



---

# FFI-RAPPORT

---

17/16935

## Military use of space

### WP1 Space-based geospatial intelligence

—

Tonje Nanette Arnesen Hannevik

Knut Eldhuset

Øyvind K. Lensjø

Dan J. Weydahl

Richard B. Olsen

Bert van den Broek (TNO)

Rob Dekker (TNO)

Mark van Persie (NLR)

Hein Noorbergen (NLR)

Arjen Oostdijk (NLR)

Rob van Swol (NLR)



# **Military use of space**

## **WP1 Space-based geospatial intelligence**

Tonje Nanette Arnesen Hannevik

Knut Eldhuset

Øyvind K. Lensjø

Dan J. Weydahl

Richard B. Olsen

Bert van den Broek (TNO)

Rob Dekker (TNO)

Mark van Persie (NLR)

Hein Noorbergen (NLR)

Arjen Oostdijk (NLR)

Rob van Swol (NLR)

---

## **Keywords**

Syntetisk apertur-radar (SAR)

Satellitter

Skipsdeteksjon

Interferometri

Polarisasjon

## **FFI-rapport**

FFI-RAPPORT 17/16935

## **Prosjektnummer**

1441

## **ISBN**

P: 978-82-464-2992-2

E: 978-82-464-2993-9

## **Approved by**

Richard B. Olsen, *Research Manager*

Johnny Bardal, *Director*



---

---

## Summary

SMART MILSpace is a project where Norway and the Netherlands are cooperating strategically about military space research. The project started in 2013, and the first part ended in December 2016. This is a final report that summarizes the work done in WP1 “Space-based geospatial information”.

---

## **Sammendrag**

SMART MILSpace er et prosjekt hvor Norge og Nederland samarbeider strategisk om militær romforskning. Prosjektet startet i 2013, og del en ble avsluttet desember 2016. Dette er en sluttrapport som oppsummerer arbeidet som er gjort i arbeidspakke 1 "Space-based geospatial information".

---

---

# Content

<b>Summary</b>	<b>3</b>
<b>Sammendrag</b>	<b>4</b>
<b>1 Introduction</b>	<b>7</b>
1.1 Background	7
1.1.1 SMART MILSpace project	7
1.1.2 WP1 Space-based geospatial information	7
1.2 Purpose of the report	8
<b>Appendix</b>	<b>9</b>
<b>A Military use of space. WP1 space-based geospatial information (GEOINT)</b>	<b>9</b>



---

---

# 1 Introduction

## 1.1 Background

### 1.1.1 SMART MILSpace project

The first part of the SMART MILSpace project started in June 2013, and carried out until the end of 2016. Through this project Norway and the Netherlands have been cooperating strategically about military space research. The project is a joint research and technology project with the focus on military use of space. SMART is short for Strategic Mutual Assistance Research and Technology. The institutes involved in the research have been Forsvarets Forskningsinstitutt (FFI) from Norway and TNO (Netherlands Organisation for Applied Scientific Research) and NLR (National Aerospace Laboratory) from the Netherlands under the control from the Norwegian and Dutch Ministries of Defence. The SMART MILSpace project included many different themes and topics of military interest:

- WP1: Space-based Geospatial Intelligence
- WP2: Satellite Communication
- WP3: Satellite Navigation
- WP4: Space Situational Awareness
- WP5 & WP6: Microsatellite Mission Concepts

### 1.1.2 WP1 Space-based geospatial information

Synthetic Aperture Radar (SAR) satellites are non-intrusive and have all weather and day/night capability. Thus, SAR together with optical satellites are reliable sources for geospatial information. Fusing geospatial information with other sources makes it geospatial intelligence (GEOINT). GEOINT is important for the military users when planning military missions.

Most of the satellites in orbit today are commercial, making it difficult to make sure the user will get the wanted satellite image over the right area at the right time. In addition, it is necessary to have some background knowledge about satellites to be able to order images. It will help the military to have a set of tools to translate the required information request into required satellite data, locate providers that can deliver the required satellite data, extract features from the satellite data and combine these features to information products including fusion with other sources, and deliver the information as products in standards that are commonly used in the military systems. The goal for WP1 is to develop a tool set like that based on open source standards and internet protocols similar to civil use of data.

---

---

The general objective is to develop and validate algorithms that can extract useful military geospatial information from open-source space-based data and deliver this information as products that can be accepted by the military communities. The main results delivered are pre-operational algorithms for generation of geospatial information products standards that are used in military communities.

The work package is divided in four sub work packages:

- WP1.1 Geospatial information definition (TNO lead)
- WP1.2 Geospatial information extraction (TNO lead)
- WP1.3 Geospatial products generation and dissemination (FFI lead)
- WP1.4 Geospatial information testbed (NLR lead)

## **1.2 Purpose of the report**

The report presents the work done under WP1 in the SMART MILSpace project. The deliverable has the title “Military use of space. WP1 Space-based geospatial intelligence”, and is presented in appendix A as a full separate document.

---

---

## **Appendix**

### **A Military use of space. WP1 space-based geospatial information (GEOINT)**

# Military Use of Space

## WP1 Space-based Geospatial Intelligence

---

FFI report no. FFI 16/02182

NLR report no. CR-2016-545

TNO report no. TNO 2016 R11404

Date: 31 December 2016

### Authors:

Bert van den Broek, Rob Dekker, TNO

Mark van Persie, Hein Noorbergen, Arjen Oostdijk, Rob van Swol, NLR

Tonje N.A. Hannevik, Knut Eldhuset, Øyvind K. Lensjø, Dan J. Weydahl, Richard B. Olsen, FFI

*Document created under the Technical Arrangement No "SMART-01" to ERG Arrangement No.1 under the EUROPA MOU between the Minister of Defence of the Kingdom of the Netherlands and the Minister of Defence of the Kingdom of Norway concerning Military Use of Space S&T.*

*All rights reserved. No part of this document may be reproduced or transmitted in any form or by any means, electronic, mechanical, photocopying, recording, or otherwise, without prior written permission of FFI, NLR or TNO.*

Approved by:

Author	Reviewer	Manager
Date:	Date:	Date:

**CLASSIFICATION: UNCLASSIFIED**



## Contact information

The following individuals can be contacted for any questions regarding the current document:

Authors:	TBD	TBD
TNO work package lead:	Bert van den Broek	+31 88 866 4075 bert.vandenbroek@tno.nl
NLR work package lead:	Mark van Persie	+31 88 5114256 mark.van.persie@nlr.nl
FFI work package lead:	Richard Olsen	+47 63 807468 richard.olsen@ffi.no

### CLASSIFICATION: UNCLASSIFIED

*All rights reserved. No part of this document may be reproduced or transmitted in any form or by any means, electronic, mechanical, photocopying, recording, or otherwise, without prior written permission of FFI, NLR or TNO.*

## Summary

The GeoInt (Geospatial Intelligence) work package within the research programme Military Use of Space has been studying automation of workflows for producing geographical oriented intelligence where the use of satellite data plays a crucial role. The focus is here on open source satellites which increasingly are available both in the optical/infrared and radar wavelength domain.

The activities in the work package followed the intelligence cycle ranging from data collection, data definition and acquisition, processing, fusion to final product, and dissemination.

In the first place, military information requirements are discussed, as well as the relevant operational military conditions and infrastructure. Tools for acquisition planning and searching of archives are discussed, as well as an overview of open source satellite data which are presently available.

Since the availability of satellite imagery increases, the revisit time for monitoring specific locations is reduced enabling longer time series of comparable satellite imagery. The availability of free data in the ESA (European Space Agency) Copernicus program is also relevant here. Thus, an important topic for studying information extraction from satellite imagery has been the automation of multi-temporal change detection using both optical and radar data. Information about activities and trends can be observed and current open source high resolution satellites, such as Worldview/Digitalglobe in the optical domain and TerraSAR-X/Comso\_Skymed in the microwave domain can be used to further identify the detections.

The detection of ships using AIS (Automatic Identification System) receivers from space is currently becoming more and more operational and FFI (Norwegian Defence Research Establishment) is operating its own satellites for this purpose. FFI is doing studies doing ship detection in SAR (Synthetic Aperture Radar) imagery and fusing the detections with AIS messages.. A ship detection tool Aegir has been developed, and adapted for the use of Sentinel data from the Copernicus program.

In this work package the information from the satellite data is considered as a half-product, which has to be enriched with context data to produce a final product. A discussion about how to fuse the data and what the sources of uncertainty to deal with are can be found in this report.

### **CLASSIFICATION: UNCLASSIFIED**

*All rights reserved. No part of this document may be reproduced or transmitted in any form or by any means, electronic, mechanical, photocopying, recording, or otherwise, without prior written permission of FFI, NLR or TNO.*

GIS (Geographical Information System) data are essential context data and the accuracy of the various sources for elevation data has been evaluated.

Dissemination of information based on satellite data requires a network architecture which can handle large amounts of data. Results of the NATO MAJIIC (Multi-sensor Aerospace-ground Joint ISR Interoperability Coalition) project and the recommendation for standardisation are a key issue here and are presented in the report. Results of the INSPIRE project which proposes a reference architecture are discussed in the context of the report.

An important goal of the work has been the development of a test bed that can demonstrate the different workflows. This is done on basis of use cases comprising a number of locations and certain type of satellite data. The test bed extraction components comprises subcomponents for optical data and SAR data focusing on multi-temporal change detection, and for SAR data also on ship detection in combination with AIS. Finally, the information from the subcomponents is combined in one single picture in a fusion component.

The results of the work package have been demonstrated to various representatives of the NLMOD (Netherlands Military of Defence) and NOMOD (Norwegian Military of Defence). A contribution to a workshop organised by the Netherlands school of intelligence (DIVI) has been made, and a report of the workshop can be found in the appendix.

From the discussions with the MOD (Military of Defence) it becomes clear that open source data can be a valuable source for information gathering. The intermediate resolution data, such as data from the Sentinel satellites, which can be accessed freely, can be used to determine trends and to detect anomalies. Higher resolution data can be acquired subsequently to characterise the detections further. Also the use of UAVs (Unmanned Aerial Vehicles), which is possible with AGS (Airborne Ground Surveillance), could further reduce the revisit time interval. However, due to limited resources for analysts the processing should be done as automated as possible, and the required infrastructure should be developed for this. The test bed presented here is a first step in this direction.

## **CLASSIFICATION: UNCLASSIFIED**

*All rights reserved. No part of this document may be reproduced or transmitted in any form or by any means, electronic, mechanical, photocopying, recording, or otherwise, without prior written permission of FFI, NLR or TNO.*

## Contents

<b>Contact information</b>	<b>2</b>
<b>Summary</b>	<b>3</b>
<b>Acronyms and Abbreviations</b>	<b>16</b>
<b>1 Introduction</b>	<b>21</b>
1.1 Background	21
1.2 Objective	22
1.3 Synopsis	22
<b>2 Geospatial information definition</b>	<b>23</b>
2.1 Introduction	23
2.2 Military information requirements & current operational workflows	23
2.2.1 NLMOD operational workflows: status of use of satellite data	24
2.2.2 NOMOD operational workflows: FSGI	26
2.3 Acquisition planning and data retrieval	30
2.3.1 Acquisition planning tools	30
2.3.2 Open source data retrieval and portals	32
2.4 Data description	35
<b>3 Geospatial information extraction</b>	<b>40</b>
3.1 Introduction	40
3.2 Optical methods	41
3.2.1 Optical satellite image time series	41
3.2.2 Optical analysis methods	42
3.2.2.1 Pre-processing	43
3.2.2.2 Single image transformations	46
3.2.3 Multi image transformation and filtering	48
3.2.4 Detection and analysis of change	49
3.3 SAR methods	52
3.3.1 Inventory of SAR methods	52
3.3.2 Selection of SAR methods	62
3.3.3 Implementation of SAR methods	64

### **CLASSIFICATION: UNCLASSIFIED**

*All rights reserved. No part of this document may be reproduced or transmitted in any form or by any means, electronic, mechanical, photocopying, recording, or otherwise, without prior written permission of FFI, NLR or TNO.*

3.4	Ship detection methods/ sea clutter/polarimetry	66
3.4.1	Dual-polarised SAR data	68
3.4.2	Quad-polarised SAR data	73
3.4.3	Compact polarimetry	86
<b>4</b>	<b>Geospatial information products and dissemination</b>	<b>93</b>
4.1	Introduction	93
4.2	Geospatial context data - 3D models from space	93
4.2.1	Inventory of relief data	93
4.2.2	Evaluation	94
4.2.3	Recommendation	99
4.3	Product generation - Fusion and Information products based on space data	100
4.3.1	Introduction	100
4.3.2	Half-finished products from imagery	101
4.3.3	Geospatial information products	104
4.3.4	Production and fusion methods	106
4.3.5	Data preparation, quality and validation	109
4.4	Dissemination and standards	110
4.4.1	The MAJIC project	110
4.4.1.1	Standardisation	111
4.4.2	A Reference architecture for dissemination of large volumes of space borne data	114
4.4.2.1	Description of the Architecture	114
4.4.3	OGC and ISO standards	117
4.4.4	CSD and services	117
4.4.5	Big Data and Cloud-based processing	117
<b>5</b>	<b>Geospatial information testbed &amp; demonstration</b>	<b>118</b>
5.1	Introduction	118
5.2	Test bed description	118
5.3	Use cases and demonstration	122
5.3.1	Use case description	125
5.3.1.1	Use case 1: Nikel	125
5.3.1.2	Use case 2: Barents sea	127
5.3.1.3	Use case 3: Caribbean	129
5.3.1.4	Use case 4: Rotterdam	131

**CLASSIFICATION: UNCLASSIFIED**

*All rights reserved. No part of this document may be reproduced or transmitted in any form or by any means, electronic, mechanical, photocopying, recording, or otherwise, without prior written permission of FFI, NLR or TNO.*

5.3.1.5	Use case 5: UV2014	142
5.3.1.6	Use case 6: Kaliningrad	143
5.4	Description of optical test bed components	148
5.4.1	Technical setup	148
5.4.2	Demonstration workflow	148
5.4.3	Graphical user interface	149
5.4.4	Technical implementation	150
5.4.4.1	Technical workflow	150
5.4.4.2	Erdas GUI customization	155
5.4.4.3	Python and Erdas	156
5.4.5	Results	156
5.4.6	Evaluation.	160
5.5	Description of SAR test bed components	161
5.6	Description ship detection test bed component	165
5.7	Description of fusion test bed component	171
<b>6</b>	<b>Conclusions</b>	<b>175</b>
6.1	Summary	175
6.2	Recommendations	177
	<b>References</b>	<b>179</b>
<b>Appendix A</b>	<b>Geospatial analysis workshop, DIVI, 't Harde, 18-20 November 2014</b>	<b>181</b>

**CLASSIFICATION: UNCLASSIFIED**

*All rights reserved. No part of this document may be reproduced or transmitted in any form or by any means, electronic, mechanical, photocopying, recording, or otherwise, without prior written permission of FFI, NLR or TNO.*

**CLASSIFICATION: UNCLASSIFIED**

*All rights reserved. No part of this document may be reproduced or transmitted in any form or by any means, electronic, mechanical, photocopying, recording, or otherwise, without prior written permission of FFI, NLR or TNO.*

## List of Figures

Figure 1 IPE with examples form the JDP2.1 document. ....	23
Figure 2 Intelligence cycle in the background, with the main topics of the GeoInt test bed in overlay. ....	24
Figure 3 A general overview of the FSGI concept. ....	28
Figure 4 FSGI concept in more detail. ....	29
Figure 5 The MEOS software tool and user interface. ....	31
Figure 6 Results from a SAR planning exercise using MEOS ....	32
Figure 7 Search results for the ESA scientific data hub for Sentinel-1A over Kaliningrad. ....	33
Figure 8. Portals of USGS (left) and ESA (right) for access to Landsat and Sentinel satellite data .....	35
Figure 9 Comparison of satellite examples for Rotterdam harbour. Left to right: Formosat, Digital globe (GE) (top), Sentinel SM, TerraSAR ST (bottom). ....	40
Figure 10. Applications for different scales of temporal and spatial observation. ....	42
Figure 11. Overview of processing steps for satellite image series analysis .....	43
Figure 12. Found tie-points between Landsat and DMC image and the relative deviations. ....	44
Figure 13. Landsat image before (top) and after (bottom) radiometric and atmospheric correction. ....	45
Figure 14. Image classification with Erdas Knowledge Engineer. Investigation of spectral characteristics (top right), application of classification rules (left), resulting classification (bottom right). ....	47
Figure 15. Detection of ship pixels and number of ships within harbour sectors. ....	48
Figure 16. Filtering of clouds (orange) and noise (red) from large ships (dark green) and small ships (light green) .....	49
Figure 17. Detection of anomalies based on filtered mean and standard deviation. ....	51
Figure 18. Change detection between series of land use classified image segments. ....	52
Figure 19 Example of the numerous patches used when doing the co-registration of the two SAR images .....	53
Figure 20 Satellite SAR change detection during an exercise at Setermoen, north of Norway..	54
Figure 21 Amplitude change imagery for Meymaneh, Afghanistan. Original SAR data: © COSMO-SkyMed™ Product-ASI 2010, distributed by e-GEOS. ....	55
Figure 22 RGB colour composite of COSMO-SkyMed imagery for Rotterdam harbour .....	55
Figure 23 TerraSAR-X images (15 and 26 June 2013) for the Ørland area (courtesy Fraunhofer IOSB) with changes due to tide and relocatable vehicles (red overlay). ....	56

### CLASSIFICATION: UNCLASSIFIED

*All rights reserved. No part of this document may be reproduced or transmitted in any form or by any means, electronic, mechanical, photocopying, recording, or otherwise, without prior written permission of FFI, NLR or TNO.*



Figure 24 Amplitude and coherence image from COSMO-SkyMed image pair for Meymaneh city in Afghanistan..... 58

Figure 25 Coherence images from COSMO-SkyMed image pair. Left one day interval. Right 8 day interval..... 59

Figure 26 Sub-set of COSMO-SkyMed SAR coherence images over Meymaneh in Afghanistan..... 60

Figure 27 Colour fusion of SAR amplitude and coherence changes over a period of 8-days over part of the Meymaneh city in Afghanistan..... 61

Figure 28 Coherence image from TerraSAR-X image pair for Ørland airbase..... 62

Figure 29 Workflow for RGB visualization ..... 64

Figure 30 Workflow for visualization of the ratio ..... 65

Figure 31 Workflow for the extraction of information from a temporal array ..... 65

Figure 32 MATLAB tool showing detected multi-temporal changes in red overlay. .... 66

Figure 33 Workflow for coherent changes ..... 66

Figure 34. Norwegian ocean areas. © www.fao.org..... 68

Figure 35. ScanSAR polarisation combinations showing how the combined channel gives better ship to sea contrast. .... 69

Figure 36. RADARSAT-2 Standard quad-pol HH- and HV-polarisation segments on November 19<sup>th</sup> 2009..... 69

Figure 37. Signature of Norne FPSO in VV-channel (top left), VH-channel (top right) and the combined case (bottom). .... 70

Figure 38. 3D reflections of vessels and the sea background in a segment of 600 pixels x 600 pixels. Top left: VV-channel, top right: VH-channel, bottom: combined case. .... 71

Figure 39. Pauli decomposition of six vessels and the ocean background over the Norne field. All six vessels are clearly visible and Norne FPSO is third from the top. .... 73

Figure 40. Segments of a RADARSAT-2 quad-polarised image over the Oslofjord are combined using different polarimetric decomposition methods. Top: Pauli, middle: Krogager and bottom: Yamaguchi. .... 76

Figure 41. RADARSAT-2 quad-polarised data over the Oslofjord is shown in different ways from top to bottom: HH-polarisation, VV-polarisation, HV-polarisation, Pauli, Krogager and Yamaguchi rotated. .... 78

Figure 42. 600 pixels x 600 pixels shown in 2D segments of a RADARSAT-2 quad-polarisation image on November 29<sup>th</sup> 2009. .... 79

Figure 43. 600 pixels x 600 pixels 2D segments of RADARSAT-2 quad-polarisation data over the Norne field in different polarisations and polarisation combinations. Top left: HH, top right:

**CLASSIFICATION: UNCLASSIFIED**

*All rights reserved. No part of this document may be reproduced or transmitted in any form or by any means, electronic, mechanical, photocopying, recording, or otherwise, without prior written permission of FFI, NLR or TNO.*

VV, middle left: HV, middle right: VH and bottom left: (HH-VV)\*HV. The different vessels are shown to the bottom right. .... 80

Figure 44. 600 pixels x 600 pixels shown in 3D of a RADARSAT-2 quad-polarisation image on November 29<sup>th</sup> 2009..... 81

Figure 45. 600 pixels x 600 pixels segments of RADARSAT-2 quad-polarisation data on December 10<sup>th</sup> 2009 in different polarisations and polarisation combinations. Top left: HH, top right: VV, bottom left: HH-VV, bottom right: (HH-VV)×HV. Norne FPSO (right) and Ocean Prince (left) are shown with the arrows. .... 82

Figure 46. 600 pixels x 600 pixels segments of RADARSAT-2 quad-polarisation data on December 10<sup>th</sup> 2009 in circular basis decomposition, RR (left) and RL (right). Norne FPSO (right) and Ocean Prince (left) are shown with the arrows. .... 82

Figure 47. 600 pixels x 600 pixels segments of RADARSAT-2 quad-polarisation data on December 10<sup>th</sup> 2009 in Krogager decompositions. Top left: kDiplane, top right: kHelix and bottom: kSphere. Norne FPSO (right) and Ocean Prince (left) are shown with the arrows. .... 83

Figure 48. 600 pixels x 600 pixels segments of RADARSAT-2 quad-polarisation data on December 10<sup>th</sup> 2009 using Yamaguchi decomposition method. Top left: Yamaguchi helix rotated, top right: volume rotated, bottom left: double rotated and bottom right: surface rotated. Norne FPSO (right) and Ocean Prince (left) are shown with the arrows..... 83

Figure 49. Top: DCP double bounce simulation (HH-VV). Bottom: Quad-polarisation double bounce (HH-VV). .... 88

Figure 50. Top: DCP surface simulation (HH+VV). Bottom: Quad-polarisation surface (HH+VV). .... 89

Figure 51. Top: DCP volume simulation (HV). Bottom: Quad-polarisation volume (HV). .... 90

Figure 52. Top: DCP Pauli decomposition. Bottom: Quad-polarisation Pauli decomposition... 91

Figure 53. Top: Quad-polarisation volume (HV) scattering. Bottom: DCP product (HH-VV)\*HV..... 92

Figure 54 Example of SRTM data before and after void filling (NGA) of Mt Rainier and Mt Adams in the Cascade Mountain range (USA). .... 95

Figure 55 GDEM (left) and SRTM DEM (right). .... 95

Figure 56 Comparison of the different levels of elevation data from radar (SAR) measurements. .... 97

Figure 57 Comparison of open source elevation data based on topographical maps (left) compared to GDEM (right) for the area of Nikel. .... 97

Figure 58 Comparison of Norwegian survey elevation data (left) compared to GDEM (right) for the area near Ørland air base. Global view (top) and detailed view (bottom). .... 98

Figure 59 AHN (version 1) example for Rotterdam, where oil terminals stand out clearly. .... 99

**CLASSIFICATION: UNCLASSIFIED**

*All rights reserved. No part of this document may be reproduced or transmitted in any form or by any means, electronic, mechanical, photocopying, recording, or otherwise, without prior written permission of FFI, NLR or TNO.*

Figure 60 Fusion and Information products in the GeoInt workflow. ....	101
Figure 61 Water bodies derived using spectral indices from multispectral Landsat imagery ..	102
Figure 62 Land use classification on basis of series of Landsat imagery. ....	103
Figure 63 Multi-temporal change detection showing changes in the utilization of assembly areas (peaks in the upper-right view) in the city of Nikel. ....	103
Figure 64 Workflow with various ingestion and egestion channels. ....	106
Figure 65 Operational picture indicating the MAJIIC project goals. ....	111
Figure 66 Reference Architecture. ....	115
Figure 67 Technology Application to Layers. ....	116
Figure 68 Workflow with the various test bed components. ....	121
Figure 69. Overview of test bed components and demonstration of use cases. ....	123
Figure 70 Demonstration set-up. ....	124
Figure 71 The Nikel area and the Nikel melt plant. ....	125
Figure 72. Radar data (three dates in the RGB colour channels) projected over a Landsat image,. The border between Norway and Russia is indicated. ....	126
Figure 73 Landsat multispectral image showing the area and a multi-spectral image in the near infrared revealing more land use details. ....	127
Figure 74 Top left: Coverage of Sentinel-1A IW VV/VH image on December 9 <sup>th</sup> 2015. Top right: SAR image and ship detections done by Aegir in both polarisation channels. Bottom: Close-up of some of the detections. ....	128
Figure 75 Coverage of Sentinel-1A image on May 30 <sup>th</sup> 2015 at 10:06 covering part of the Caribbean. © Google Earth. ....	129
Figure 76 Sentinel-1A IW image on May 30 <sup>th</sup> 2015 with land mask and ship detections in the VV-channel. ....	130
Figure 77 Sentinel-1A IW image on May 30 <sup>th</sup> 2015 shown in Google Earth together with SAR ship detections. © Google Earth. ....	130
Figure 78 Ship detections and AIS data shown together. © Google Earth. ....	131
Figure 79 Port of Rotterdam (source: World Topo Map ESRI). ....	132
Figure 80 Port of Rotterdam overlaid with satellite image that encompasses 22.5 km x 26.5 km. ....	133
Figure 81 DMC recordings between April and September 2013. ....	134
Figure 82 Sentinel-2A recordings from 2016. ....	136
Figure 83. COSMO-SkyMed data showing three dates in the RGB color channels. ....	137
Figure 84 Radarsat2 XF mode data for three dates in the RGB channels. ....	137
Figure 85 Sentinel 1A SM data for two dates in the RGB channels. ....	138
Figure 86 Sentinel 1A IW data for three dates in the RGB channels. ....	138

**CLASSIFICATION: UNCLASSIFIED**

*All rights reserved. No part of this document may be reproduced or transmitted in any form or by any means, electronic, mechanical, photocopying, recording, or otherwise, without prior written permission of FFI, NLR or TNO.*

Figure 87 Coverage of Sentinel-1A image on June 1 <sup>st</sup> 2015 covering Rotterdam.....	139
Figure 88 Sentinel-1A IW image on June 1 <sup>st</sup> 2015 in VH-polarisation showing Rotterdam and the sea outside Rotterdam. ....	140
Figure 89 Sentinel-1A IW image on June 1 <sup>st</sup> 2015 in VV-polarisation with land mask.....	140
Figure 90 Sentinel-1A IW image on June 1 <sup>st</sup> 2016 with land mask and ship detections done by Aegir in yellow. Green diamonds mean that the SAR ship detections are confirmed by AIS data. ....	141
Figure 91 Sentinel-1A IW image on June 1 <sup>st</sup> 2016 with ship detections done by Aegir (yellow) as well as AIS data (red). Green diamonds mean that the SAR ship detections are confirmed by AIS data. ....	141
Figure 92 Overview of the radar data for the Ørland airbase.....	142
Figure 93 Sentinel image used for the Kaliningrad Oblast.....	143
Figure 94 Coverage of Sentinel-1A image on August 16 <sup>th</sup> 2016 covering Kaliningrad. ....	144
Figure 95 Sentinel-1A IW image on August 16 <sup>th</sup> 2016 with ship detections done by Aegir (yellow) as well as AIS data (red) Green diamonds mean that the SAR ship detections are confirmed by AIS.....	145
Figure 96 Coverage of Sentinel-1A image on September 9 <sup>th</sup> 2016 covering Kaliningrad. © Google Earth .....	145
Figure 97 Sentinel-1A IW image on September 9 <sup>th</sup> 2016 with land mask and ship detections in the VV-channel done by Aegir. ....	146
Figure 98 Sentinel-1A IW image on September 9 <sup>th</sup> 2016 with land mask and ship detections in the VV- and VH-channel done by Aegir. ....	146
Figure 99 Sentinel-1A IW image on September 9 <sup>th</sup> 2016 with land mask and AIS data.....	147
Figure 100 Sentinel-1A IW image on September 9 <sup>th</sup> 2016 with ship detections done by Aegir (yellow) as well as AIS data (red) Green diamonds mean that the SAR ship detections are confirmed by AIS data. ....	147
Figure 101 Milspace demonstration tab with user workflow (ships).....	149
Figure 102. Main components of graphical user interface.....	150
Figure 103. Overview of anomaly detection, with anomalies in green in left viewer, temporal profile of anomalies (0,1), and temporal profile of reflections (red curve) in separate windows. ....	152
Figure 104. Overview of export products (red/grey anomaly image (left) and text output file.	153
Figure 105 Results of ship intensity detection activities: anomalous harbour sections (left, yellow) and detected ships at a selected data (right).....	154

**CLASSIFICATION: UNCLASSIFIED**

*All rights reserved. No part of this document may be reproduced or transmitted in any form or by any means, electronic, mechanical, photocopying, recording, or otherwise, without prior written permission of FFI, NLR or TNO.*

Figure 106 Overview of the ship anomaly evaluation: selected anomaly harbour sectors (left, yellow), and temporal profile of number of ships in the selected sector (red line in right window). ..... 155

Figure 107. Anomaly detection result (left), showing new buildings in green and the smoke plume of a power plant (right). The temporal reflection profile for the building anomaly shows that the anomaly occurs in the fourth observation (1 may 2013). ..... 157

Figure 108 Anomalies detected in a series of 19 Sentinel-2A images. The colors show the number of detected anomalies over time. .... 158

Figure 109. Temporal ship intensity plotted for different harbour types. .... 159

Figure 110 Results of ship detection in Sentinel-2A (top) compared to DMC (bottom). ..... 160

Figure 111 Workflow for the multi-temporal change detection tool. .... 161

Figure 112 Interface of the multi-temporal change detection tool showing use case Nikel .... 162

Figure 113 Interface of the multi-temporal change detection tool showing use case Rotterdam. .... 163

Figure 114 Interface of the multi-temporal change detection tool showing analysis results for use case Rotterdam. .... 163

Figure 115 Interface of the multi-temporal change detection tool showing temporal behaviour of oil terminal content. .... 164

Figure 116 Interface of the multi-temporal change detection tool showing use case UV2014 (top) and the analysis for displacement of aircraft (bottom). ..... 165

Figure 117. Workflow for the automatic ship detector Aegir for dual-polarisation or quad-polarisation data. .... 167

Figure 118 Aegir’s main image display and GUI when Aegir is running. .... 168

Figure 119 When ice is present in the image, a manual mask can be created over the ice in addition to the automatic land mask over Jan Mayen in this RADARSAT-2 image. .... 168

Figure 120. Location where it is possible to choose the fused polarimetric “channel” (see red circle to the left). ..... 169

Figure 121 SAR detections can be shown in Google Earth. © Google Earth. .... 170

Figure 122 Overview of test bed components and workflow ..... 171

Figure 123 Interface of the fusion component showing use case Kaliningrad. .... 172

Figure 124 Interface of the fusion component showing use case Kaliningrad and retrieval of radar change detection results. .... 173

Figure 125 Interface of the fusion component showing use case Rotterdam. .... 174

Figure 126 Interface of the fusion component showing use case Rotterdam and retrieval of optical change detection results. .... 174

**CLASSIFICATION: UNCLASSIFIED**

*All rights reserved. No part of this document may be reproduced or transmitted in any form or by any means, electronic, mechanical, photocopying, recording, or otherwise, without prior written permission of FFI, NLR or TNO.*

## List of Tables

Table 1 Medium resolution satellites that provide open data. ....	37
Table 2 High resolution satellites.....	38
Table 3 Overview of SAR methods and software packages. ....	64
Table 4. Maximum amplitude divided by mean sea (R) for the oil production vessel Norne FPSO in 26 RADARSAT-2 ScanSAR dual-polarisation images. ....	72
Table 5. Maximum amplitude divided by mean sea for Norne FPSO on November 29 <sup>th</sup> 2009 and December 1 <sup>st</sup> 2009 for different polarisations and polarisation combinations.....	84
Table 6. Maximum amplitude divided by mean sea for Norne FPSO on December 10 <sup>th</sup> 2009..	85
Table 7. Maximum intensity divided by mean sea intensity for Norne FPSO on December 10 <sup>th</sup> 2009. ....	86
Table 8 Fusion methods. ....	107
Table 9 Information products.....	108
Table 10 Test bed components.....	120
Table 11 Overview of use cases.....	122
Table 12 Reports produced after ship detection is done. ....	170

### **CLASSIFICATION: UNCLASSIFIED**

*All rights reserved. No part of this document may be reproduced or transmitted in any form or by any means, electronic, mechanical, photocopying, recording, or otherwise, without prior written permission of FFI, NLR or TNO.*

## Acronyms and Abbreviations

A	Ascending
AGS	Airborne Ground Surveillance
AHN	Actueel Hoogtebestand Nederland
AIS	Automatic Identification System
AOI	Area of Interest
ARC	Archive
ASI	Agenzia Spaziale Italiana
BMS	Battle Field Management System
BOA	Bottom of Atmosphere
CADRG	Compressed ARC Digitized Raster Graphic
CCD	Coherent Change Detection
CCDO	Certificate of Competence for Demolition Operatives
CORBA	Common Object Request Broker Architecture
Core GIS	Core Geographical Information System
CP	Circular Polarimetry
CSD	Coalition Shared Database
CSK	Cosmo SkyMed
CTLR	Circular Transmit - Linear Receive
D	Descending
DCP	Dual Circular Polarimetry
DEM	Digital Elevation Model
DG	Dienst Geografie
DIVI	Netherlands School of Intelligence
DLR	German Aerospace Center
DMC	Disaster Monitoring Constellation
DN	Digital Number
DP	Darkest Pixel
DTED	Digital Terrain Elevation Data
DWT	Discrete Wavelet Transformation
EADS	European Aeronautic Defense and Space Company
ELINT	Electronic signals Intelligence
ENL	Equivalent Number of Looks
EO	Earth Observation
EOWEB	Earth Observation Web

### **CLASSIFICATION: UNCLASSIFIED**

*All rights reserved. No part of this document may be reproduced or transmitted in any form or by any means, electronic, mechanical, photocopying, recording, or otherwise, without prior written permission of FFI, NLR or TNO.*



EPSCG	European Programme Strategy Group
ERG	European Research Council
ESA	European Space Agency
ESB	Enterprise Service Bus
ESRI	Earth Sciences and Resource Institute
FFI	Forsvarets Forskningsinstitutt – Norwegian Defence Research Establishment
FFT	Fast Fourier Transform
FMGT	Forsvarets Militærgeografiske Tjeneste – Norwegian Military Geographic Service
FSGI	Felles Satellitt- og Geoinformasjonscenter – Common Satellite and Geoinformation Centre
FTP	File Transfer Protocol
GDAL	Geospatial Data Abstraction Library
GDEM	Global Digital Elevation Map
GE	Google Earth
GeoInt	Geospatial Intelligence
GFS	Grouped Frequent Sequential
GIF	Graphics Interchange Format
GIS	Geographical Information System
GMTI	Ground Moving Target Indicator
GRDH	Ground Range Detected High
GSA	GeoSpatial Analyst
GUI	Graphical User Interface
HANTS	Harmonic Analysis of Time Series
H	Horizontal
HH	Horizontal transmit – Horizontal receive
HV	Horizontal transmit – Vertical receive
HRSI	High Resolution Satellite Imagery
IDD	Interface Design Document
IMINT	Image Intelligence
INREP	Intelligence Report
InSAR	Interferometric SAR
INTSUM	Intelligence Summary
IPE	Intelligence Preparation of the Environment
ISIS	Integrated Staff Information System
ISR	Intelligence, Surveillance, Reconnaissance

**CLASSIFICATION: UNCLASSIFIED**

*All rights reserved. No part of this document may be reproduced or transmitted in any form or by any means, electronic, mechanical, photocopying, recording, or otherwise, without prior written permission of FFI, NLR or TNO.*



ISRSPOTREP	Intelligence, Surveillance, Reconnaissance SPOT report
IW	Interferometric Wide
JDP	Joint Doctrine Publication
JINT	Joint Intelligence
KSAT	Kongsberg Satellite Services
L	Left
LAI	Leaf Area Index
LL	Left Left circular
LR	Left Right circular
LRIT	Long Range Identification and Tracking
MAJIC	Multi-sensor Aerospace-ground JointISR Interoperability
MEOS	Multi-Mission Earth Observation System
MGCP	Multinational Geospatial Co-Production Program
MHT	Multi Hypothesis Tracker
MIDIS	Multi-Intelligence Data Integration Services
MilGeo	Military Geography
MIR	Middle Infrared
MIVD	Militaire Inlichtingen en Veiligheidsdienst
MMSI	Maritime Mobile Service Identity
MNF	Minimum Noise Fraction
MOD	Military of Defence
MS	Multispectral Bands
NASA	National Aeronautics and Space Administration
NATO	North Atlantic Treaty Organization
NDVI	Normalized Difference Vegetation Index
NDWI	Normalized Difference Water Index
NGA	National Geospatial-Intelligence Agency
NIR	Near Infrared
NLMOD	Netherlands Military of Defence
NLR	Nationaal Lucht- en Ruimtevaartlaboratorium / National Aerospace Laboratory
NOMOD	Norwegian Military of Defence
NoSQL	Not only SQL
NSIF	NATO Secondary Imagery Format
NSO	National Space Organization
OGC	Open Geospatial Consortium
OSM	Open Street Map

**CLASSIFICATION: UNCLASSIFIED**

*All rights reserved. No part of this document may be reproduced or transmitted in any form or by any means, electronic, mechanical, photocopying, recording, or otherwise, without prior written permission of FFI, NLR or TNO.*

PCA	Principal Component Analysis
PDF	Probability Density Function
PoL	Patterns of Life
R	Right
RCM	Radarsat Constellation Mission
REST	Representational State Transfer
RFI	Request For Information
RGB	Red Green Blue
RL	Right Left
RMS	Root Mean Square
ROC	Receiver Operating Curve
RR	Right Right
S&T	Science & Technology
S2A	Sentinel-2A
SAR	Synthetic Aperture Radar
SAVI	Soil Adjusted Vegetation Index
SCN	ScanSAR Narrow
SCW	ScanSAR Wide
SDI	Spatial Data Infrastructures
SET	Sensors and Technology
SITS	Satellite Image Time Series
SMTP	Simple Mail Transfer Protocol
SOA	Service Oriented Architecture
SOAP	Service Oriented Architecture Protocol
SQL	Structured Query Language
SRTM	Shuttle Radar Topography Mission
ST	Staring Spotlight
STGP	Shared Tactical Ground Picture
TAI	Target Areas of Interest
TNO	Organisatie voor Toegepast Natuurwetenschappelijk Onderzoek / Netherlands Organisation for Applied Scientific Research
TOA	Top of Atmosphere
TREX	TanDEM-X-High Resolution Elevation Data Exchange Program
UAV	Unmanned Aerial Vehicle
USGS	US Geological Survey
UTM	Universal Transverse Mercator

**CLASSIFICATION: UNCLASSIFIED**

*All rights reserved. No part of this document may be reproduced or transmitted in any form or by any means, electronic, mechanical, photocopying, recording, or otherwise, without prior written permission of FFI, NLR or TNO.*

UV	Unified Vision
UV	Ultraviolet
V	Vertical
VH	Vertical transmit – Horizontal receive
VMS	Vessel Monitoring System
VV	Vertical transmit – Vertical receive
WorldDEM	World Digital Elevation Model
WPI	WorkPoint Interface
WSDL	Web Service Description Language
XF	Extrafine
XML	Extensible Markup Language

**CLASSIFICATION: UNCLASSIFIED**

*All rights reserved. No part of this document may be reproduced or transmitted in any form or by any means, electronic, mechanical, photocopying, recording, or otherwise, without prior written permission of FFI, NLR or TNO.*

## 1 Introduction

### 1.1 Background

Geospatial information (and if fused with other classified information: Geospatial Intelligence: GeoInt) is an important source for intelligence and planning of military missions. Because of their non-intrusive character and all weather capability, Synthetic Aperture Radar (SAR) satellites are a reliable source for geospatial information. Optical satellites are also a good source.

However, the exploitation of this information source for operational practise is not easy. An in-depth knowledge of the satellite and sensor characteristics is required to order the best suited satellite data as source for specific military information (data acquisition modes can have varying size, resolution, polarisation, viewing angles and frequency bands). Also the procedures to order and access the satellite data once they have been acquired might be complex. Finally the data formats that are used are not always compatible with military systems.

Apart from the data access aspect, the automatic extraction of reliable intelligence information from the satellite images is a complex process. Practical methodologies, automatic procedures and tools need to be developed and integrated in the military workflow. These should be based on the latest research results and image exploitation tools, and suited for the newest satellite observation capabilities.

What would help the military to make use of geospatial information would be a set of tools supporting a (semi-) automatic workflow that is able to:

- Translate the required information request into required satellite data
- Identify providers that can deliver the required satellite data
- Extract features from the satellite data and combine these features to information products including fusion with other sources
- Deliver the information as products in standards that are commonly used in the military systems

Such a tool set, based on open source standards and internet protocols similar to civil use of data, is developed in this work package.

### **CLASSIFICATION: UNCLASSIFIED**

*All rights reserved. No part of this document may be reproduced or transmitted in any form or by any means, electronic, mechanical, photocopying, recording, or otherwise, without prior written permission of FFI, NLR or TNO.*

## 1.2 Objective

The general objective of this work package is to develop and validate algorithms for extracting useful military geospatial information from open-source space-based data and for delivering this information as products that can be accepted by the military communities.

This means that the information has to be delivered according to operational standards in terms of contents and data formats. What information is useful for military operations follows from interviews with military stakeholders done during the first months of the work package.

The main results of the work package are pre-operational algorithms implemented as semi-automatic workflows for the generation of geospatial information products using standards that are used in the military communities. In follow-on projects, these operational algorithms may be actually implemented in military systems.

To focus the work a number of use cases have been selected such as mapping, ship monitoring and monitoring of activities in harbours and airfields. These activities are detected on basis of multi-temporal change detection techniques using time series for the open source satellites. Specific focus was on the use of satellite SAR images with its high-resolution modes over land areas, lower-resolution modes over sea, as well as on the use of multispectral medium resolution optical imagery.

The work package has followed a rapid proto-typing method of two cycles to achieve the overall objective. In the first cycle (initial development) a testbed has been set-up in which the work package partners have developed and validated algorithms for workflows to extract information from open source satellite data and to generate products according to standards that are accepted among the military communities. In the second cycle the testbed and workflow have been applied to current available satellite data such as Sentinel data from the Copernicus program.

## 1.3 Synopsis

The activities within WP1 (Work Package 1) are distributed over four main topics. The work and results are presented in chapters 2-5 respectively:

- Chapter 2: Geospatial information definition
- Chapter 3: Geospatial information extraction
- Chapter 4: Geospatial information products generation and dissemination
- Chapter 5: Geospatial information testbed and demonstration

### **CLASSIFICATION: UNCLASSIFIED**

*All rights reserved. No part of this document may be reproduced or transmitted in any form or by any means, electronic, mechanical, photocopying, recording, or otherwise, without prior written permission of FFI, NLR or TNO.*

## 2 Geospatial information definition

### 2.1 Introduction

The main objective of the work described in this chapter is to identify what military information is required, and what type of operational military conditions and infrastructure are relevant. The requirements are seen in the context of the military intelligence cycle and a possible solution for a military data acquisition service is presented. Tools for acquisition planning and searching of archives are discussed as well as an overview of open source satellite data which are presently available.

### 2.2 Military information requirements & current operational workflows

The military information requirements (with a reference to information from satellites) can be derived at a high level from the NATO (North Atlantic treaty Organization) joint JDP-2.1 document, and in general focus on the intelligence preparation of the environment (IPE) and subsequent surveillance phases. Two main topics can be distinguished (see figure 1 for details):

- Terrain analysis including the infrastructure.
- Activity patterns.

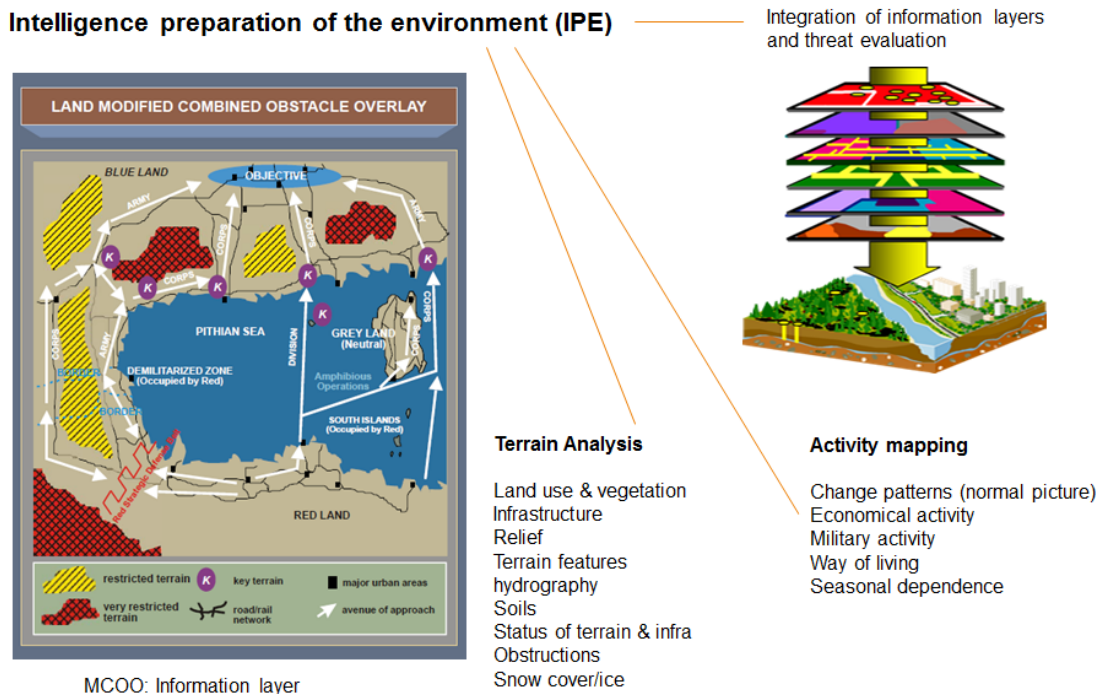


Figure 1 IPE with examples form the JDP2.1 document.

## CLASSIFICATION: UNCLASSIFIED

All rights reserved. No part of this document may be reproduced or transmitted in any form or by any means, electronic, mechanical, photocopying, recording, or otherwise, without prior written permission of FFI, NLR or TNO.

On basis of the intelligence collection information layers can be produced which are integrated with threat evaluation results to produce IPE products.

### 2.2.1 NLMOD operational workflows: status of use of satellite data

Within the framework of the Milspace WP1 on GeoInt a number of interviews had been held on the current use by the Netherlands MOD (Military of Defence) of satellite data for intelligence purposes. We report here on this topic following the phases in intelligence cycle.

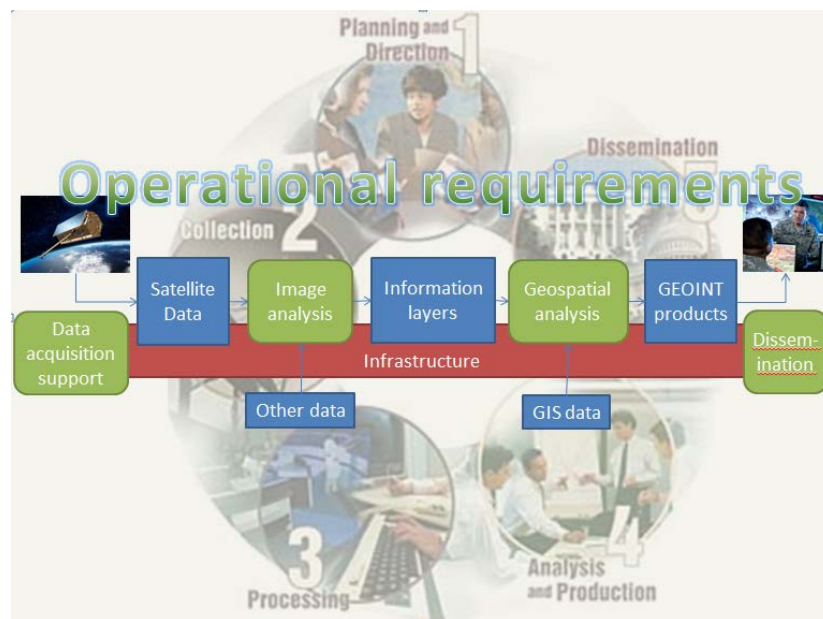


Figure 2 Intelligence cycle in the background, with the main topics of the GeoInt test bed in overlay.

#### Planning & direction

The various MOD departments themselves decide whether they need satellite imagery. Sometimes the need is initiated on individual basis by an employee who has expertise in satellite imagery. Departments which have requested imagery are e.g. the intelligence service, the school for intelligence, military engineers, special forces and the military geographical office.

#### Collection

The MOD itself does not have direct contact with satellite operators. They buy data from local (Dutch) resellers (e.g. Geoserve). The latter company is screened for working with classified data.

### CLASSIFICATION: UNCLASSIFIED

All rights reserved. No part of this document may be reproduced or transmitted in any form or by any means, electronic, mechanical, photocopying, recording, or otherwise, without prior written permission of FFI, NLR or TNO.

In principle the data are collected by the military geographical office (Milgeo). They have a front office which collects the requests. They can give advice with respect to the request and they contact the reseller for acquisition and store the data upon reception in the so-called data warehouse, before it will be distributed within the MOD. If possible the reseller organizes the geo-registration. In some cases geo-registration can be done by the Milgeo office.

Most of the requested data comprise single high resolution imagery. Sometimes also existing and freely available lower resolution imagery (Landsat, Aster & Blue Marble) is used, e.g. for C2 systems as background pictures. Radar data is not yet used by the Netherlands MOD, but is possible in the future when these data become more available (F35, Male UAV, etc.).

The military intelligence service also collects data independently from the Milgeo office, since some of the intelligence topics are classified. The main task of the Intelligence service is to produce intelligence. Deploying scarce human and financial sources to 'ordinary' requests for data & maps does not fall within the service's description. If the data are not classified it should also be stored in the Milgeo data warehouse for other users.

The Navy collects data through the Hydrographic office. This office orders data through the local reseller. They share the data with the Milgeo office for storage in the data warehouse. In the near future the NLMOD (Netherlands MOD) geoportal is foreseen. In the first stage data can be found by searching through metadata. In a later stage data may be downloaded. Also classification levels are considered, so that classified data may be shared through this portal too.

### **Processing and analysis**

Mostly the images are inspected as a picture. For geotagging software such as Erdas and ESRI/ArcMap is used.

Military intelligence services are divided in a strategic and operational/tactical level. At the strategic level imagery and observations are translated into analysis reports and information is geo-tagged when possible. In this sense this intelligence service does not produce GeoInt, but rather applies geo-referenced intelligence fusion to produce geo-related intelligence. Sometimes information is vectorised so that it can be used for further geographical processing.

At the operational/tactical level imagery is processed into fused intelligence products and also geo-referenced GIS (Geographical Information System) products are produced. In this sense at the operational/tactical level the intelligence services are more focused on producing GeoInt.

## **CLASSIFICATION: UNCLASSIFIED**

*All rights reserved. No part of this document may be reproduced or transmitted in any form or by any means, electronic, mechanical, photocopying, recording, or otherwise, without prior written permission of FFI, NLR or TNO.*



Sometimes multispectral data is used by the school for military intelligence and the military engineers to extract surface properties. Within the MGCP project data are processed by the land registry office and are handled following the procedure for aero-cartography. No multispectral or radar data are used.

### **Production & dissemination**

Dissemination follows the standard links in the military network. Usual data formats (shape files, geotiff) are used. In cases of C2 systems compressed data formats (CADRG – Compressed ARC Digitized Raster Graphic) are used. The Milgeo office takes care for the conversion to such formats.

### **Remarks (conclusions)**

- Data are used on case by case basis. Often individual experts request for data and handle these themselves.
- Budgets are limited to buy data.
- Radar data is not (yet) used, but the expectation is that for the future radar data will become more important.

Change detection and the use of time series of satellite imagery to reveal patterns of life is not used. The topic to observe patterns of life (PoLs) is however identified by the Netherlands school of intelligence (DIVI) as an important but rather complex intelligence topic, which has not yet been standardized.

### **2.2.2 NOMOD operational workflows: FSGI**

In Norwegian context the common satellite- and geo-information centre (In Norwegian: “Felles Satellitt- og Geo-Informasjonscenter” = FSGI) is presented here.

### **Background**

- Many different commercial satellite images are available today.
- Too many systems and image types to cope with for an end user.

### **Solution**

- Establish a common national concept for ordering, archiving and processing of commercial satellite image products on a regular basis.

### **Advantages**

- One contact point for the end user:
  - Giving input to the FSGI system by using Request for Information (RFI).

## **CLASSIFICATION: UNCLASSIFIED**

*All rights reserved. No part of this document may be reproduced or transmitted in any form or by any means, electronic, mechanical, photocopying, recording, or otherwise, without prior written permission of FFI, NLR or TNO.*

- Short response time (hours/days).
- Output through data/product reception.
- Easier to share the products (open source) with others.
- One contact point towards the commercial market:
  - Establish good contracts based on foreseen volume and product needs.
  - Asking for and ordering new satellite image acquisitions.
  - Ordering satellite images from archive.
- One node for satellite image products generation:
  - A more effective use of standard, but expensive state-of-the-art hardware and software solutions.
  - Incorporating routines for high level data handling and management.
  - Fusing data from satellite images and existing geo-information systems.
  - Enabling re-use of satellite image data for different end users.
  - Maintaining a high degree of readiness through daily/weekly throughput.
- One node for distributing data and products to the end users.

### **The FSGI concept**

In figure 3 the FSGI concept is depicted. The FSGI stands for the common satellite- and geo-information centre.

## **CLASSIFICATION: UNCLASSIFIED**

*All rights reserved. No part of this document may be reproduced or transmitted in any form or by any means, electronic, mechanical, photocopying, recording, or otherwise, without prior written permission of FFI, NLR or TNO.*

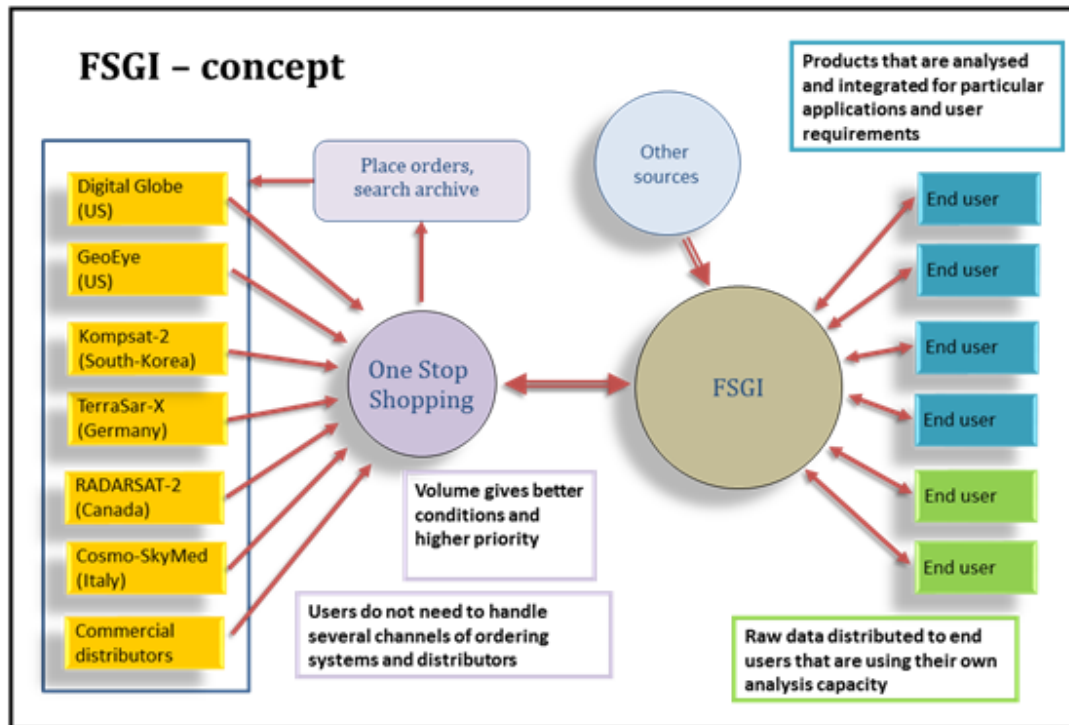


Figure 3 A general overview of the FSGI concept.

An overview of the FSGI (The common satellite- and geo-information centre) concept with specific entities plotted into the various blocks is given in the figure 4. Here, FMGT is the Norwegian Military Geographic Service, and KSAT is the company Kongsberg Satellite Services located in Tromsø, Norway. KSAT is the present (in year 2013) common node for ordering satellite data and downloading data, but other commercial firms do also exist in the European market.

**CLASSIFICATION: UNCLASSIFIED**

All rights reserved. No part of this document may be reproduced or transmitted in any form or by any means, electronic, mechanical, photocopying, recording, or otherwise, without prior written permission of FFI, NLR or TNO.

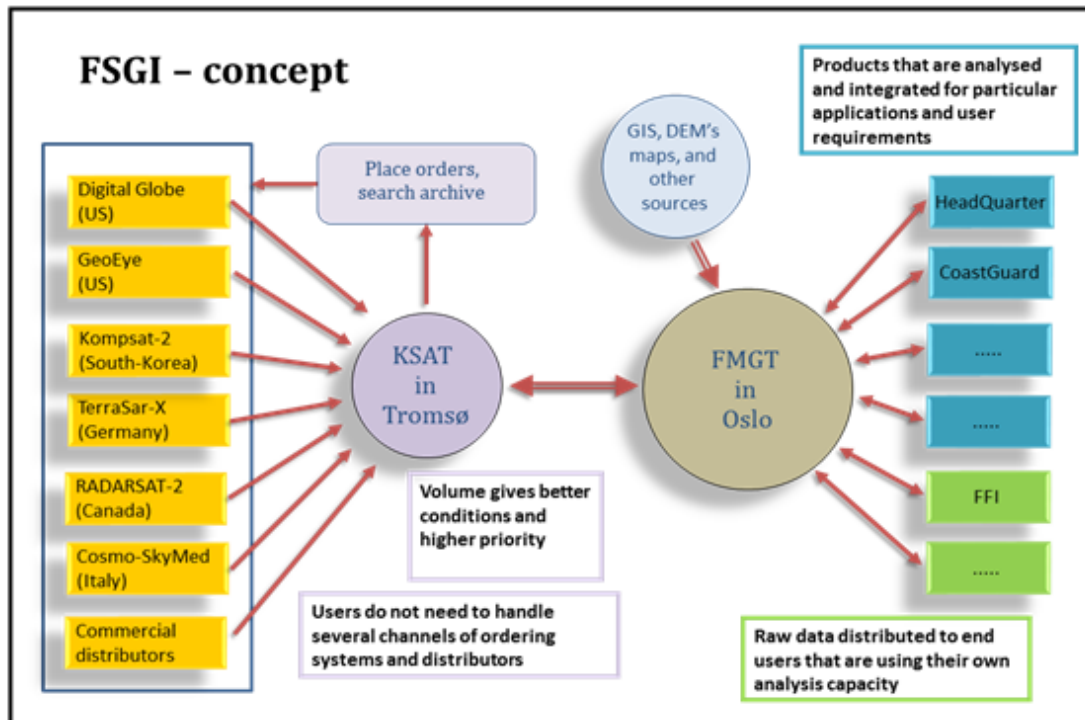


Figure 4 FSGI concept in more detail.

### Development of FSGI

An operational test carried out in 2011 used an initial version of the FSGI concept to order, distribute and analyse both optical and SAR satellite images. From that time onwards, the FSGI concept has been under constant development with updates and modifications from time to time. FSGI is in use today.

### FSGI processing tools

- Secure WS FTP (File Transfer Protocol) Server
  - Download satellite data
- Erdas Imagine
  - Satellite image analysis and satellite map generation
- Remote View
  - Satellite image analysis and GeoInt report generation
- MEOS (Multi-Mission Earth Observation System) developed by Kongsberg Spacetec AS
  - A system for scheduling, receiving and achieving optical and SAR satellite image data
- MEOS MissionPlanner (Kongsberg Spacetec AS)
  - A tool for mission planning of optical and SAR satellite images
- Aegir (FFI-developed software)

### **CLASSIFICATION: UNCLASSIFIED**

All rights reserved. No part of this document may be reproduced or transmitted in any form or by any means, electronic, mechanical, photocopying, recording, or otherwise, without prior written permission of FFI, NLR or TNO.

- Analysis of satellite SAR images for maritime applications
- Erdas Apollo
  - Distribution of satellite images and analysis results over low bandwidth communication lines
  - Establish a Geo Data Manager for the satellite image database
- SOCET GXP
  - Image analysis and management

### **FSGI products**

- Raw data
- Georeferenced satellite images
- Satellite image maps
- Topographic maps
- Digital Elevation Models (DEMs)
- Analysis reports

### **Restrictions on data distribution**

- The commercial satellite images are normally unclassified upon arrival
- Developed products can be tailored to the individual end user:
  - Data and information that are added onto the unclassified satellite image, may lead to a higher classification level.
- Restrictions regarding follow-on distribution:
  - The license agreement from the satellite image operator may lead to some restrictions.
  - The value-added production may lead to certain restrictions.

## **2.3 Acquisition planning and data retrieval**

### **2.3.1 Acquisition planning tools**

For acquisition planning purposes predictions about the satellite overpasses and its observing footprint are to be made. This is done on basis of orbit prediction.

The MEOS software developed by Kongsberg Spacetec AS is a generic tool which allows acquisition prediction of satellites on basis of the orbit and satellite parameters. The satellite parameters can be configured so that a new satellite can be added. The goal of the MEOS software is to obtain a complete overview over possible satellite image acquisitions over a specific geographic location in time by using one single software tool. Today, there are several

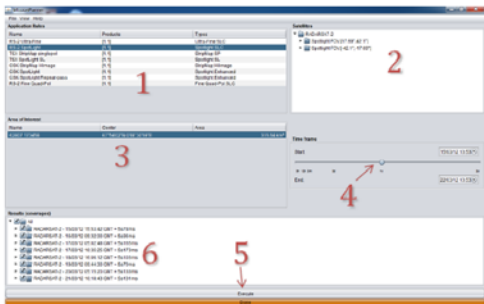
## **CLASSIFICATION: UNCLASSIFIED**

*All rights reserved. No part of this document may be reproduced or transmitted in any form or by any means, electronic, mechanical, photocopying, recording, or otherwise, without prior written permission of FFI, NLR or TNO.*

commercial satellite systems available, such as Quickbird, Ikonos, Worldview, RADARSAT-2, TerraSAR-X, TanDEM-X, COSMO-SkyMed, where the three first are optical and four last are SAR systems. However, most of them will require separate software tools for planning a set of data acquisitions over a region of interest. This is suboptimal for an end user who would like to know the overall acquisition possibilities from several sensors and SAR image providers. The mission planning tool (MEOS MissionPlanner™) incorporates the orbital parameters and acquisition modes for several of the satellite SAR platforms (and also optical image platforms) frequently in use today.

Tests with several case studies have shown the feasibility of the MEOS MissionPlanner™ and usefulness when it comes to choosing the most optimal image combination for a given application on land or at sea. This software tool will also enable the end user to be more flexible when it comes to the choice of satellite image providers, sensor, and mode. In the figures below a SAR planning case has been elaborated.

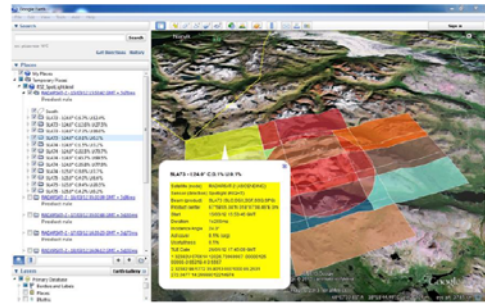
**2. Software tool**  
 Using the single tool MEOS MissionPlanner™ software from Kongsberg Spacetec AS, it is possible to obtain a complete overview of the foreseen SAR coverages over an area of interest given a fixed time-span of some days or weeks.



Graphic User Interface and workflow steps (1-6) for MEOS MissionPlanner™

It is also possible to program the tool in an expert mode:

- to obtain the best configuration for repeat-pass change detection
- adapt to upcoming stereo SAR events
- investigate future interferometric SAR acquisitions



Example of MEOS MissionPlanner™ results viewed in Google Earth®.

Figure 5 The MEOS software tool and user interface.

**CLASSIFICATION: UNCLASSIFIED**

All rights reserved. No part of this document may be reproduced or transmitted in any form or by any means, electronic, mechanical, photocopying, recording, or otherwise, without prior written permission of FFI, NLR or TNO.



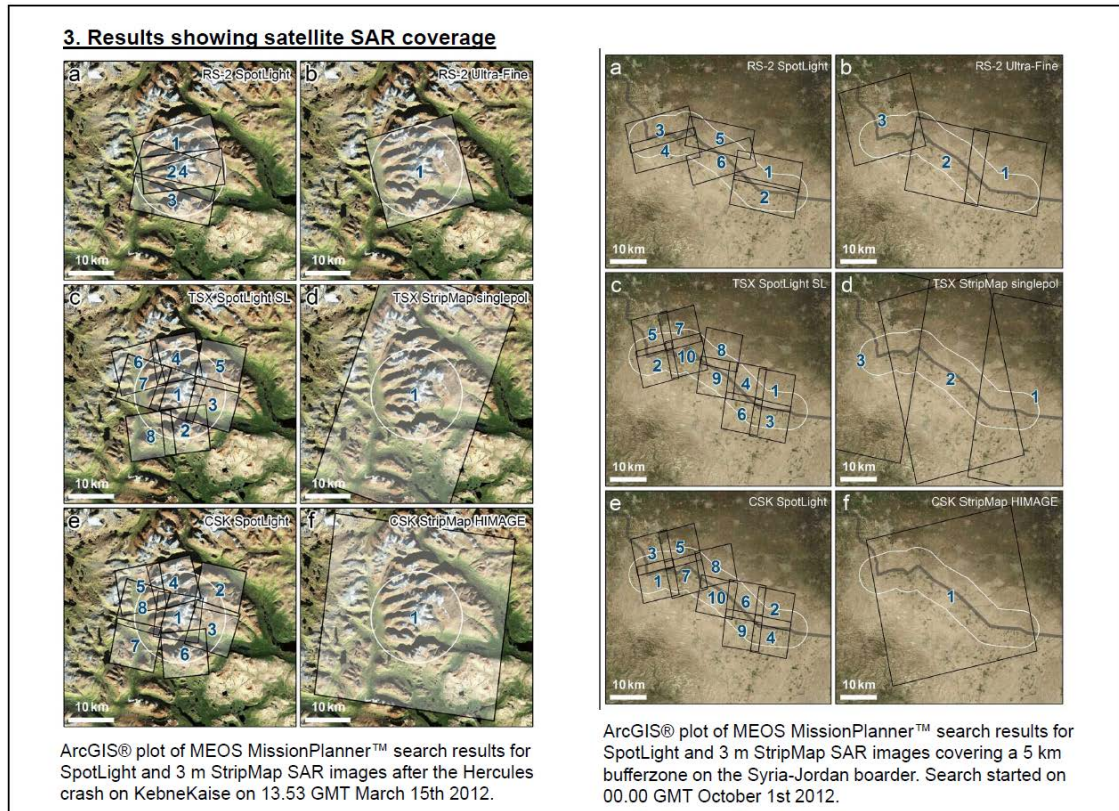


Figure 6 Results from a SAR planning exercise using MEOS

### 2.3.2 Open source data retrieval and portals

Satellite data which have been collected can be found in archives. These archives can be searched online using the so-called geoportals. There are various portals like that, usually related to dealers which sell the data. Open source catalogues are provided by the German Aerospace Center (DLR) (EOWEB – Earth Observation Web), European Space Agency (ESA) (Sentinel data hub) and US Geological Survey (USGS) (Landsat). Some of the web addresses are listed here:

- EOLI-SA (<https://earth.esa.int/web/guest/home>)
- EOWEB (<https://geoservice.dlr.de/egp/>)
- EarthExplorer (<https://earthexplorer.usgs.gov/>)
- ESA scientific Data Hub (<https://scihub.copernicus.eu/>)

Most of these open source geoportals allow download of free data, for example Landsat and Sentinel data.

## CLASSIFICATION: UNCLASSIFIED

All rights reserved. No part of this document may be reproduced or transmitted in any form or by any means, electronic, mechanical, photocopying, recording, or otherwise, without prior written permission of FFI, NLR or TNO.

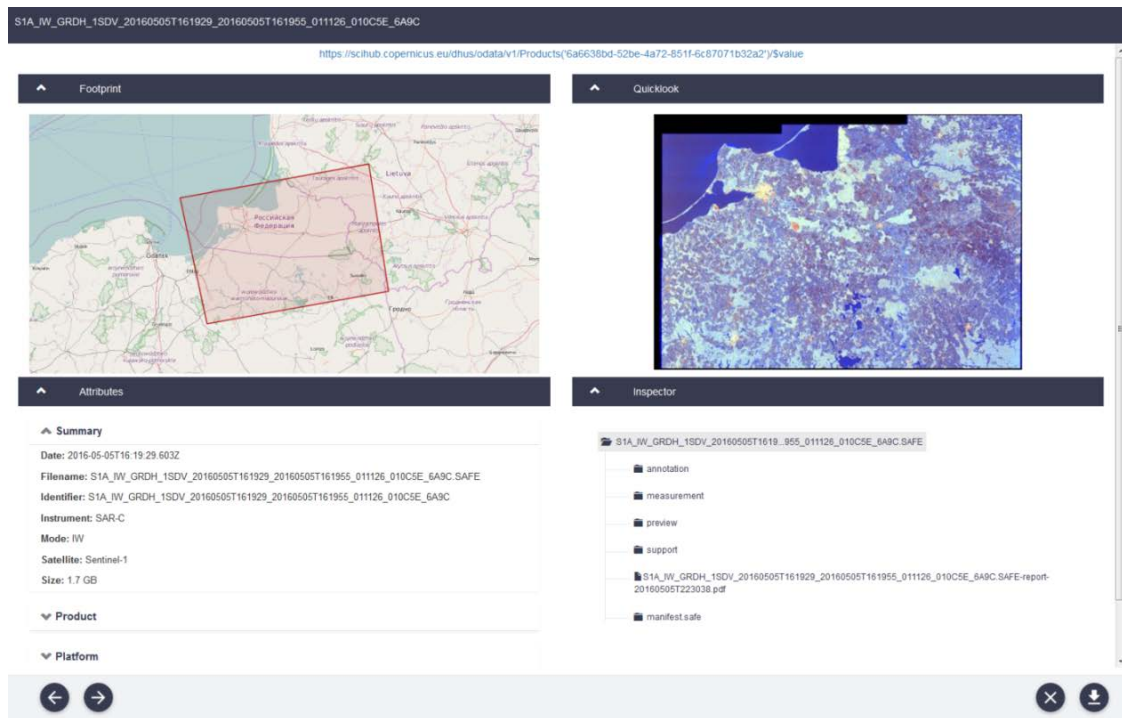


Figure 7 Search results for the ESA scientific data hub for Sentinel-1A over Kaliningrad.

Currently some 125 earth observation satellites are orbiting our globe taking a variety of daily recordings. An increasing number of countries are active in the manufacturing and launch of earth observation satellites and in the dissemination of resulting imagery; in particular USA, Europe, Russia, India, China and several South East Asian countries. A rough division can be made between the geostationary satellites that are at a height of about 36.000 km above the Earth, of lower resolution and specifically tasked for meteorological purposes and the polar-orbiting satellites that are at a height of about 600-700 km of higher resolution and aimed at detection of Earth details and processes. All types of data can be of interest for military information requirements. In this study the emphasis is on the polar orbiting satellites and then especially the ones that generate medium- to high resolutions of 5-50 metres to 0.25-5 metres respectively. All the above mentioned countries launch these types of satellites but the availability of the data differs per country. On the one end are for example USA and European countries that make satellite data broadly available for general use while on the farthest other end are countries like Russia and China that hardly reveal anything about launch and use of their satellites. As for the common available medium- and high resolution satellites some general tendencies can be recognised:

- Satellites are manufactured and launched as part of a satellite programme following a planned schedule which ensures continuity and improvement of recording quality. The Landsat, SPOT and ERS/ENVISAT/Sentinel programmes are examples of this approach.

### **CLASSIFICATION: UNCLASSIFIED**

All rights reserved. No part of this document may be reproduced or transmitted in any form or by any means, electronic, mechanical, photocopying, recording, or otherwise, without prior written permission of FFI, NLR or TNO.



- The number of spectral bands and radiometric resolution, recording detail (spatial resolution) and flexibility in timely recording and dissemination (temporal resolution) improves constantly.
- Medium resolution data of the bigger programmes are becoming available for free, which opens an enormous reservoir of historic and actual data and enables new ways of using the information. Landsat and Sentinel data in the resolution range of 10 to 30 metres is free of cost nowadays.
- There is a growth in satellite constellations, bigger numbers of (small) satellites that are manufactured and launched simultaneously, dedicated to the same task and each taking care of a part of that task. Further information about these developments can be found in paragraph 2.4.

At a national Dutch level, during the past four years, a selection of satellite data covering The Netherlands has been made available for free by the Dutch Government (NSO, National Space Organisation). During these years the Dutch user community could make use of optical medium and high resolution data (DMC (Disaster Monitoring Constellation), SPOT and Formosat) and radar data (Radarsat). This in preparation to the arrival of freely available Sentinel radar and optical imagery. The data was provided to the Dutch users by making use of the existing dissemination system of the Astrium consortium (nowadays EADS, European Aeronautic Defense and Space company), the DataDoors electronic catalogue.

In general satellite data is made available via electronic catalogues, also called data hubs, in which users can search, select and download data. Dozens of electronic catalogues exist, varying from very well accessible and to a great extent automated to difficult accessibility and demanding more traditional communication. The open satellite data from the Landsat satellites are made available in the USGS Global Visualization Viewer (amongst others) and the data of Sentinel missions are accessible through the ESA Sentinel scientific data hub. See Figure 8 with left and right the appearances of USGS and ESA catalogues.

## **CLASSIFICATION: UNCLASSIFIED**

*All rights reserved. No part of this document may be reproduced or transmitted in any form or by any means, electronic, mechanical, photocopying, recording, or otherwise, without prior written permission of FFI, NLR or TNO.*

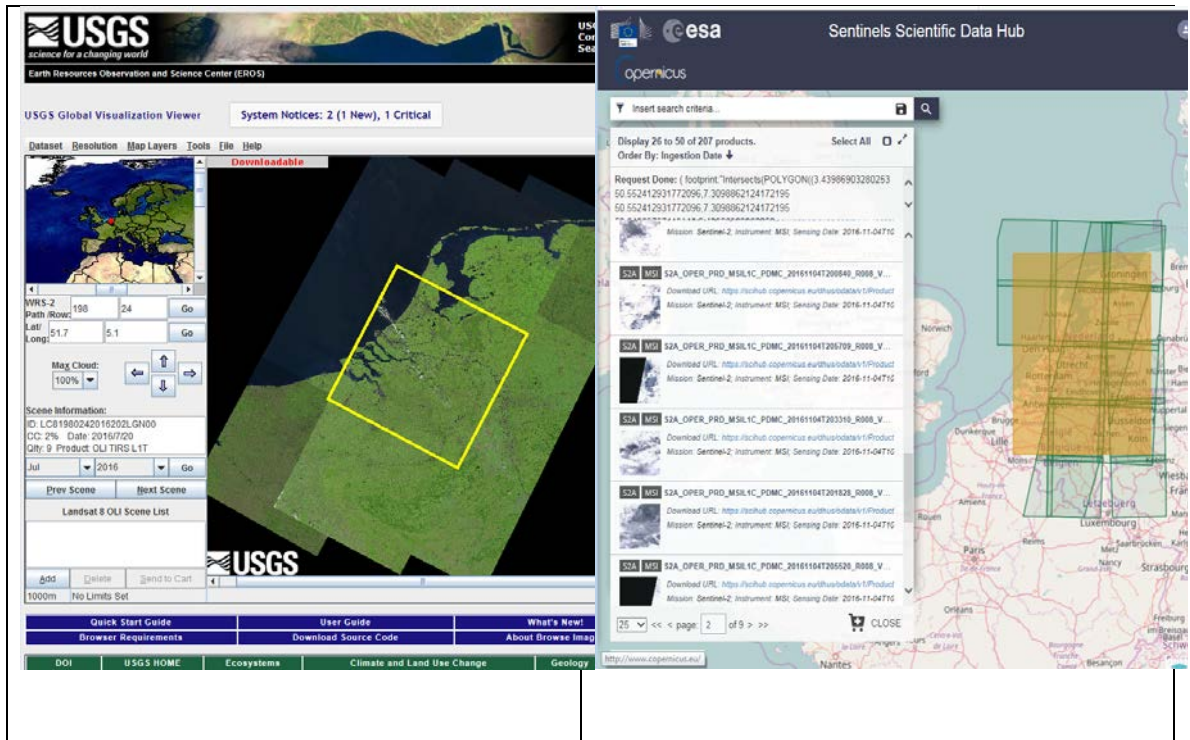


Figure 8. Portals of USGS (left) and ESA (right) for access to Landsat and Sentinel satellite data

Most catalogues offer search filters like acquisition period and geographic area of interest, selection and download instructions. Initiatives are undertaken to select recordings fully automated, based on predefined criteria (area of interest, time-period, cloud cover limits and so on).

Apart from the freely available medium resolution imagery, high resolution imagery in the resolution range from 0.25 to 5 meters is also readily accessible albeit on payment. Important suppliers of high resolution data are Digital Globe (WorldView, Quickbird), SpotImage (SPOT, Formosat, Pleiades) and ISRO (Cartosat). The suppliers of high resolution imagery can be contacted directly or else the help from a national data broker (advise and order support) can be called upon. Regular common pricing and ordering conditions for high resolution imagery are about €20/km<sup>2</sup> and minimum order of areas of 100 km<sup>2</sup>. There are numerous additional conditions.

## 2.4 Data description

Most satellites, especially the radar satellites have various modes allowing high resolution data as spotlight imagery or lower resolution wide area imagery. Obviously the higher the resolution,

### **CLASSIFICATION: UNCLASSIFIED**

All rights reserved. No part of this document may be reproduced or transmitted in any form or by any means, electronic, mechanical, photocopying, recording, or otherwise, without prior written permission of FFI, NLR or TNO.

the smaller the area imaged. Also when more optical/infrared spectral bands or polarisations (radar) are used the resolution is generally lower than for one band (PAN).

An overview is given of past, current and future optical earth observing satellites. A main division, in two separate tables, is made between the medium resolution open satellite data (5-50 meters) and the commercial available high resolution satellite data (0.25-5 meters). Therefore, the first table (Table 1) is a selection of satellites providing data free of cost (obviously there are many more medium resolution satellites) and the second table (Table 2) is an extensive overview of all high resolution satellites. Gray fields in the table indicate satellites that are expired (but still of interest because of historic archives), white fields are currently operated satellites and green fields indicate future satellites. In the tables the numbers between brackets in the MS (Multispectral) column mean the number of spectral bands.

Almost all optical high resolution earth observation satellites carry a panchromatic camera together with a multispectral camera. The panchromatic wavelength range is broader than the multispectral ranges resulting in a stronger amount of reflection per area unit which subsequently results in a higher resolution. Panchromatic bands are often a factor 2 to 4 sharper in detail compared to the multispectral bands (MS).

Multispectral bands of the newer earth observation satellites show a trend to become greater in number and smaller in range. For example, the number of Landsat spectral bands has increased from 6 to 8 and the number of Sentinel spectral bands has increased even further to 13. Some of these bands are aimed at observation of specific earth objects, like the reflection characteristics of vegetation and minerals, and are smaller in spectral range. Some of the Sentinel spectral bands are comparable to the Landsat spectral bands, like the visible bands and the near infrared. Sentinel spectral bands can also differ in spatial resolution; 10 meter resolution for the 4 bands in the visible- and near-infrared part, 20 meter resolution for 6 near- and mid-infrared spectral bands and 60 meter resolution for 3 spectral bands (UV (Ultraviolet) and mid-infrared).

DMC is in this table because these data have been temporary available free of cost, thanks to the 4 years arrangement from the Dutch Government/NSO. The number of spectral bands of DMC is limited: only visible green, visible red and near-infrared, which is the traditional spectral band combination for construction of false colour imagery.

## **CLASSIFICATION: UNCLASSIFIED**

*All rights reserved. No part of this document may be reproduced or transmitted in any form or by any means, electronic, mechanical, photocopying, recording, or otherwise, without prior written permission of FFI, NLR or TNO.*

Table 1 Medium resolution satellites that provide open data.

Satellite	Launch date	Country	PAN (m)	MS (m)	SAR (m)	Swath (km)
DMC Deimos-1	20090729	Spain		22 (3)		600
UK-DMC-2	20090729	UK		22 (3)		600
Landsat 4	19820716	USA		30 (6)		185
Landsat 5	19840301	USA		30 (6)		185
Landsat 7	19990415	USA	15	30 (6)		185
Landsat 8	20130211	USA	15	30 (8)		185
Sentinel 1A	20140403	Europe			4-80	80-400
Sentinel 1B	20160425	Europe			4-80	80-400
Sentinel 2A	20150623	Europe		10-20-60 (13)		290
Sentinel 2B	Apr2017	Europe		10-20-60 (13)		290

**CLASSIFICATION: UNCLASSIFIED**

All rights reserved. No part of this document may be reproduced or transmitted in any form or by any means, electronic, mechanical, photocopying, recording, or otherwise, without prior written permission of FFI, NLR or TNO.

Table 2 High resolution satellites.

Satellite	Launch date	Country	PAN (m)	MS (m)	SAR (m)	Swath (km)
<a href="#">Cartosat-2 (IRS P7)</a>	20070110	India	0.8			9.6
<a href="#">Cartosat 2A</a>	20080428	India	0.8			9.6
<a href="#">Cartosat-2C</a>	20140731	India	0.65	2 (4)		10
<a href="#">Cartosat-2E</a>	2017-jul	India	0.65	2 (4)		10
<a href="#">Cartosat-3</a>	2018	India	0.25	1 (2)		16
<a href="#">Cartosat-3A</a>	2019	India	0.25	1		16
<a href="#">Cartosat-3B</a>	2019	India	0.25	1		16
<a href="#">COSMO SkyMed CSG-1</a>	2016-dec	Italy			0.8	10
<a href="#">COSMO SkyMed CSG-2</a>	2017-dec	Italy			0.8	10
<a href="#">EROS B</a>	20060425	Israel+USA	0.7			13.5
<a href="#">EROS C</a>	2009	Israel+USA	0.5	2		12
<a href="#">Gaofen-2</a>	20140819	China	0.8	3.2 (4)		45
<a href="#">GeoEye-1 (Orbview-5)</a>	20080906	USA	0.46	1.84 (4)		15.2
<a href="#">Ikonos 2</a>	19990924	USA	1	4 (4)		13
<a href="#">KazEOSat-1</a>	20140430	Kazachstan	1	4 (4)		20
<a href="#">KOMPSAT-3</a>	20120517	Korea	0.7	2.8 (4)		15
<a href="#">KOMPSAT-3A</a>	20150325	Korea	0.55	2.2 (4)		12
<a href="#">Pleiades-1A</a>	20111216	France	0.5	2 (4)		20
<a href="#">Pleiades-1B</a>	20121202	France	0.5	2 (4)		20
<a href="#">Quickbird 2</a>	20011018	USA	0.61	2.44 (4)		16.5
<a href="#">Resurs-P N1</a>	20130625	Russia	1	3 (5)		38
<a href="#">Resurs-P N2 t/m N5</a>	2016-2019	Russia	1	3 (5)		38
<a href="#">Resurs-PM N1</a>	2020	Russia	0.4	1.6 (8)		19
<a href="#">Resurs-PM N2</a>	2021	Russia	0.4	1.6 (8)		19
<a href="#">Resurs-PM N3</a>	2023	Russia	0.4	1.6 (8)		19
<a href="#">Resurs-PM N4</a>	2024	Russia	0.4	1.6 (8)		19
<a href="#">SkySat-1</a>	20131121	USA	0.9	2 (4)		
<a href="#">SkySat-2</a>	20140708	USA	0.9	2 (4)		
<a href="#">TerraSAR-X</a>	20070615	Germany			0.25	
<a href="#">TripleSat</a>	20150710	India	0.8	3.2 (4)		23.8
<a href="#">WorldView-1</a>	20070918	USA	0.5			17.6
<a href="#">WorldView-2</a>	20091008	USA	0.46	1.84 (8)		16.4
<a href="#">WorldView-3</a>	20140813	USA	0.31	1.24 (8)		16.4
<a href="#">WorldView-4</a>	20160915	USA	0.31	1.24 (8)		13.1

**CLASSIFICATION: UNCLASSIFIED**

All rights reserved. No part of this document may be reproduced or transmitted in any form or by any means, electronic, mechanical, photocopying, recording, or otherwise, without prior written permission of FFI, NLR or TNO.

Special attention should be paid to the rise of the satellite constellations. These are usually a cluster of similar small satellites that are launched together and that orbit the Earth in a coordinated, sophisticated pattern so that areas of interest can be revisited as often as possible. The oldest satellite constellation is the Disaster Monitoring Constellation (DMC) that was manufactured by Surrey Satellite Technology Ltd, UK around 2003 and of which the first generation consisted of four small satellites that were funded and operated by four countries: Algeria, Nigeria, Turkey and UK. These satellites were used for retrieving quick information at several global disasters such as tsunamis, flooding, hurricanes and wildfires. The resolution of the imagery is 32 meters. The first generation DMC expired around 2011. The second generation DMC also consists of four satellites funded and operated by China, UK, Spain and Nigeria. These satellites are all still operational today, except for the Chinese satellite. The resolution of the second generation satellites is 22 meters. A third generation DMC constellation, called TripleSat was launched in 2015. These satellites provide higher resolution data (see Table 2). Newer satellite constellations involve Pleiades, Sentinel, COSMO-SkyMed, RapidEye).

By using multiple satellites in a well-chosen configuration the revisit time decreases. The revisit for a specific area can also be reduced by varying the incidence angle. However this hinders change detection since the imaging geometry is different.

Recently much larger satellite constellations are in development. One example of this is the initiative of the Google company that is supporting a service provided by Terra Bella (formerly Skybox Imaging) focusing on high-resolution Earth observation satellite imagery combined with high-definition video from space. The spatial resolution is in the order of one meter and the satellites are based on the SmallSat concept so that an extensive constellation is possible. This allows high-resolution satellite imagery of any place on Earth multiple times a day. Momentarily (autumn 2016) SkySAT 1-7 are in orbit. Other examples of large satellite constellations are Planet Lab (60 sun synchronous optical satellites with 3 meters resolution to be launched in 2017), Blacksky (6 satellites with 1 meter resolution in preparation with 60 other satellites planned) and Satellogic (large constellation of 2 meters spatial resolution satellites planned).

Some examples are shown below for the oil terminal area in Rotterdam harbour for Formosat (2 meter), Digitalglobe imagery (extracted from GE, about 1 meter), Sentinel strip map (5 meter) and TerraSAR ST imagery (about 1 meter).

## **CLASSIFICATION: UNCLASSIFIED**

*All rights reserved. No part of this document may be reproduced or transmitted in any form or by any means, electronic, mechanical, photocopying, recording, or otherwise, without prior written permission of FFI, NLR or TNO.*



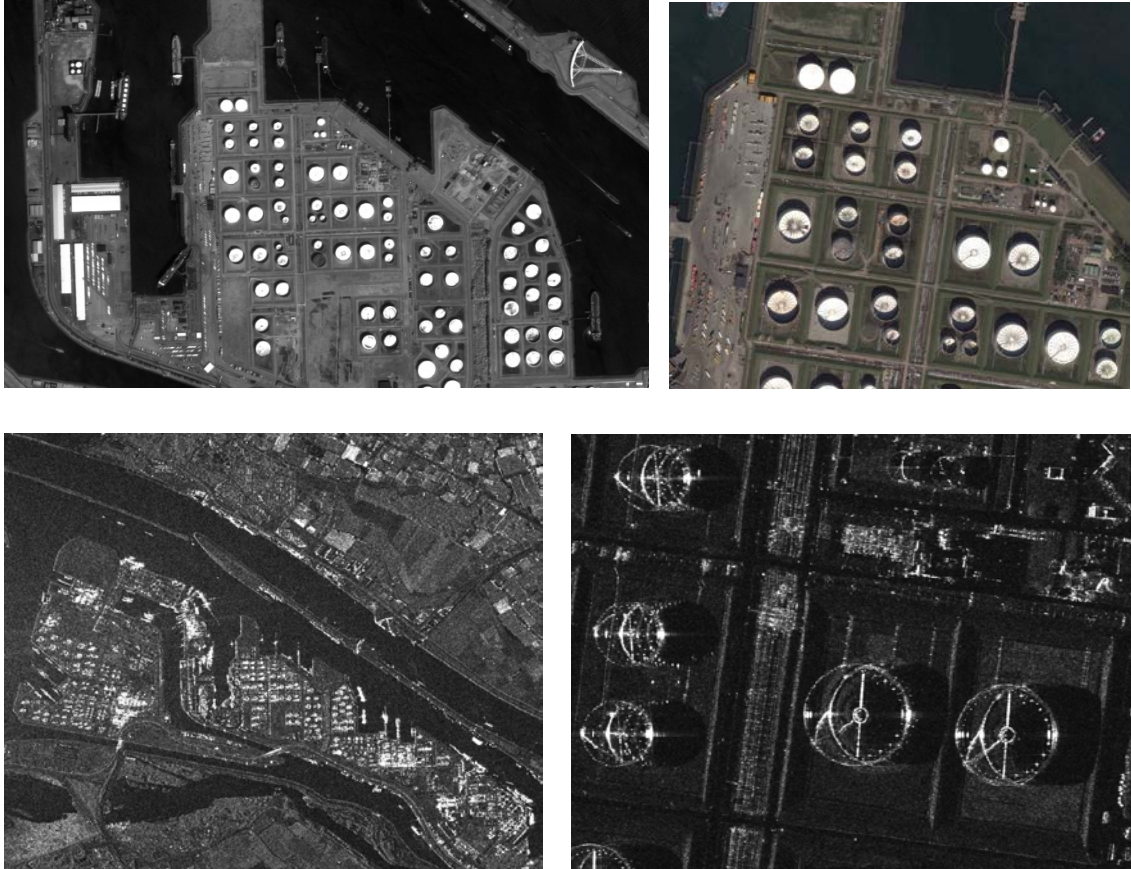


Figure 9 Comparison of satellite examples for Rotterdam harbour. Left to right: Formosat, Digital globe (GE) (top), Sentinel SM, TerraSAR ST (bottom).

### 3 Geospatial information extraction

#### 3.1 Introduction

In this chapter a number of data analysis techniques for extracting the required military information from the open source satellite data are described. The focus is on change detection and in particular the changes from time series (multi-temporal change detection). First techniques for optical data are described, where also the benefit of multispectral data in this context is discussed. Secondly techniques for SAR data are described, which also allows coherent change detection that can reveal changes that are otherwise not observable. The last part focuses on ship detection with SAR data and the role of polarimetry for the suppression of sea clutter to improve the sensitivity of ship detection.

#### **CLASSIFICATION: UNCLASSIFIED**

All rights reserved. No part of this document may be reproduced or transmitted in any form or by any means, electronic, mechanical, photocopying, recording, or otherwise, without prior written permission of FFI, NLR or TNO.

## 3.2 Optical methods

### 3.2.1 Optical satellite image time series

For the optical image extraction activities NLR (National Aerospace Laboratory) concentrated on the analysis of satellite image time series (SITS). First some information will be given on the availability and usability of satellite image time series.

The availability of extensive image time series for an area of interest increases. Reasons for this are the increasing number of commercial and military observation satellites, with increasing quality and lower costs. At the same time the archives of historic images are opened up and the technology for fast access, transfer and processing of the images is developing. Especially for medium resolution governmental satellites like Landsat and Sentinel the databases of historic and actual images are made available for free, which gives access to series of 30 years of optical observations.

As a consequence new analysis strategies and methods can be applied. The focus is no longer on one or a very limited number of observations from a specific area, but instead using extensive time series of satellite images from larger areas during longer periods acquired by multiple systems. For this the term SITS (Satellite Image Time Series) is used. Using these time series the analysis can focus on the identification of temporal and spatial trends and patterns and the detection of anomalies with respect to these. In this way surveillance of larger areas can be performed over time, generating triggers of specific locations or moments where further detailed analysis can take place.

Looking at satellite image time series different parameters are of importance. First the temporal dimension, which can be subdivided into the period over which the monitoring/observations take place and into the temporal frequency at which the observations are taken. The period can vary from year/season to a month/week/day to hour/minute and the temporal frequency from months to weeks to minutes or seconds. Secondly the spatial dimension, which can be subdivided into the size of the area that is observed and the spatial scale with which it is observed. The size can vary from the whole world or a large region, to a country or province, to a city or harbour, down to a specific street or building. The spatial resolutions may vary from 100 m up to 20 cm.

The temporal and spatial variation can be structured in main categories so that a matrix is obtained. For the most relevant combinations examples of applications are given, see Figure 10. For the Milspace project the focus has been laid on the medium resolution imagery of 10-20 m

## **CLASSIFICATION: UNCLASSIFIED**

*All rights reserved. No part of this document may be reproduced or transmitted in any form or by any means, electronic, mechanical, photocopying, recording, or otherwise, without prior written permission of FFI, NLR or TNO.*



spatial detail and observation frequencies in the order of 2 weeks over a one year period. In the Milspace project the focus was laid on the processing of medium resolution imagery of the DMC, Landsat and Sentinel 2 satellites.

Area (detail)	Period (freq)	Year/season (weeks-days)	Month/week/day (days-hours)	Hour/min (min-sec)
World/region (100m)		climate zones deforestation	flooding wildfire	
Country/province (20m)		infrastructure geography	infrastructure agriculture, crops snow/ice coverage flooding, wildfire night time lights	calamities like flooding, wildfire
City/harbour (2m)			infrastructure, raw materials, containers water resources pattern of life, cars, ships damage	pattern of life, cars, ships, damage
Building/street (0.3m)				persons, cars, objects

Figure 10. Applications for different scales of temporal and spatial observation.

### 3.2.2 Optical analysis methods

For the proper analysis of SITS several processing steps need to be taken into account, as shown in Figure 11. First the images need to be pre-processed, involving the geometric and radiometric calibration of the images. This is essential for the proper relation of the observations to each other.

**CLASSIFICATION: UNCLASSIFIED**

All rights reserved. No part of this document may be reproduced or transmitted in any form or by any means, electronic, mechanical, photocopying, recording, or otherwise, without prior written permission of FFI, NLR or TNO.

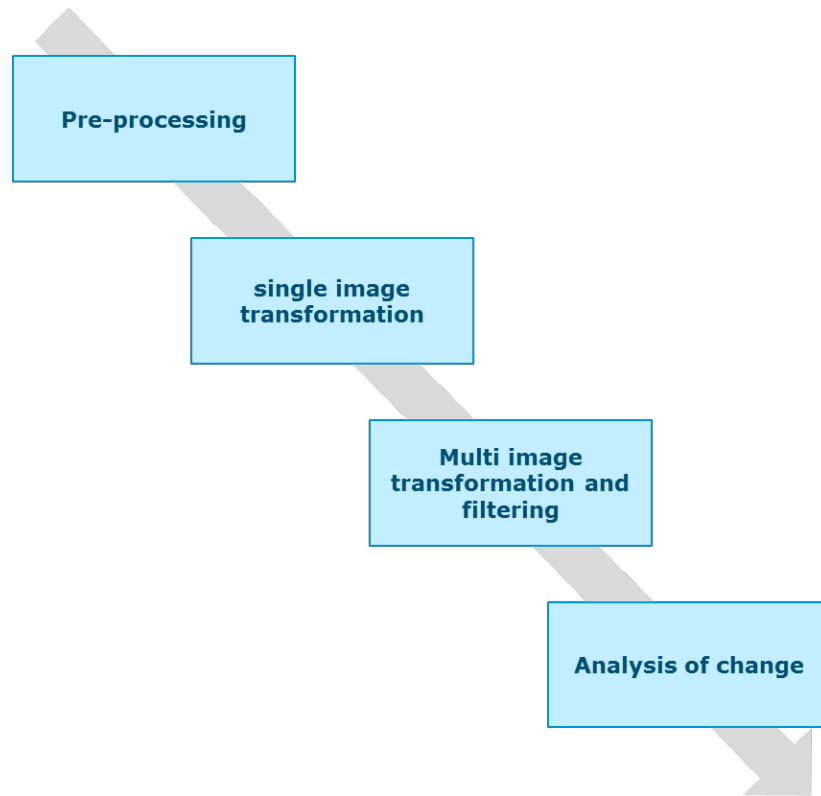


Figure 11. Overview of processing steps for satellite image series analysis

### 3.2.2.1 Pre-processing

#### Overview of methods

First the satellite imagery needs to be pre-processed in order to make proper relation of the observations to each other possible. This may involve the following activities:

- Accurate geometric registration.
- Radiometric calibration or normalization, also including atmospheric correction.
- Noise filtering: in spatial, temporal or frequency domain.

The calibration can be done absolute to physical quantities, after which observations can be related via the same standard reference and absolute parameters and thresholds can be applied. Calibration can also be done relatively, where the data within one dataset is corrected relatively to each other to form a consistent dataset. In this case only relative parameters and thresholds for the specific dataset can be applied.

## **CLASSIFICATION: UNCLASSIFIED**

*All rights reserved. No part of this document may be reproduced or transmitted in any form or by any means, electronic, mechanical, photocopying, recording, or otherwise, without prior written permission of FFI, NLR or TNO.*

### Selected methods

#### *Automated geo-referencing of DMC images*

In the project for a set of DMC satellite images an automated geometric correction procedure was investigated. The geo-referencing accuracy of the DMC images as supplied by the receiving ground stations is rather limited and shows deviations in the order of up to 2 km. For the automatic geo-correction the Keystone system (version 3.6) of Spacemetric was used. With the system a hierarchic approach could be configured where for a defined grid of points of the DMC image corresponding points were searched in a 15 m spatial resolution panchromatic Landsat reference image using image correlation techniques. After some experimentation an approach was used, starting from coarse pixels of 640 m and ending after four steps at the actual resolution of 22 m. In most cases in the order of 700 correlating points were found and based on that the model parameters of the camera and satellite orbit model were adjusted, after which the image was resampled. In most cases the resulting overall planimetric root mean square (RMS) value was in the order of 10 m. In 85% of the cases the automatic correlation process was successful, in the other cases first a number of manual control points needed to be digitized for the first iteration. In Figure 12 a corrected DMC image is shown, projected over the reference Landsat image, the purple arrows show the relative errors at each tie-point (extent and direction of desired correction).

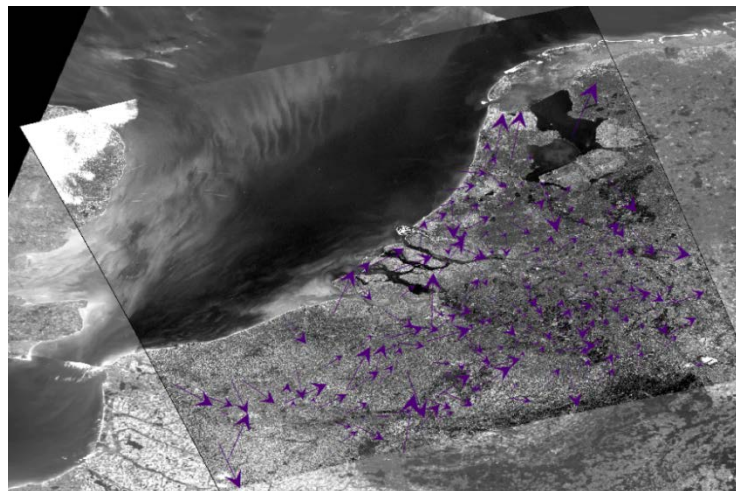


Figure 12. Found tie-points between Landsat and DMC image and the relative deviations.

#### *Landsat radiometric and atmospheric correction*

For the correction of Landsat a spatial model was developed in the Erdas environment. The spatial model combines the formula for the conversion to bottom of atmosphere (BOA) radiances (L) to reflections with the correction for the atmospheric path based on the darkest pixel method.

### **CLASSIFICATION: UNCLASSIFIED**

All rights reserved. No part of this document may be reproduced or transmitted in any form or by any means, electronic, mechanical, photocopying, recording, or otherwise, without prior written permission of FFI, NLR or TNO.

$$L = (DN-DP) * \text{gain} + \text{offset}$$

$$\rho = \pi * d^2 * L / E_o * \cos\theta$$

L = radiance

DN = Digital Number

DP = Darkest Pixel

$\sigma$  = reflection value

d = distance Sun – Earth

E = exoatmospheric irradiance

$\theta$  = zenith angle Sun

With the model the meta information on gain and offset values is read from the file header, besides additional parameters on sun angle, irradiation and distance. Information on darkest pixels can be provided manually or obtained from the image statistics. The same methodology was applied for the DMC images and can also be applied to the Sentinel images. The result of the radiometric and atmospheric correction is shown in figure 13.

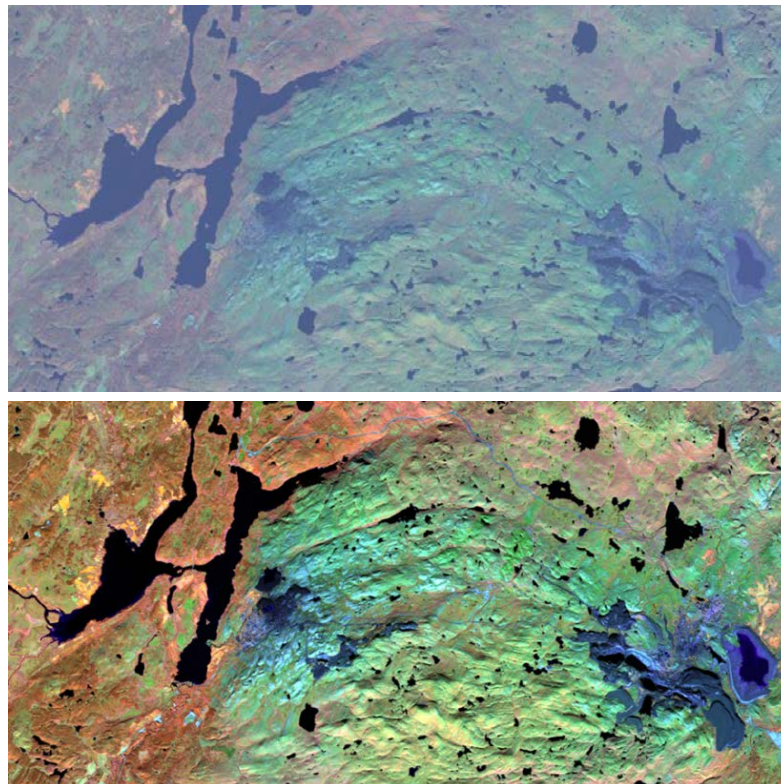


Figure 13. Landsat image before (top) and after (bottom) radiometric and atmospheric correction.

### **CLASSIFICATION: UNCLASSIFIED**

All rights reserved. No part of this document may be reproduced or transmitted in any form or by any means, electronic, mechanical, photocopying, recording, or otherwise, without prior written permission of FFI, NLR or TNO.

### 3.2.2.2 Single image transformations

#### Overview of methods

Individual images may be converted to specific geophysical or mathematical parameters (half products) that are suited for further spatio-temporal analysis, more than the raw image spectrum. The half products may eliminate (absolute) calibration inaccuracies, reduce data dimensions or highlight differences between the observations. Examples are:

- Conversion to uncorrelated variables: PCA (Principal Component Analysis), MNF (Minimum Noise Fraction)
- Derivation of indices for e.g. vegetation, water, materials: NDVI (Normalized Difference Vegetation Index), LAI (Left Area Index), Tasseled Cap, NDWI (Normalized Difference Water Index)
- Derivation of specific parameters, like temperature
- Spectral pre-classification into main classes
- Derivation of geospatial attributes, like texture values.

#### Selected methods

##### *Spectral pre-classification*

For the Nikel Landsat dataset a spectral classification method was applied for translating of a single Landsat image to a number of land use classes. The idea is that this methodology can be applied to all images of the time series, so that the changes can be detected at land cover class level and not at spectral level. For the spectral classification use was made of the Erdas Knowledge Engineer, see figure 14. This is a tool in which a set of classification rules can be defined interactively, inspected and saved (left). The result can be applied on a complete set of images. To define the classification rules, an analysis was made of the spectral characteristics of different land cover types and materials and their behaviour over time (right-up). Also different indices were computed and integrated in the classification process (vegetation, moisture, iron). The resulting land cover classification is shown right down.

##### *Derivation of indices*

For the case of the analysis of the series of DMC images of the Rotterdam area a number of spectral and temporal parameters were derived for each pixel, such as average min and max values per spectral band over time, as well as the NDVI average. Furthermore on basis of the NDVI start and end, the duration of crop growth, and a number of harvesting times were derived. Based on these parameters, further classification and temporal analysis of the images could take place.

## **CLASSIFICATION: UNCLASSIFIED**

*All rights reserved. No part of this document may be reproduced or transmitted in any form or by any means, electronic, mechanical, photocopying, recording, or otherwise, without prior written permission of FFI, NLR or TNO.*



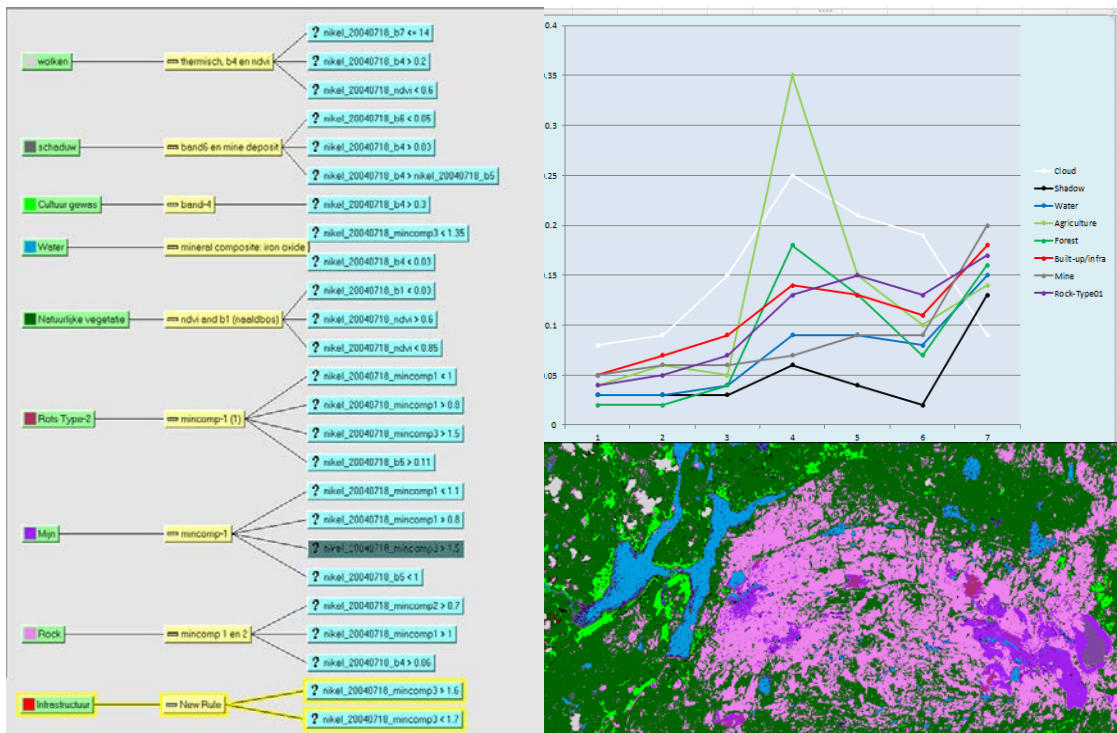


Figure 14. Image classification with Erdas Knowledge Engineer. Investigation of spectral characteristics (top right), application of classification rules (left), resulting classification (bottom right).

#### Derivation of specific parameters

For the analysis of anomalies in the ship intensity in the harbour of Rotterdam in a first step the number of ships were detected for each harbour sector. A ship detection routine was developed that detects ship pixels and clusters neighbouring pixels to ship clumps. The ship detection routine uses a land-water mask as input. The reflection level of the water is normalized by subtracting a low bandwidth filtered image from the original, after which a single threshold can be applied. These ships were classified in small and large ships. For each harbour sector the number of ships was counted for each image. Based on these ship intensity parameters an anomaly detection routine could be applied. See also figure 15 for detection of ship pixels and number of ships within harbour sectors.

### CLASSIFICATION: UNCLASSIFIED

All rights reserved. No part of this document may be reproduced or transmitted in any form or by any means, electronic, mechanical, photocopying, recording, or otherwise, without prior written permission of FFI, NLR or TNO.

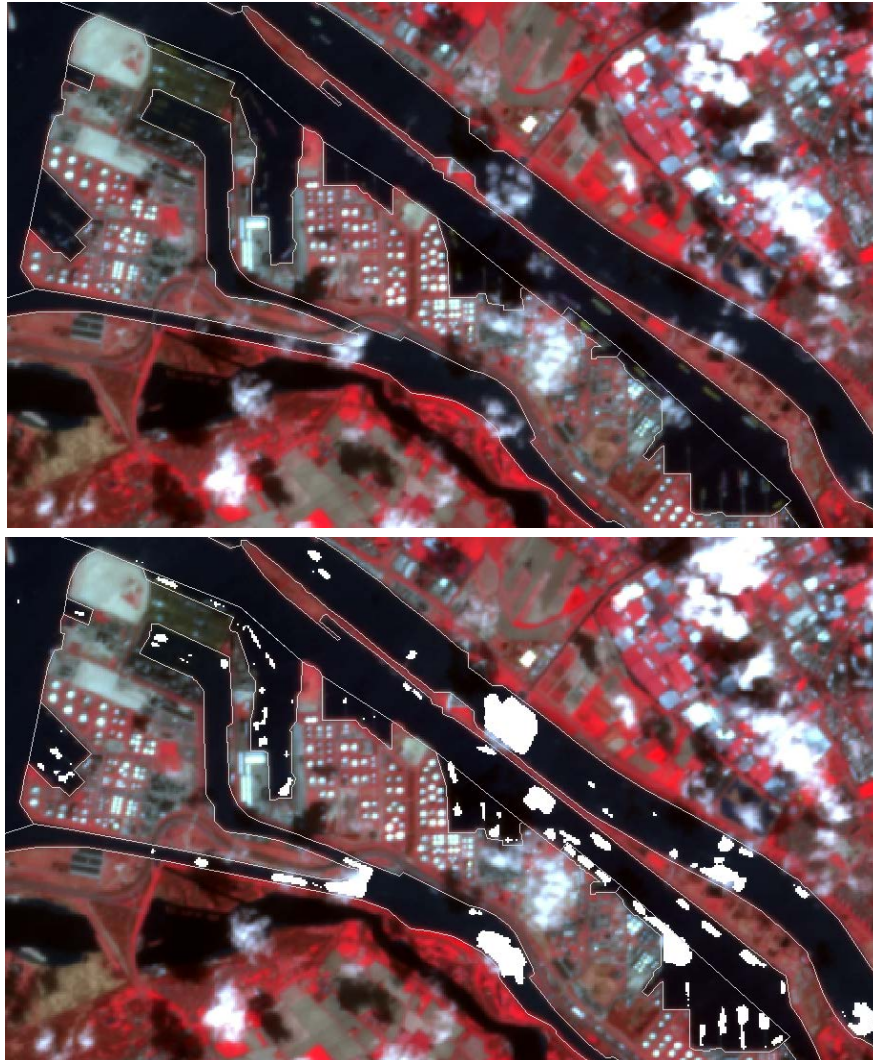


Figure 15. Detection of ship pixels and number of ships within harbour sectors.

### 3.2.3 Multi image transformation and filtering

#### Overview of methods

Transformation of the data may be applied in order to enhance the temporal, spatial and radiometric quality and consistency of the data series or make it better suited for further analysis:

- Aggregation: replace set of consecutive values by the mean value
- Data smoothing and outlier removal
- Gap filling for missing data

#### **CLASSIFICATION: UNCLASSIFIED**

All rights reserved. No part of this document may be reproduced or transmitted in any form or by any means, electronic, mechanical, photocopying, recording, or otherwise, without prior written permission of FFI, NLR or TNO.

- Discretization: smaller sub-sequences as discrete values
- Signal processing: changing (or reducing) the dimensional representation, e.g. fast Fourier transformation (FFT, like HANTS Harmonic Analysis of Time Series) or discrete wavelet transformation (DWT).

### Selected methods

#### *Outlier removal for ship detection*

For the detection of the ship intensity parameter per harbour sector filtering of outliers was applied. Ship clumps smaller than 4 pixels were supposed to be noise and ships larger than 70 pixels were supposed to be clouds or misclassifications (see Figure 16).



Figure 16. Filtering of clouds (orange) and noise (red) from large ships (dark green) and small ships (light green)

#### *Cloud filtering*

Imagery parts covered by clouds and cloud shadows were detected by comparing individual images with a cloud free reference image (mean image of several cloud free images). On the difference image thresholds and filtering was applied.

### **3.2.4 Detection and analysis of change**

#### Overview of methods

The change might be a combination of temporal and spatial change. Different types of temporal change can be distinguished:

- Event change (catastrophic fires, disasters, (dis)appearing of car or ship)
- Short term change (synoptic weather event)
- Directional change (urban development, trends)

### **CLASSIFICATION: UNCLASSIFIED**

All rights reserved. No part of this document may be reproduced or transmitted in any form or by any means, electronic, mechanical, photocopying, recording, or otherwise, without prior written permission of FFI, NLR or TNO.



- Multi-directional change (deforestation & regeneration)
- Cyclic change (seasonal phenology)

Also different types of spatial change can be distinguished:

- Individual pixel change. Change of a single pixel with respect to an absolute external standard or relatively to the rest of dataset
- Contextual change. Change of a pixel with respect to neighbouring samples
- Change of groups (segment) of pixels
- Change of the area shape of pixel groups (grow, decrease, shift, etc.)

Different approaches exist for the combined analysis of the temporal and spatial aspects of changes, either starting in the temporal domain followed by looking to spatial aspects, or the other way around. Examples are:

- Derivation of the changes over time for each pixel and formulation of these in a change vector. Besides spatial patterns for these change vector are grouped (the so-called Grouped Frequent Sequential (GFS) patterns).
- Segmentation of the dataset, followed by derivation of spatial and spectral characteristics of the segments, after which the temporal behaviour of these characteristics are evaluated.

The detected changes can be characterized and compared to expected trends using several methods:

- Post-classification. Clustering of changes in comparable types (e.g. nearest neighbour, clustering, sectors (quadrants) of change).
- Derivation of expected or mean behaviour. Finding trends (consistent change) and identification of discontinuity in that trends (e.g. regression analysis).

### Selected methods

#### *Pixel based anomaly detection*

A relatively simple anomaly detection method was applied for pixel based anomaly detection in a series of DMC or Sentinel images was applied. First areas with clouds, water and vegetation were masked out in order to concentrate the anomaly detection on urban areas. For each pixel the time series of spectral values was evaluated. This is done by computing the mean values over time for each spectral band and applying and detecting values with large deviations from that mean above a specified threshold. In case large deviations occur in all spectral bands, the

## **CLASSIFICATION: UNCLASSIFIED**

*All rights reserved. No part of this document may be reproduced or transmitted in any form or by any means, electronic, mechanical, photocopying, recording, or otherwise, without prior written permission of FFI, NLR or TNO.*

pixel at that time is supposed to be an anomaly. In the next step, clusters of anomalies pixels are identified by a clumping routine, so that also a spatial element is obtained.

*Harbour ship intensity anomaly detection*

The harbour ship intensity stands for the number of ships that is detected within the area of a specific harbour sector. The procedure for this is described in section 3.2.2.2. The ship intensity over time for each harbour section is evaluated and large deviations are detected as anomalies. Deviations are detected by applying a moving filter that takes into account the last five values of ship intensity and determine the mean and standard deviation for this. In case the new intensity value deviates more than 3 times the standard deviation from the mean, the new intensity is defined as an anomaly. This approach makes it possible to handle smooth variations over the seasons. See an example of detection of anomalies in figure 17.

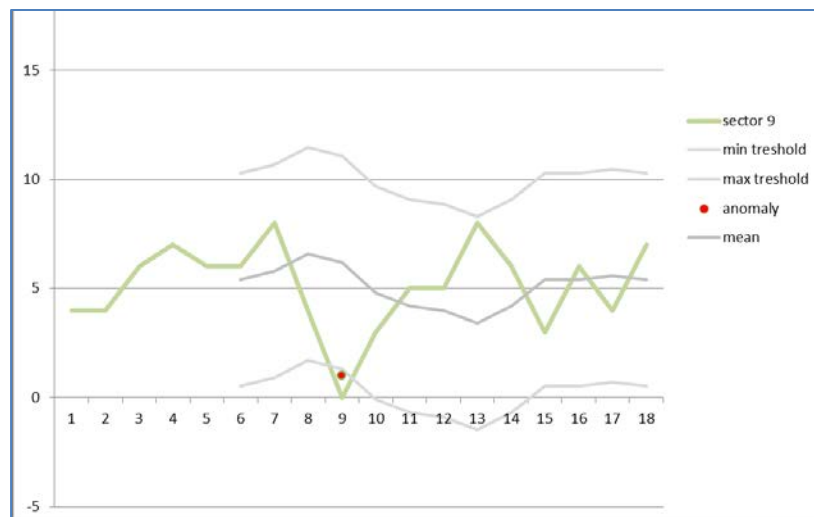


Figure 17. Detection of anomalies based on filtered mean and standard deviation.

*Segment based change detection*

For the evaluation of changes in land use in the rural area south of Rotterdam an approach was used where first segmentation was applied to divide the area in segments with comparable pixel behaviour. In a next step for each image the segments were classified in land use classes, based on the spectral features of the pixels of each segment. In a third step a change in the type of land use for a segment was identified as an anomaly. See figure 18 for an example.

**CLASSIFICATION: UNCLASSIFIED**

All rights reserved. No part of this document may be reproduced or transmitted in any form or by any means, electronic, mechanical, photocopying, recording, or otherwise, without prior written permission of FFI, NLR or TNO.

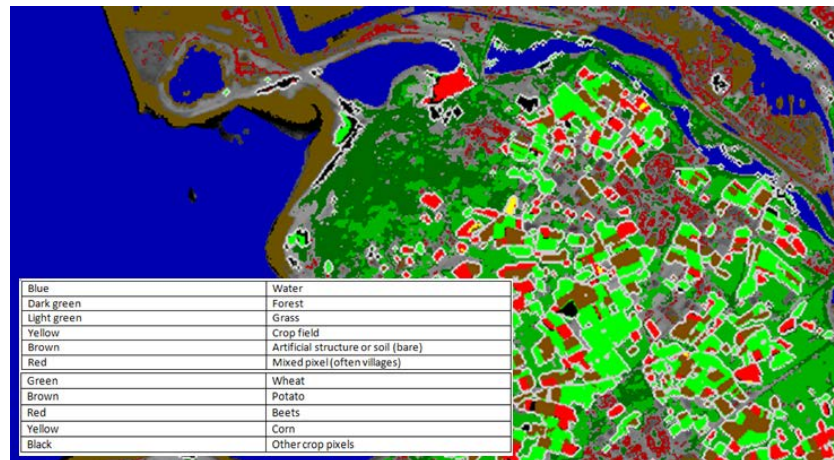


Figure 18. Change detection between series of land use classified image segments.

### 3.3 SAR methods

#### 3.3.1 Inventory of SAR methods

We focus here on change detection methods for multi-temporal analysis of SAR imagery. A pre-condition for change detection is an accurate geo-registration of the images and calibration of the pixel values.

An image matching procedure can be used to co-registrare two and two SAR images. Small patches throughout the two images are correlated using FFT (see illustration in Figure 19). The sub-pixel shifts in the x- and y-directions are then fit to a linear model for the entire area. Finally, a four-point bicubic algorithm is used to resample one of the two SAR images with sub-pixel accuracy to the geometry of the other SAR image. Then the SAR amplitude and coherence images can be geocoded to the WGS84 ellipsoid, resulting in SAR image products that will have a geometry that is more easily compared to maps [16]. In Figure 19 two COSMO-SkyMed (distributed by e-GEOS) SAR images from January 9<sup>th</sup> and 10<sup>th</sup> 2010 are shown.

## CLASSIFICATION: UNCLASSIFIED

All rights reserved. No part of this document may be reproduced or transmitted in any form or by any means, electronic, mechanical, photocopying, recording, or otherwise, without prior written permission of FFI, NLR or TNO.

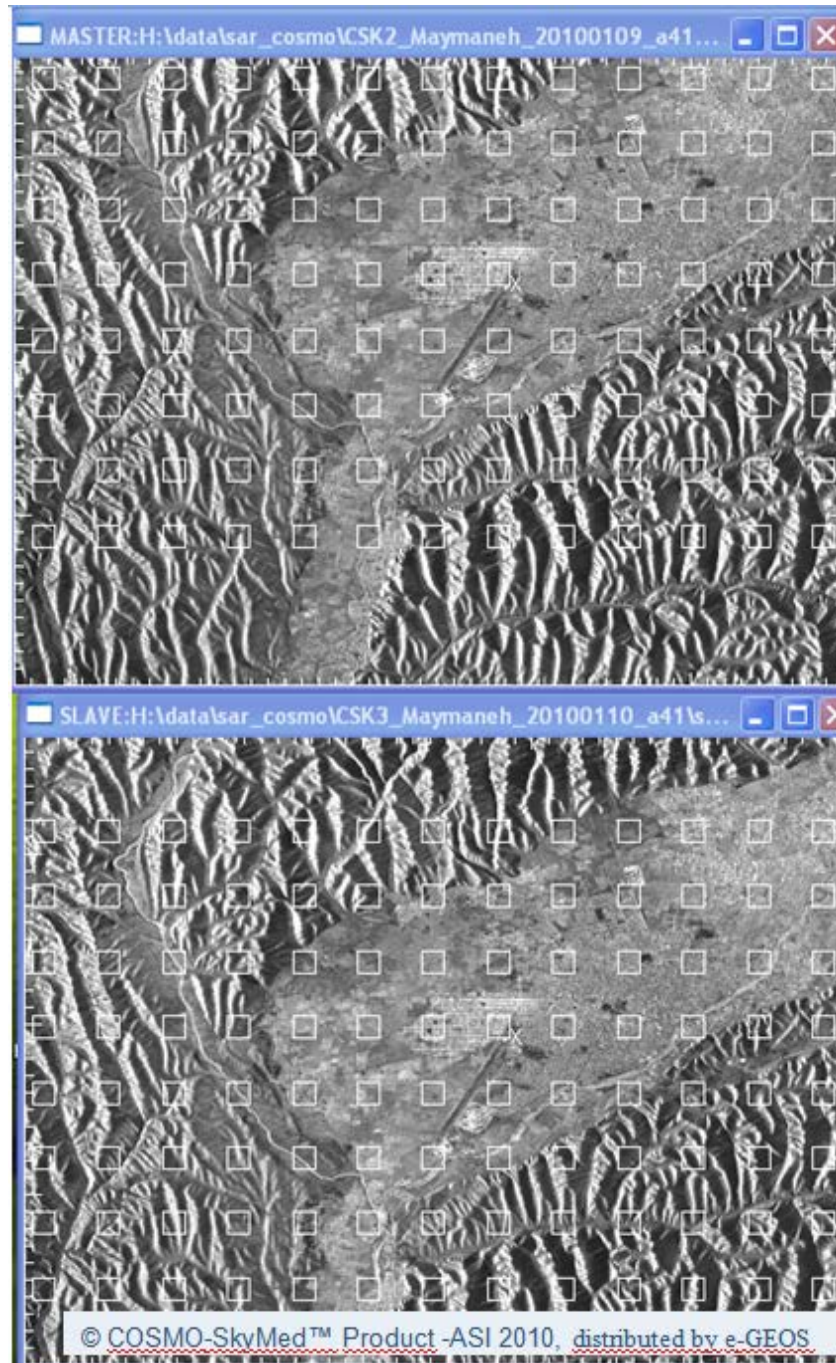


Figure 19 Example of the numerous patches used when doing the co-registration of the two SAR images

#### Colour composite of layer stack

A basic method for visual analysis of multi-temporal information is to present the multiple greyscale SAR images in the RGB (Red Green Blue) channels of a colour display. This way

### **CLASSIFICATION: UNCLASSIFIED**

All rights reserved. No part of this document may be reproduced or transmitted in any form or by any means, electronic, mechanical, photocopying, recording, or otherwise, without prior written permission of FFI, NLR or TNO.



differences will be highlighted by a colour, and non-changed objects by a tone of grey. The RGB method is only applicable for two or three images, so that when more images are available various sets of RGB image are to be inspected. Figure 20 shows an example of SAR change detection in Norway. In *Figure 21* SAR amplitude image changes within different time periods in Meymaneh, Afghanistan are shown. The left image shows 8-days amplitude change between January 1<sup>st</sup> and January 9<sup>th</sup>. The left image shows 1-day change between January 9<sup>th</sup> and January 10<sup>th</sup>. In *Figure 22* change imagery for COSMO-SkyMed spot light imagery (Blue/Green/Red: 30 June/3 July/ 7 July 2011) for the Rotterdam harbour is shown [9]. Change due to relocation of ship is clearly visible in the colours, while the infrastructure is mostly grey due to no change.



Feb. 10<sup>th</sup>



March 10<sup>th</sup>

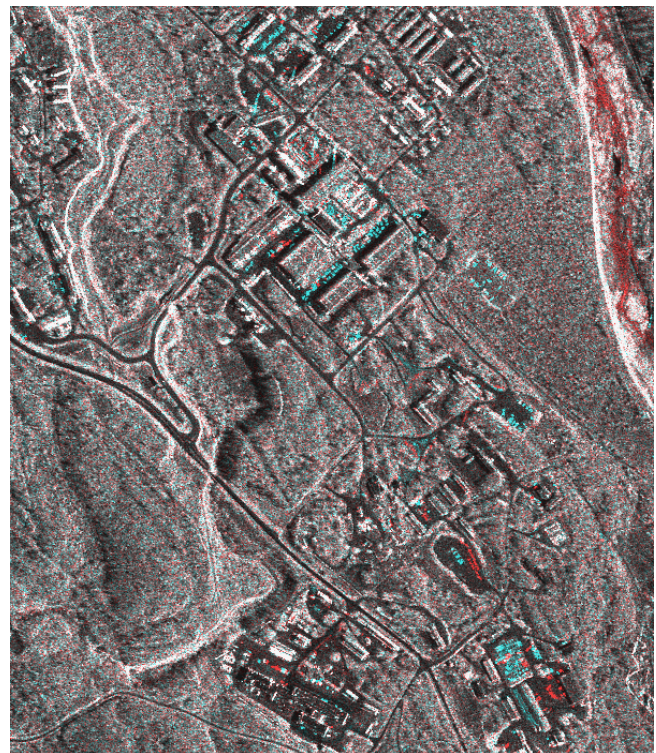


*Figure 20 Satellite SAR change detection during an exercise at Setermoen, north of Norway.*

**CLASSIFICATION: UNCLASSIFIED**

*All rights reserved. No part of this document may be reproduced or transmitted in any form or by any means, electronic, mechanical, photocopying, recording, or otherwise, without prior written permission of FFI, NLR or TNO.*





Figure 21 Amplitude change imagery for Meymaneh, Afghanistan. Original SAR data: © COSMO-SkyMed™ Product-ASI 2010, distributed by e-GEOS.

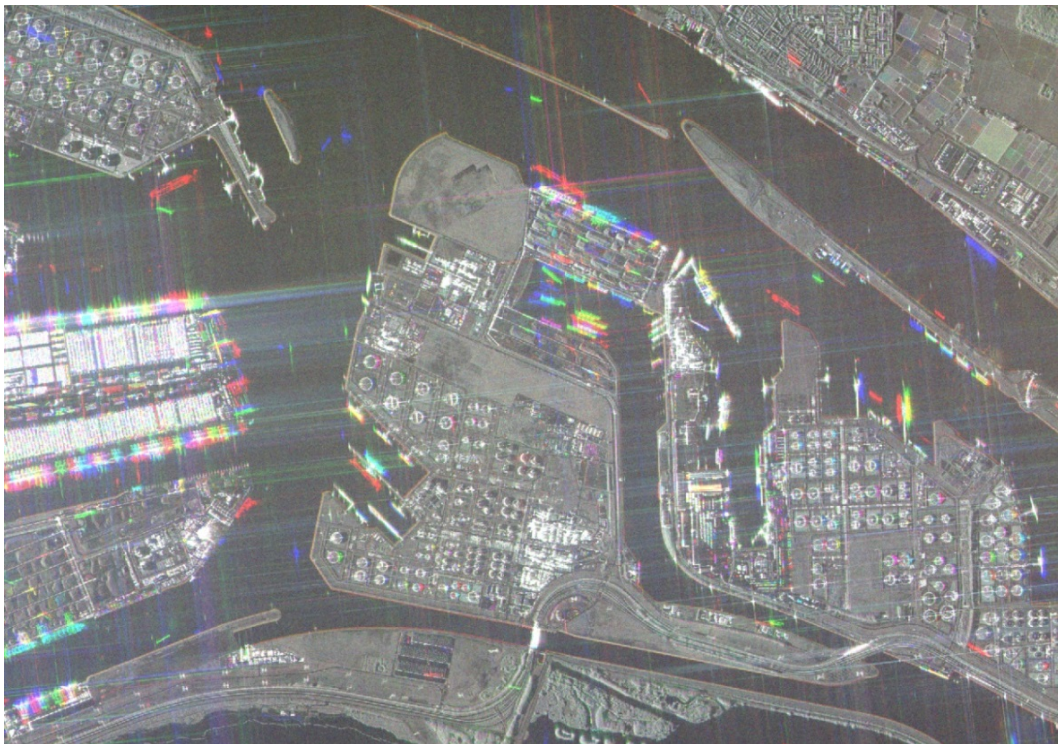


Figure 22 RGB colour composite of COSMO-SkyMed imagery for Rotterdam harbour

**CLASSIFICATION: UNCLASSIFIED**

All rights reserved. No part of this document may be reproduced or transmitted in any form or by any means, electronic, mechanical, photocopying, recording, or otherwise, without prior written permission of FFI, NLR or TNO.



### Division or subtraction

Another method of visualising changes is by dividing or subtracting the images. This method applies only to image pairs. Which method to choose, either dividing or subtracting, depends on the representation of the images. In case of amplitude or power images, it is best to choose division, while for log-scaled images it is best to choose subtraction [10]. The disadvantage of applying such operations to SAR images is that speckle can hinder interpretation of the changes. However, speckle filters have been developed to reduce that effect. Division or subtraction can be done on a pixel basis or on an object basis where multi-temporal segmentation can be applied to define objects [14]. The advantage of segmentation is that it reduces speckle too, and that the result is easy to vectorise. After division or subtraction changes can be detected using a threshold. In Figure 23 these detected changes are made visible in a red overlay.



Figure 23 TerraSAR-X images (15 and 26 June 2013) for the Ørland area (courtesy Fraunhofer IOSB) with changes due to tide and relocatable vehicles (red overlay).

### Statistical analysis of multi-layer stack

In case multiple images are to be analysed for changes and multi-temporal trends, a so-called layer stack can be used. In a layer stack, the stacks span the temporal domain and the map the geospatial domain. For detecting temporal changes averages can be taken for a (moving) window in the spatial domain, resulting in a temporal array. This array can be analysed for temporal trends or be used to detect changes by finding outliers using the average (e.g. the mean or median) and the standard deviation.

## **CLASSIFICATION: UNCLASSIFIED**

All rights reserved. No part of this document may be reproduced or transmitted in any form or by any means, electronic, mechanical, photocopying, recording, or otherwise, without prior written permission of FFI, NLR or TNO.

### Coherent change detection

SAR interferometry (InSAR) enables coherent change detection (CCD) in which the decorrelation of the phase between two consecutive acquisitions is determined [18]. The decorrelation can be caused by thermal noise (thermal decorrelation), the baseline between the platform tracks (baseline or spatial decorrelation), and temporal effects (temporal decorrelation). Temporal decorrelation generally follows from physical changes of the earth surface over a certain period of time, due to weather, soil motion, or human activities. Examples of human activities that disturb the surface are mining, tillage, building activities, damage, and vehicle tracks. Especially in dry (arid) areas (no change due to natural causes), changes in the coherency map indicate human activities.

The estimated SAR coherence is influenced by man-made changes, natural vegetation growth and varying surface moisture conditions. The number of false alarms can be reduced if more than three coherent SAR images are jointly analysed.

Coherence change detection can be used to inspect the water level in rivers. Figure 24 shows high coherence level from the wide river in the 1-day repeat-pass data set from Meymaneh city in Afghanistan, indicating extremely low water level in the river in January 2010. There is a small stream still running, and the stable radar scatterers come from the dry river bed. Low coherence will appear also in areas where there is an exceptional low SAR backscatter. Figure 24 shows one example where there is a paved surface close to and at the northern side of the airport runway. The interferometric phase measurement will be uncertain when the SAR backscatter is low, and hence the coherence level will be low. Thus, to avoid misinterpretations, it is important to compare low coherence levels with the SAR amplitude backscatter [16]. COSMO-SkyMed (distributed by e-GEOS) spotlight SAR images from January 2010 show Meymaneh city in Afghanistan. The left image is an amplitude SAR image from January 9<sup>th</sup> with the main river marked in blue in the upper half part of the image. The right image shows a 1-day coherence image between SAR acquisitions made on January 9<sup>th</sup> and 10<sup>th</sup>, where the low coherence areas with man-made activities are shown up with a black or dark grey colour.

## **CLASSIFICATION: UNCLASSIFIED**

*All rights reserved. No part of this document may be reproduced or transmitted in any form or by any means, electronic, mechanical, photocopying, recording, or otherwise, without prior written permission of FFI, NLR or TNO.*





*Figure 24 Amplitude and coherence image from COSMO-SkyMed image pair for Meymaneh city in Afghanistan.*

Figure 25 is another example of coherent change detection. The area of a stamp mill industry is marked with a square. When studying the 1-day coherence image to the left, the low coherence areas (dark areas) clearly show that there is some on-going activity. The 8-days coherence image to the right shows that the activity is steadily going on. The low-coherence areas are even extending over a larger part of the stamp mill area. The circles indicate increased activity on certain roads (low coherence). It is also possible to see some low coherence lines within the river bed when investigating more closely the 8-days coherence image. During the dry seasons of the year parts of the river is used as an additional road from time to time for big trucks.

Low coherence images can also be used to get a clear indication on which agricultural fields that are used at the time being. Thus, it is possible to obtain a kind of “activity” map over the region: a map telling us where and when the activity (for example agricultural practices like ploughing and harrowing) is taking place. To some extent, it is also possible to see which roads or trails that are used in connection to the various agricultural fields. See examples on the left part of the coherence images in Figure 25 [16]. The figure shows COSMO-SkyMed spotlight SAR acquisitions (distribution by e-Geos) from January 2010 over parts of Meymaneh city in Afghanistan. The left image shows a 1-day coherence SAR image using acquisitions from January 9<sup>th</sup> and 10<sup>th</sup>. The right image shows an 8-day coherence SAR image using acquisitions from January 1<sup>st</sup> and 9<sup>th</sup>. Low coherence areas with man-made activities are shown as a black colour.

**CLASSIFICATION: UNCLASSIFIED**

*All rights reserved. No part of this document may be reproduced or transmitted in any form or by any means, electronic, mechanical, photocopying, recording, or otherwise, without prior written permission of FFI, NLR or TNO.*

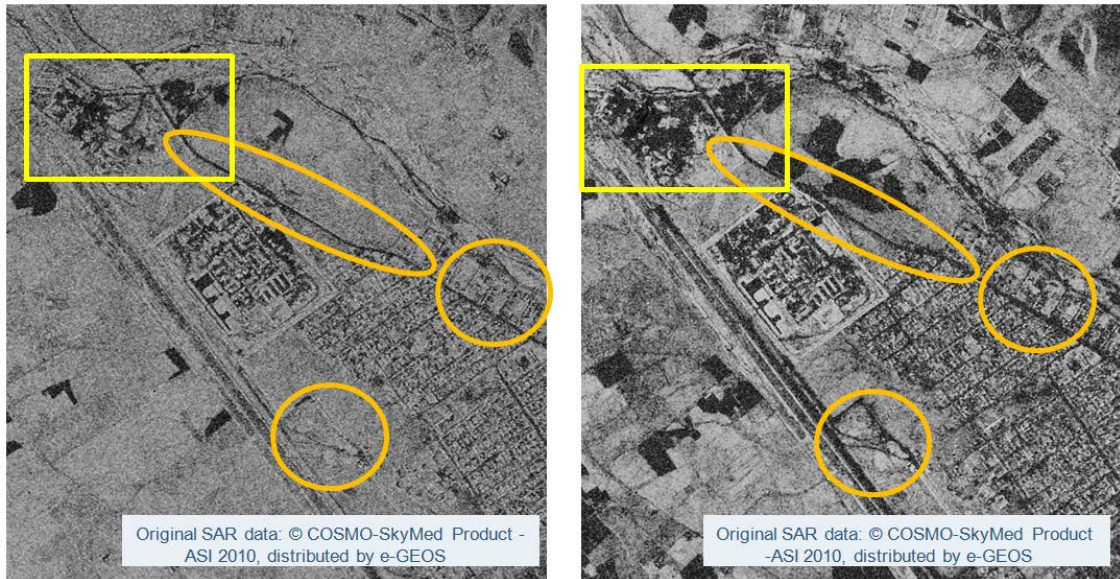


Figure 25 Coherence images from COSMO-SkyMed image pair. Left one day interval. Right 8 day interval.

Figure 26 illustrates man-made activities over different time-slots well. The SAR coherence of the first 8 days is shown in the left image. On-going changes over the next day (1-day coherence) are shown up as dark areas in the image to the right. Some roads are still in use between the January 9<sup>th</sup> and 10<sup>th</sup>, while others were only used in the first time period. In the figure a sub-set of COSMO-SkyMed SAR images over Meymaneh in Afghanistan in 2010 is shown to the left with 8-day coherence SAR image using acquisitions from January 1<sup>st</sup> and 9<sup>th</sup>. The image to the right shows a 1-day coherence SAR image using acquisitions from January 9<sup>th</sup> and 10<sup>th</sup>. Some agricultural fields and roads show low SAR coherence (black), but with different concentration during the two time periods.

The “pattern of life” can be mapped by monitoring the evolution of changes in the region by analysing repeat-pass SAR images. Changing weather conditions can hamper the coherence SAR images. Snow, thawing, precipitation, changing ground surface moisture conditions etc. can have an influence of the resulting coherence SAR image pairs. Thus, weather forecasts should be used when planning SAR acquisitions. Figure 27 shows a fusion of SAR amplitude and coherence changes over a period of 8-days over part of the Meymaneh city in Afghanistan.

### **CLASSIFICATION: UNCLASSIFIED**

*All rights reserved. No part of this document may be reproduced or transmitted in any form or by any means, electronic, mechanical, photocopying, recording, or otherwise, without prior written permission of FFI, NLR or TNO.*



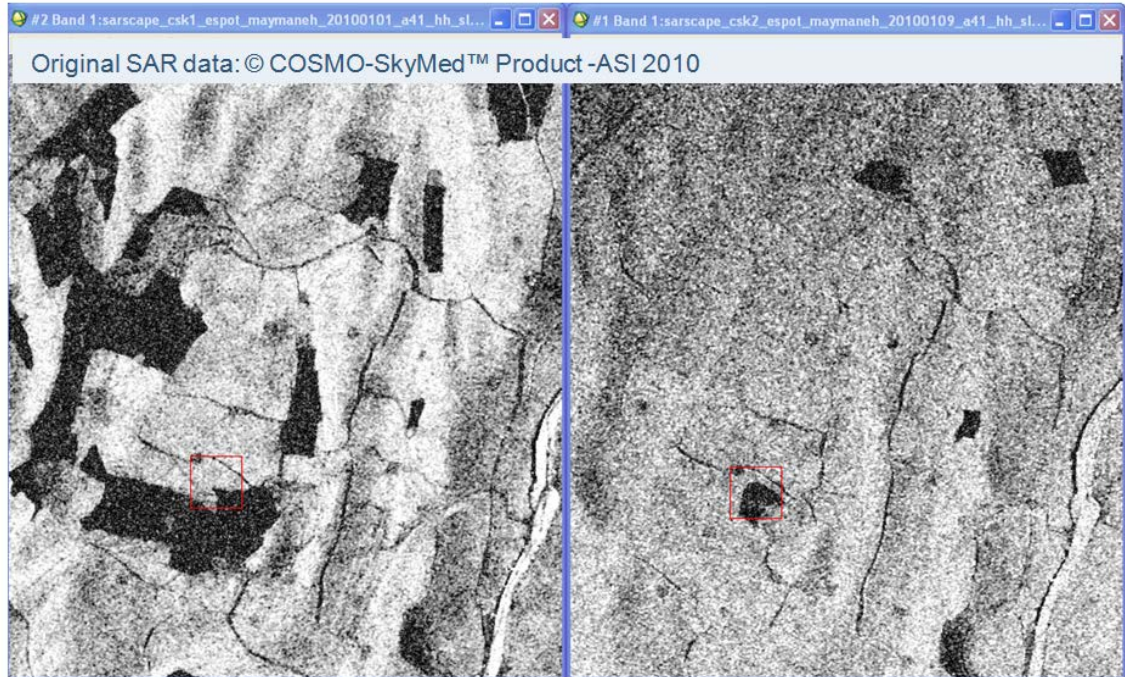
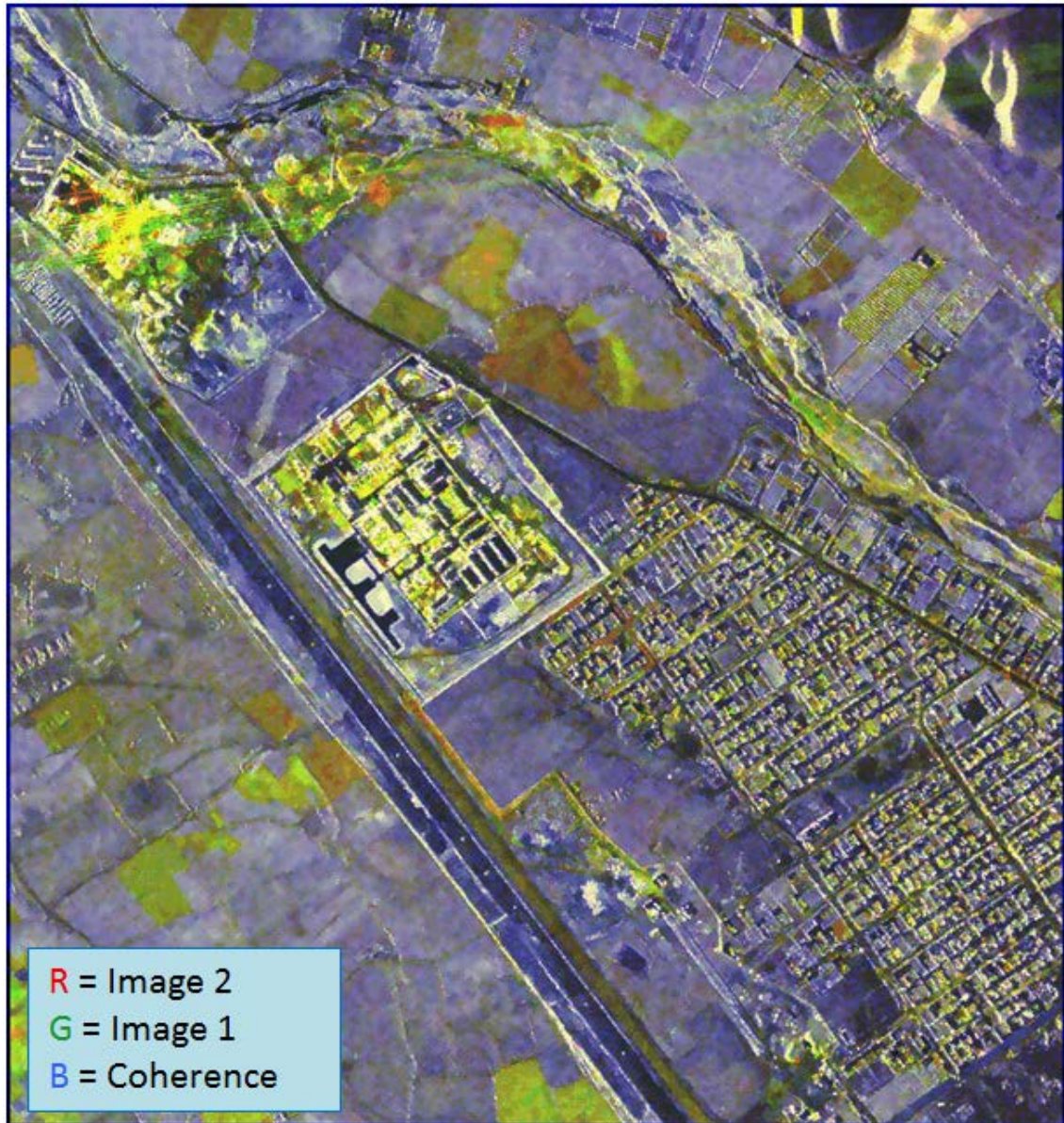


Figure 26 Sub-set of COSMO-SkyMed SAR coherence images over Meymaneh in Afghanistan.

**CLASSIFICATION: UNCLASSIFIED**

All rights reserved. No part of this document may be reproduced or transmitted in any form or by any means, electronic, mechanical, photocopying, recording, or otherwise, without prior written permission of FFI, NLR or TNO.



*Figure 27 Colour fusion of SAR amplitude and coherence changes over a period of 8-days over part of the Meymaneh city in Afghanistan.*

Figure 28 shows the coherency in the TerraSAR-X images (15 and 26 June 2013) for the Ørland area (courtesy Fraunhofer IOSB). Infrastructural (air base, urban area) and rocky areas show high coherency (no change), while other areas with vegetation show low coherency (change due to small changes in the vegetation layer).

### **CLASSIFICATION: UNCLASSIFIED**

*All rights reserved. No part of this document may be reproduced or transmitted in any form or by any means, electronic, mechanical, photocopying, recording, or otherwise, without prior written permission of FFI, NLR or TNO.*





Figure 28 Coherence image from TerraSAR-X image pair for Ørland airbase.

### 3.3.2 Selection of SAR methods

Different commercial software packages support part of the methods described in the previous sections. Among these software packages are:

#### Erdas Imagine

This is originally a remote sensing image analysis package widely used in the GeoInt community. Erdas Imagine has many additional toolkits, including tools for processing of vector information and information from SAR images. The latter include calibration, geocoding, co-registration, change detection, speckle reduction, texture analysis, and interferometry. Geocoding is the process of projecting a satellite image from radar geometry into a map projection (e.g. UTM (Universal Transverse Mercator) WGS84). This can be done by assuming the earth as an ellipsoid, or by adding the local elevation model. Speckle reduction can be applied to reduce the image noise that is characteristic for SAR images (noise intensity is inversely proportional to the equivalent number of looks (ENL)). Interferometry is a technique to measure the terrain elevation, subsidence, and coherent change detection. Coherent change detection is based on the phase of the radar signal, conventional change detection on the amplitude or power (i.e. image intensity).

## **CLASSIFICATION: UNCLASSIFIED**

*All rights reserved. No part of this document may be reproduced or transmitted in any form or by any means, electronic, mechanical, photocopying, recording, or otherwise, without prior written permission of FFI, NLR or TNO.*

### ENVI SARscape

ENVI is a popular image analysis package in the hyperspectral imaging community, but has also a toolkit for SAR image analysis (SARscape). This toolkit is similar to the SAR toolkit of Erdas Imagine, but also has many capabilities for the analysis of polarimetric SAR images. ENVI for ArcGIS makes it possible to integrate a part of the SAR functions in ArcGIS.

### BAE Socet GXP

This package is similar to Erdas Imagine, but provides only part of its functionality. Analysis of SAR images is limited. An interesting function is the analysis of moving objects based on sub-aperture images (images based on a sub-section of the antenna aperture). A question remains how to obtain the sub-apertures. Socet GXP supports analysis of video.

### ESRI ArcGIS

ArcGIS is a generic Geographical Information software package that is good at processing of vector information and thematic rasters. It is widely used in the GEOINT community. ArcGIS has many extensions, including tools for geostatistics, spatial analysis, and 3D analysis. ArcGIS has no functions of its own for (SAR) image analysis, but ENVI for ArcGIS makes it possible to integrate a part of the SAR functions in ArcGIS. ArcGIS is widely used in the GEOINT community.

To summarise, methods for SAR are best supported by Erdas Imagine and ENVI SARscape. The latter can be integrated with ArcGIS, but which functions this applies to are unknown. Functions that are not supported, such as statistical analysis of multi-layer stacks, can be implemented using for instance Matlab, a general purpose fourth-generation computer language that provides many different toolboxes (including a mapping toolbox providing GIS functions). The table below gives an overview of which software packages support the different SAR methods.

## **CLASSIFICATION: UNCLASSIFIED**

*All rights reserved. No part of this document may be reproduced or transmitted in any form or by any means, electronic, mechanical, photocopying, recording, or otherwise, without prior written permission of FFI, NLR or TNO.*

Table 3 Overview of SAR methods and software packages.

Method	Erdas Imagine	ENVI SARscape	Socet GXP	ArcGIS
Geocoding	•	•		
Co-registration	•	•		
Colour composite	•	•	•	•
Division, subtraction (pixel based)	•	•		
Speckle filtering	•	•		
Multi-temporal segmentation	•	•		
Coherent Change Detection	•	•		
Statistical analysis of multi-layer stack	(•)	(•)		

### 3.3.3 Implementation of SAR methods

#### Colour composite of layer stack

Basic workflow of this method is shown in the diagram below. Depending on the SAR product that has been obtained, the image has to be geocoded or not. Depending on the accuracy of geocoding, additional co-registration is necessary. Erdas Imagine and ENVI provide functions for layer stacking. A layer stack can be viewed by all software packages, such as an RGB image in which each colour channel shows one image layer. Brightness and contrast can be adjusted (e.g. by using the wheels in Erdas Imagine).

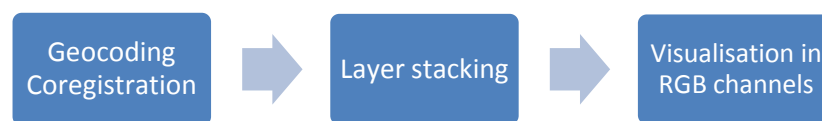


Figure 29 Workflow for RGB visualization

#### Division or subtraction

Start of this workflow is the same as the previous workflow. Optionally, to suppress speckle noise, a filter or multi-temporal segmentation can be applied. In multi-temporal segmentation, a stack of images (instead of one image) is input to the segmentation process. Both Erdas Imagine and ENVI provide different speckle filters, functions for image segmentation, and image division and subtraction. Visualisation of the ratio or difference can be done in one channel, as

### **CLASSIFICATION: UNCLASSIFIED**

All rights reserved. No part of this document may be reproduced or transmitted in any form or by any means, electronic, mechanical, photocopying, recording, or otherwise, without prior written permission of FFI, NLR or TNO.

greyscale image or pseudo-colour. In some cases, due to stretching of fore-shortened objects, it is better to do the geocoding after division/subtraction, to reduce the number of false alarms. A threshold can be applied to make a selection of changes.



Figure 30 Workflow for visualization of the ratio

Statistical analysis of multi-layer stack

This workflow starts with geocoding and registration followed by layer stacking which is analogous to the previous methods. In the packages described here no standard way to extract the temporal arrays and to analyse these arrays, followed by visualisation are available.

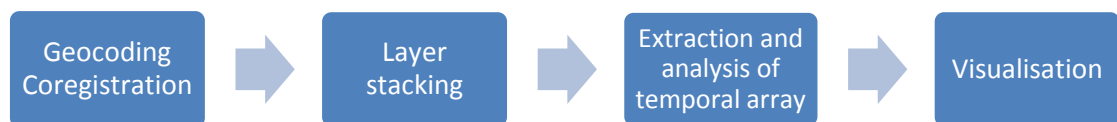


Figure 31 Workflow for the extraction of information from a temporal array

In Erdas a spectral profile (in the multispectral tab) can be inspected, which gives limited insight. In this project a user defined approach implemented in MATLAB is used. In the figure below a user-defined MATLAB tool is showing detected multi-temporal changes (red overlay), to the right the temporal behaviour for the lower left corner and a Google Earth image to provide the context for interpretation of the change. Change is due to parking of trucks in an assembly area in July in the city of Nikel.

**CLASSIFICATION: UNCLASSIFIED**

All rights reserved. No part of this document may be reproduced or transmitted in any form or by any means, electronic, mechanical, photocopying, recording, or otherwise, without prior written permission of FFI, NLR or TNO.



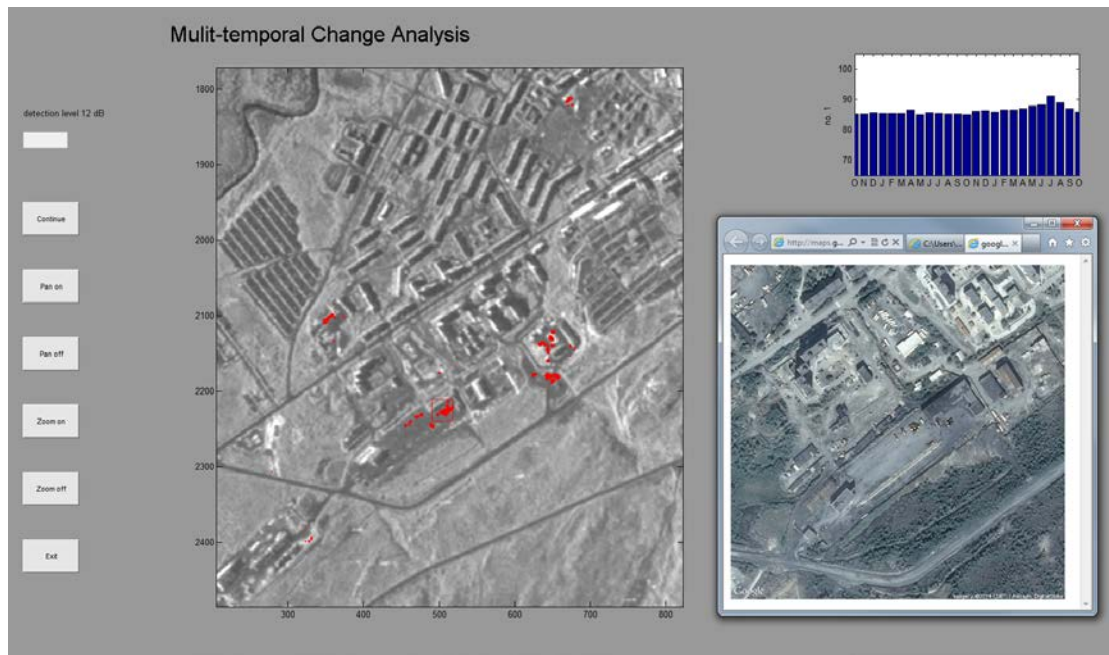


Figure 32 MATLAB tool showing detected multi-temporal changes in red overlay.

### Coherent change detection

This workflow starts with a different co-registration procedure than in the previous workflows. Actually, in this process phase correlation is applied to obtain sub-pixel accuracy that is needed to have a clear view of the temporal decorrelation. Erdas Imagine and ENVI both provide interferometry packages that support this process. Geocoding is generally done after computation of the coherence map. Visualisation of the coherence map can be done in one channel, as greyscale image or pseudo-colour. Note that when sub-pixel co-registration has been done, it is also possible to compute the amplitude or power and apply conventional change detection by division or subtraction.

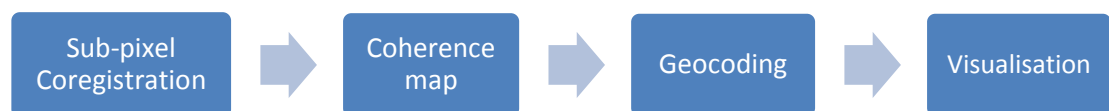


Figure 33 Workflow for coherent changes

### 3.4 Ship detection methods/ sea clutter/polarimetry

There are many SAR satellites in orbit today, which offer dual- and/or quad-polarised data. The first commercial SAR satellites, ERS, ENVISAT and RADARSAT-1, offered single-polarised SAR data. It is possible to get more information out of multi-polarised SAR data. Newer

## **CLASSIFICATION: UNCLASSIFIED**

All rights reserved. No part of this document may be reproduced or transmitted in any form or by any means, electronic, mechanical, photocopying, recording, or otherwise, without prior written permission of FFI, NLR or TNO.

satellites, such as the Canadian RADARSAT-2, the European Sentinel-1A and -1B, the German TerraSAR-X and TanDEM-X and the Italian COSMO-SkyMed satellites are all in orbit, and can now commercially provide at least dual-polarised data.

Norway has large ocean areas, and there is increased shipping and fishing in these areas (see Figure 34). To ease the task of monitoring these large ocean areas, FFI has developed an automatic ship detection tool, Aegir, which uses all polarisation channels to detect bright objects in the available SAR images.

Radar images used operationally in Norway today have linear polarisation. The radar can transmit horizontal (H) and/or vertical (V) polarisation and receive horizontal (H) and/or vertical (V) polarisation. The images can have these polarisation combinations:

- HH – Horizontal transmit and horizontal receive
- VV – Vertical transmit and vertical receive
- HV – Horizontal transmit and vertical receive
- VH – Vertical transmit and horizontal receive

FFI has done research on different ways of combining the available polarisation channels to increase the ship to sea contrast. There are options in Aegir to analyse the different polarisation channels manually and automatically. The more information that is available, the easier the ship detection process gets. Using more polarisation channels may give the opportunity to discriminate between vessels and ice. Co-polarisation is the best option at large incidence angles when the ocean clutter is minimized and the ship to sea contrast is maximized. Backscatter from the ocean is less prominent in cross-polarisation, making this channel less dependent on imaging geometry and wind conditions. Using cross-polarisation opens up the opportunity to use lower incidence angles to do ship detection.

## **CLASSIFICATION: UNCLASSIFIED**

*All rights reserved. No part of this document may be reproduced or transmitted in any form or by any means, electronic, mechanical, photocopying, recording, or otherwise, without prior written permission of FFI, NLR or TNO.*



Figure 34. Norwegian ocean areas. © www.fao.org

### 3.4.1 Dual-polarised SAR data

Norway uses RADARSAT-2 SAR data operationally today, and most of the data used is dual-polarised. Dual-polarised data gives better temporal coverage and wider swath widths than quad-polarised data and more information than single polarised data. The two channels can be analysed separately or they can be combined and analyses can be done on the fused “channel”. Figure 35 shows an example of ScanSAR polarisation combinations, and how the combined channel gives better ship to sea contrast and better contrast between land and ocean.

Figure 36 shows 3D segments of a SAR image in HH- and HV-polarisation on November 29<sup>th</sup> 2009 over the Norne oil production field outside the Norwegian west coast. The segments of

## CLASSIFICATION: UNCLASSIFIED

All rights reserved. No part of this document may be reproduced or transmitted in any form or by any means, electronic, mechanical, photocopying, recording, or otherwise, without prior written permission of FFI, NLR or TNO.

600 pixels x 600 pixels show how much the ocean is suppressed in cross-polarisation compared to co-polarisation.

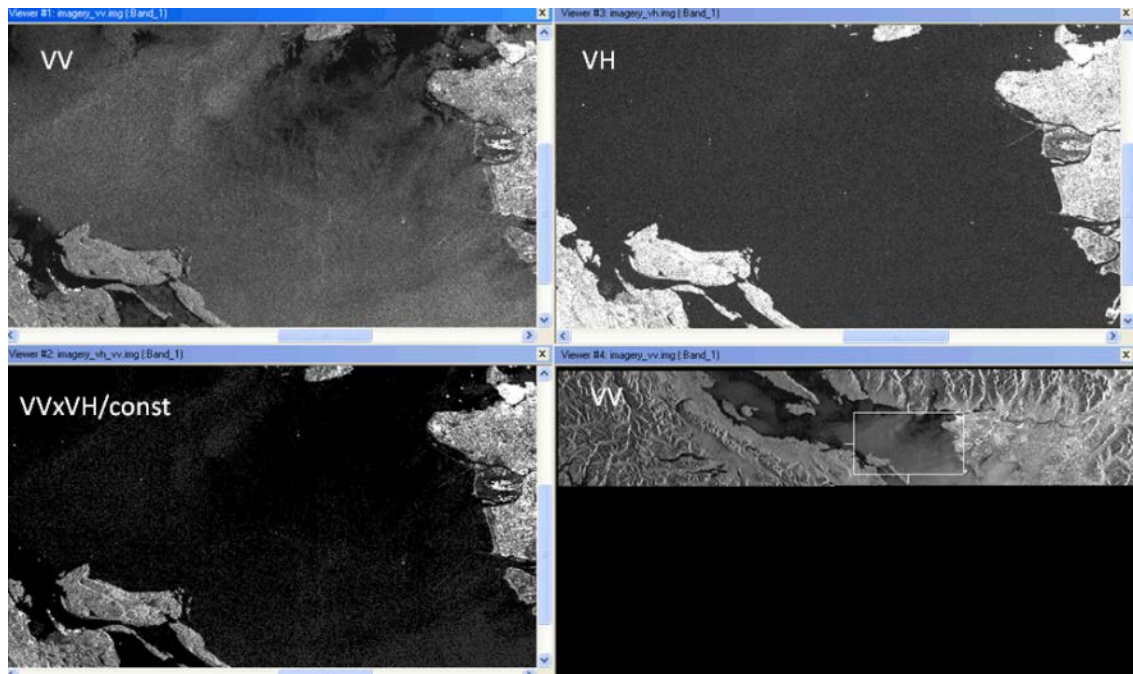


Figure 35. ScanSAR polarisation combinations showing how the combined channel gives better ship to sea contrast.

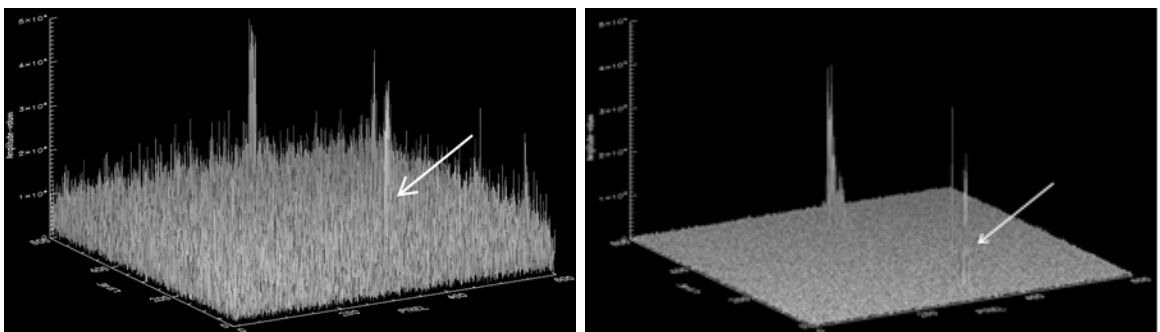


Figure 36. RADARSAT-2 Standard quad-pol HH- and HV-polarisation segments on November 19<sup>th</sup> 2009.

Figure 37 shows signatures of Norne FPSO in the Norne field on June 30<sup>th</sup> 2010. The vessel is shown in 3D presentation in HH-, HV-polarisation and in the combined case, HH×HV, in segments of 60 pixels x 60 pixels. The ship to sea contrast is best when the two available polarisation channels are combined. The sea clutter is almost absent, compared with the ship backscatter, when combining the two polarisation channels. The contrasts between the maximum values of the vessel divided by the mean sea backgrounds are 47 for HH-polarisation,

**CLASSIFICATION: UNCLASSIFIED**

All rights reserved. No part of this document may be reproduced or transmitted in any form or by any means, electronic, mechanical, photocopying, recording, or otherwise, without prior written permission of FFI, NLR or TNO.

34 for HV-polarisation and 975 for the combined case when the vessel is at an incidence angle of 35.3°.

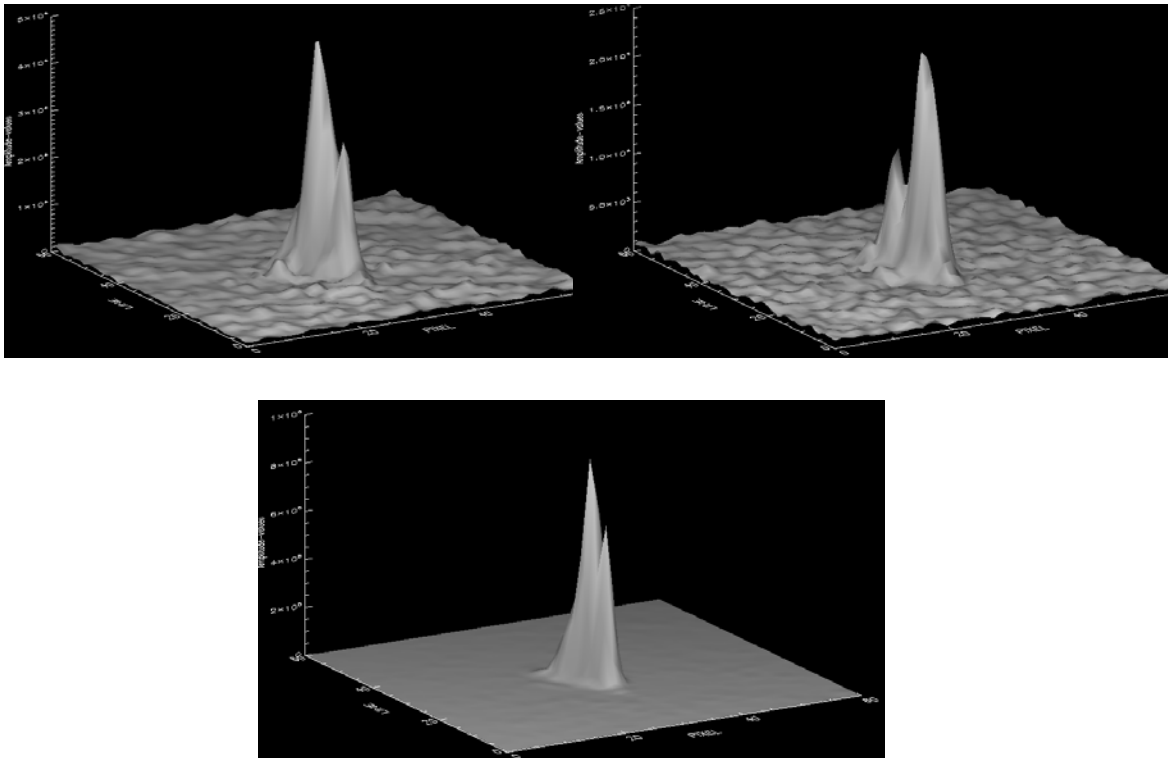


Figure 37. Signature of Norne FPSO in VV-channel (top left), VH-channel (top right) and the combined case (bottom).

Figure 38 shows signatures of vessels and the sea background over the Norne field outside the west coast of Norway on March 31<sup>st</sup> 2010. The vessels are shown in 3D segments of 600 pixels x 600 pixels in VV-, VH-polarisation and in the combined case VV×VH. The ship to sea contrast is best when combining the two polarisation channels and the VH-channel also gives good contrast. The contrast between the maximum value of Norne FPSO divided by the mean sea background is 9 for VV-polarisation, 35 for VH-polarisation and 40 for the combined case.

**CLASSIFICATION: UNCLASSIFIED**

All rights reserved. No part of this document may be reproduced or transmitted in any form or by any means, electronic, mechanical, photocopying, recording, or otherwise, without prior written permission of FFI, NLR or TNO.



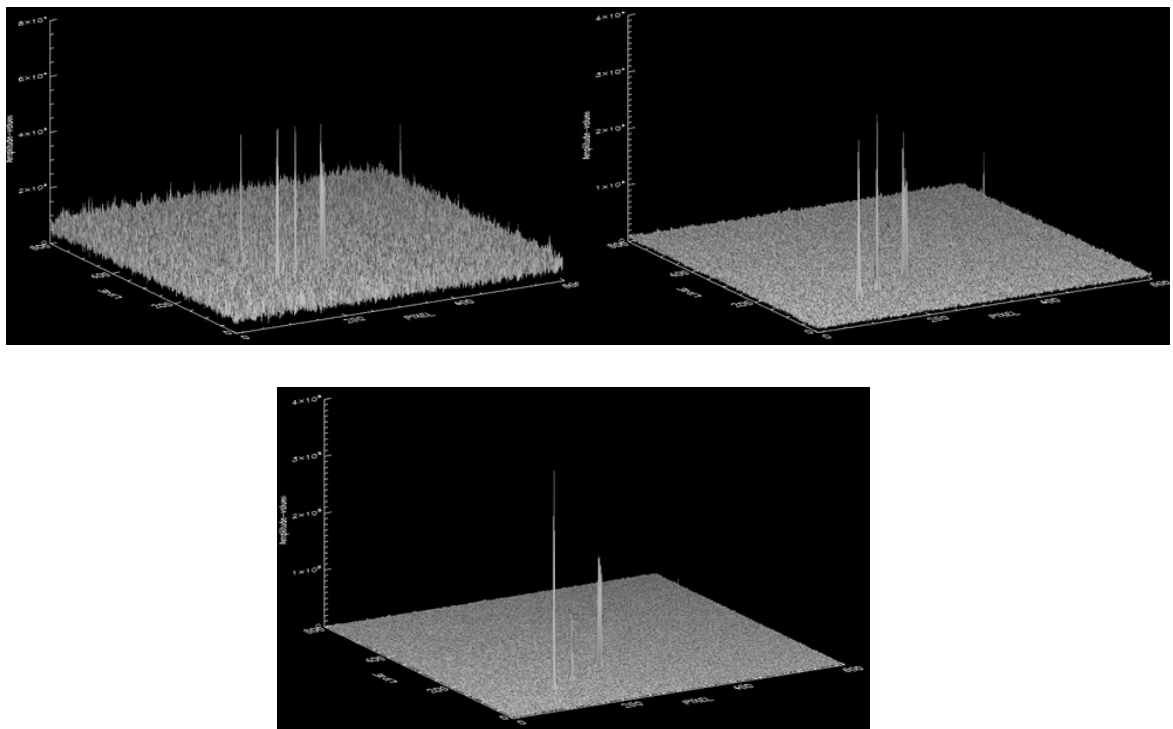


Figure 38. 3D reflections of vessels and the sea background in a segment of 600 pixels x 600 pixels. Top left: VV-channel, top right: VH-channel, bottom: combined case.

Table 4 shows maximum amplitude divided by mean sea for Norne FPSO in 26 RADARSAT-2 dual-polarised images, ScanSAR Wide (SCW) and ScanSAR Narrow (SCN) images. A means ascending and D means descending. Combining the two available polarisation channels shows evident improvements of the ship to sea contrast when combining the polarisation channels for ship detection for low incidence angles. The improvements of the ship to sea contrasts when combining the polarisation channels for ship detection for medium and high incidence angles are very clear. HH-polarisation gives better contrast than VV-polarisation for all incidence angles. Cross-polarisation mostly gives better results for low and medium incidence angles.

**CLASSIFICATION: UNCLASSIFIED**

All rights reserved. No part of this document may be reproduced or transmitted in any form or by any means, electronic, mechanical, photocopying, recording, or otherwise, without prior written permission of FFI, NLR or TNO.

Table 4. Maximum amplitude divided by mean sea ( $R$ ) for the oil production vessel Norne FPSO in 26 RADARSAT-2 ScanSAR dual-polarisation images.

Date	Time	Mode	A/D	Inc. angle	HH	VV	HV/VH	Sqrt ( $co \times cross$ )
14/4-10	16:39:35	SCN	A	23,5		3	7	16
25/6-10	16:39:37	SCN	A	23,5	5		27	107
26/6-10	06:18:08	SCN	D	23,7	13		11	133
15/4-10	06:18:07	SCN	D	23,7		2	6	5
7/4-10	16:43:44	SCN	A	26,4		7	32	253
12/7-10	16:43:01	SCN	A	26,4	7		22	152
23/12-09	06:14:02	SCN	D	26,6	9		22	199
22/4-10	06:13:58	SCN	D	26,7		36	30	801
31/3-10	16:47:54	SCN	A	29,3		8	32	249
5/7-10	16:47:10	SCN	A	29,3	15		27	335
24/4-10	16:47:56	SCN	A	29,3		15	27	352
10/7-10	06:09:47	SCN	D	29,4	19		35	642
30/12-09	06:09:52	SCN	D	29,5	8		27	202
28/6-10	16:51:21	SCN	A	32,2	33		23	630
24/3-10	16:52:04	SCN	A	32,2		53	22	912
17/4-10	16:52:05	SCN	A	32,2		25	14	287
18/12-09	16:51:10	SCN	A	32,3	16		18	232
12/4-10	06:05:37	SCN	D	32,4		7	27	112
23/6-10	06:05:38	SCN	D	32,4	59		39	2828
20/12-09	06:01:09	SCW	D	33,7	8		10	105
10/4-10	16:56:14	SCN	A	35,2		23	45	544
21/6-10	16:55:31	SCN	A	35,2	8		19	148
30/6-10	06:09:52	SCN	D	35,3	47		34	975
19/4-10	06:01:27	SCN	D	35,3		13	30	376
3/4-10	17:00:24	SCN	A	38,1		21	26	507
14/12-09	17:08:56	SCW	A	41,5	41		23	884

**CLASSIFICATION: UNCLASSIFIED**

All rights reserved. No part of this document may be reproduced or transmitted in any form or by any means, electronic, mechanical, photocopying, recording, or otherwise, without prior written permission of FFI, NLR or TNO.

### 3.4.2 Quad-polarised SAR data

Quad-polarised data gives four images with four different polarisations, which can be combined in many different ways. The information that is possible to get out of the quad-polarised data is superior compared to single-polarised data, and the data give more complete information about the vessels and the background. For more information about the decomposition methods, see [12].

When applying the Pauli decomposition method, the components surface scattering (HH+VV), volume scattering (HV or VH) and double bounce (HH-VV) are used. Figure 39 shows an example of the Pauli decomposition where the six vessels in the image segment are clearly visible. The surface scattering is displayed in blue and scaled with a scaling factor  $(HH+VV)^{0.7}$ , the double bounce is displayed in red and scaled with the same scaling factor  $(HH-VV)^{0.7}$ , while the volume scattering is displayed in green and scaled with two scaling factors  $(\sqrt{2} \times (HV+VH))^{0.7}$  [15].

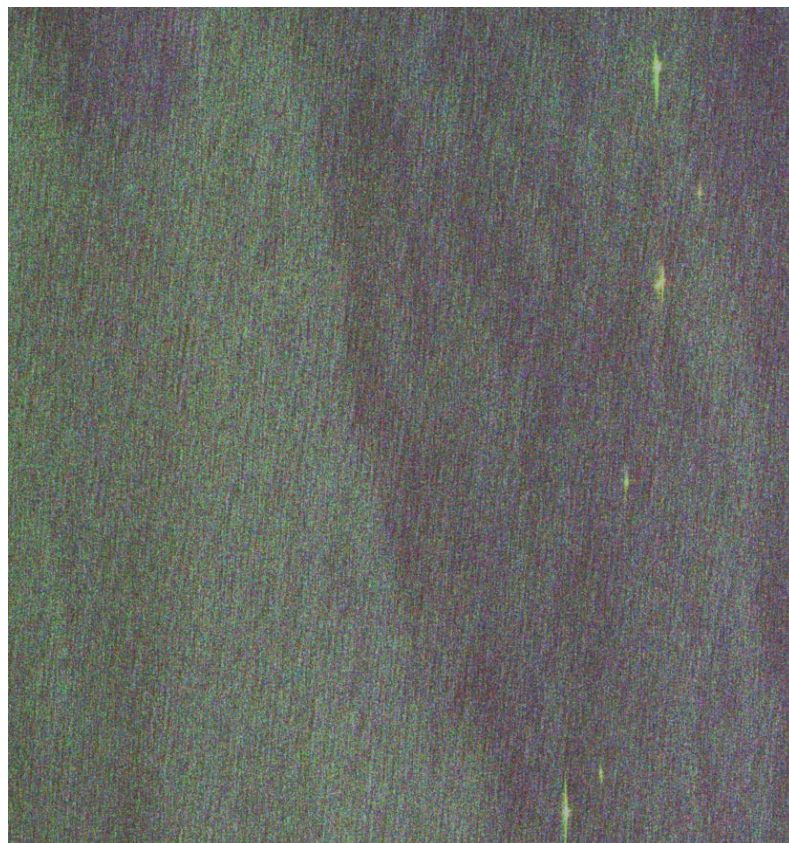


Figure 39. Pauli decomposition of six vessels and the ocean background over the Norne field. All six vessels are clearly visible and Norne FPSO is third from the top.

### **CLASSIFICATION: UNCLASSIFIED**

All rights reserved. No part of this document may be reproduced or transmitted in any form or by any means, electronic, mechanical, photocopying, recording, or otherwise, without prior written permission of FFI, NLR or TNO.



Another way of combining quad-polarised data is to use the Circular Basis decomposition method. The quad-polarised data are decomposed into four elements. The double bounce, HH-VV, and the sum of the volume scattering, HV+VH, are found in the  $S_{RL}$  (Right Left circular) and  $S_{LR}$  (Left Right circular) elements. The surface scattering, HH+VV, is found in the  $S_{RR}$  (Right Right circular) and  $S_{LL}$  (Left Left circular) elements. The double bounce case is expected to be best for ship detection since the ocean surface scattering is suppressed.

In the Krogager decomposition, the polarisation data is decomposed into three coherent components, sphere ( $k_s$ ), diplane ( $k_d$ ) and helix ( $k_h$ ) under a change of rotation.

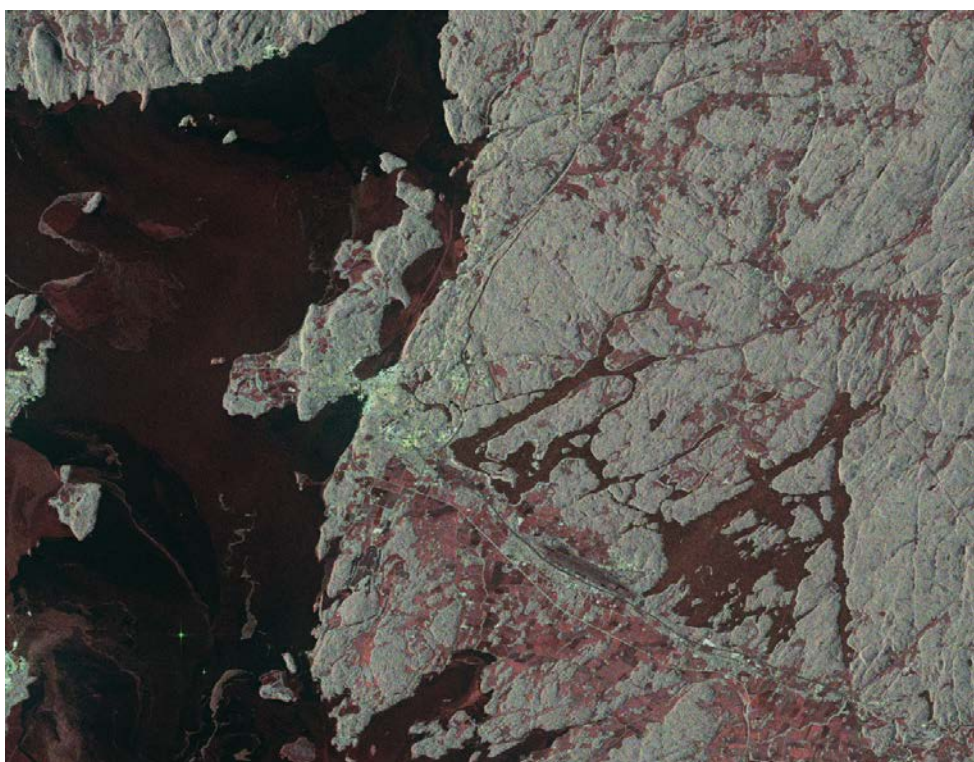
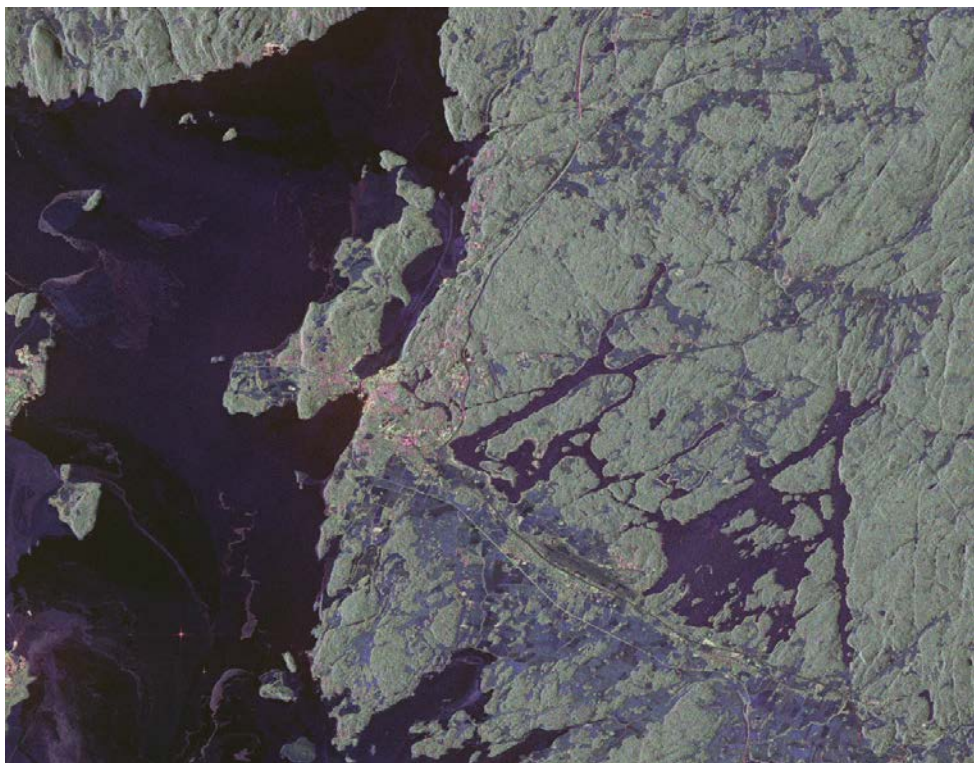
Yamaguchi proposed a four-component scattering model in [17] that can be applied with or without rotation of the coherence matrix.

The double bounce and the volume scattering (HH-VV)\*HV are combined and implemented into the automatic ship detector Aegir. All the polarimetric decompositions are implemented in Aegir, and can be used to analyse vessels, ice, ocean background and areas on land.

Figure 40 shows Pauli, Krogager and Yamaguchi decompositions over segments of a RADARSAT-2 quad-polarisation image including land, sea, vessels and sea ice in and around the Oslofjord on February 7<sup>th</sup> 2010. The example shows how buildings, ships, ice and other natural features scatter differently in different polarisation combinations. The Yamaguchi decomposition method shows that the forest exhibits mostly volume scattering (green) and agricultural fields are dominated by surface scattering (blue) while most of the double bounce scattering (red) comes from buildings and manmade objects. Figure 41 shows segments from the same RADARSAT-2 image in HH-polarisation, VV-polarisation, HV-polarisation, Pauli, Krogager and Yamaguchi rotated. Two vessels are shown in circles, and it is shown that the vessels appear differently in the different polarisations and polarisation combinations.

## **CLASSIFICATION: UNCLASSIFIED**

*All rights reserved. No part of this document may be reproduced or transmitted in any form or by any means, electronic, mechanical, photocopying, recording, or otherwise, without prior written permission of FFI, NLR or TNO.*



**CLASSIFICATION: UNCLASSIFIED**

*All rights reserved. No part of this document may be reproduced or transmitted in any form or by any means, electronic, mechanical, photocopying, recording, or otherwise, without prior written permission of FFI, NLR or TNO.*



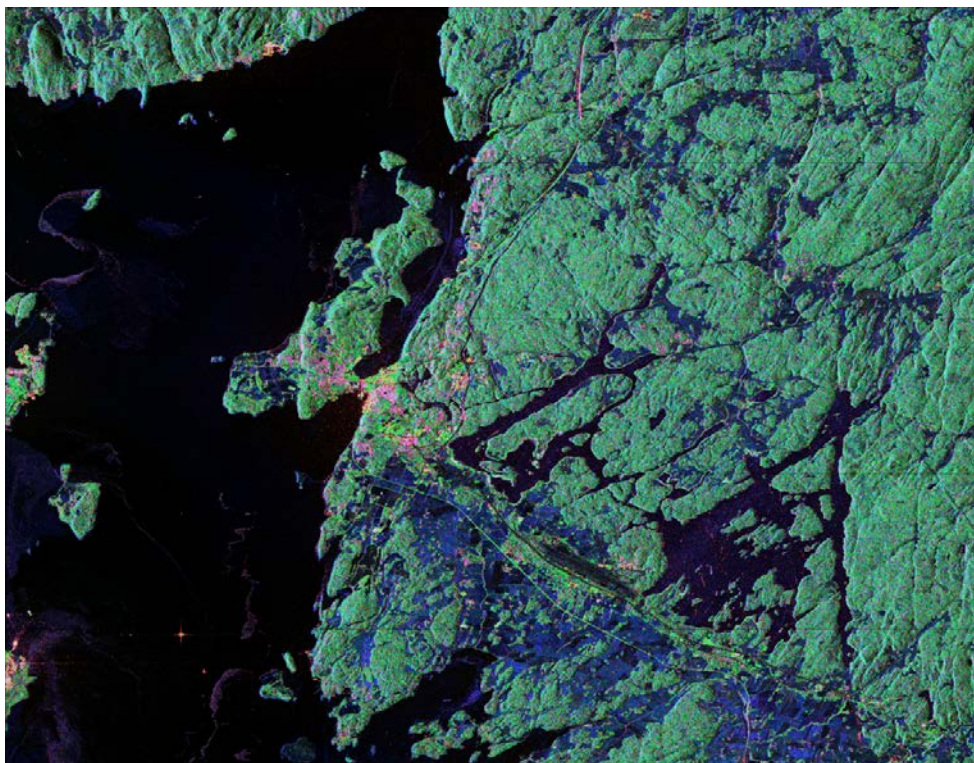
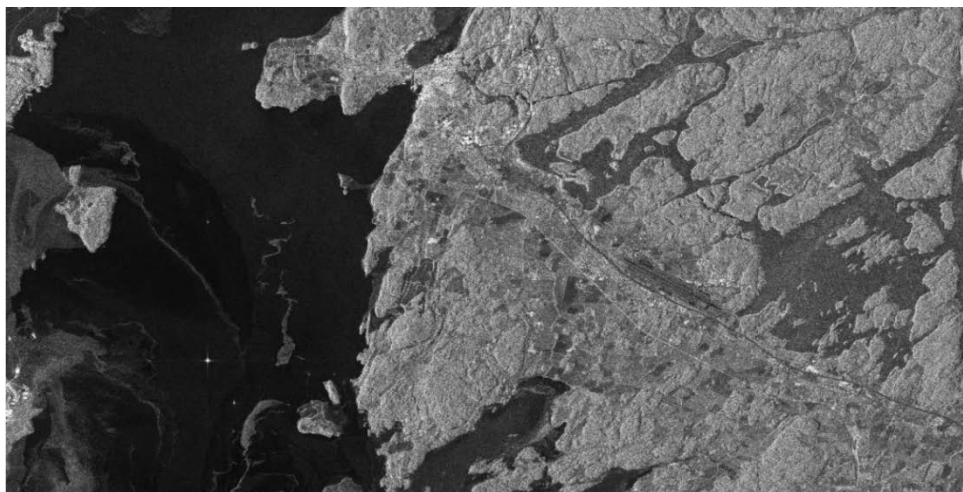
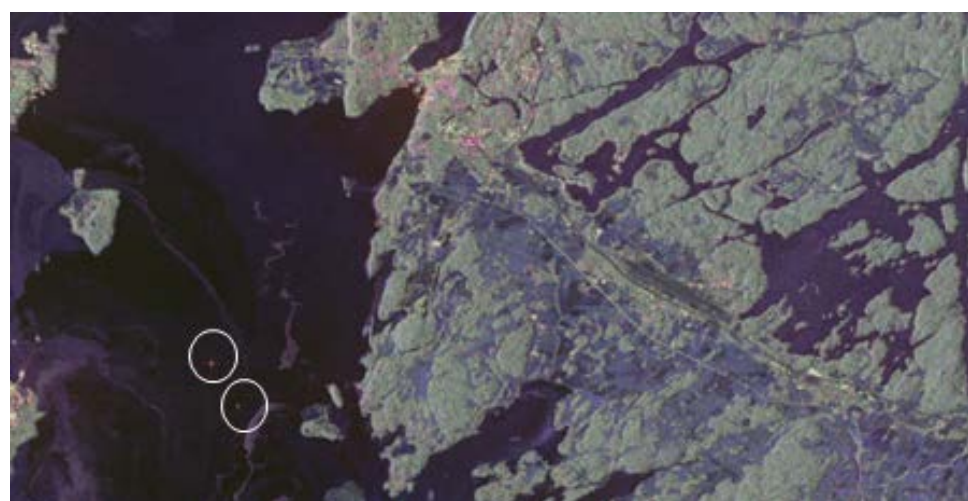
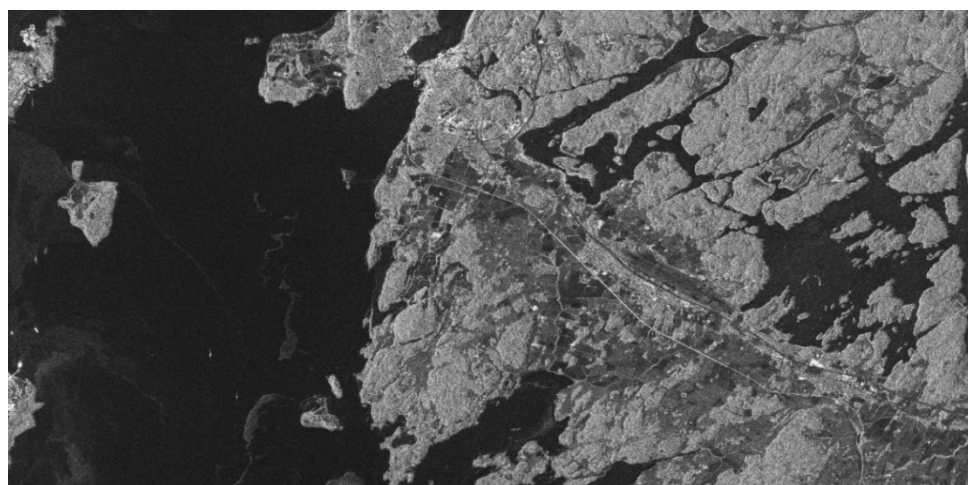
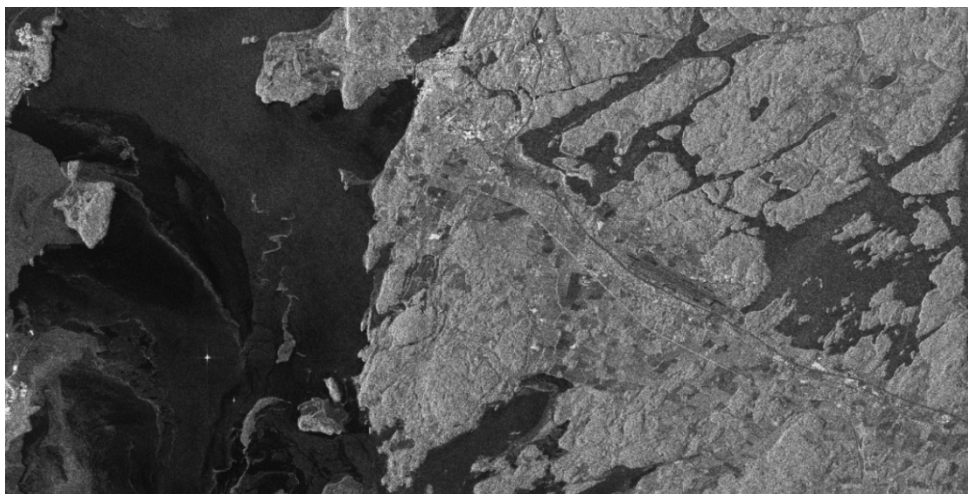


Figure 40. Segments of a RADARSAT-2 quad-polarised image over the Oslofjord are combined using different polarimetric decomposition methods. Top: Pauli, middle: Krogager and bottom: Yamaguchi.



### **CLASSIFICATION: UNCLASSIFIED**

All rights reserved. No part of this document may be reproduced or transmitted in any form or by any means, electronic, mechanical, photocopying, recording, or otherwise, without prior written permission of FFI, NLR or TNO.



**CLASSIFICATION: UNCLASSIFIED**

*All rights reserved. No part of this document may be reproduced or transmitted in any form or by any means, electronic, mechanical, photocopying, recording, or otherwise, without prior written permission of FFI, NLR or TNO.*



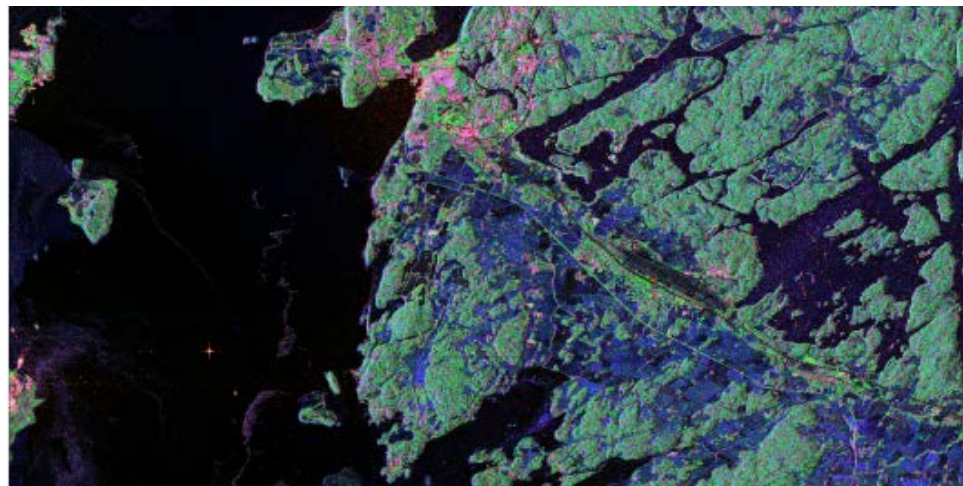
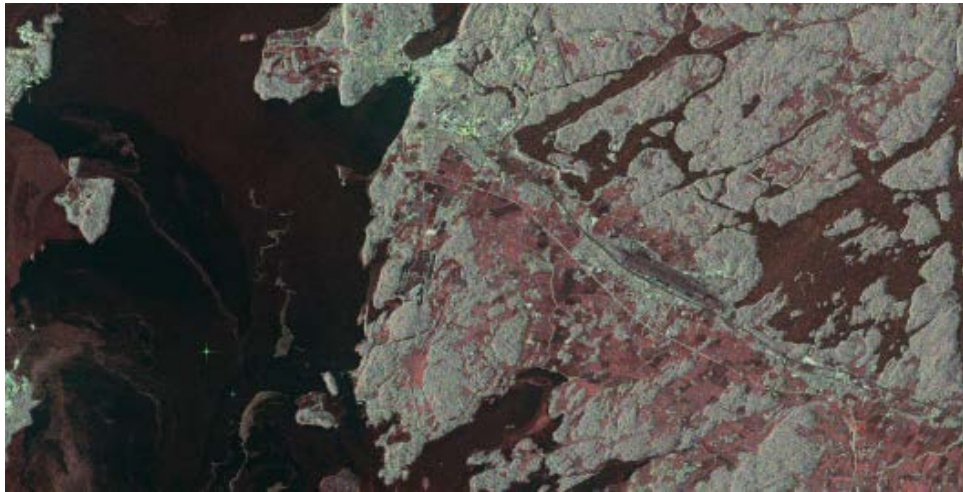


*Figure 41. RADARSAT-2 quad-polarised data over the Oslofjord is shown in different ways from top to bottom: HH-polarisation, VV-polarisation, HV-polarisation, Pauli, Krogager and Yamaguchi rotated.*

Figure 42 and figure 43 show 600 pixels x 600 pixels segments in 2D presentation of RADARSAT-2 quad-polarisation images. The ocean is suppressed in cross-polarisation and even more when multiplying cross-polarisation (HV) with double bounce (HH-VV). The vessels are less visible in surface (HH+VV) scattering and the ocean waves are visible. The ship to sea contrasts are best with cross-polarisation or for the combination (HH-VV) x HV.

### **CLASSIFICATION: UNCLASSIFIED**

*All rights reserved. No part of this document may be reproduced or transmitted in any form or by any means, electronic, mechanical, photocopying, recording, or otherwise, without prior written permission of FFI, NLR or TNO.*

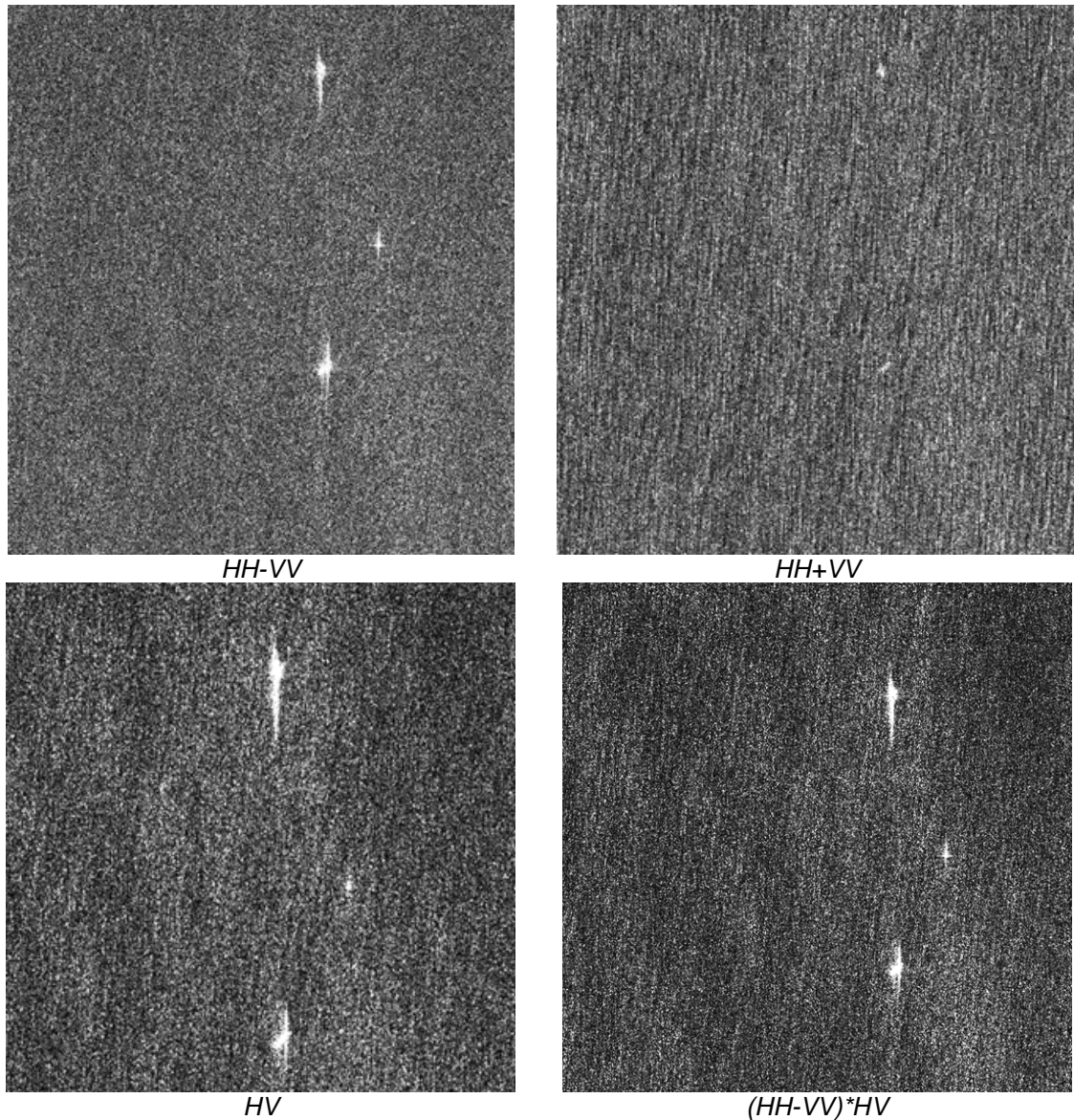


Figure 42. 600 pixels x 600 pixels shown in 2D segments of a RADARSAT-2 quad-polarisation image on November 29<sup>th</sup> 2009.

**CLASSIFICATION: UNCLASSIFIED**

All rights reserved. No part of this document may be reproduced or transmitted in any form or by any means, electronic, mechanical, photocopying, recording, or otherwise, without prior written permission of FFI, NLR or TNO.



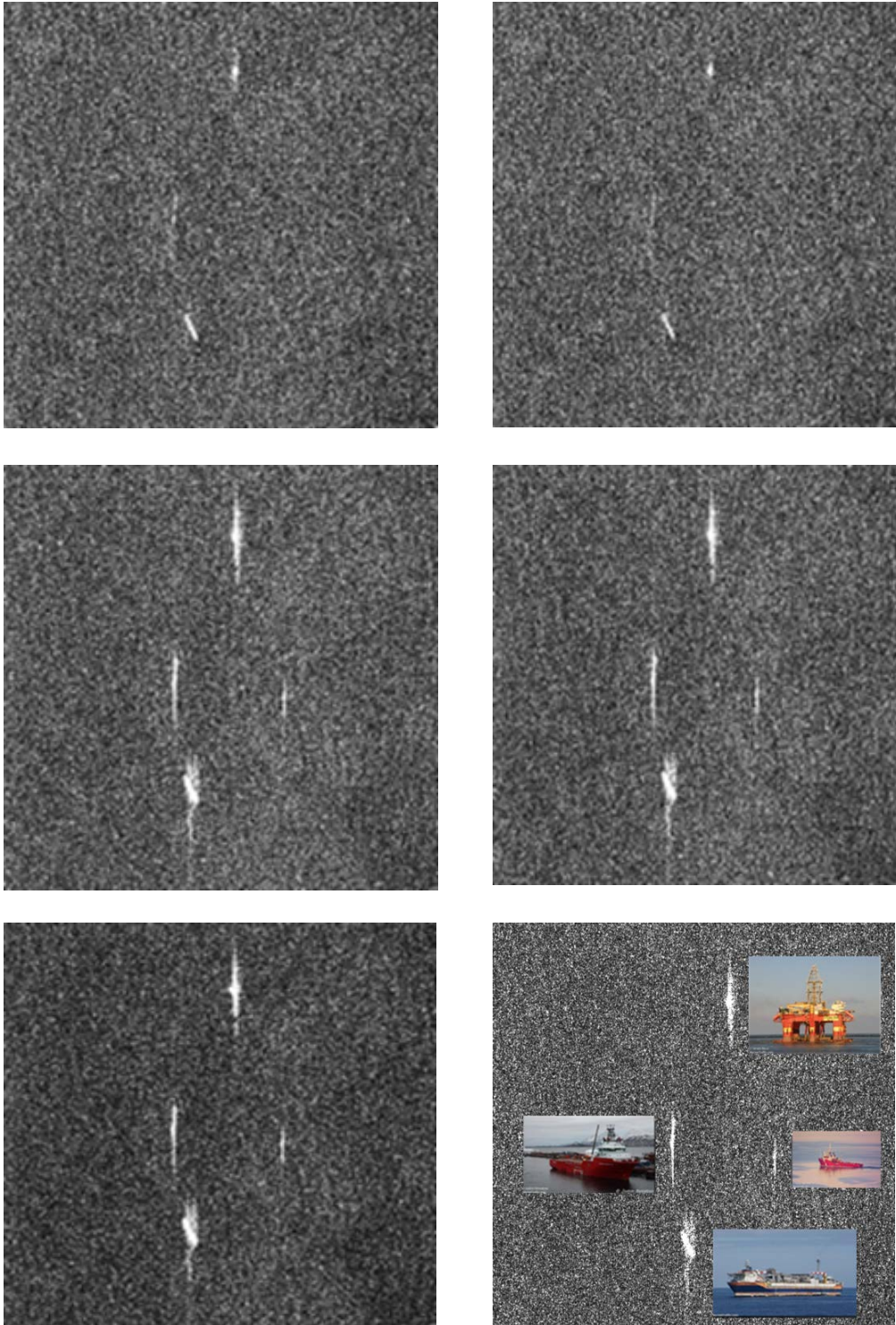


Figure 43. 600 pixels x 600 pixels 2D segments of RADARSAT-2 quad-polarisation data over the Norne field in different polarisations and polarisation combinations. Top left: HH, top right: VV, middle left: HV, middle right: VH and bottom left:  $(HH-VV)*HV$ . The different vessels are shown to the bottom right.

**CLASSIFICATION: UNCLASSIFIED**

All rights reserved. No part of this document may be reproduced or transmitted in any form or by any means, electronic, mechanical, photocopying, recording, or otherwise, without prior written permission of FFI, NLR or TNO.



Figure 44 shows 600 pixels x 600 pixels segments in 3D presentation of a RADARSAT-2 quad-polarisation image on November 29<sup>th</sup> 2009. It is shown how the ocean background can be suppressed by using different polarisations and polarisation combinations. (HH-VV)xHV gives clearly the best result with regards to suppressing the ocean background.

Figure 45- figure 48 show segments of 600 pixels x 600 pixels in 3D presentations of a RADARSAT-2 quad-polarisation image on December 10<sup>th</sup> 2009 and how the reflections differ in the different polarisation channels and polarisation combinations. Figure 45 shows HH, VV, HH-VV (double bounce) and (HH-VV)xHV (double bounce times volume scattering). Norne FPSO is at the top, Ocean Prince in the middle to the left and Skandi Mongstad (vessel) and Stenda Don (oil platform) are at the bottom (lying close together looking like one object in the SAR image). Figure 46 shows circular basis decomposition method, RR and RL, figure 47 shows Krogager decomposition method, while figure 48 shows Yamaguchi decomposition method with rotation. Surface waves are visible in Yamaguchi surface rotated. Norne FPSO is at incidence angle 40.9°.

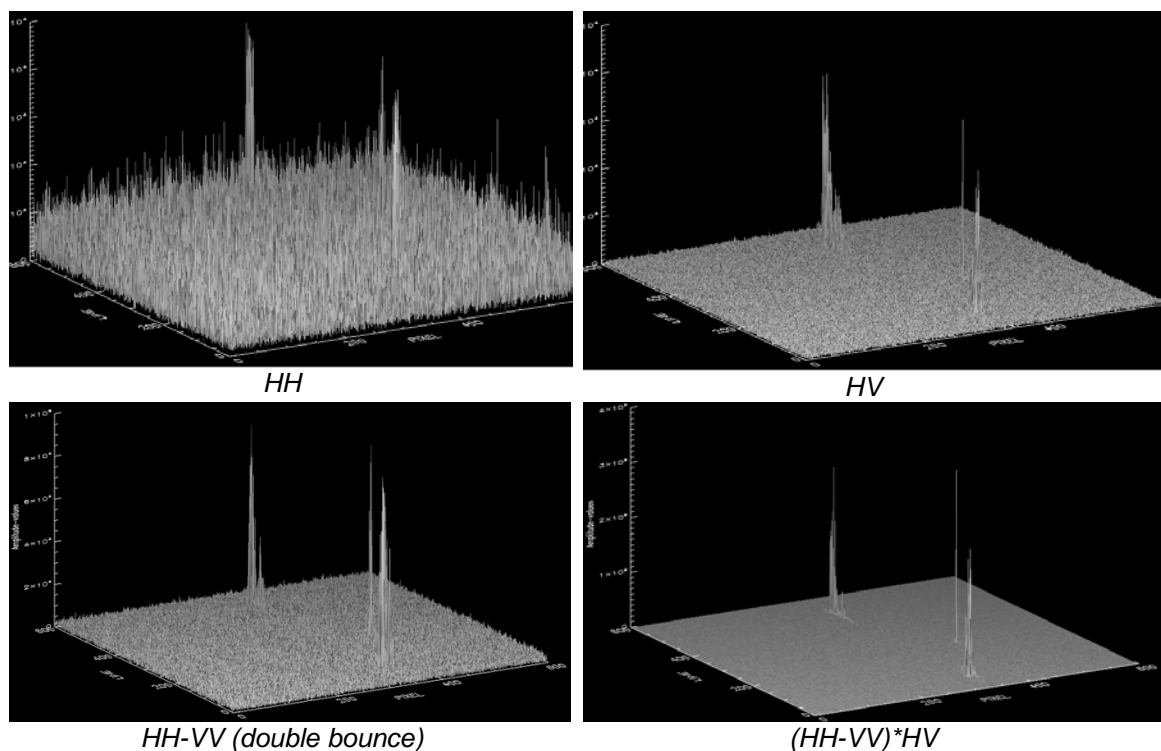


Figure 44. 600 pixels x 600 pixels shown in 3D of a RADARSAT-2 quad-polarisation image on November 29<sup>th</sup> 2009.

**CLASSIFICATION: UNCLASSIFIED**

All rights reserved. No part of this document may be reproduced or transmitted in any form or by any means, electronic, mechanical, photocopying, recording, or otherwise, without prior written permission of FFI, NLR or TNO.

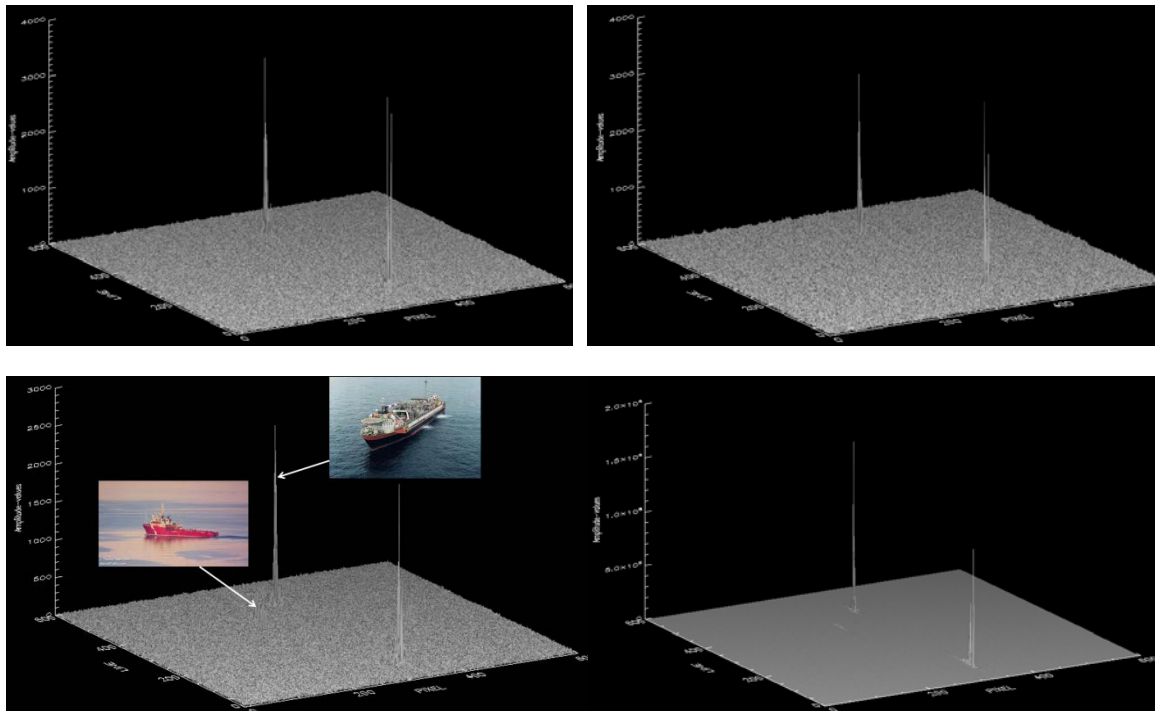


Figure 45. 600 pixels x 600 pixels segments of RADARSAT-2 quad-polarisation data on December 10<sup>th</sup> 2009 in different polarisations and polarisation combinations. Top left: HH, top right: VV, bottom left: HH-VV, bottom right: (HH-VV)xHV. Norne FPSO (right) and Ocean Prince (left) are shown with the arrows.

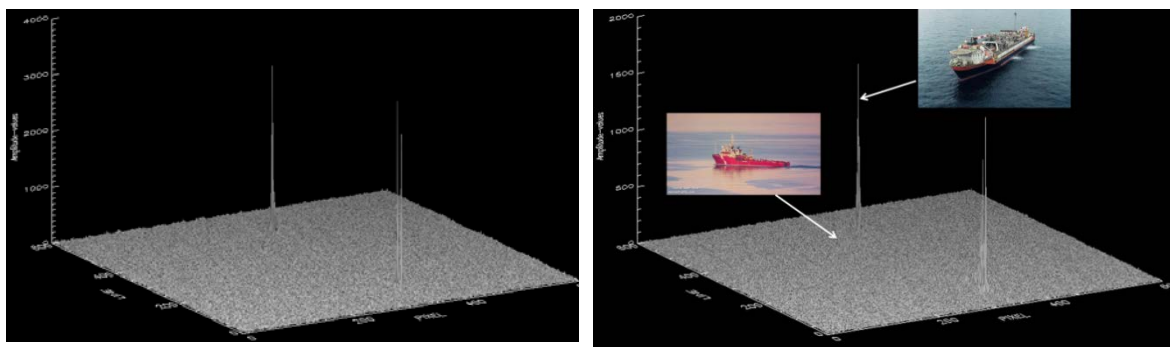


Figure 46. 600 pixels x 600 pixels segments of RADARSAT-2 quad-polarisation data on December 10<sup>th</sup> 2009 in circular basis decomposition, RR (left) and RL (right). Norne FPSO (right) and Ocean Prince (left) are shown with the arrows.

**CLASSIFICATION: UNCLASSIFIED**

All rights reserved. No part of this document may be reproduced or transmitted in any form or by any means, electronic, mechanical, photocopying, recording, or otherwise, without prior written permission of FFI, NLR or TNO.

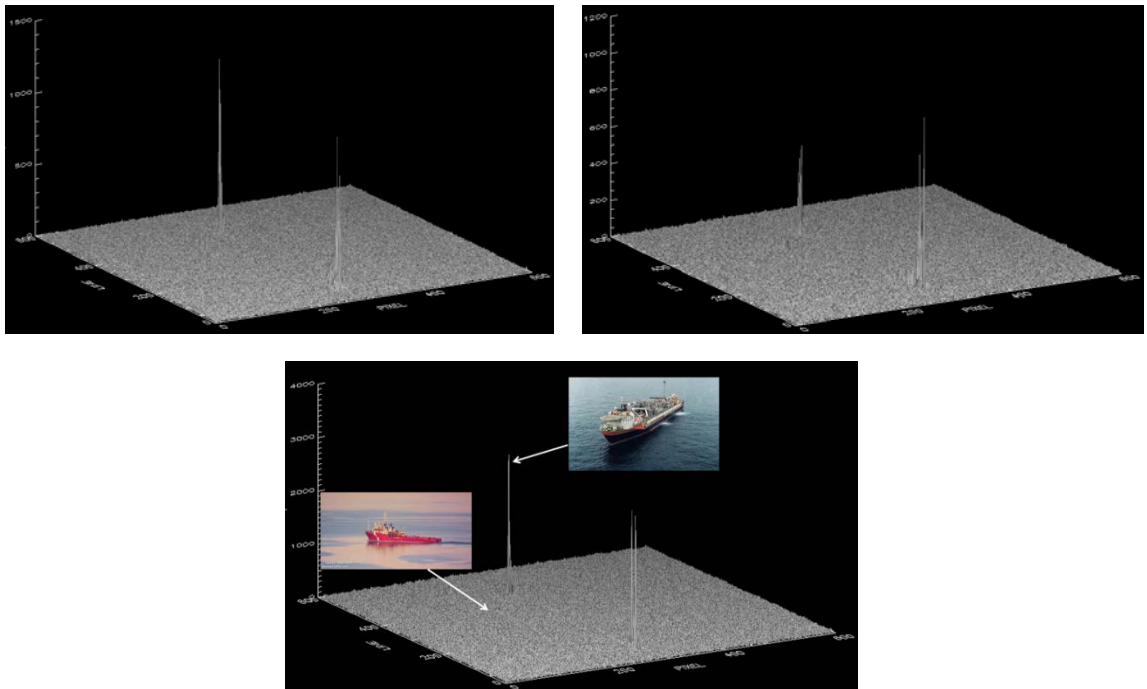


Figure 47. 600 pixels x 600 pixels segments of RADARSAT-2 quad-polarisation data on December 10<sup>th</sup> 2009 in Krogager decompositions. Top left: kDiplane, top right: kHelix and bottom: kSphere. Norne FPSO (right) and Ocean Prince (left) are shown with the arrows.

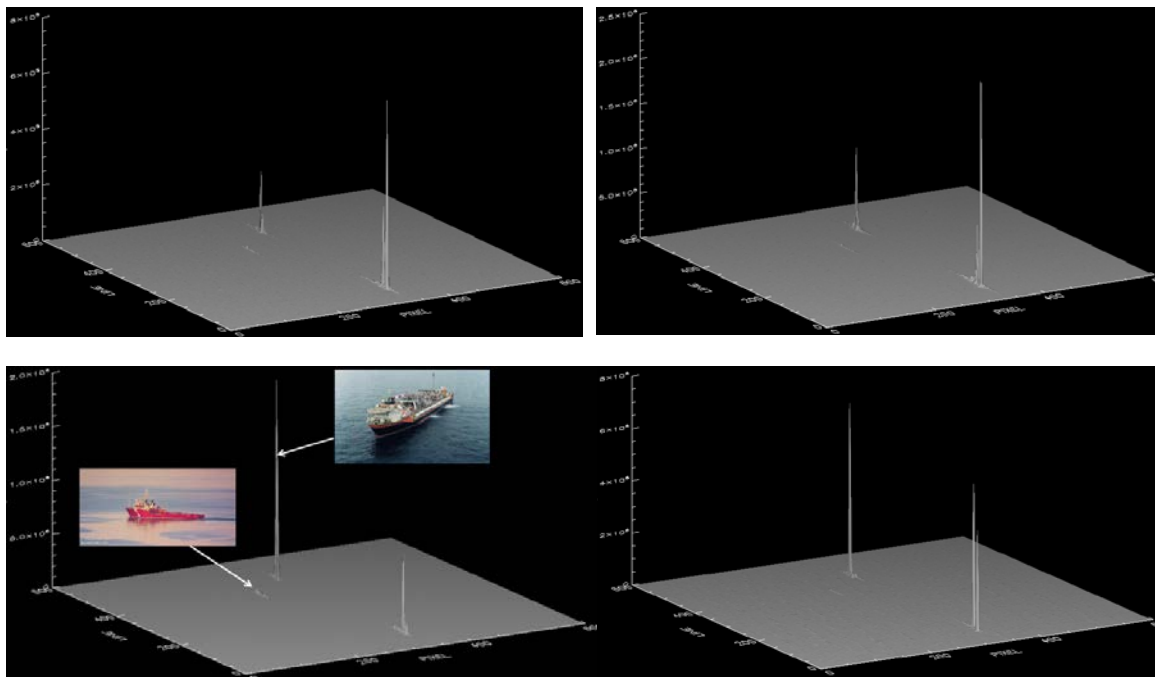


Figure 48. 600 pixels x 600 pixels segments of RADARSAT-2 quad-polarisation data on December 10<sup>th</sup> 2009 using Yamaguchi decomposition method. Top left: Yamaguchi helix rotated, top right: volume rotated, bottom left: double rotated and bottom right: surface rotated. Norne FPSO (right) and Ocean Prince (left) are shown with the arrows.

**CLASSIFICATION: UNCLASSIFIED**

All rights reserved. No part of this document may be reproduced or transmitted in any form or by any means, electronic, mechanical, photocopying, recording, or otherwise, without prior written permission of FFI, NLR or TNO.

Table 5 shows ship to sea contrasts of the oil production vessel Norne FPSO and Ocean Prince for different polarisations and different polarisation combinations. Table 6 and 7 contrast measures, both amplitude and intensity, of Norne FPSO and Ocean Prince for different polarisations and polarisation combinations. The results indicate what we have seen in the previous figures.

*Table 5. Maximum amplitude divided by mean sea for Norne FPSO on November 29<sup>th</sup> 2009 and December 1<sup>st</sup> 2009 for different polarisations and polarisation combinations.*

		R = Maximum amplitude / mean sea									
Date	Time	HH	VV	HV	VH	RR	LL	RL	LR	HH-VV	HH-VV * HV
29/11-09	06:14	7	7	59	60	6	6	60	50	46	1991
1/12-09	16:48	8	6	40	41	6	6	46	35	33	1100

**CLASSIFICATION: UNCLASSIFIED**

*All rights reserved. No part of this document may be reproduced or transmitted in any form or by any means, electronic, mechanical, photocopying, recording, or otherwise, without prior written permission of FFI, NLR or TNO.*

Table 6. Maximum amplitude divided by mean sea for Norne FPSO on December 10<sup>th</sup> 2009.

Method	Max. amplitude / mean sea	
	Norne FPSO	Ocean Prince
<i>HH</i>	193	18
<i>VV</i>	112	8
<i>HV</i>	123	22
<i>VH</i>	135	23
<i>HH-VV</i>	155	22
<i>RR</i>	150	8
<i>RL</i>	169	17
<i>kSphere</i>	150	8
<i>kHelix</i>	112	32
<i>Sqrt((HH-VV)×HV)</i>	149	20
<i>Sqrt(Yamaguchi helix)</i>	79	13
<i>Sqrt(Yamaguchi volume)</i>	81	11
<i>Sqrt(Yamaguchi surface)</i>	80	5
<i>Sqrt(Yamaguchi double)</i>	230	31
<i>Sqrt(Yamaguchi double rot.)</i>	234	29

**CLASSIFICATION: UNCLASSIFIED**

All rights reserved. No part of this document may be reproduced or transmitted in any form or by any means, electronic, mechanical, photocopying, recording, or otherwise, without prior written permission of FFI, NLR or TNO.

Table 7. Maximum intensity divided by mean sea intensity for Norne FPSO on December 10<sup>th</sup> 2009.

	Max. intensity / mean sea intensity	
Method	Norne FPSO	Ocean Prince
<i>HH<sup>2</sup></i>	28982	253
<i>VV<sup>2</sup></i>	9833	56
<i>HV<sup>2</sup></i>	11843	382
<i>(HH-VV)×HV</i>	18707	349
<i>Yamaguchi helix</i>	5044	141
<i>Yamaguchi volume</i>	5950	120
<i>Yamaguchi surface</i>	6012	21
<i>Yamaguchi double</i>	35521	748
<i>Yamaguchi double rot.</i>	39374	671

### 3.4.3 Compact polarimetry

Compact polarimetry seems to be the preferred choice for the wide swath modes of some of the future radar satellites. The Indian satellite RISAT is in orbit and the Canadian Radarsat Constellation Mission (RCM) is planned for launch in 2018. Both missions offer compact polarimetry. Simulations can be done on compact polarimetry based on quad-polarised data from RADARSAT-2. Some examples of simulations of compact polarimetry from RADARSAT-2 quad-polarisation data will be shown in this sub-chapter.

In quad-polarised data the radar transmits both in horizontal and vertical polarisation and receives both in horizontal and vertical polarisation, giving four different polarisation options: HH, VV, HV and VH. Compact polarimetry can be implemented in three different modes:

1. Dual Circular Polarimetry (DCP) mode where 1 circular polarisation (either R or L) is transmitted and both circular polarisations are received (R and L).
2. Circular Transmit – Linear Receive (CTLR) mode where 1 circular polarisation (either R or L) is transmitted and both linear polarisations are received (H and V).
3. Pi/4 mode where 1 pi/4 (H + V) is transmitted and both horizontal and vertical polarisation are received (H and V).

### **CLASSIFICATION: UNCLASSIFIED**

All rights reserved. No part of this document may be reproduced or transmitted in any form or by any means, electronic, mechanical, photocopying, recording, or otherwise, without prior written permission of FFI, NLR or TNO.



The CTRLR mode has been selected as the CP (Circular Polarimetry) mode in the RCM Satellites. FFI (Norwegian Defence Research Establishment) has used RADARSAT-2 quad-polarisation data to simulate Dual Circular Polarimetry (DCP) mode. The circular polarisation components RR and RL are first computed from the quad-polarisation data. The Pauli components surface scattering (HH+VV), double bounce scattering (HH-VV) and cross-polarisation (HV) are then computed directly from (RR,RL). The product which maximizes the ship to sea contrast for ship detection is (HH-VV)\*HV, and this product can then easily be computed.

Figure 49 shows Dual Circular Polarimetry (DCP) mode double bounce simulation and quad-polarisation double bounce (HH-VV). The compact polarimetry estimates the double bounce slightly different from full polarimetry. Figure 50 shows DCP mode surface simulation and quad-polarisation surface (HH+VV). The compact polarimetry estimates the surface scattering close to quad-polarisation data. Figure 51 shows DCP mode cross-polarisation (HV) scattering simulation and quad-polarisation HV-scattering. It can be seen from figure 51 that the compact polarimetry overestimates the HV-scattering in urban areas. The same is observed by Nord et al. [13], and they conclude that all compact polarimetric modes tend to overestimate the HV-scattering contribution. Figure 52 also shows what was shown by Nord et al that DCP overestimates the HV-scattering contribution. Blue is surface scattering, red is double bounce scattering and green is cross-polarisation scattering. Figure 53 shows quad-polarisation HV and DCP mode product (HH-VV)\*HV (double bounce times HV), and it is shown that the vessels are more easily visible in the DCP product which is promising for ship detection. It can also be seen that the ocean background is more suppressed in the simulated DCP product image than in the quad-polarisation HV-image.

## **CLASSIFICATION: UNCLASSIFIED**

*All rights reserved. No part of this document may be reproduced or transmitted in any form or by any means, electronic, mechanical, photocopying, recording, or otherwise, without prior written permission of FFI, NLR or TNO.*



Figure 49. Top: DCP double bounce simulation (HH-VV). Bottom: Quad-polarisation double bounce (HH-VV).

**CLASSIFICATION: UNCLASSIFIED**

All rights reserved. No part of this document may be reproduced or transmitted in any form or by any means, electronic, mechanical, photocopying, recording, or otherwise, without prior written permission of FFI, NLR or TNO.

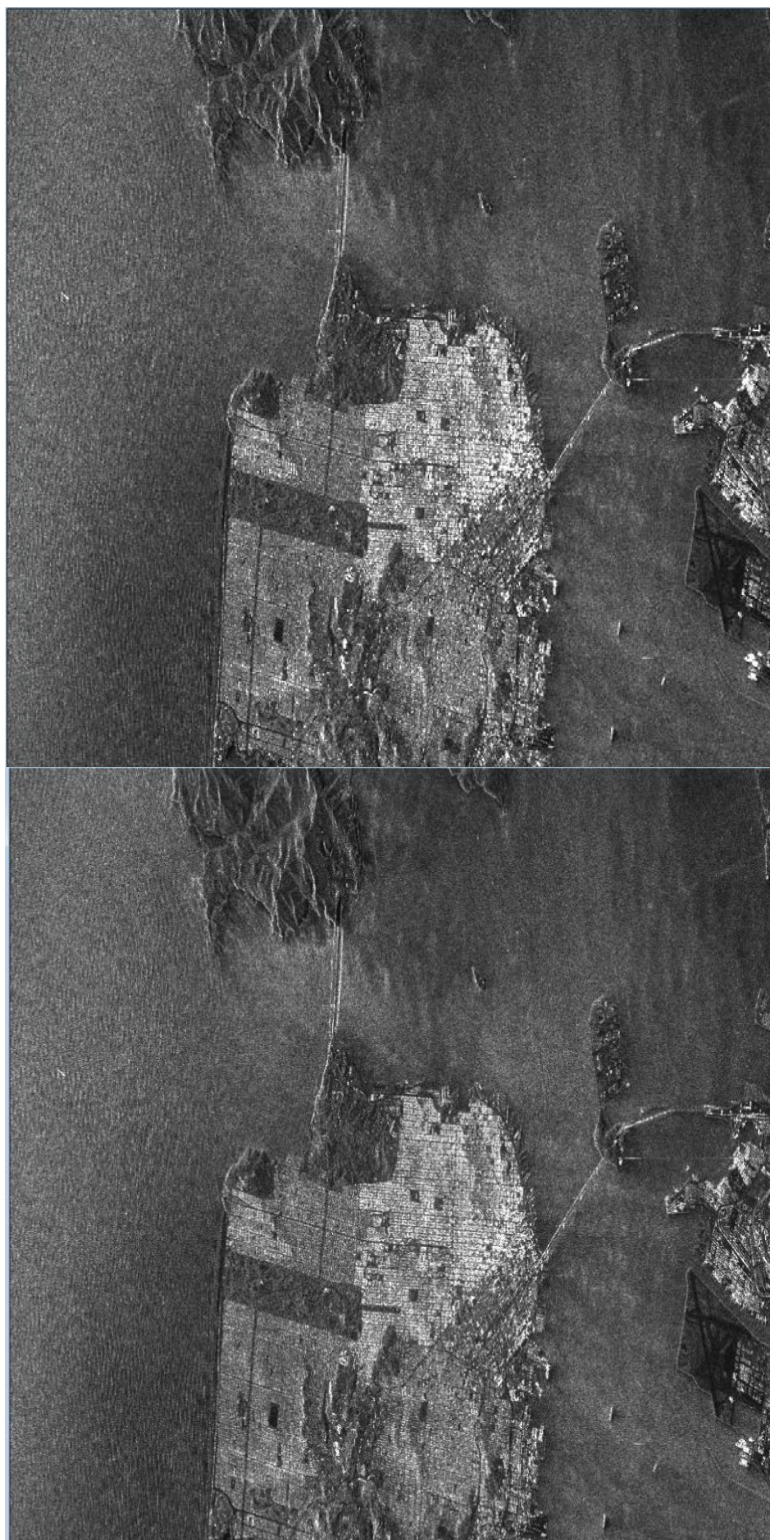


Figure 50. Top: DCP surface simulation (HH+VV). Bottom: Quad-polarisation surface (HH+VV).

**CLASSIFICATION: UNCLASSIFIED**

All rights reserved. No part of this document may be reproduced or transmitted in any form or by any means, electronic, mechanical, photocopying, recording, or otherwise, without prior written permission of FFI, NLR or TNO.





*Figure 51. Top: DCP volume simulation (HV). Bottom: Quad-polarisation volume (HV).*

**CLASSIFICATION: UNCLASSIFIED**

*All rights reserved. No part of this document may be reproduced or transmitted in any form or by any means, electronic, mechanical, photocopying, recording, or otherwise, without prior written permission of FFI, NLR or TNO.*

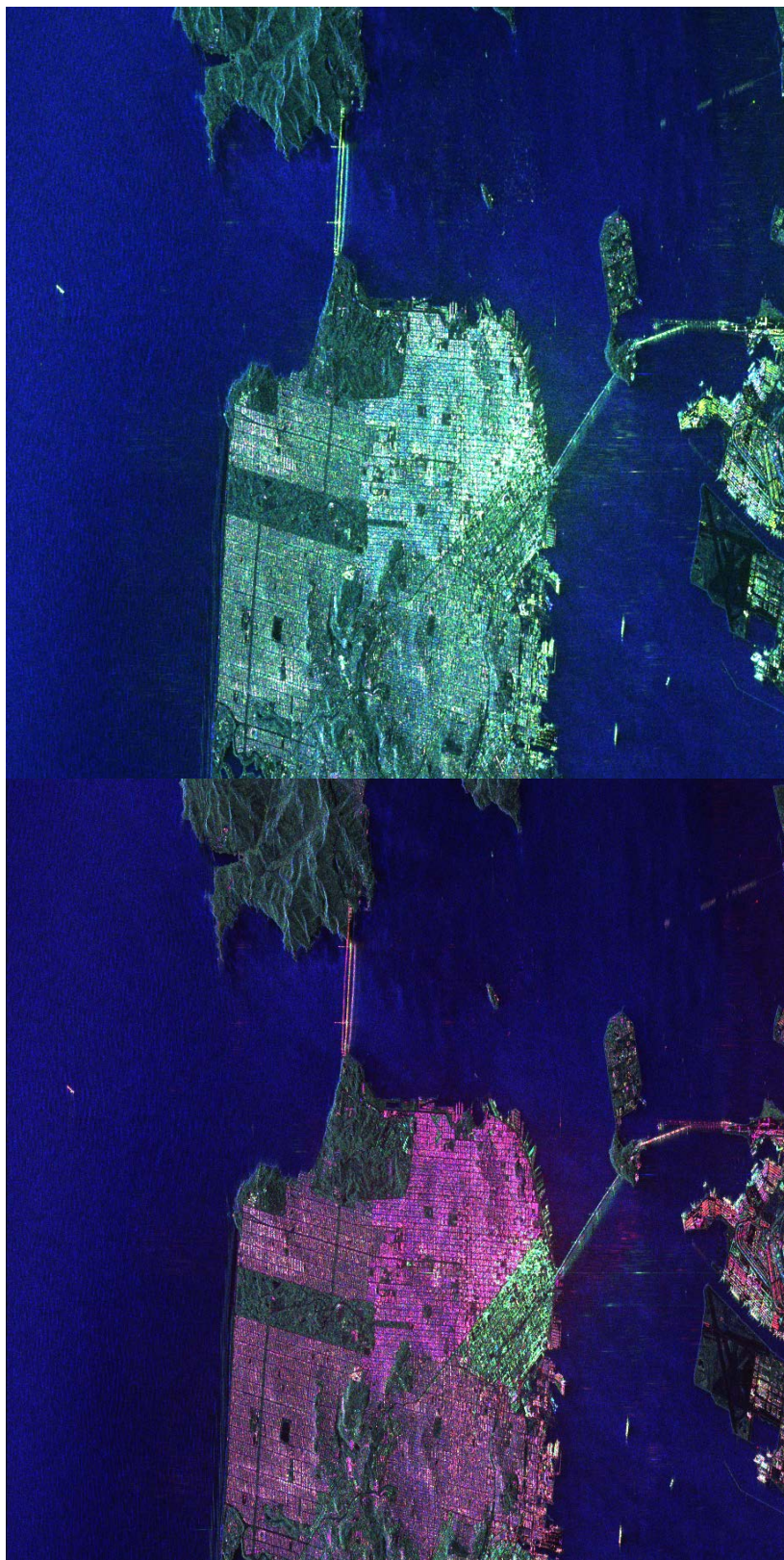


Figure 52. Top: DCP Pauli decomposition. Bottom: Quad-polarisation Pauli decomposition.

**CLASSIFICATION: UNCLASSIFIED**

All rights reserved. No part of this document may be reproduced or transmitted in any form or by any means, electronic, mechanical, photocopying, recording, or otherwise, without prior written permission of FFI, NLR or TNO.



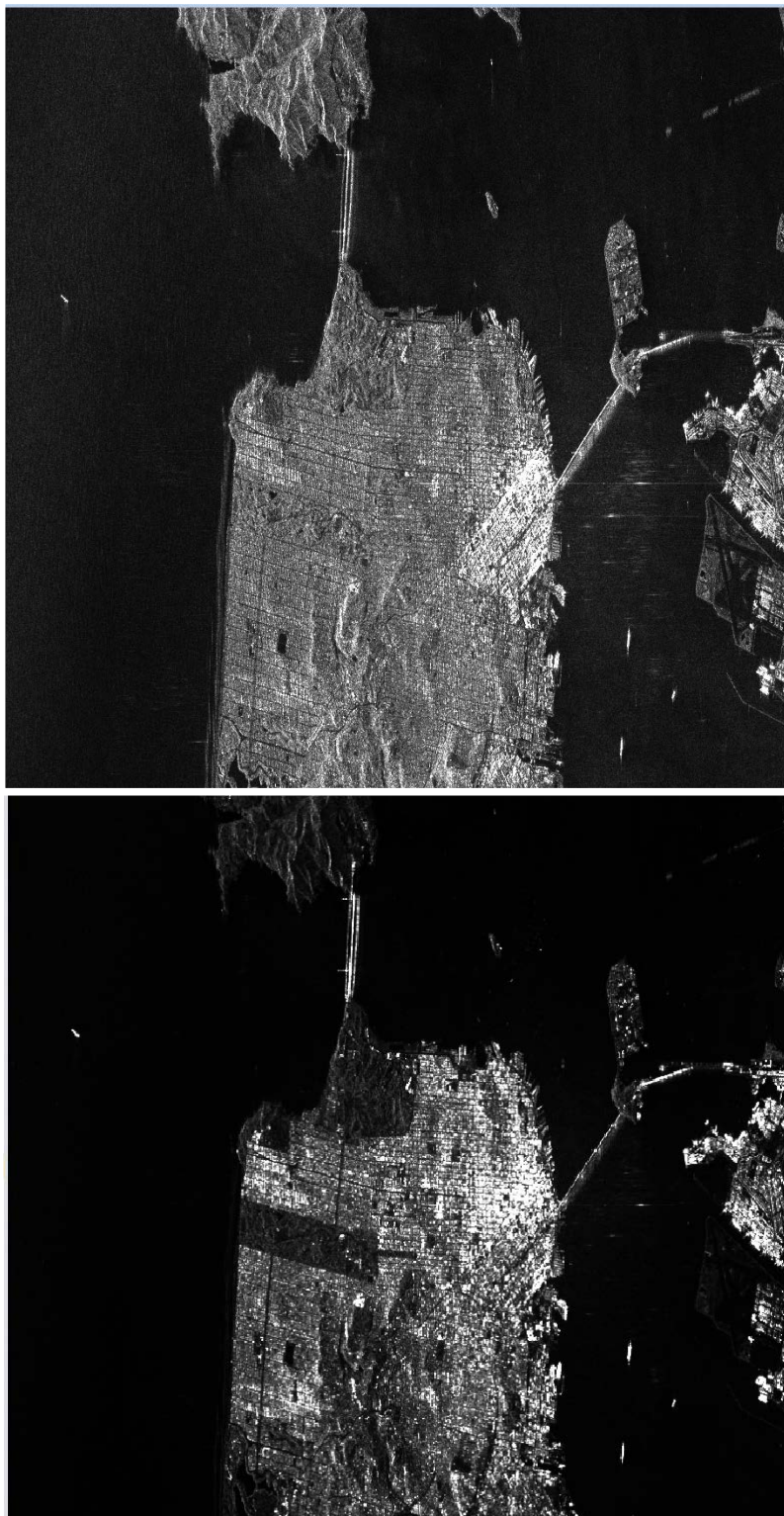


Figure 53. Top: Quad-polarisation volume (HV) scattering. Bottom: DCP product (HH-VV)\*HV.

**CLASSIFICATION: UNCLASSIFIED**

All rights reserved. No part of this document may be reproduced or transmitted in any form or by any means, electronic, mechanical, photocopying, recording, or otherwise, without prior written permission of FFI, NLR or TNO.



## 4 Geospatial information products and dissemination

### 4.1 Introduction

This chapter focuses on information products based on satellite data. Information is produced using extraction techniques described in the previous sections, and combined with context information to answer military questions. Important context information is given by elevation data which are often based on space-borne data. An overview of elevation data is given and the quality of the various elevation data sets is discussed.

Usually space borne data can only give a part of the answer of a military question. We will describe workflows of satellite data to half-finished products and to final GeoInt products when fused with other (context) data. Finally the dissemination of GeoInt products is discussed, where standardisation plays an important role.

### 4.2 Geospatial context data - 3D models from space

#### 4.2.1 Inventory of relief data

Elevation (height) models or DEMs give height values for grid cells (posting) in a map. The height value is usually given as meters above the sea surface or more accurately above the Earth Gravitational Model 1996 (EGM96). Values are usually expressed in signed 16 bit (2 bytes). The height can refer to the terrain level (terrain models) or can include the height of surface objects such as vegetation, buildings etc (surface models). Traditionally the height is derived from triangular measurements and later on from stereo photogrammetry. Currently height measurements are also obtained by satellites using optical stereo measurements and interferometry with radar. Also LIDAR measurements from airplanes are used. Height models are important to assess the line-of-sight, the slope and to correct for distortions in images due to oblique or slant range viewing.

There are national digital and global elevation models. Global elevation models have been defined by the [National Geospatial-Intelligence Agency](#) (NGA), called DTED (Digital terrain elevation data). There are several levels to discriminate, of which level 1 and 2 are most commonly used (posting 90 m/3 arcsec and 30 m/1 arcsec). The present (open) sources to obtain global models are:

- SRTM data (<http://www2.jpl.nasa.gov/srtm/>). Available for 90 meter (3 arcsec posting) as open source. For military use 1 arcsec is available, see DTED level 2.

## **CLASSIFICATION: UNCLASSIFIED**

*All rights reserved. No part of this document may be reproduced or transmitted in any form or by any means, electronic, mechanical, photocopying, recording, or otherwise, without prior written permission of FFI, NLR or TNO.*

- Aster GDEM (Global Digital Elevation Map), posting 30 meters, (<http://asterweb.jpl.nasa.gov/gdem.asp> or <http://gdem.ersdac.jspacesystems.or.jp/>)
- Tandem-X worldDEM, 12m posting (<http://www.astrium-geo.com/en/168-tandem-x-global-dem>).

For a collection of open source global elevation data a number of web sites can be found. e.g.

- Collection of global elevation data from open sources on <http://www.viewfinderpanoramas.org/dem3.html>

For National elevation data we refer here to:

- Norway: Elevation data with 10 posting are available (kartverket\_terrengmodeller). (<http://www.statkart.no/Kart/Kartdata/Terrengmodeller/Terrengmodell-10-meters-grid/> )
- Netherlands: AHN (Actueel Hoogtebestand Nederland) data with are available with a posting of 5 meter, resampled from 0.5 meter based on laser altimetry measurements (<http://www.ahn.nl/>).

#### **4.2.2 Evaluation**

##### **SRTM**

Data are from the C-band and X-band antenna on board of the Shuttle Radar Topographical Mission (SRTM) in February 2000 and are processed interferometrically to height models. Due to shadowing and interferometric effects for steep slopes the model contain so-called voids, especially in steep terrain which have to be corrected. A number of studies have been addressed to this topic. For example the Cigliar consortium has produced a void free version (<http://www.cgiar-csi.org/data/srtm-90m-digital-elevation-database-v4-1>). Also SRTM Void filled data from USGS are available. These data are filled with interpolation and additional sources if needed (<https://lta.cr.usgs.gov/node/375>). The free data always refer to the 90 meter posting data. Height accuracy is in the order 5 m (relative) and 10 m (absolute). A disadvantage is that these data are only available for latitudes below 60 degrees North and above 56 degrees South due to the orbit of the Shuttle. The SRTM data are currently the standard global DEM. On average the data are reliable, except that in mountainous areas reliability can vary due to the void filling.

### **CLASSIFICATION: UNCLASSIFIED**

*All rights reserved. No part of this document may be reproduced or transmitted in any form or by any means, electronic, mechanical, photocopying, recording, or otherwise, without prior written permission of FFI, NLR or TNO.*

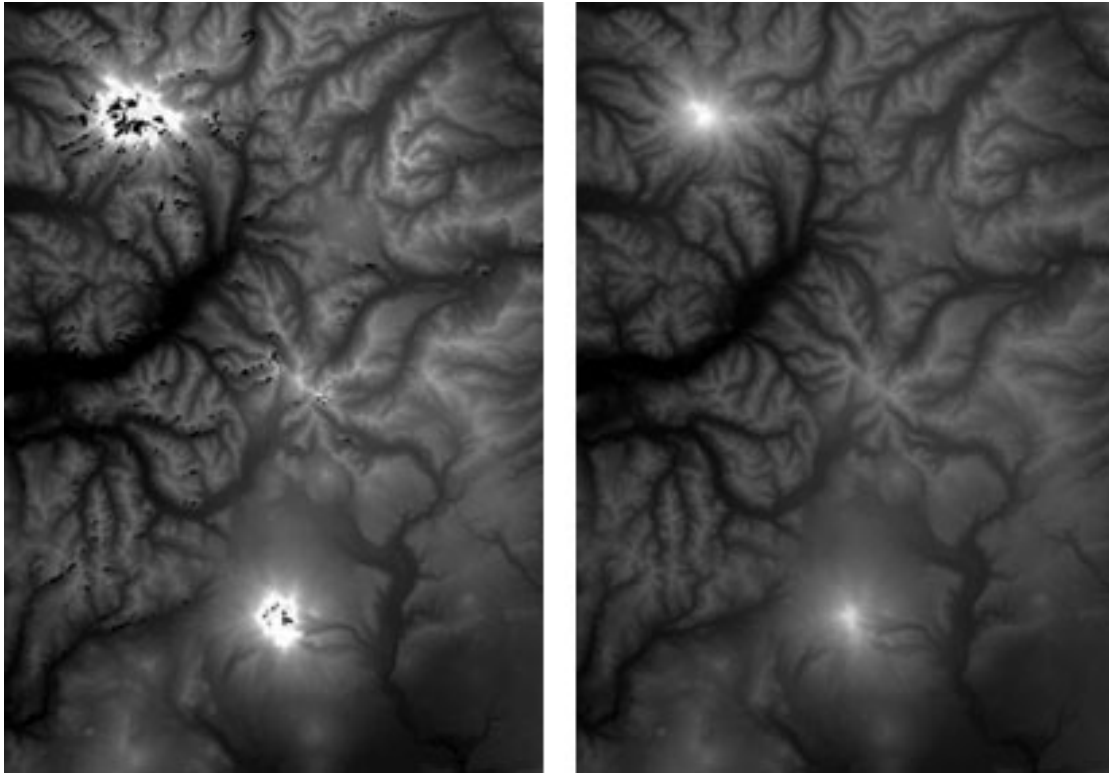


Figure 54 Example of SRTM data before and after void filling (NGA) of Mt Rainier and Mt Adams in the Cascade Mountain range (USA).

### GDEM

The Aster GDEM is produced on basis of stereo data from the multispectral Aster instrument on board of the Terra satellite. Data are collected over several years and cover the whole earth with a resolution of 15 to 90 meters. The Aster GDEM has the advantage that is available also for the higher latitudes compared to the SRTM data. The posting is 30 meters. For an impression see below (left ASTER GDEM) and (right SRTM DEM)

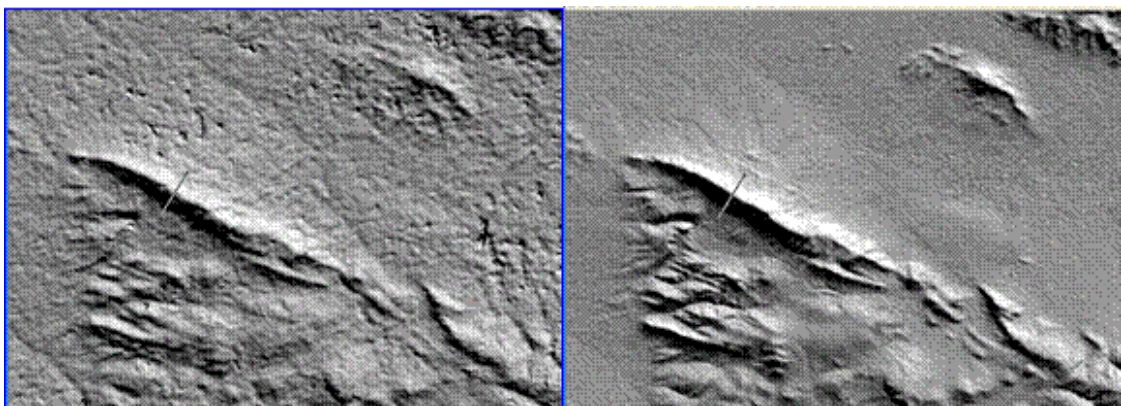


Figure 55 GDEM (left) and SRTM DEM (right).

### **CLASSIFICATION: UNCLASSIFIED**

All rights reserved. No part of this document may be reproduced or transmitted in any form or by any means, electronic, mechanical, photocopying, recording, or otherwise, without prior written permission of FFI, NLR or TNO.

An extensive comparison can be found on the NIMA website (<http://earth-info.nima.mil/GandG/elevation/index.html>). It is concluded in this document that:

Overall, the quality of the ASTER GDEM appears to be less than the SRTM DTED<sup>®</sup> 2. Although the aggregated error statistics are not that bad in many areas, the data in its present form would be very difficult to trust and use without careful review and editing. Within the SRTM coverage area (56° S to 60° N), the ASTER data may be useful for filling voids in the SRTM DTED<sup>®</sup> on a case-by-case basis after a thorough examination. Above 60° N where no SRTM DTED<sup>®</sup> are available and where other DEM data are scarce, ASTER has problems. There are obviously ASTER scenes available at these latitudes, but the data need to be reprocessed to remove the major anomalies and artefacts that are present. Even then, one would need to examine an area's data for inconsistencies before using them. The lack of water body depiction and the frequency of artefacts would require extensive editing and filtering of the ASTER GDEM to convert it to a DTED<sup>®</sup> product. At best, the ASTER GDEM can be used as an independent source of elevation data for areas where no other reliable data exist, and could be used on a case-by-case basis to support specific applications.

The general conclusion is that Aster GDEM data are generally less reliable and useful than the SRTM data, especially for the details.

### **Tandem-X (WorldDEM).**

Tandem-X WorldDEM (World Digital Elevation Model) data are derived from the interferometry processing from the twin TerraSAR-X satellites, and aim to be much more precise (DTED level 3, posting 12 meters, height resolution 2 meters relative and 4 meter absolute) than the SRTM data (DTED level 2). Data collection is still continuing and the first global DEM data will be available in 2014. Processing is huge task and for military purposes a project comparable to the MGCP project has been defined (TRES – TanDEM-X High Resolution Elevation Data Exchange Program). An impression of the Tandem-X data compared to the STRM data is shown below.

## **CLASSIFICATION: UNCLASSIFIED**

*All rights reserved. No part of this document may be reproduced or transmitted in any form or by any means, electronic, mechanical, photocopying, recording, or otherwise, without prior written permission of FFI, NLR or TNO.*



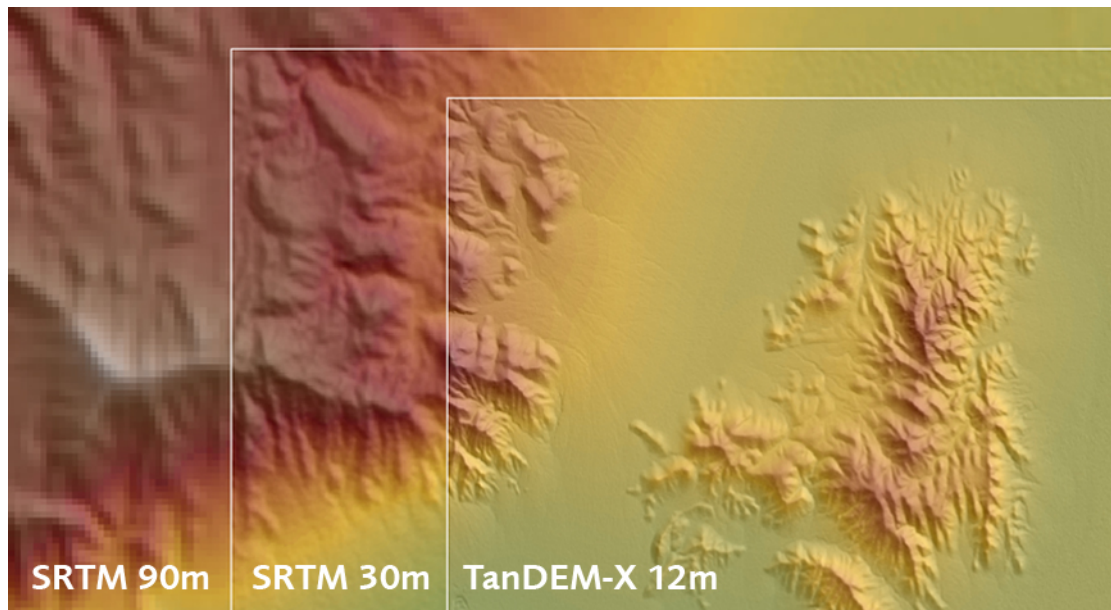


Figure 56 Comparison of the different levels of elevation data from radar (SAR) measurements.

**Comment on open source data.**

The *viewfinderpanoramas* site (<http://viewfinderpanoramas.org/>) is an open source site where elevation data is collected on personal initiative by Jonathan de Ferranti BA for viewing 3D panoramas. The site shows a professional impression and references to the data are given, although it is often difficult to determine the reliability of the data. 3 arcsec data are derived from the SRTM mission and 1 arcsec data are from national surveys if they are made available publically (e.g. the Alps). For Northern Europa (Norway, Finland and Denmark) 10 meter data are also available. For Sweden, Germany and Northern Russia the 10 meter DEM is derived using the contours extracted from 1:100,000 Russian topographic maps. Below a comparison of these 10 meter data compared to GDEM data is shown. The GDEM data clearly show artefacts not present in the data from the *viewfinderpanoramas* site.

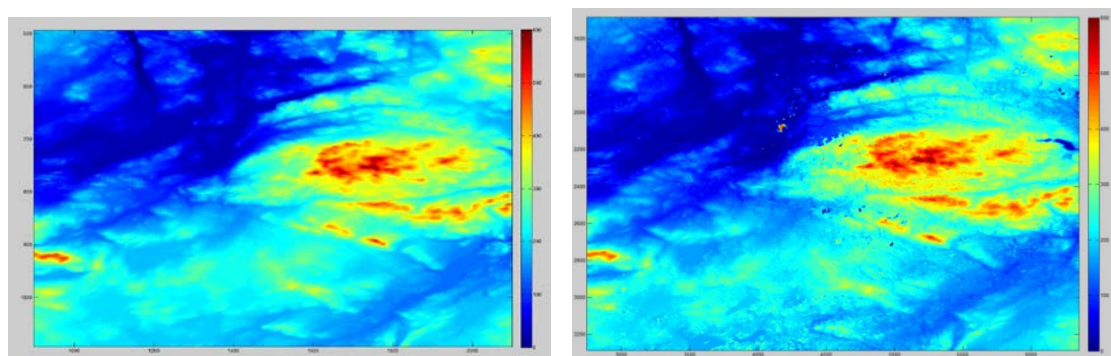


Figure 57 Comparison of open source elevation data based on topographical maps (left) compared to GDEM (right) for the area of Nikel.

**CLASSIFICATION: UNCLASSIFIED**

All rights reserved. No part of this document may be reproduced or transmitted in any form or by any means, electronic, mechanical, photocopying, recording, or otherwise, without prior written permission of FFI, NLR or TNO.



**Norway DEM**

The Norwegian survey gives DEM data with 10 meter posting with accuracies of 2-6 meters. Figure 58 shows an example for the area near the Ørland airbase. The left shows the Norwegian survey DEM and the right shows the corresponding GDEM. At global level the DEMs are comparable (top level), but at detailed level showing the peninsula with the airfield, the Norwegian DEM is clearly of superior quality compared to the GDEM.

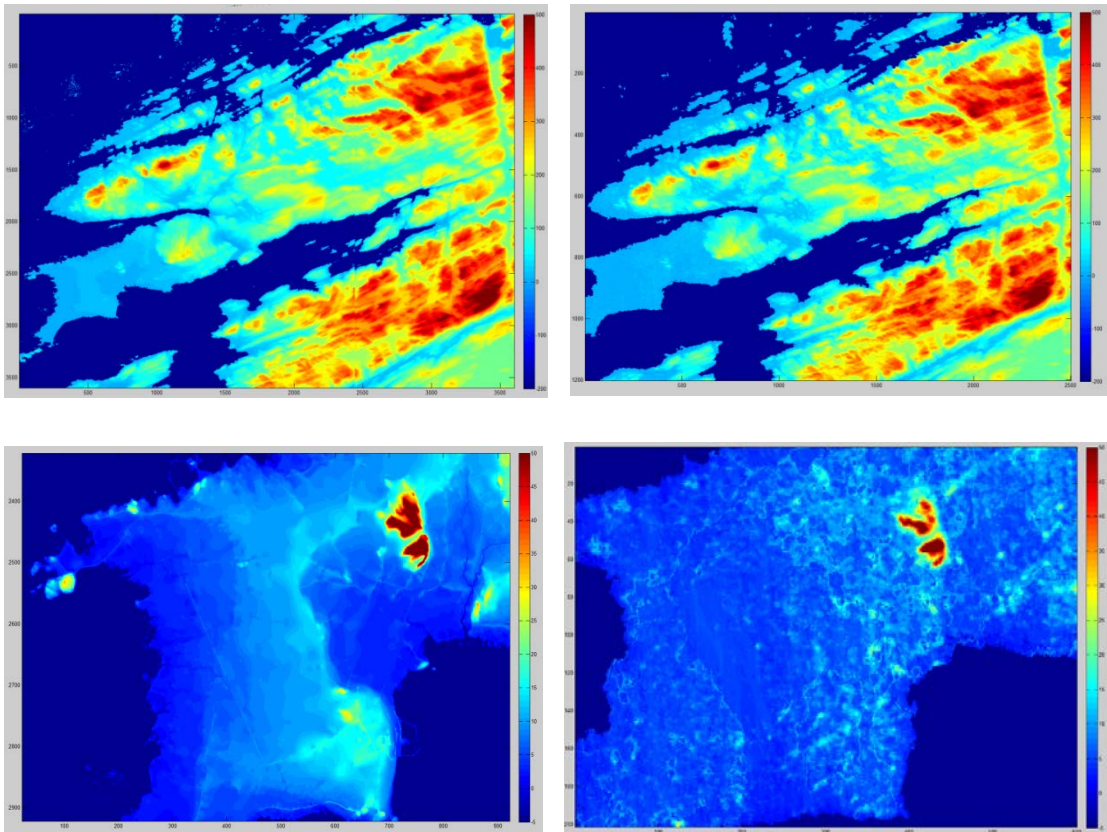


Figure 58 Comparison of Norwegian survey elevation data (left) compared to GDEM (right) for the area near Ørland air base. Global view (top) and detailed view (bottom).

**Netherlands DEM**

A large part of the Netherlands is flat within a few meters, so that the global DEMs do not give much information. For water management and governance purposes a very accurate height model (AHN) has been measured using LIDAR measurements (starting in 1996), which is recently available as open source. The original posting is 50 cm and a practical posting is 5 meters. The systematic accuracy is 5 cm, but the actual accuracy is determined by the statistical

**CLASSIFICATION: UNCLASSIFIED**

All rights reserved. No part of this document may be reproduced or transmitted in any form or by any means, electronic, mechanical, photocopying, recording, or otherwise, without prior written permission of FFI, NLR or TNO.

variation within the posting. The DEM is typically a surface height model showing the height of vegetation and buildings (see Figure 59).

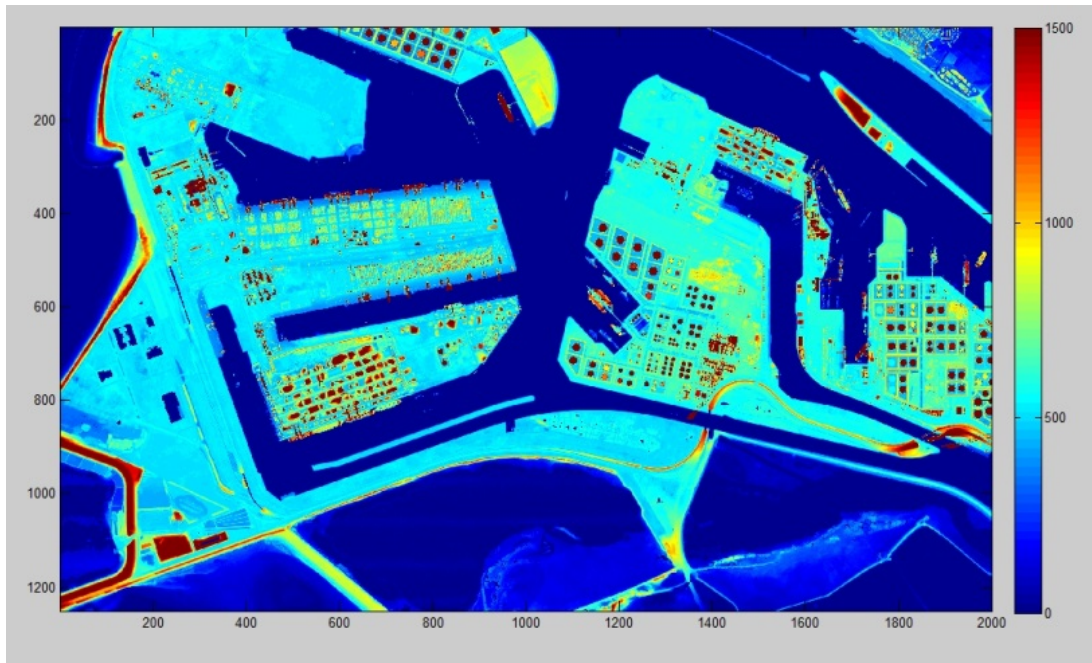


Figure 59 AHN (version 1) example for Rotterdam, where oil terminals stand out clearly.

#### 4.2.3 Recommendation

Height models are important to assess the line-of-sight, the slope and to correct for distortions in images due to oblique or slant range viewing. We focus here on the use of satellite imagery, so that distortions in the images due to relief and the height of objects are the main issue here.

Factors of importance here are:

- 1) The degree of distortion
- 2) The resolution in the image versus the DEM accuracy.
- 3) What is to be corrected for: distortion due to terrain relief or land cover (buildings and vegetation).

Obviously in mountainous areas distortions are significant. In the optical it is possible to select images with a minimum oblique viewing angle so that the distortions are also limited and a DEM can be used to remove the distortions. In that case a standard DEM (corresponding level 1 or 2) is sufficient.

For SAR imagery, the scene is always viewed from the side, so artefacts such as shadowing and foreshortening are always present. Geometrical distortions due to foreshortening can be

### **CLASSIFICATION: UNCLASSIFIED**

*All rights reserved. No part of this document may be reproduced or transmitted in any form or by any means, electronic, mechanical, photocopying, recording, or otherwise, without prior written permission of FFI, NLR or TNO.*

corrected for, but resolution is degraded. Although the resolution should match the image resolution, a somewhat lower DEM posting is acceptable since also the resolution is already degraded due to the foreshortening.

In these cases the filled SRTM DEM is the best choice if more accurate models from national surveys are not available. For the future the DEM derived for the TanDEM-X mission is probably a better choice.

In case of high resolution images where buildings and trees are present a correction for the height of these objects may be necessary. In that case a high resolution DEM ('urban DEM' or DTED level V) is necessary with a posting in the order of one meter and also a (sub)meter accuracy for the height is necessary. These DEMs are obtained through aero-cartography or with LIDAR measurements. Such DEMs are only available for certain areas or should be obtained through dedicated measurement campaigns.

The main recommendations are summarized here:

1. Use optical images with no or less oblique view (e.g. Landsat) to minimize geometric distortion.
2. Use radar images with incidence angles near 45 degrees to get an average between shadowing and foreshortening.
3. A standard DEM such as SRTM can be used for slight to moderate distortions
4. For mountainous areas at least level 2 is necessary, such as the Norway DEM or the DEMs for the Alps.
5. For buildings an 'urban' DEM with (sub) meter accuracy is necessary. In that case the surface model should match the reflection or scattering surface in the image.
6. Surfaces which are changing in the scene such as vegetation and moving objects cannot always be corrected for.

#### **4.3 Product generation - Fusion and Information products based on space data**

##### **4.3.1 Introduction**

This section discusses the use of information derived from satellite images for producing geospatial intelligence and refers to deliverables 2.4, 2.5 and 3.2 of the planning document for Milspace WP1: data and information fusion, validation and preparation of GeoInt products. In the workflow below *image analysis* refers to the processing of satellite images for producing *half-finished products*. These *half-finished products* are processed in the *geospatial analysis*

### **CLASSIFICATION: UNCLASSIFIED**

*All rights reserved. No part of this document may be reproduced or transmitted in any form or by any means, electronic, mechanical, photocopying, recording, or otherwise, without prior written permission of FFI, NLR or TNO.*

part to produce finished GeoInt products for dissemination. This document focuses on the right-hand part of the workflow (indicated by red ellipse).

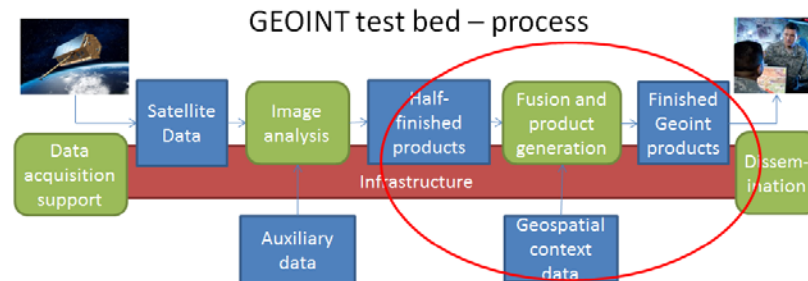


Figure 60 Fusion and Information products in the GeoInt workflow.

For discussing above mentioned workflow we need to discriminate between two main phases for military operations:

- Preparation phase: intelligence preparation of the environment (IPE)
- Operational/tactical phase

In the IPE picture building is important, and terrain analysis (soils, relief, vegetation, hydrography, infrastructure, population) is a main item. Obviously satellite imagery can give actual and detailed information of the terrain. Also with multi-temporal change detection patterns of life can be extracted. In the operational phase, usually a geospatial context is already available, and satellite imagery is used to fill in missing detailed information or is used for confirmation/verification.

#### 4.3.2 Half-finished products from imagery

When analysing satellite imagery, a number of products can be produced. These are discussed here and can be considered as half-products which have to be fused with other information to answer the actual intelligence question.

##### *Classification products.*

Classification products can be used to get information about vegetation, infrastructure hydrology flooding etc. Multispectral data is useful for this purpose since various spectral incidences correlate with different land types. In this way agricultural fields can be inspected or the outlines of water bodies in the case of flooding can be determined. A special case is height extraction using spectroscopic information (optical) or interferometric information (radar).

### **CLASSIFICATION: UNCLASSIFIED**

*All rights reserved. No part of this document may be reproduced or transmitted in any form or by any means, electronic, mechanical, photocopying, recording, or otherwise, without prior written permission of FFI, NLR or TNO.*



For the IPE usually some general geospatial information is a starting point (e.g. large scale information or information from the MGCP (Multinational Geospatial Co-Production Program) project; scales 1:50,000 – 1:100, 000). Satellite imagery can then be used to get an actual and more detailed overview. An example is water bodies and their outline which can be inspected (see Figure 61).

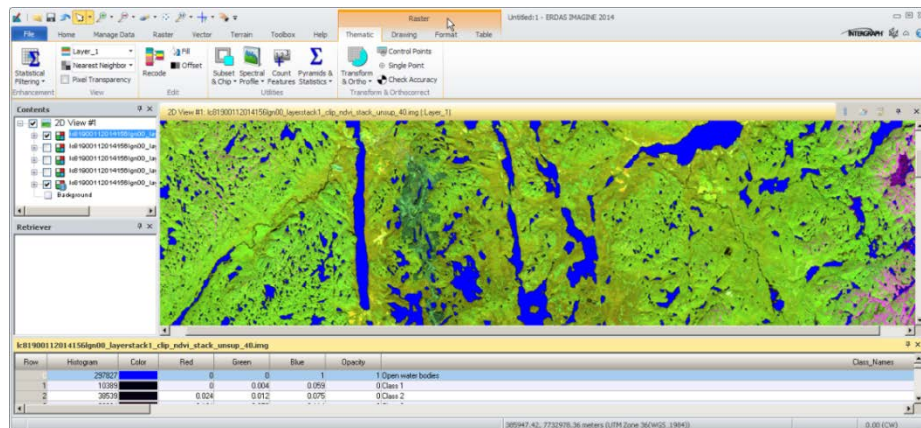


Figure 61 Water bodies derived using spectral indices from multispectral Landsat imagery

Product types are raster images or shapefiles containing polygons and attributes containing information about the properties. Above mentioned products are typically produced in the IPE. In some cases (e.g. flooding, presence of a particular kind of vegetation) such products are also produced during the operational phase.

*Change detection products.*

For the IPE collection of historical images and more recent images can be used to detect patterns of life. For example series of historical Landsat imagery can be used to get information about changes in land use (see Figure 62) and infrastructure. Other higher resolution optical data can give information about harbour activities.

**CLASSIFICATION: UNCLASSIFIED**

All rights reserved. No part of this document may be reproduced or transmitted in any form or by any means, electronic, mechanical, photocopying, recording, or otherwise, without prior written permission of FFI, NLR or TNO.



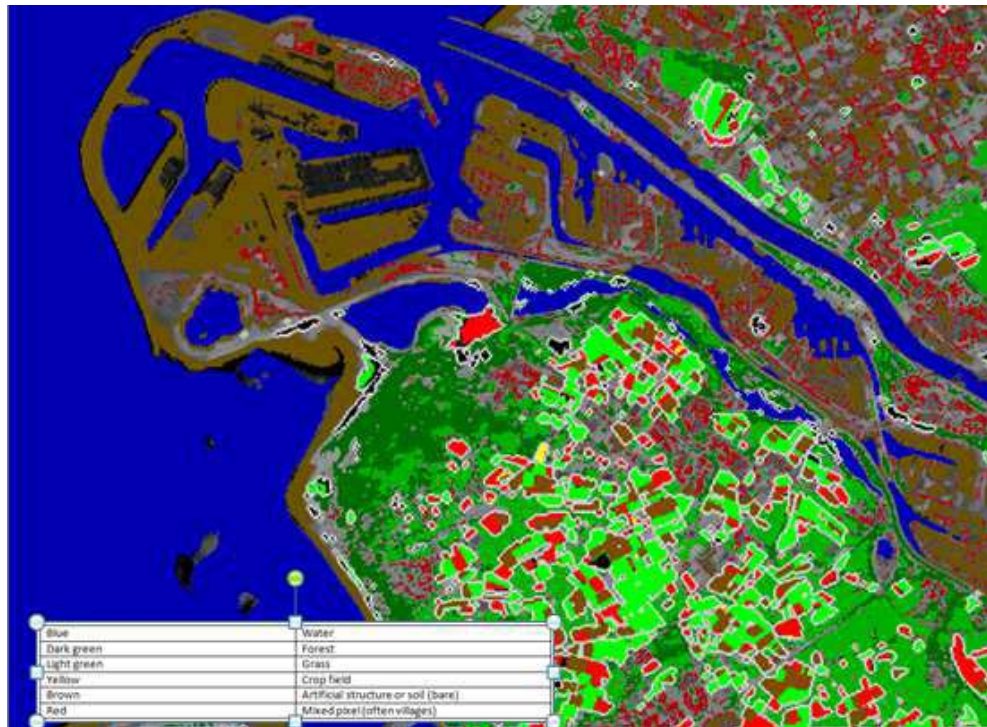


Figure 62 Land use classification on basis of series of Landsat imagery.

Series of high resolution radar imagery also gives information about harbour activities, as well as other urban and industrial activities (see figure 63). Advantage of the radar imagery is that regular monitoring intervals are more ensured due to its all-weather and day-night capability.

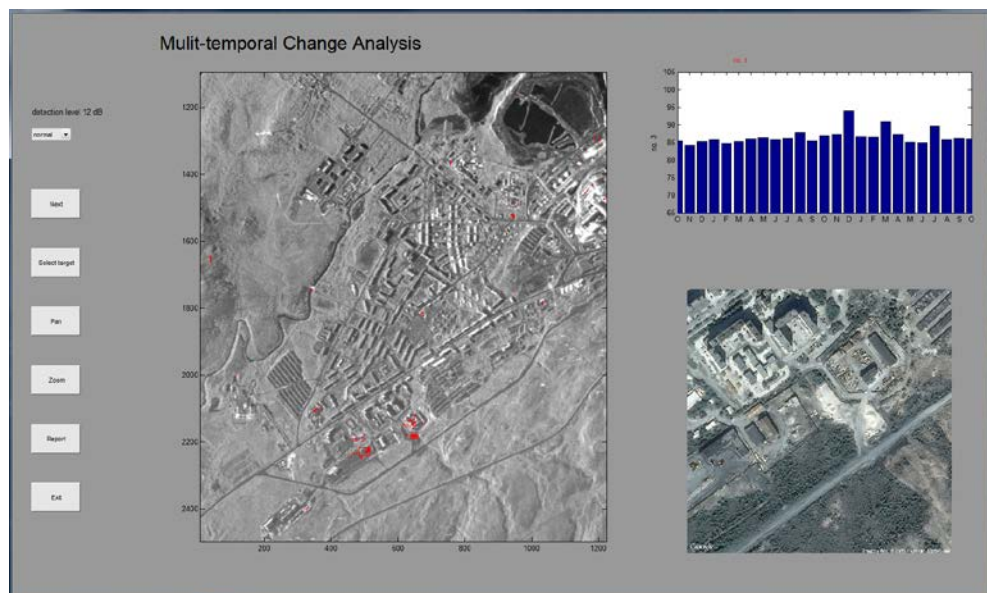


Figure 63 Multi-temporal change detection showing changes in the utilization of assembly areas (peaks in the upper-right view) in the city of Nikel.

**CLASSIFICATION: UNCLASSIFIED**

All rights reserved. No part of this document may be reproduced or transmitted in any form or by any means, electronic, mechanical, photocopying, recording, or otherwise, without prior written permission of FFI, NLR or TNO.

Product types are annotated change images or shapefiles containing positions or polygons indicating the changes and possibly associated information describing the detected pattern. These products describing patterns are relevant in the IPE. Operationally they can be used for surveillance, e.g. by producing an alert when a detected change is anomalous for the pattern.

#### *Ship detection products.*

Satellites can monitor large and remote areas to detect ship activity. Ships are efficient scatterers of radar radiation, and wide swath radar imagery is quite suitable for automatically detecting ships. SAR satellites also have all-weather and day-night capability. The ship detection results can be compared with AIS for verification. In harbour areas higher resolution radar and optical imagery can be used to detect ships. An example is the Norwegian coast and the street between Svalbard and Norway where ship traffic and illegal fisheries needs to be monitored by the Norwegian Coast Guard and the Norwegian intelligence services. Products are for example lists with ship positions including attributes with the properties of the ships. These products can be used both for picture building (determining the normal pattern) and operationally for surveillance indicating anomalous presence of ships

#### *Detailed analysis products.*

Currently submeter resolution optical satellite imagery is available and even short video clips can be obtained from space (Google skybox). Such images can be used to recognize objects on the ground in so-called target areas interest (TAIs) and to give a detailed description of infrastructure and individual buildings. The TAIs are indicated during the IPE. An example can be the military analysis of a bridge, an airfield or the analysis of a nuclear power plant. The product is usually an annotated picture. Annotation can be used as a separate layer where the annotations are geotagged. These products are used to fill in the existing context with detailed information and are therefore most relevant for the operational phase. They can be combined with other information to produce so-called target packages (see section 4.3.3).

### **4.3.3 Geospatial information products**

GeoInt covers a wide range of topics. In this context GeoInt comprises three categories: base layers (“the map”), half-finished products and finished products.

#### *Base layers:*

Base layers are typically products which are prepared by the military geographical offices. Dissemination is usually done using multimedia storage devices (DVD etc). Future

## **CLASSIFICATION: UNCLASSIFIED**

*All rights reserved. No part of this document may be reproduced or transmitted in any form or by any means, electronic, mechanical, photocopying, recording, or otherwise, without prior written permission of FFI, NLR or TNO.*

dissemination is also foreseen using national MOD geoportals (web mapping services). In NATO context COREGIS (Core Geographical Information System), a web mapping service using Open GeoSpatial Consortium (OGC) standards, is relevant. COREGIS is based on ESRI (Earth Science Resource Institute) software. The advantage of web mapping services is that the source data stays at the server and that the user can compose its own map suitable for his operational task.

*Half-finished products:*

These are typically shapefiles, thematic maps or density maps, which contain elements of information. ESRI software is often leading here (ARCGIS), and this kind of information stays preferably in the ESRI environment. An example is here ESRI's ARCGIS server and ARCSDE, the ESRI technology for accessing and managing geospatial data within relational databases. It supports reading and writing of multiple (OGC) standards. The half-products stay with the owner, but can be accessed through the military network by the user for further interpretation and fusion to produce enhanced half-products or eventually finished products. Wider dissemination between NATO partners is possible using the coalition shared database (CSD). Half-products in the form of annotated imagery and still imagery can be stored (STANAG 4545) as well as video clips/streams (STANAG 4609). Other formats can be stored such as maps and shapefiles (zip format) as long as appropriate meta data is also specified (STANAG 2433 in prep.) See also section 4.4.1.1.

*Finished products:*

Geographical finished products can be published in the geopdf format. Sometimes the KML format is used. For dissemination of intelligence between partners the coalition shared database is used. When storing files in the CSD, it is essential that potential users can discover the information. This implies that appropriate meta data is also specified and stored together with the information file. Work is in progress (MAJIIC - Multi-sensor Aerospace-ground Joint ISR Interoperability Coalition) to standardise multi-source intelligence (STANAG 2433) where the meta data covers 5 domains (the pentagram): event, location, organisation, person and means. At the moment no standardisation specifically for GeoInt products is foreseen. Finished GeoInt products can also be used as layers in C2 systems, such as the BMS (battle field management system) or ISIS (integrated staff information system) for the NLMOD. In that case a specific format may be needed. In Figure 64 we show the workflow and various ingestion and egestion channels.

**CLASSIFICATION: UNCLASSIFIED**

*All rights reserved. No part of this document may be reproduced or transmitted in any form or by any means, electronic, mechanical, photocopying, recording, or otherwise, without prior written permission of FFI, NLR or TNO.*

## GEOINT test bed – ingestion & dissemination

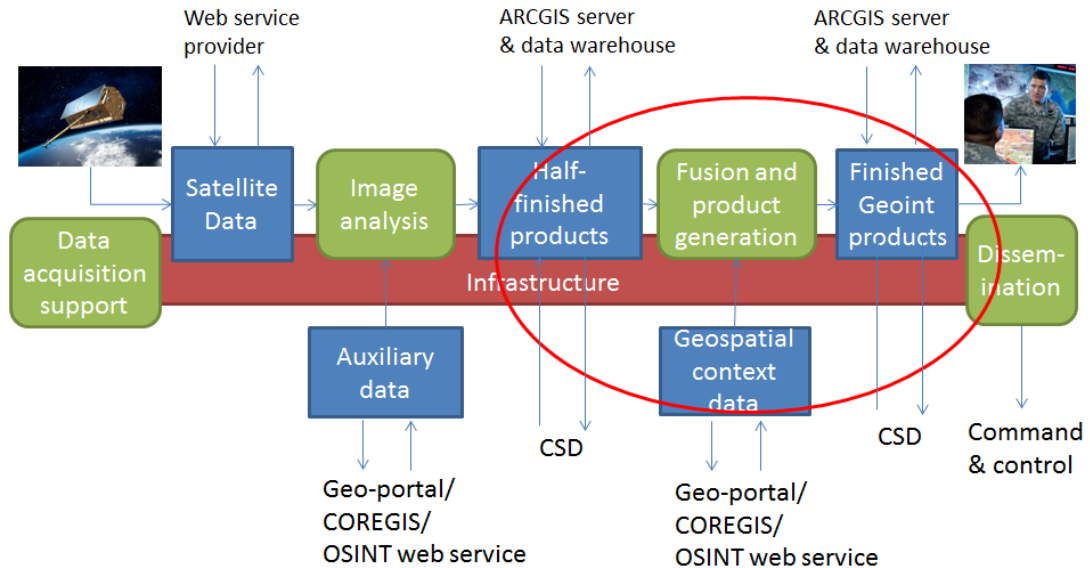


Figure 64 Workflow with various ingestion and egestion channels.

### 4.3.4 Production and fusion methods

In the previous sections we have summarized half-finished products which can be obtained from the satellite image analysis and the type of GeoInt products which can be used and produced. To produce GeoInt products the half-finished products are usually combined with other geospatial context data to enhance the products or to finish the product. The geospatial context data is usually obtained through a geo-portal or a web service, which may be an internal military service or an open source type of service. Below we summarize various examples of context data and a number of fusion methods in a table.

**CLASSIFICATION: UNCLASSIFIED**

All rights reserved. No part of this document may be reproduced or transmitted in any form or by any means, electronic, mechanical, photocopying, recording, or otherwise, without prior written permission of FFI, NLR or TNO.

Table 8 Fusion methods.

Products from satellite information	Geospatial context data	Fusion methods
Classification	Reference GIS (MGCP feature data 50-100K)	Layer stacking.
Change detection	Topographic maps	RGB colour coding
Ship detection	High-resolution optical reference (Google Earth/aerial photography)	Video
Detailed analysis	Open street map (OSM) data	ArcGIS modelling
	Elevation data (DTED level II-V)	Advanced models
	Shorelines/land masks	Neighbourhood analysis
	AIS (stream)	
	Operationally defined areas	

On basis of the fusion methods information products are defined for a number of use cases (see section 5.3.1). In the following table a list of information products is shown.

**CLASSIFICATION: UNCLASSIFIED**

All rights reserved. No part of this document may be reproduced or transmitted in any form or by any means, electronic, mechanical, photocopying, recording, or otherwise, without prior written permission of FFI, NLR or TNO.



Table 9 Information products.

	<b>Half-finished products</b>	<b>Geospatial context</b>	<b>Fusion method</b>	<b>Enhanced/ finished products</b>
<b>Maritime</b>				
<ul style="list-style-type: none"> <li>Barents Sea</li> </ul>	Ship detection with Radarsat/Sentinel wide	AIS, land masks	Layer stacking, neighbourhood analysis	Annotated imagery, ship position lists, shapefiles
<ul style="list-style-type: none"> <li>Caribbean</li> </ul>	Ship detection with Radarsat/Sentinel wide	AIS, land masks	Layer stacking, neighbourhood analysis	Annotated imagery, ship position lists, shapefiles
<b>Air</b>				
<ul style="list-style-type: none"> <li>Ørland, Norway (UV2014) (Unified Vision)</li> </ul>	Change detection with TerraSAR	Maps, defined areas, elevation	Advanced models	Annotated imagery, shapefiles
<b>Land</b>				
<ul style="list-style-type: none"> <li>Rotterdam</li> </ul>	Multi-temporal change detection with COSMO-SkyMed Multitempoal analysis with DMC	Formosat, Landsat, OSM data, AIS	RGB colour coding  Layer stacking	Annotated imagery  Layers in GeoPDF
<ul style="list-style-type: none"> <li>Nikel</li> </ul>	Multi-temporal change detection with Radarsat Video of Landsat changes Multitemporal change detection with Landsat	High-resolution optical reference (Google Earth), OSM data, elevation	Advanced models  Layer stacking  Video	Annotated imagery  Layers in GeoPDF

**CLASSIFICATION: UNCLASSIFIED**

All rights reserved. No part of this document may be reproduced or transmitted in any form or by any means, electronic, mechanical, photocopying, recording, or otherwise, without prior written permission of FFI, NLR or TNO.

#### **4.3.5 Data preparation, quality and validation**

##### *Change detection*

In the change detection procedure a threshold is applied to detect a change. If a low value is used smaller changes are detected, i.e. the probability of detection increases, but also the probability that irrelevant changes (false alarms) due to noise, light conditions (optical) or speckle (radar) increases. The choice for the threshold depends on the operational conditions. If not missing a detection is important one should allow false alarms and the threshold should be low. If the effort for inspecting false alarms should be limited, the threshold should be high. The function with the threshold as parameter in the Pod, Fa diagram is often called the ROC curve and is a property of the observation system.

##### *Classification*

Classification, e.g. land use with multispectral data should be compared with a reference land use set in order to get information about the accuracy. For this reference set ground truth information is needed.

##### *Positional accuracy*

When different geographical sources are combined they should be geo-registered. The geometrical accuracy should be accurate enough to allow an appropriate and meaningful combination. For change detection it is essential that the images which are compared are accurately co-registered, since otherwise more false alarms will be generated. For example the SRTM land mask should fit the observed land sections in the SAR images. Mismatches can arise from different registration methods and from differences in resolution.

For checking the registration accuracy ground control points (e.g. corner reflectors in SAR images) may be used for which the position is very accurately known

##### *Multi-temporal observations*

When multi-temporal observations are used to detect activities and activities pattern, it is important that the observation times and intervals should match the dynamics of the phenomena to be observed. For example in the case of Nickel each month an image has been acquired. This is good enough to see seasonal changes, such as vegetation and ice growth variations. However if we want to monitor the activities of the Nickel melt plant, for example by detecting the trains

### **CLASSIFICATION: UNCLASSIFIED**

*All rights reserved. No part of this document may be reproduced or transmitted in any form or by any means, electronic, mechanical, photocopying, recording, or otherwise, without prior written permission of FFI, NLR or TNO.*

delivering ore, we may require images each day. To determine the monitoring schedule we should therefore have prior information (or have an expectation) about temporal characteristics.

#### **4.4 Dissemination and standards**

In this section we first discuss the MAJIIC project, followed by a listing of standards to be used in this context. The second part presents reference architecture for the dissemination of large amounts of space borne data.

##### **4.4.1 The MAJIIC project**

MAJIIC (Multi-sensor Aerospace-ground Joint ISR Interoperability Coalition) has been a project for developing and testing several standards and interfaces for distributed intelligence gathering and sharing of data and intelligence products (see figure 65). The focus was on the use of NATO sensors where the Coalition shared database (CSD) and associated services plays a crucial role. In the focus of this report the dissemination of the GeoInt products are relevant as the acquisition of satellite data was beyond the scope of MAJIIC.

The output of MAJIIC is a list of STANAGs and implementation procedures which should be applied by the participating countries, such as the STANAG 4559 (CSD) describing the NATO Standard ISR Library Interface, STANAG 4545, describing the NATO Secondary Imagery Format (NSIF). Figure 65 shows the operational picture indicating the MAJIICMAJIIC goals. In the next subsection a list of applicable standards and engineering guides can be found.

For the dissemination of intelligence products standardisation of the products and a distribution architecture infrastructure is necessary. Since GeoInt products have a geospatial reference it is important to align with the current trend for GIS services. Some nations exploit the use the Open Geospatial consortiums definition of Web Map Service, Web Coverage Service and Web Feature service for exchange of Geo Intelligence. Examples are US GEOINT visualisation service and NATO's Interim Geo Spatial Intelligence tool. Applicable document regarding the use of GIS services within NATO and MAJIIC are:

- Bi-Strategic Commands Automated Information System Core Geographic Services CO-11424-GIS: extensive description of the NATO Core GIS services by Siemens.
- MAJIIC COREGIS IMPLEMENTATION GUIDE.

### **CLASSIFICATION: UNCLASSIFIED**

*All rights reserved. No part of this document may be reproduced or transmitted in any form or by any means, electronic, mechanical, photocopying, recording, or otherwise, without prior written permission of FFI, NLR or TNO.*

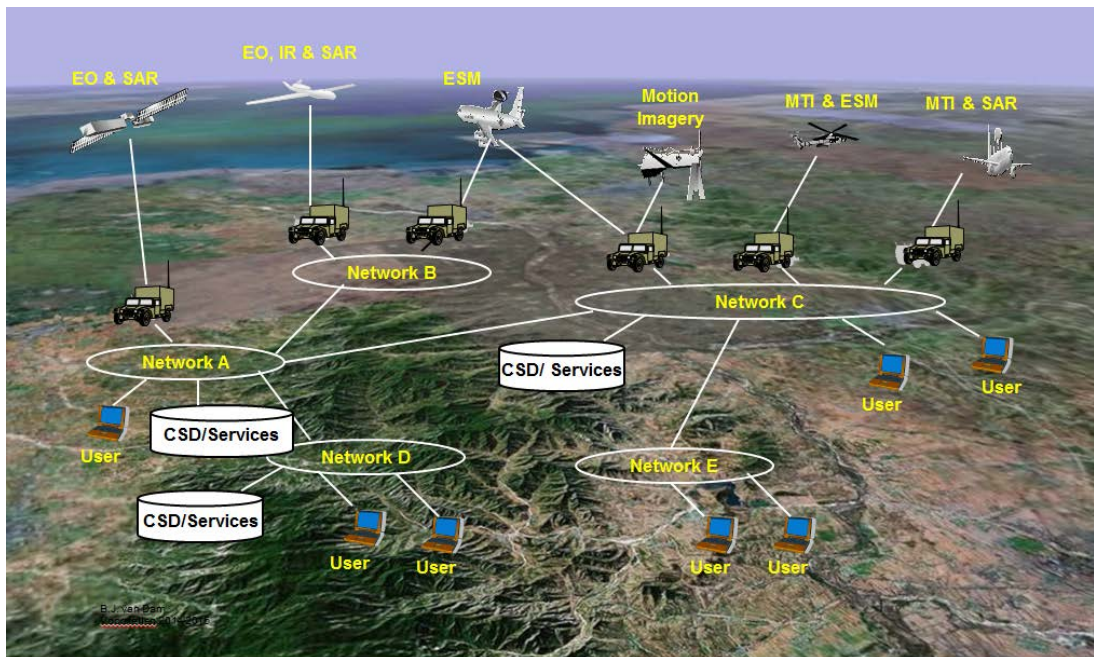


Figure 65 Operational picture indicating the MAJIIC project goals.

#### 4.4.1.1 Standardisation

MAJIIC has two baselines: an operational baseline and an experimental baseline. Parties outside the MAJIIC community are expected to use the operational baseline since this is an established version, while the experimental baseline is continuously subject of change. Therefore the operational baseline as was available at the time (2014) this part of the document was written is used. It is the expectation that a new operational baseline will be defined including the latest XML schema's after the Unified Vision 2014 exercise. Below the products which are applicable in the context of geographic intelligence including the references to applicable STANAGs and engineering guides are listed:

##### *MAJIIC CSD:*

- DOP-MAJIIC-14|2.4|Sep 2010 Coalition Shared Data (CSD) Server Interface Design Document (IDD)
- STANAG 4559|Edition 3|Nov 2010 NATO Standard ISR Library Interface
- AEDP-5|Edition 2|May 2013 NATO Standard ISR Library Interface (NSILI) Implementation Guide

##### *Still Imagery:*

- Still Imagery according to STANAG 4545

### **CLASSIFICATION: UNCLASSIFIED**

All rights reserved. No part of this document may be reproduced or transmitted in any form or by any means, electronic, mechanical, photocopying, recording, or otherwise, without prior written permission of FFI, NLR or TNO.

- STANAG 4545|Edition 2 Draft 1|Nov 2008, NATO Secondary Imagery Format (NSIF)
- AEDP-4|Edition 2|May 2013 NATO Secondary Imagery Format (NSIF) STANAG 4545 (Edition 2) Implementation Guide.
- DOP-MAJIC2-006|3.3 Draft 1|Jun 2012 MAJIC 2 STANAG 4545 NSIF Implementation Guide.
- Reconnaissance Exploitation Report Imagery exploitation report format according to the RECCEXREP format of STANAG 3377 and target reporting of STANAG 3596 in XML format.
  - XSD:RECCEXREP|1.0|Mar 2009 RECCEXREP<sup>1</sup>
    - STANAG 3377|Edition 6|Nov 2002 Air Reconnaissance Intelligence Report Forms
  - XSD: STANA3596|1.0|Apr 2010 STANAG 3596
    - STANAG 3596 Ed 6 Air Reconnaissance Requesting and Reporting Guide, Nov 2007.

*Motion Imagery:*

- Motion Imagery according to STANAG 4609:
  - STANAG 4609|Edition 3|Oct 2009 NATO Digital Motion Imagery Standard.
  - AEDP-8|Edition 3|Dec 2009 NATO Motion Imagery (MI) STANAG 4609 (Edition 3) Implementation Guide.
  - DOP-MAJIC2-009|3.0|Apr 2011 MAJIC STANAG 4609 MI Implementation Guide.
- Motion Imagery Exploitation Report supports reporting on moving target extracted from video and target reporting according to STANAG 3596:
  - XSD:MIEXREP|1.0|May 2010 MIEXREP
  - XSD: STANA3596|1.0|Apr 2010 STANAG 3596
    - STANAG 3596 Ed 6 Air Reconnaissance Requesting and Reporting Guide, Nov 2007

*Global Moving Target Indicator:*

- NATO Ground Moving Target Indicator (GMTI) Format according to STANAG 4609
  - STANAG 4607|Edition 3|Sep 2010 NATO Ground Moving Target Indicator (GMTI) Format

---

<sup>1</sup> All reports XSD's include also XSD:COMMON|0.71|Sep 2009 COMMON (common definitions ISR domain) and XSD: GENERICREPORT|1.0|May 2009 providing a generic report header

**CLASSIFICATION: UNCLASSIFIED**

All rights reserved. No part of this document may be reproduced or transmitted in any form or by any means, electronic, mechanical, photocopying, recording, or otherwise, without prior written permission of FFI, NLR or TNO.



- AEDP-7|Edition 2|May 2013 NATO Ground Moving Target Indicator Format (GMTIF) STANAG 4607 Implementation Guide
- MAJIIC 2 STANAG 4607 GMTI Implementation guide|1.1|May 2012
- MTI Exploitation Report allowing report on GMTI observations.
  - XSD: MTIEXREP|1.1|May 2010 MTIEXREP

*ISR Tracks:*

- STANAG 4676, Edition 1 Ratification Draft 1), “NATO Intelligence Surveillance and Reconnaissance Tracking Standard (NITS)”, Ratification request November 2011
- MAJIIC 2 STANAG 4676 NATO Intelligen|1.0 Draft|Jan 2012 MAJIIC 2 STANAG 4676 NATO Intelligence, Surveillance, Reconnaissance (ISR) Tracking Standard (NITS) Implementation Guide
- AEDP-12|Edition A Version 1 Ratification Draft|Oct 2012 NATO ISR Tracking Standard (NITS)

*Generic/Multi INT Intelligence Reports:*

- ISRSPT Report: used for quick reporting allowing a free-text description of the results:
  - XSD:ISRSPTREP|1.0|May 2010 ISRSPTREP
- Intelligence report INTREP (XML) and INTSUM (Intelligence Summary) (XML):
  - Is now part of experimental baseline. Will become part of a new operational baseline.
    - STANAG 2511|Edition 1|Jan 2003 Intelligence Reports Intelligence summary INTSUM (XML):
- PENTAGRAM report (XML) format for Multi-INT information dissemination using a Pentagon.
  - Is now part of experimental baseline and may become part of a future operational baseline.
    - STANAG 2433 JINT (Joint Intelligence) (EDITION 4) (RATIFICATION DRAFT 1) – THE NATO MILITARY INTELLIGENCE DATA EXCHANGE STANDARD – AINTP-3 EDITION C VERSION 1

*Documents:*

- The MAJIIC CSD allows to post MS Office documents, portable document format (pdf) including geo pdf and plain text documents. The MAJIIC community does not promote to post exploitation results and analysis through documents, but it is possible to do so. Operational users have a strong preference to post finished intel through Office documents.

**CLASSIFICATION: UNCLASSIFIED**

*All rights reserved. No part of this document may be reproduced or transmitted in any form or by any means, electronic, mechanical, photocopying, recording, or otherwise, without prior written permission of FFI, NLR or TNO.*

#### **4.4.2 A Reference architecture for dissemination of large volumes of space borne data**

A generic technical infrastructure required for the dissemination of large volumes of data (i.e. still imagery) to end-users is described here. The focus is on the functional components within this infrastructure and the related existing and new technologies and standards. Because of the variety of end-users that can be identified and of all the different use cases that can be defined, no attempt is made to define an all-encompassing infrastructure which supports all the dissemination scenarios one can think of. Instead, a generic network-based architecture is to be used containing all the relevant components related to finding, viewing, downloading and processing of data. Thereby, it is assumed that the exact implementation of these components will depend on the different use-case scenarios. The reference architecture can also serve as the baseline for an operational demonstration of still imagery dissemination in which new, but proven technology is used to implement a realistic infrastructure for a few selected scenarios. In the following subsection a summary of the topic described is given.

##### **4.4.2.1 Description of the Architecture**

The reference architecture that will be used here is a so-called Service Oriented Architecture (SOA), which is a network architecture in which loosely-coupled services provide dedicated functionality. SOA based infrastructures provide a high level of interoperability, are extendible and support incorporation of legacy systems, meaning that existing functionality can be used where needed. It supports interoperable communication and data exchange between different partners in a distributed environment. The architecture that will be adopted here as reference architecture resembles many of the architectures developed for (geo-) spatial data infrastructures (SDIs). In particular, the INSPIRE Network Services Architecture [3] is considered as a very useful example of an architecture for finding, publishing, viewing, downloading and processing of geospatial information, but more similar architectures exist.

SOA (Service Oriented Architecture) can be designed using various communications standards of which (Service Oriented Architecture Protocol) SOAP/WSDL (Web Service Description Language) is the most popular one. But also CORBA (Common Object Request Broker Architecture) can be used as communication technology between the services. SOAP/WSDL based SOA architectures are adopted in various domains, notably Air Transport Management (civil and military) and Spatial Data Infrastructures (SDI's). The recommendation to use SOA is in line with the findings of [4] where a service based ISR (Intelligence, Service, Reconnaissance) information dissemination system is proposed implemented within a service oriented architecture (SOA). Figure 66 shows the reference architecture and its components. The components are grouped within a number of layers.

### **CLASSIFICATION: UNCLASSIFIED**

*All rights reserved. No part of this document may be reproduced or transmitted in any form or by any means, electronic, mechanical, photocopying, recording, or otherwise, without prior written permission of FFI, NLR or TNO.*

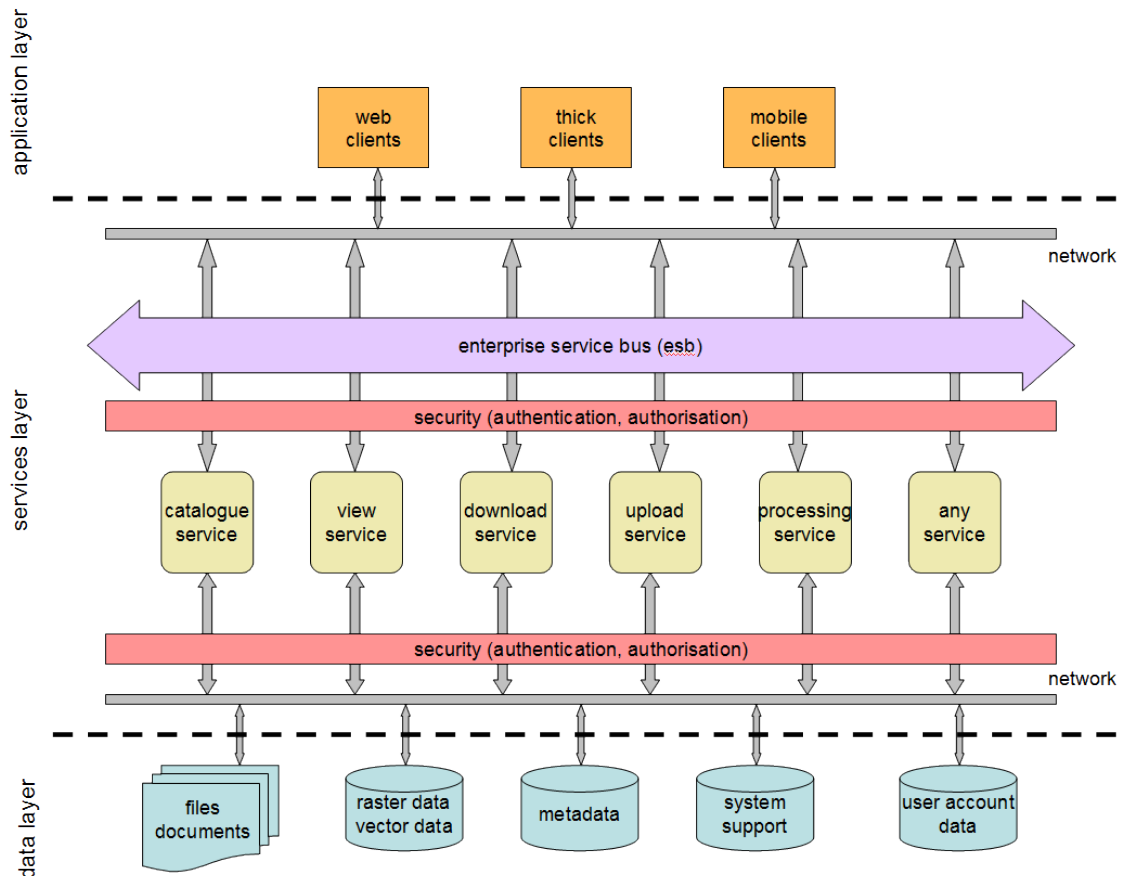


Figure 66 Reference Architecture.

**Data layer:** this layer contains the data sources and their metadata. Typically these data sources contain raster data (i.e. satellite images, aerial photography data, maps) or vector data (i.e. digital elevation models, boundary data ...). Very important in this layer is the metadata describing the data and the metadata describing the available services in the service layer. Also registry data such as user information, thesauri, administration data and system support data are part of this layer.

**Services layer:** services are contained in the service layer and provide the functionality of the system. Basic services are related to: discovering datasets (by providing search mechanisms based on associated metadata); viewing of the data (by providing mechanisms to visual inspect the spatial data and relevant parts of the metadata, including zoom, pan and overlay functions); downloading of data (by providing means to retrieve datasets, or a part of a dataset); uploading of data; processing of data (by providing means to start off-line or on-the-fly processes to generate customized products from existing data sources).

### CLASSIFICATION: UNCLASSIFIED

All rights reserved. No part of this document may be reproduced or transmitted in any form or by any means, electronic, mechanical, photocopying, recording, or otherwise, without prior written permission of FFI, NLR or TNO.

**Application layer:** from this layer the service layer is accessed by a variety of client programs. Clients can be thin, like browser based web applications or can be thick, like advanced image processing environments. The type of client that is actually used will depend amongst others on end user requirements, available tools and available bandwidth.

**Security layer:** access to the system and to the individual services is controlled within the security layer. Authentication and authorisation methods will take care of control and granting access to data sources using user and product dependant criteria.

**Middleware layer (Service bus):** the middleware layer comprises the enterprise service bus (ESB). The ESB provides the software architecture which offers the standardized interfaces for communication between the client and the services. Examples of these interfaces are SOAP/WSDL, REST (Representational State Transfer), HTTP and SMTP (Simple Mail Transfer Protocol).

**Network layer:** the network layer deals with communication technologies, network protocols and quality of service issues.

For each of the above layers existing or new technologies can be identified, which might be applied when implementing the components building up the layer. In deliverable [2] these technologies are reviewed. Their applicability will depend on the use cases, and can be assessed by taking the different scenarios into account. A comprehensive overview of many of the technologies involved and grouped at architecture layer level is given in Figure 67.

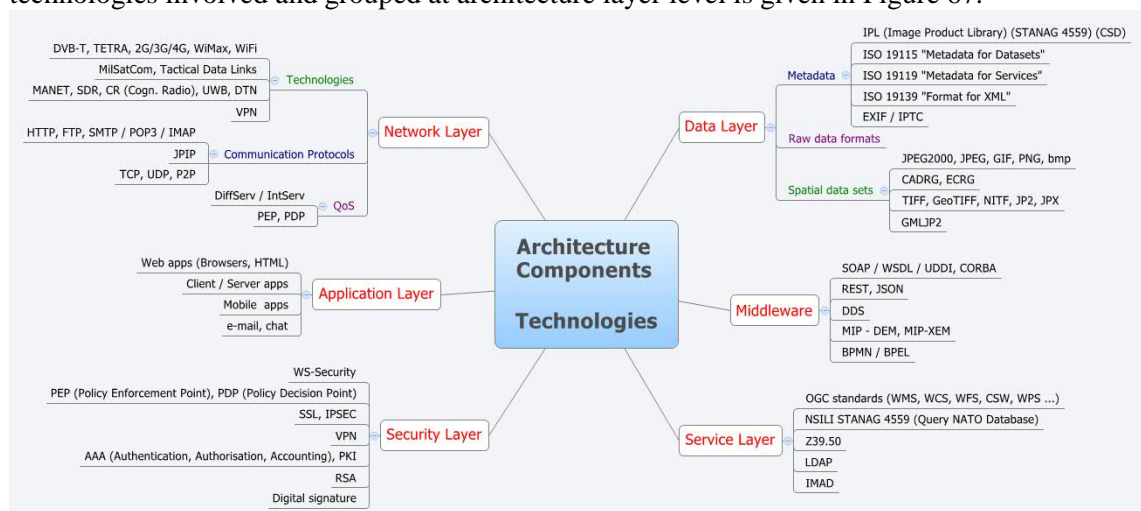


Figure 67 Technology Application to Layers.

**CLASSIFICATION: UNCLASSIFIED**

All rights reserved. No part of this document may be reproduced or transmitted in any form or by any means, electronic, mechanical, photocopying, recording, or otherwise, without prior written permission of FFI, NLR or TNO.

#### **4.4.3 OGC and ISO standards**

Another important aspect that has been addressed is the use of standards for data description (metadata), data discovery and data exchange. The Open Geospatial Consortium (OGC) is leading the development of standards for geospatial and location based services. Closely related to the OGC specifications are the ISO standards 19115, 19119 and 19139 for describing data and services. The OGC standards and the ISO standards allow the development of geospatial information services in a SOA environment. The most relevant specifications in this context are the standards relating to data discovery (CSW [6]), the view (WMS [5]) and download (WCS [7]) services. It is proposed to also adopt the OGC standards and the ISO application profiles for dissemination of geospatial products such as imagery or maps to the different geospatial applications and geospatial product consumers in a military environment.

#### **4.4.4 CSD and services**

With respect of data discovery and data serving, the use of the Coalition Shared Database (CSD) forms NATO's baseline scenario. Integration of CSD in a SOA requires several issues to be solved. Because CSD is CORBA based, effort has to be put into the integration into a SOAP/WSDL based architecture. Secondly, to bring the use of CSD for data discovery in line with OGC standards requires access to the CSD using the CSW standard. Since, CSW can be made available as a SOAP service; this would solve the first issue as well. However, currently no software tools exist which exposes CSD as a CSW service to the outside world and at the same time offers all the features of CSD. Another option is not to use the CSD for discovery but a CSW service, assuming that the metadata (from the CSD) can be made available according to the ISO 19115 standard or that a STANAG application profile is defined for the CSW.

With respect to client functionality, in NATO/Coalition project Shared Tactical Ground Picture (STGP), the content of a STANAG 4559 based [8] CAESAR/MAJIIC Coalition Shared Database (CSD) is exposed through Web Services, meaning that users can access the CSD from a web application communicating with a web service which serves as a proxy to the CSD. This has the advantage of clients not having to implement CORBA communications. In principle, a web application can in this case provide CSD client functionality.

#### **4.4.5 Big Data and Cloud-based processing**

A new technology that looks rather promising for large volume data processing for geo-intelligence is Big Data technology. Often Big Data is described by the characteristics Volume, Variety and Velocity and many more. These terms relate to the enormous amount of data, the diversity of the data and data sources and the time required to process the data. In order to meet

### **CLASSIFICATION: UNCLASSIFIED**

*All rights reserved. No part of this document may be reproduced or transmitted in any form or by any means, electronic, mechanical, photocopying, recording, or otherwise, without prior written permission of FFI, NLR or TNO.*



the demands of timely information generation from a fast growing number of data sources producing even faster growing volumes of data, scalable big data systems are build using technologies like Apache Hadoop, Spark (MapReduce) and NoSQL (Not only SQL (Structured Query Language)) databases. These systems are mostly provided as cloud-based services, meaning that the required infrastructure is provided as a service and users don't have to care about managing the computers. Thus, Big Data is about content (data) and Cloud Computing is about infrastructure.

Military intelligence is a typical area that will benefit from the new ways of handling large data volumes. Automated analysis and combining data from different sources will make it possible to detect signals in the data that would remain hidden otherwise. Reference [1] describes research for the design and implementation of a prototype for scalable Multi-Intelligence Data Integration Services (MIDIS), based on a flexible data integration approach, making use of Semantic Web and Big Data technologies. The paper provides a good insight in the technology involved.

## **5 Geospatial information testbed & demonstration**

### **5.1 Introduction**

In this chapter we describe the actual test bed and workflow that has been studied and tested in the research program. This is done on basis of use cases comprising a number of locations and certain types of satellite data used to extract information for a topic of interest, such as monitoring, activities in harbours on land etc. Demonstrations are described in which a testbed component is applied to the data to extract the required information. We first give an overview of the test bed and next an overview of the various use cases.

The test bed extraction components studied here comprises subcomponents for optical data and SAR data focusing on multi-temporal changes detection and for SAR data focusing on ship detection and the combination with AIS. These can be used for demonstration purposes and are discussed in more detail in the following. Finally, the information from the subcomponents are fused in one single picture. At the end of the chapter this fusion component is presented.

### **5.2 Test bed description**

The test bed supports workflows that facilitate the use of open source satellite data for producing GeoInt products. The test bed consists of 4 main components:

## **CLASSIFICATION: UNCLASSIFIED**

*All rights reserved. No part of this document may be reproduced or transmitted in any form or by any means, electronic, mechanical, photocopying, recording, or otherwise, without prior written permission of FFI, NLR or TNO.*

- Data acquisition support
- Image analysis
- Geospatial analysis
- Dissemination

The test bed should fit to the existing processing infrastructure used by the MOD. In the Dutch context this means that use is made of the following software packages: Erdas/Imagine for image analysis and ESRI/ArcGis for the geospatial analysis. The NOMOD makes use of the Socet-GXP and also of TerraExplorer (3D visualisation) next to ESRI/ArcGIS. These expensive software packages are at TNO (Netherlands Organisation for Applied Scientific Research) (and NLR) available using floating licences and accessible at the workstation through the TNO/NLR network. Below we describe each component in more detail. In the current version of the test bed the components are implemented on a single workstation. However, also a distributed architecture can be considered.

#### **Data acquisition support**

Goal: facilitate with planning of satellite data acquisition and searching in data archives. Using the MEOS software package from Kongsberg it is possible to foresee what data will be available in the different modes from the various satellites. The MEOS software is implemented in the test bed. Data searches in data archives can be done using various websites such as EOLi from ESA and EOWEB from DLR. Also various archives from NASA (National Aeronautics and Space Administration) and USGS (EarthExplorer) can be accessed through the web. Some of these websites also allow the planning of data acquisition. The actual acquisition (buying of data) is done via a dealer. Data is usually transferred using FTP. Server architecture for making queries independent of the various websites developed in the ESA DREAM project is also considered here.

#### **Image analysis**

Goal: processing of image data to produce IMINT (Image Intelligence) products. Erdas is a suitable tool here for implementing workflows, e.g. for classifying multi-spectral data, using models and the so-called knowledge engineer. Also Python based code can be integrated easily. Alternatively ENVI can be used. In addition to the main software packages, specific tools for multi-temporal change detection (developed by TNO, based on Matlab) or ship detection (Aegir, developed by FFI) are used and implemented in the test bed. Specific software such as SARscape (ENVI based) is used in addition to Aegir by FFI for the processing of polarimetric radar data.

### **CLASSIFICATION: UNCLASSIFIED**

*All rights reserved. No part of this document may be reproduced or transmitted in any form or by any means, electronic, mechanical, photocopying, recording, or otherwise, without prior written permission of FFI, NLR or TNO.*

**Geospatial analysis**

Goal: processing of IMINT products and fusion with additional data to produce GeoInt products.

Additional data serves as context information and can consist of maps, images, GIS data (OpenStreetMap), height models as well as AIS data. Using ARCGIS it is possible to implement the workflow in Python scripts. GeoInt products are often map packages with various GIS layers which can be exported in a geopdf format for distribution. Other formats for distribution, e.g. to show positions of object such as ships, are xml or kml, where kml also supports lines and polygons.

**Dissemination**

Goal: to disseminate GeoInt products.

Focus here is the NATO coalition shared database (CSD) as is developed through the MAJIC project. An interface to communicate with the CSD is for example MAJIIC-NL. Note that there is no standard for GeoInt products. Products can be put into the CSD but should be accompanied with keywords and geo-tags to enable the traceability. Using MAJIIC-nl, klm and xml can be exploited to atomically fill in the tags and keywords, while this is not possible for the geopdf format. For the latter accompanying meta data should be available. Table 10 shows components and the software tools that are implemented at the workstation platform or accessible through the network (see also Figure 68). In Table 10 the tools used for the different testbed components are listed, while in Figure 68 a graphical overview is given of the tools in relation to the workflow.

*Table 10 Test bed components*

<i>Component</i>	<i>Tool</i>
Data acquisition	MEOS
	EOLi/EOWEB (via internetbrowser)
	FTP
Image analysis	Erdas/Imagine and Python
	Aegir
	ENVI/SARscape
Geospatial analysis	Matlab runtime tool
	ArcGis
	Adobe reader
Dissemination	MAJIIC-NL

**CLASSIFICATION: UNCLASSIFIED**

*All rights reserved. No part of this document may be reproduced or transmitted in any form or by any means, electronic, mechanical, photocopying, recording, or otherwise, without prior written permission of FFI, NLR or TNO.*

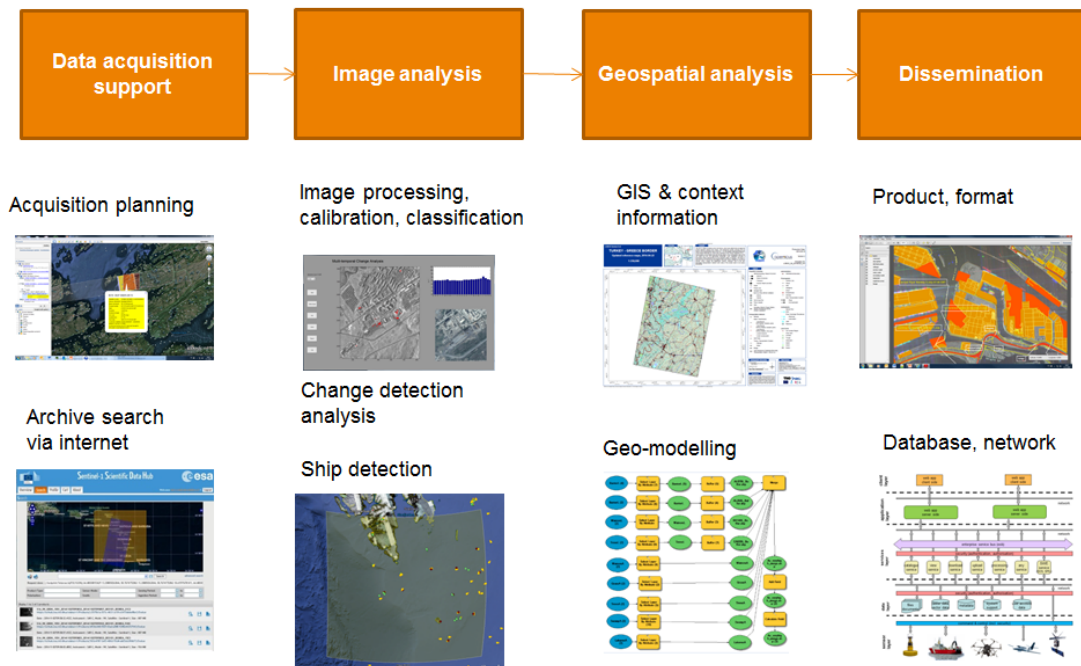


Figure 68 Workflow with the various test bed components.

**CLASSIFICATION: UNCLASSIFIED**

All rights reserved. No part of this document may be reproduced or transmitted in any form or by any means, electronic, mechanical, photocopying, recording, or otherwise, without prior written permission of FFI, NLR or TNO.

### 5.3 Use cases and demonstration

To develop the workflows and to demonstrate the test bed we have defined various use cases, which combine a location and a data type for a specific topic of interest for the three military domains. In Table 11 an overview is given.

Table 11 Overview of use cases

Use case	Location	Data type	Interest	Domain
1	Nikel	Radarsat spotlight Landsat	Activities near industrial complex and urban/land area	land
2	Barents sea	Sentinel-1A/-1B IW + AIS	Ships monitoring	maritime
3	Caribbean	Sentinel-1A/-1B IW + AIS	Ships monitoring	maritime
4	Rotterdam	COSMO- SkyMed spotlight Radarsat-2 extra fine, Sentinel IW, AIS Landsat, Formosat , DMC, Sentinel 2A	Ships monitoring & harbor activities, and land activities, incl. ELINT (simulated)	land
3	UV2014	Terra-SAR spotlight COSMO-SkyMed spotlight	CCDO (camouflage, concealment, deception and obscurants) & replacements of airplanes and vehicles	air
6	Kaliningrad	Sentinel-1A/-1B IW + AIS Sentinel-2A	Ships monitoring, harbor activities, airfield activities & activities near military complexes, incl. ELINT (simulated).	land

Use cases (Nikel, Rotterdam) are prepared as exercises for imagery analysts/ geospatial analysts (GSA) in a workshop at the Netherlands school of intelligence (DIVI). See also Appendix A,

### **CLASSIFICATION: UNCLASSIFIED**

All rights reserved. No part of this document may be reproduced or transmitted in any form or by any means, electronic, mechanical, photocopying, recording, or otherwise, without prior written permission of FFI, NLR or TNO.



For the NOMOD/coastguard the Barents Sea use case is relevant, while the Caribbean use case focuses on the Dutch effort to control drug trafficking. The Aegir component is relevant here. The Ørland use case is related to the UV2014 trials and is done in collaboration with the NATO/SET220 (Sensors & technology) working group, which is also studying the Kaliningrad test site.

The demonstration was defined using the different test bed components of TNO, NLR and FFI and on the integrated GeoInt component (realised by TNO). The integrated demonstration fuses the results of five underlying demonstrations based on the following testbed components (see figure 69).

1. Optical change detection in time series & anomalies (NLR)
2. Optical harbour ship detection (NLR)
3. SAR change detection in time series & anomalies (TNO)
4. SAR/AIS ship detection (FFI)
5. Radar emission (ELINT– Electronic signals Intelligence) detection (simulated by TNO)

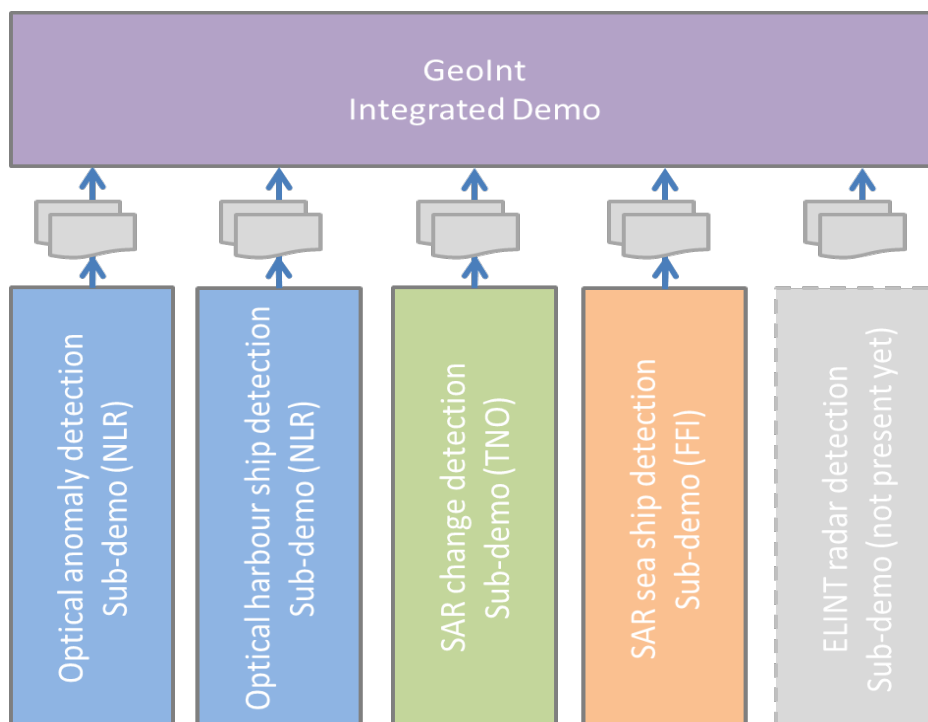


Figure 69. Overview of test bed components and demonstration of use cases

**CLASSIFICATION: UNCLASSIFIED**

All rights reserved. No part of this document may be reproduced or transmitted in any form or by any means, electronic, mechanical, photocopying, recording, or otherwise, without prior written permission of FFI, NLR or TNO.

For the integrated demonstration two scenarios are defined:

*A. Radar emission detection*

From an ELINT satellite an emission from a surveillance/fire control radar is detected (position with inaccuracies of several kilometres). A further analysis is made for this detection by using context information from other satellite images. Optical change detection in the harbour area is carried out with a series of optical observations of the last year period. A change map is shown as a grey image with the changes in red. It is possible to click on a change and then further information of the change is shown: profile of image values in time, meta information of the change, possibly a video clip of images for an AOI (Area Of Interest) around the change position. SAR change detection is carried out with a series of SAR observations of the last year period. The results are handled analogue to the optical changes as described above. Related maps and HRSI (High Resolution Satellite Imagery) images from Google can be shown.

*B. Suspect ship activities*

Suspect ship movements at sea are detected with the Aegir SAR/AIS application. Suspect ship activities in the harbour are detected with the NLR harbour ship detection application. For harbour sections of interest analyses are made of changes in this area during the last period using the SAR and Optical change detection functionality for series of satellite observations.

The demonstration set-up can be summarized as follows: The use cases are defined (see Table 11) by the location (e.g. Kaliningrad), data type (e.g. Sentinel-1A IW – Interferometric Wide) and what is of interest (e.g. harbour activities). For the demonstration a test bed component is applied to the use cases. In the next sub section we first describe the 5 use cases followed by subsections describing the test bed components. In these subsections also demonstration examples are given. Figure 70 picturizes the demonstration set-up.

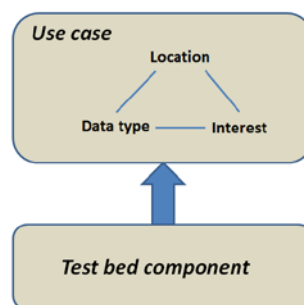


Figure 70 Demonstration set-up

**CLASSIFICATION: UNCLASSIFIED**

All rights reserved. No part of this document may be reproduced or transmitted in any form or by any means, electronic, mechanical, photocopying, recording, or otherwise, without prior written permission of FFI, NLR or TNO.

### 5.3.1 Use case description

We discuss in the following the use cases from Table 11. The combination of data type and topic of interest is always indicated too.

#### 5.3.1.1 Use case 1: Nikel

The use case Nikel is focused on the Nikel melt installation in the Murmansk Oblast which produces excessive amounts of the polluting sulphur dioxide. Its location near the Norwegian border implies that the polluting footprint is of serious concern for Norway.

Discussion about reduction of the activities and a possible shut-down is going on. The topic of interest is therefore to monitor the activities in the complex and the nearby town in order to infer the economic use of the melt plant. See figure 71 for an impression of the topic.



Figure 71 The Nikel area and the Nikel melt plant.

#### Radars data & activities near industrial complex

To monitor the activities RADARSAT-2 spotlight data have been collected each month for 2 years starting from autumn 2011 until autumn 2013 over the Nikel area (see Figure 72). The data are co-registered and projected to ground range. The resulting ground resolution is 2 x 2 meter implying that some averaging has been applied in order to reduce the speckle (multi-looking).

### CLASSIFICATION: UNCLASSIFIED

All rights reserved. No part of this document may be reproduced or transmitted in any form or by any means, electronic, mechanical, photocopying, recording, or otherwise, without prior written permission of FFI, NLR or TNO.

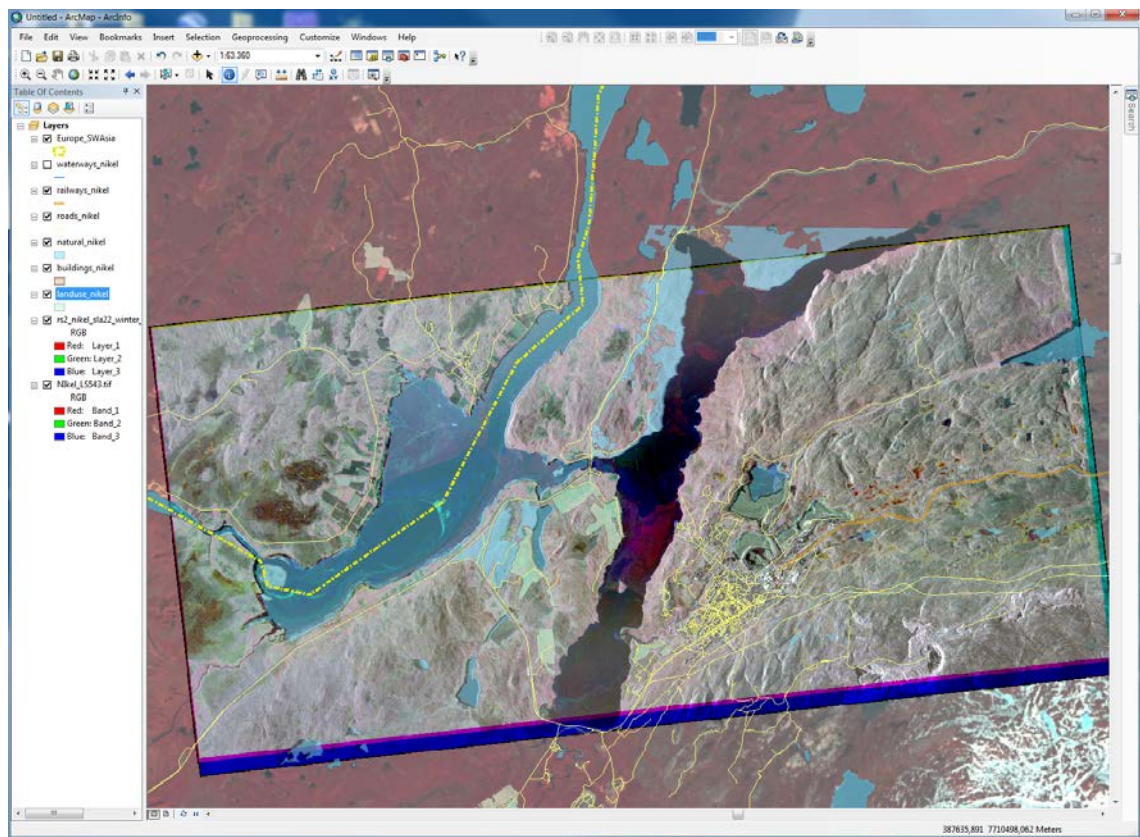


Figure 72. Radar data (three dates in the RGB colour channels) projected over a Landsat image,. The border between Norway and Russia is indicated.

### *Optical data & land activities*

To monitor activities and the development in the area Landsat data over the various years have been collected, calibrated and co-registered. The data are suitable to monitor vegetation growth, agricultural activities, and seasonal changes due to snow cover etc. Figure 73 shows the Landsat image.

## **CLASSIFICATION: UNCLASSIFIED**

All rights reserved. No part of this document may be reproduced or transmitted in any form or by any means, electronic, mechanical, photocopying, recording, or otherwise, without prior written permission of FFI, NLR or TNO.



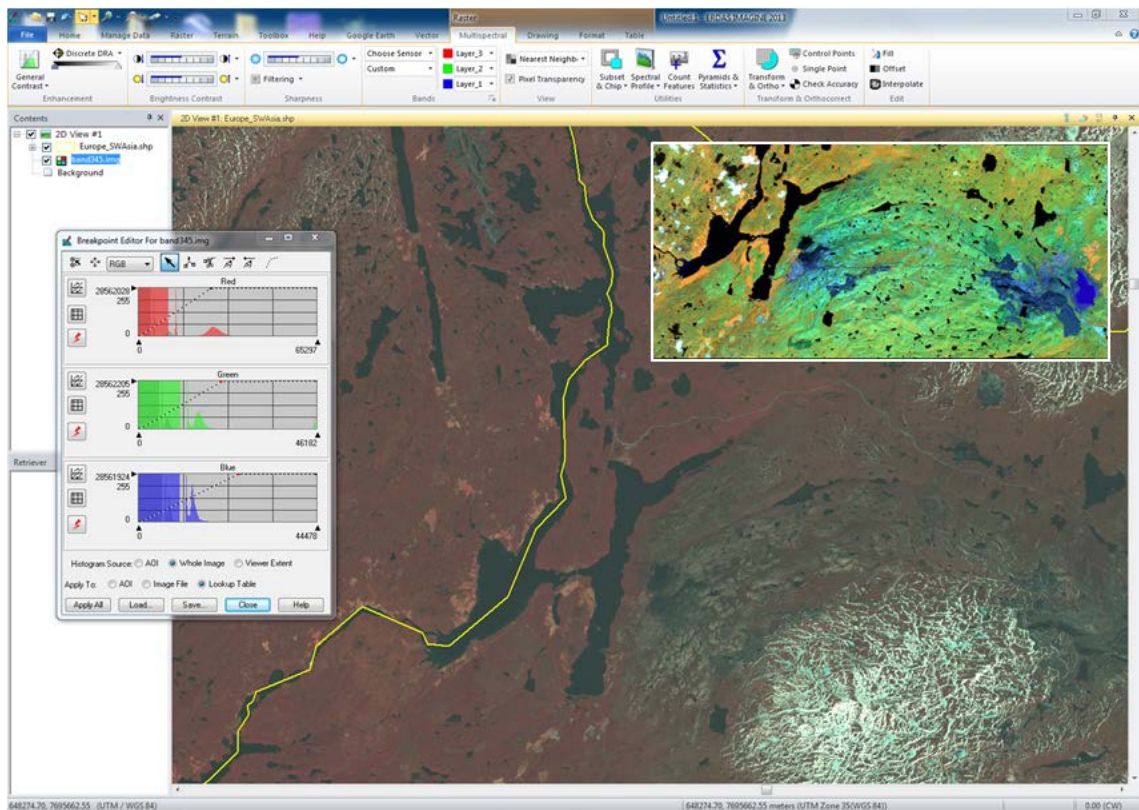


Figure 73 Landsat multispectral image showing the area and a multi-spectral image in the near infrared revealing more land use details.

### 5.3.1.2 Use case 2: Barents sea

#### Ship monitoring (Aegir) and Sentinel data

This subchapter will give some demonstration cases on the use of Aegir, the ship detection results that Aegir gives and the fusion with AIS data. Sentinel-1A images are used in these tests. When running Aegir, the data is ingested and loaded on screen, the land mask module and ship detection algorithm are run, and the ship detections are displayed on screen on top of the SAR image. The ship detections are marked in different colours depending on which channel the vessels are detected in. Figure 74 shows an example of a Sentinel-1A IW VV/VH image on December 9<sup>th</sup> 2015 from the north of Norway and the Barents Sea. Five detections are done in total outside the land mask, where two are done in the VV-channel and five detections are done in the VH-channel. Close-up of some of the detections done in Aegir is shown in the same figure.

**CLASSIFICATION: UNCLASSIFIED**

All rights reserved. No part of this document may be reproduced or transmitted in any form or by any means, electronic, mechanical, photocopying, recording, or otherwise, without prior written permission of FFI, NLR or TNO.



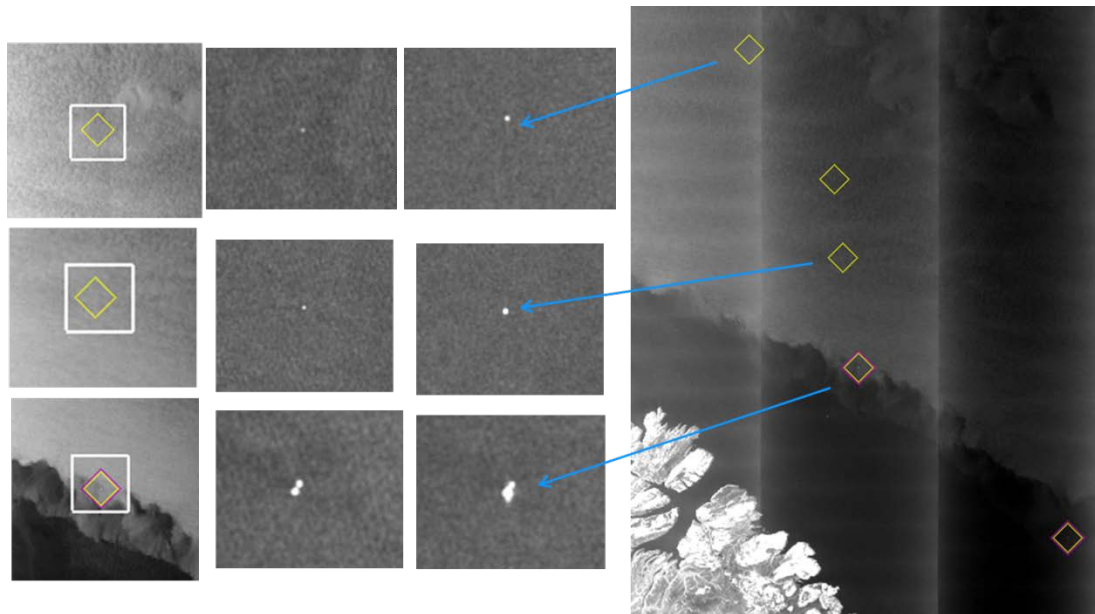
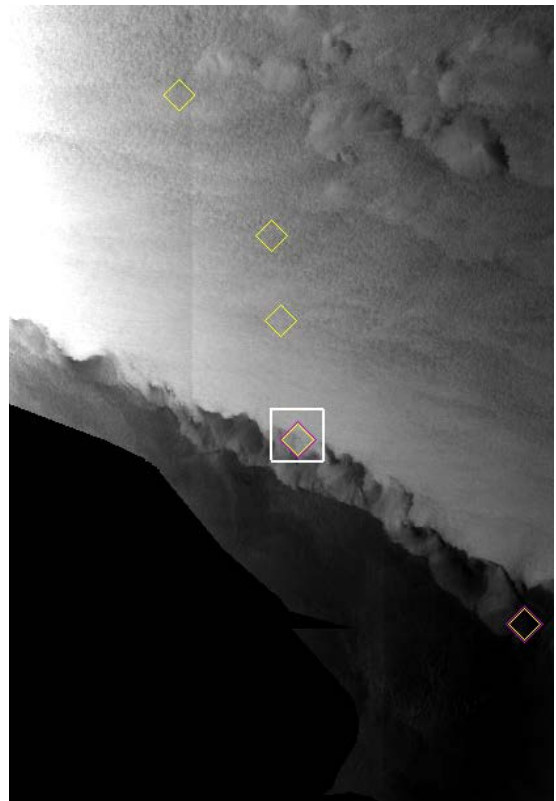


Figure 74 Top left: Coverage of Sentinel-1A IW VV/VH image on December 9<sup>th</sup> 2015. Top right: SAR image and ship detections done by Aegir in both polarisation channels. Bottom: Close-up of some of the detections.

**CLASSIFICATION: UNCLASSIFIED**

All rights reserved. No part of this document may be reproduced or transmitted in any form or by any means, electronic, mechanical, photocopying, recording, or otherwise, without prior written permission of FFI, NLR or TNO.

### 5.3.1.3 Use case 3: Caribbean

#### *Ship monitoring (Aegir) and Sentinel data*

Figure 75 shows the coverage of the Sentinel-1A IW GRDH (Ground Detected High) VV-polarisation image used in this use case. The image is from May 30<sup>th</sup> 2015 at 10:06. Figure 76 shows Sentinel-1A SAR image in VV-polarisation displayed with land mask and ship detections in purple diamonds. Figure 77 shows the same SAR image in Google Earth together with SAR ship detections and AIS data. Figure 78 shows a close up of the island Sint-Eustatius with ship detections done by Aegir where four detections are confirmed by AIS data.

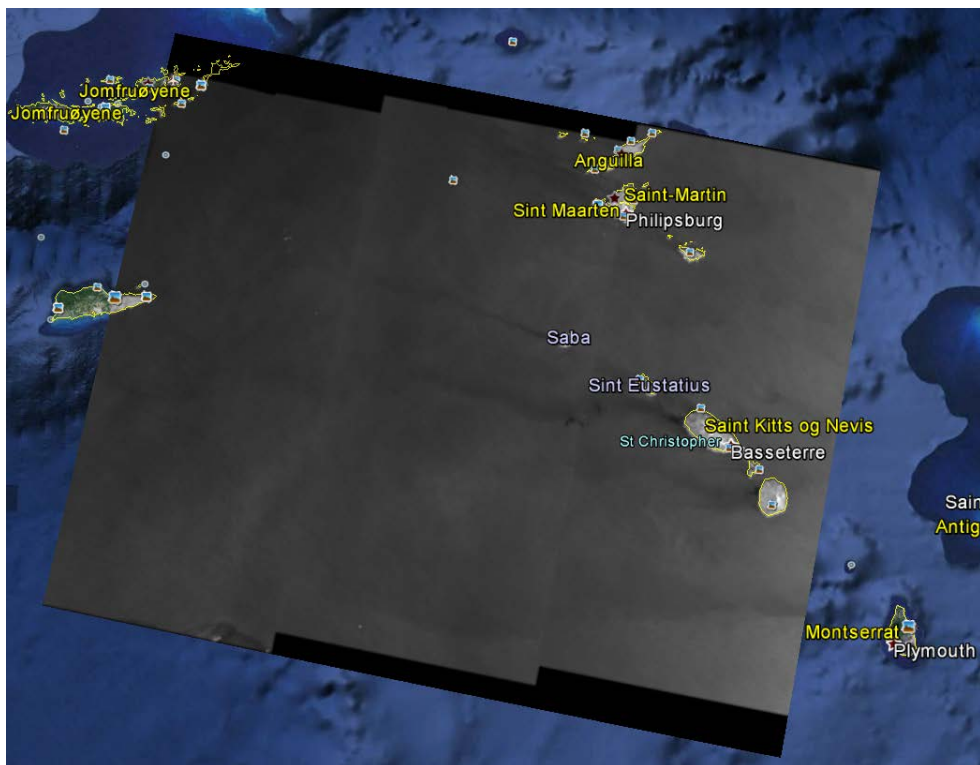


Figure 75 Coverage of Sentinel-1A image on May 30<sup>th</sup> 2015 at 10:06 covering part of the Caribbean. © Google Earth.

## **CLASSIFICATION: UNCLASSIFIED**

All rights reserved. No part of this document may be reproduced or transmitted in any form or by any means, electronic, mechanical, photocopying, recording, or otherwise, without prior written permission of FFI, NLR or TNO.

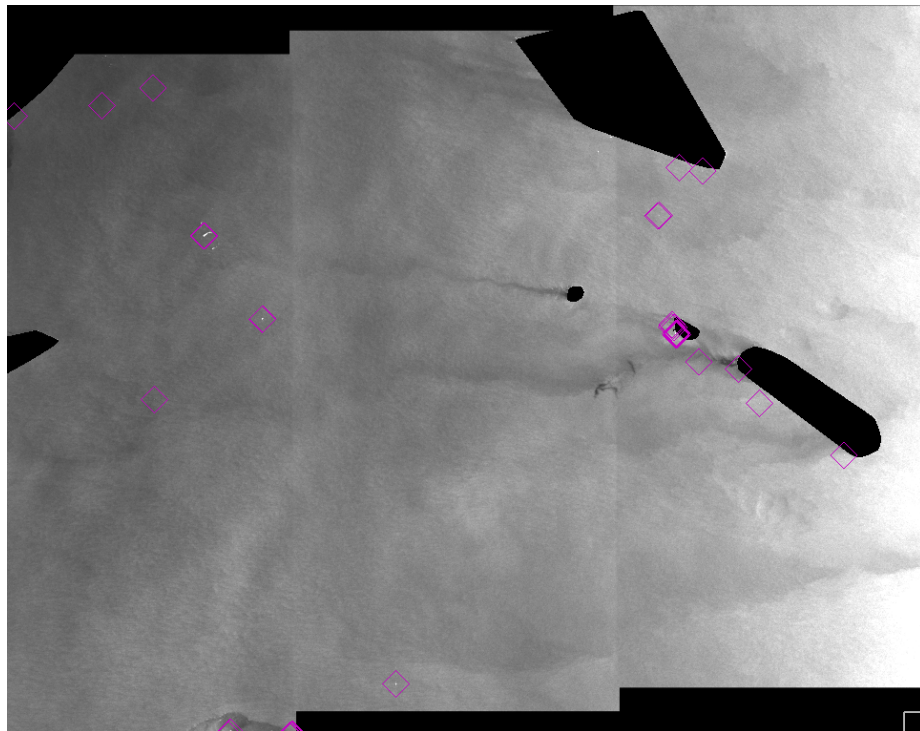


Figure 76 Sentinel-1A IW image on May 30<sup>th</sup> 2015 with land mask and ship detections in the VV-channel.

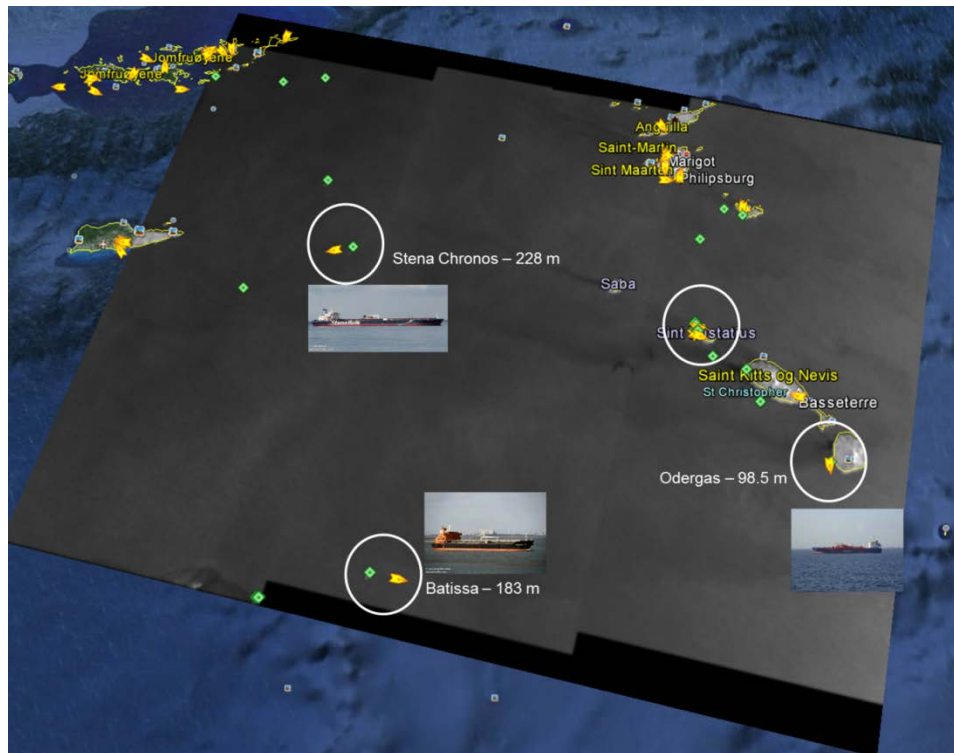


Figure 77 Sentinel-1A IW image on May 30<sup>th</sup> 2015 shown in Google Earth together with SAR ship detections. © Google Earth

**CLASSIFICATION: UNCLASSIFIED**

All rights reserved. No part of this document may be reproduced or transmitted in any form or by any means, electronic, mechanical, photocopying, recording, or otherwise, without prior written permission of FFI, NLR or TNO.



Figure 78 Ship detections and AIS data shown together. © Google Earth

#### 5.3.1.4 Use case 4: Rotterdam

##### *Optical data and harbour activities*

For the optical demonstration two sub demonstrations were worked out in the Rotterdam area

- Anomaly detection in optical time series
- Harbour ship detection

The Port of Rotterdam is the largest port in Europe, and one of the largest harbours in the world. The yearly transfer of goods sums up to 465 million tonnes. This amount, when measured in sea-containers, corresponds to 16.5 million containers. If the containers are connected, this corresponds to a total length of 100.000 km (two and a half times the circumference of the Earth). The harbour area covers 12.500 ha. Yearly some 30.000 sea ships and about 110.000 inland vessels visit the Rotterdam harbour.

For the demonstration exercises of this study, a 22.5 km by 26.5 km area was chosen that encloses the western harbour and surrounding rural landscapes north and south of it. In this way both the ship detection (ship activity within the harbour) and the anomaly detection (of broader phenomena, not only ship movements but also other infrastructural changes) can be performed.

### **CLASSIFICATION: UNCLASSIFIED**

*All rights reserved. No part of this document may be reproduced or transmitted in any form or by any means, electronic, mechanical, photocopying, recording, or otherwise, without prior written permission of FFI, NLR or TNO.*



In Figure 79 a map of the Port of Rotterdam is shown and Figure 80 shows the map overlaid with a satellite image that encompasses the 22.5 km x 26.5 km study area.



Figure 79 Port of Rotterdam (source: World Topo Map ESRI).

**CLASSIFICATION: UNCLASSIFIED**

All rights reserved. No part of this document may be reproduced or transmitted in any form or by any means, electronic, mechanical, photocopying, recording, or otherwise, without prior written permission of FFI, NLR or TNO.



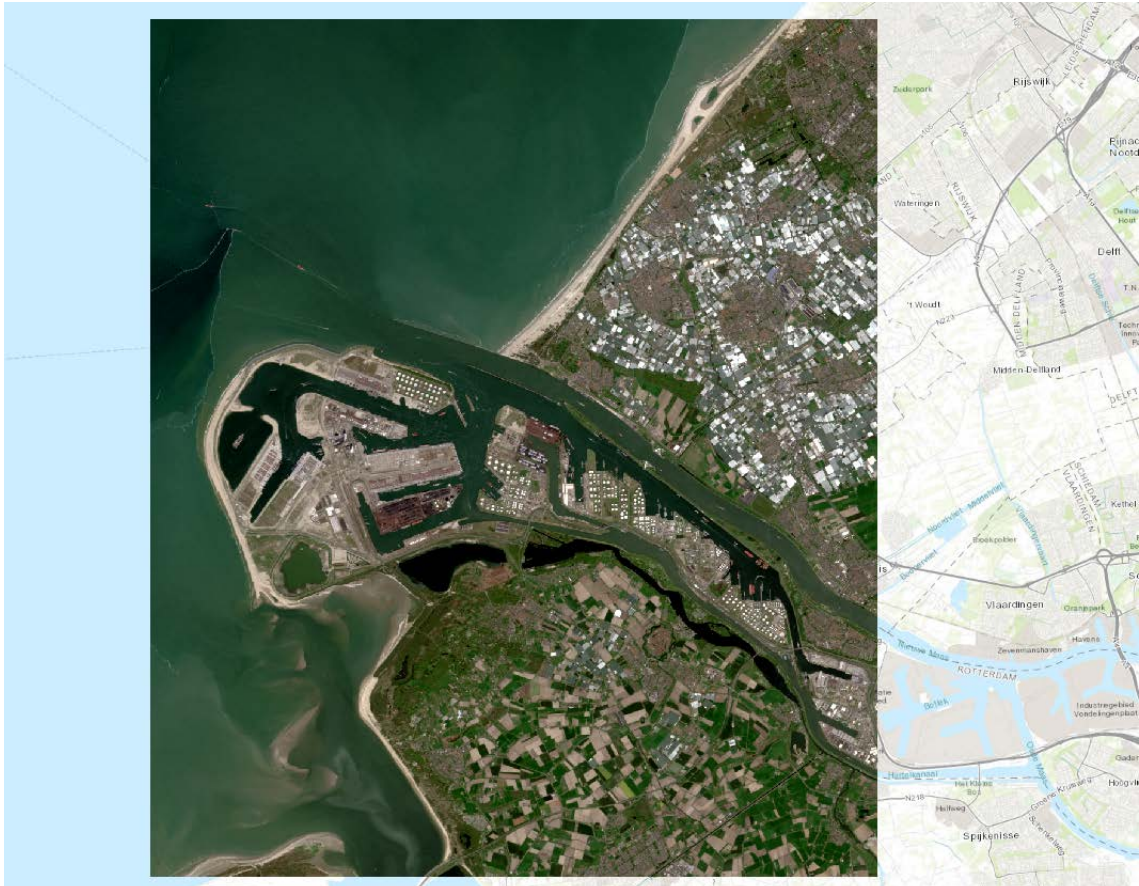


Figure 80 Port of Rotterdam overlaid with satellite image that encompasses 22.5 km x 26.5 km.

### *DMC imagery*

For the ship detection study 18 DMC satellite images were collected. The acquisition dates of the images span the period between April and September 2013. All images have been ortho-corrected to the UTM map projection (EPSG 32631 (European Programme Strategy Group)) by means of the semi-automatic Keystone processing software (see also paragraph 3.2.2.1). Next, atmospheric corrections have been applied in order to generate calibrated images that are comparable with each other. The used method is a correction towards so-called BOA reflectance. The general background explanation of this can be found in paragraph 3.2.2.1, but the method used for DMC imagery is slightly different because of the characteristics of the DMC data. Gain data have to be used as a division factor (depends on satellite and production level), and the DMC metadata offset values are not reliable (and therefore not used). That's why the two calculation steps towards BOA reflectance are now as follows:

1.  $L = (DN - DP) / \text{gain}$
2.  $\sigma = \pi * d^2 * L / E_0 * \cos\theta$

### **CLASSIFICATION: UNCLASSIFIED**

*All rights reserved. No part of this document may be reproduced or transmitted in any form or by any means, electronic, mechanical, photocopying, recording, or otherwise, without prior written permission of FFI, NLR or TNO.*

where:

- L = radiance
- DN = Digital Number
- DP = Darkest Pixel
- $\sigma$  = reflection value
- d = distance Sun – Earth
- E = exoatmospheric irradiance
- $\theta$  = zenith angle Sun

After the corrections described above are done, the DMC dataset shown in Figure 81 is available. The acquisition dates used are shown in the figure from left to right / top to bottom.

20130407	20130418	20130421	20130501	20130506
20130519	20130527	20130602	20130608	20130707
20130715	20130723	20130801	20130805	20130823
20130827	20130906	20130927		

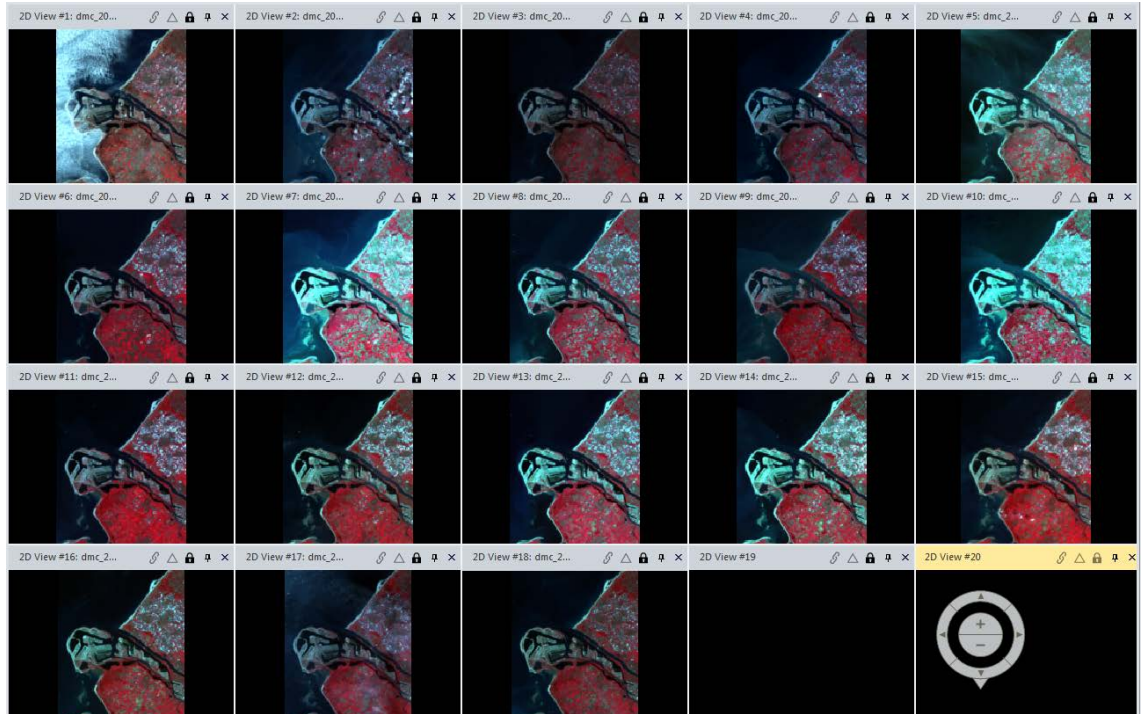


Figure 81 DMC recordings between April and September 2013.

**CLASSIFICATION: UNCLASSIFIED**

All rights reserved. No part of this document may be reproduced or transmitted in any form or by any means, electronic, mechanical, photocopying, recording, or otherwise, without prior written permission of FFI, NLR or TNO.

### *Sentinel-2A imagery*

The arrival of free of cost medium resolution Sentinel optical data in the course of the project gave cause to adding these data to the demonstration case of Rotterdam harbour. Four of the thirteen spectral bands of Sentinel 2A (S2A) have a resolution of 10 meters. These bands were selected for the demo-study. S2A data can be downloaded via the ESA Sentinel Scientific data hub (see also paragraph 2.2) and its level of processing (L1C) is such that geometric and radiometric accuracy is already of a high level.

L1C involves ortho correction towards a UTM WGS84 map projection with a geolocation accuracy of, according to the Sentinel specifications, 12.5 meters at 95% confidence level (with ground control points). The map output grid is co-registered, that holds for the mutual spectral bands as well as for different acquisition dates. In other words, pixels of any spectral band or any acquisition date will always fit exactly in the same output grid so that pixels can be projected on each other. A visual check of a S2A L1C image, projected over a World Topo Map (ESRI) learns that the satellite image fits quite well. Well enough to take the images as they are and use the dataset of 19 Sentinel recordings of 2016 in the geometric state as made available. The S2A L1C products are already converted to TOA (Top Of Atmosphere) reflectance. But the DN values are multiplied with a factor 10.000 in order to have them as integer values in a 12-bit range. For obtaining reflection files with values between 0 and 1 a simple division by 10.000 can be applied. The acquisition dates of Sentinel-2A used in Figure 82 are shown from left to right/top to bottom.

20151223	20160125	20160305	20160312	20160401
20160411	20160421	20160501	20160504	20160511
20160610	20160703	20160710	20160720	20160901
20160908	20160928	20161008	20161031	

### **CLASSIFICATION: UNCLASSIFIED**

*All rights reserved. No part of this document may be reproduced or transmitted in any form or by any means, electronic, mechanical, photocopying, recording, or otherwise, without prior written permission of FFI, NLR or TNO.*



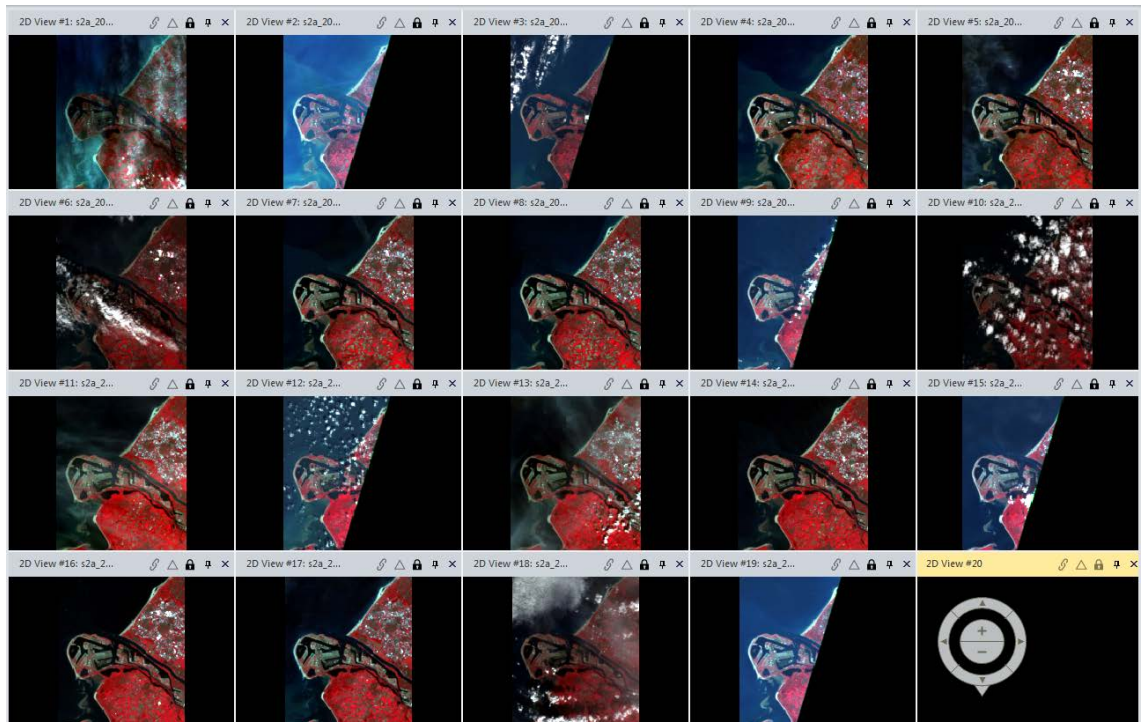


Figure 82 Sentinel-2A recordings from 2016.

#### *Radar data and harbour activities*

For the Rotterdam harbour area various radar data types have been used, ranging from high resolution to medium resolution. The highest resolution is found for COSMO-SkyMed spotlight data which have been collected in the framework of the NATO/SET145 working group. Four acquisition dates are used: 29 June, 30 June, 3 July, and 7 July 2011.

For RADARSAT Extra Fine (XF) mode data with a ground resolution of about 5 meters for 6 dates each month in autumn 2015 are used.

Sentinel-1A SM (Stripmap) mode data have been used for two dates: 20 October 2014 and 12 January 2015. The ground resolution is about 5 meter, which is comparable to the RADARSAT-2 XF mode. Sentinel-1A data IW mode have been used for several dates in 2015. Ground resolution is in the order 10 meter.

These time series are used to apply multi-temporal changes detection to detect ship displacements, changes in oil terminal content and other activities related to storage of good etc. Figure 83 – Figure 86 show examples for each data type.

### **CLASSIFICATION: UNCLASSIFIED**

*All rights reserved. No part of this document may be reproduced or transmitted in any form or by any means, electronic, mechanical, photocopying, recording, or otherwise, without prior written permission of FFI, NLR or TNO.*

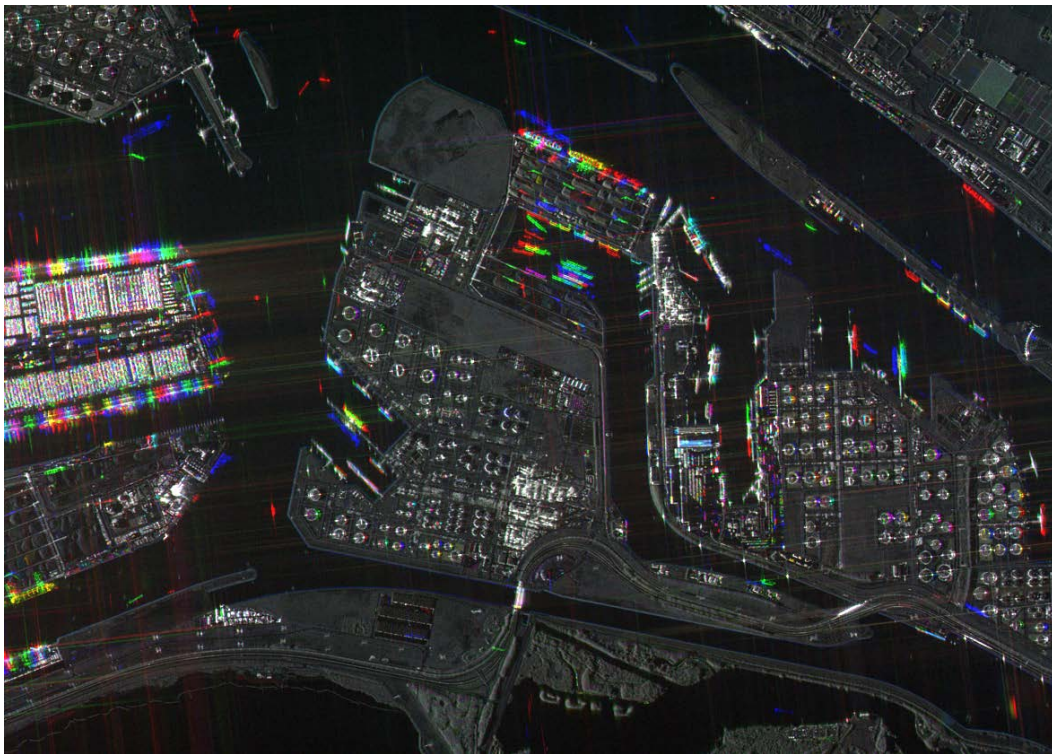


Figure 83. COSMO-SkyMed data showing three dates in the RGB color channels.

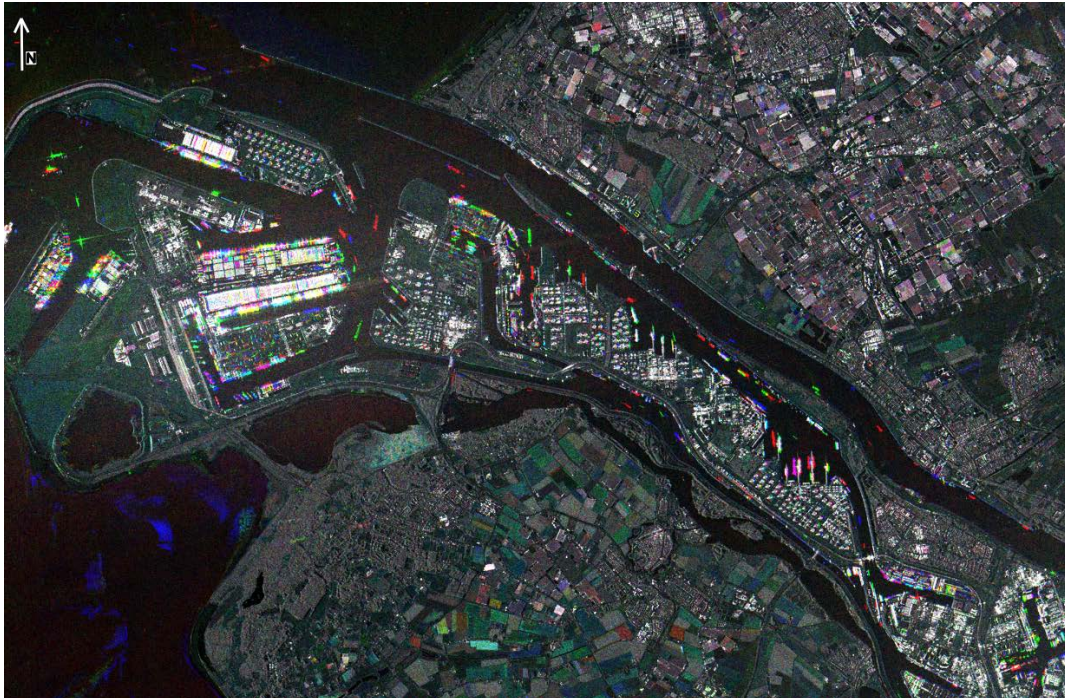


Figure 84 Radarsat2 XF mode data for three dates in the RGB channels.

**CLASSIFICATION: UNCLASSIFIED**

All rights reserved. No part of this document may be reproduced or transmitted in any form or by any means, electronic, mechanical, photocopying, recording, or otherwise, without prior written permission of FFI, NLR or TNO.



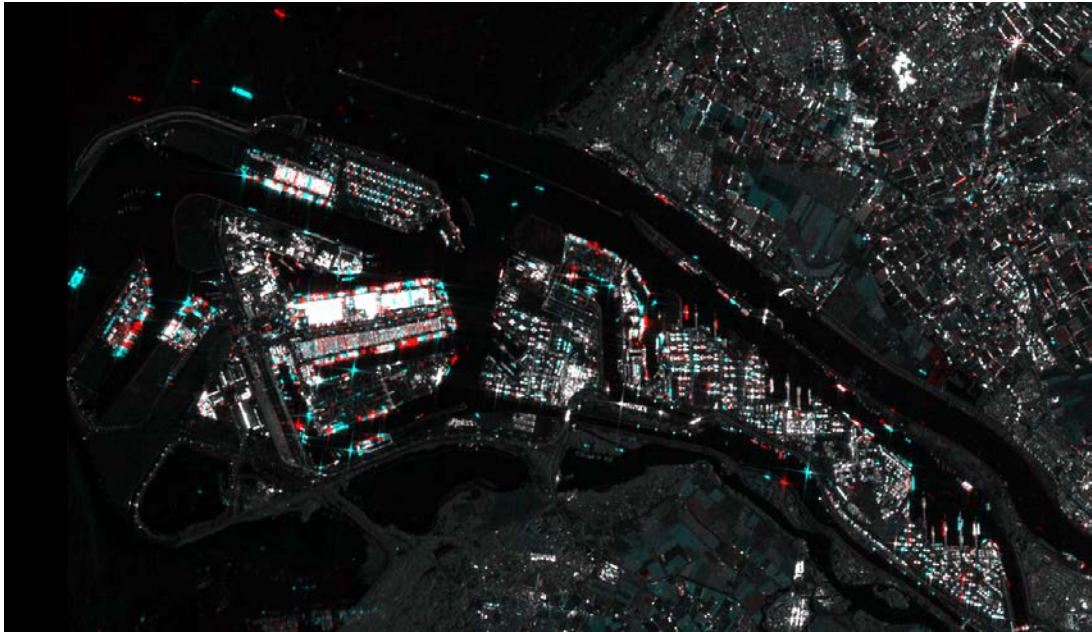


Figure 85 Sentinel 1A SM data for two dates in the RGB channels.

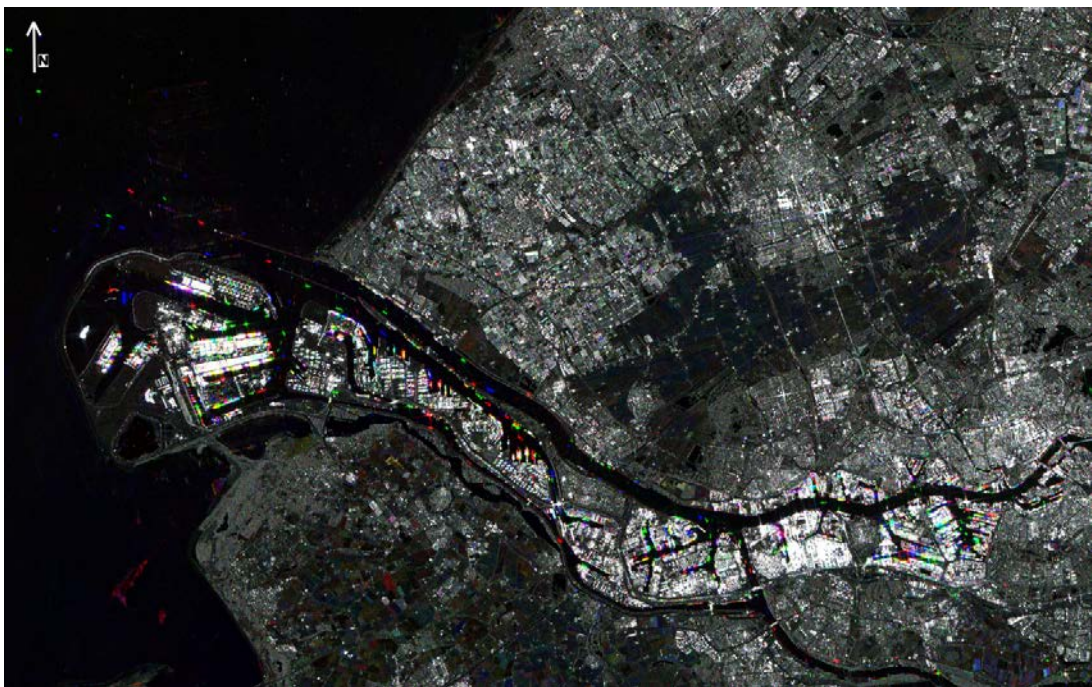


Figure 86 Sentinel 1A IW data for three dates in the RGB channels.

#### *Ship monitoring (Aegir) and Sentinel data*

Figure 87 shows the coverage of the Sentinel-1A image used in the use case. The image is IW GRDH dual-polarisation VV/VH from June 1<sup>st</sup> 2015 at 17:32. Figure 88 shows the SAR image in VH-polarisation where windmill parks and many vessels are easily visible. Figure 89 shows

### **CLASSIFICATION: UNCLASSIFIED**

All rights reserved. No part of this document may be reproduced or transmitted in any form or by any means, electronic, mechanical, photocopying, recording, or otherwise, without prior written permission of FFI, NLR or TNO.

the VV-channel with land mask and masks over the wind mill parks. Figure 90 shows the SAR image with land mask, masks over the wind mill parks, ship detections in yellow and ship detections confirmed by AIS data in green. Figure 91 shows the same as Figure 90, but here is also AIS data in red shown.

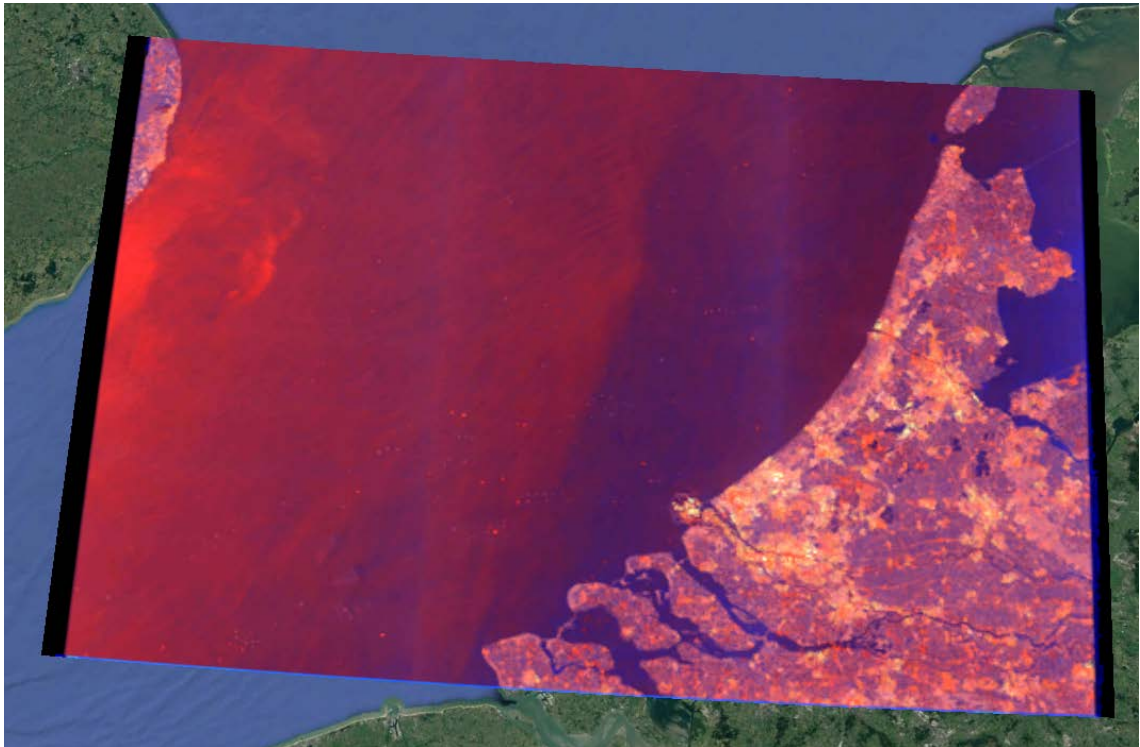


Figure 87 Coverage of Sentinel-1A image on June 1<sup>st</sup> 2015 covering Rotterdam.  
© Google Earth

**CLASSIFICATION: UNCLASSIFIED**

All rights reserved. No part of this document may be reproduced or transmitted in any form or by any means, electronic, mechanical, photocopying, recording, or otherwise, without prior written permission of FFI, NLR or TNO.



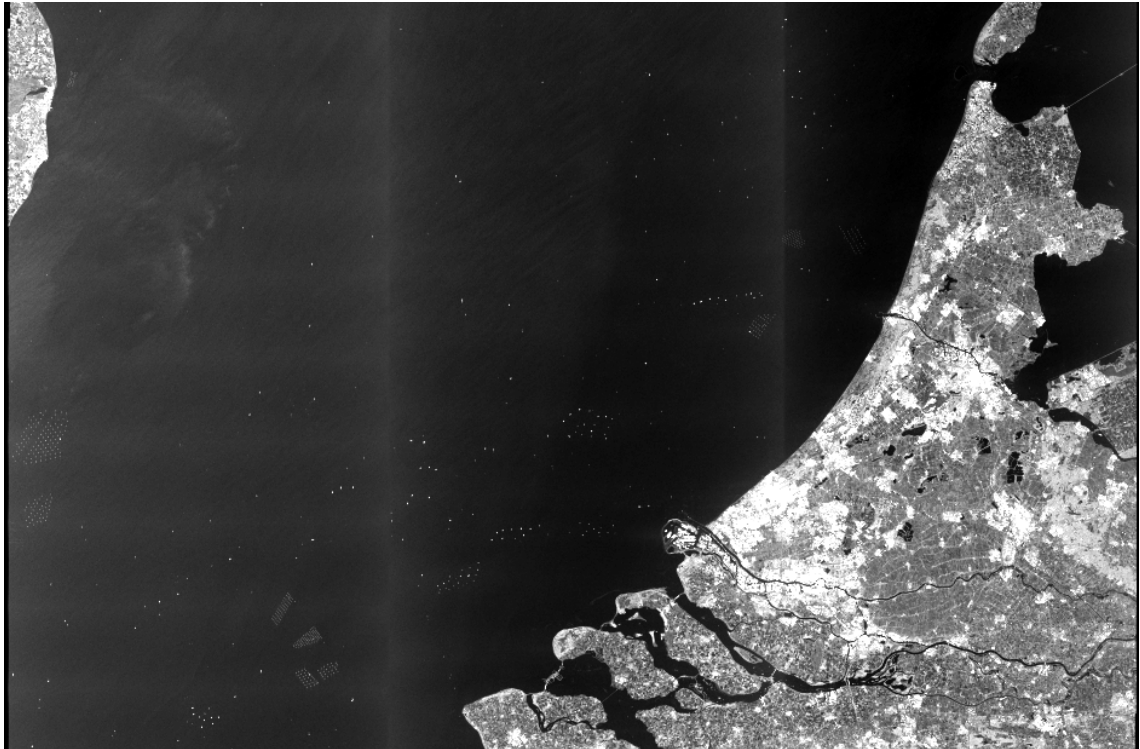


Figure 88 Sentinel-1A IW image on June 1<sup>st</sup> 2015 in VH-polarisation showing Rotterdam and the sea outside Rotterdam.

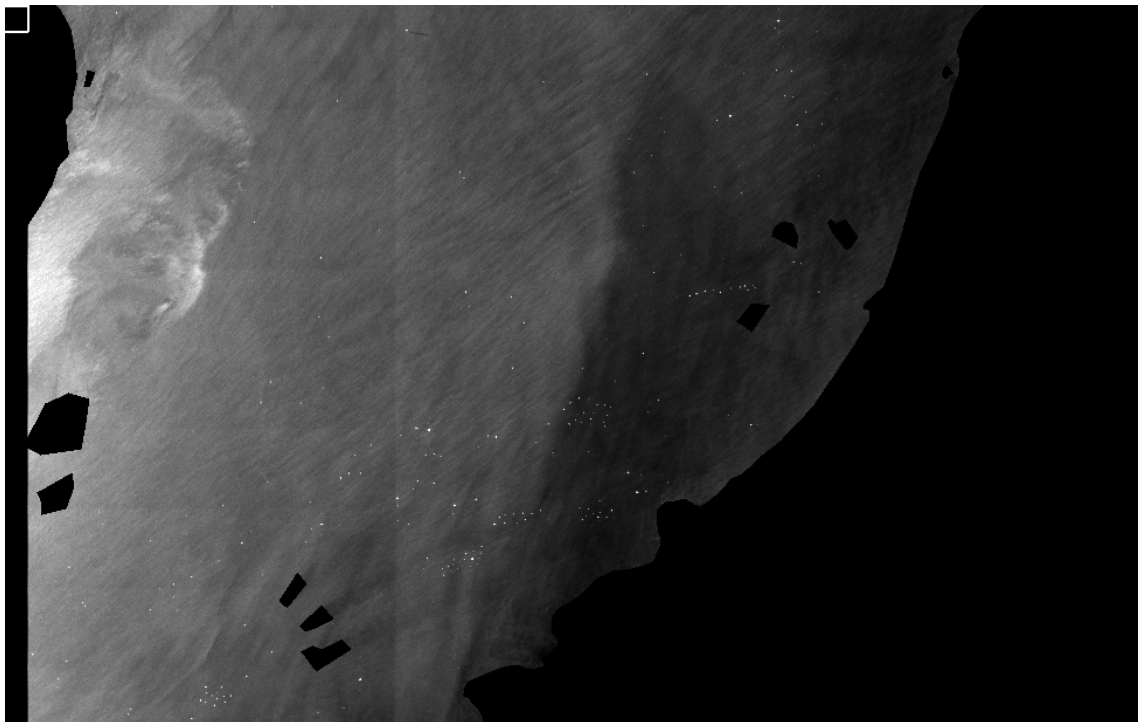


Figure 89 Sentinel-1A IW image on June 1<sup>st</sup> 2015 in VV-polarisation with land mask.

**CLASSIFICATION: UNCLASSIFIED**

All rights reserved. No part of this document may be reproduced or transmitted in any form or by any means, electronic, mechanical, photocopying, recording, or otherwise, without prior written permission of FFI, NLR or TNO.

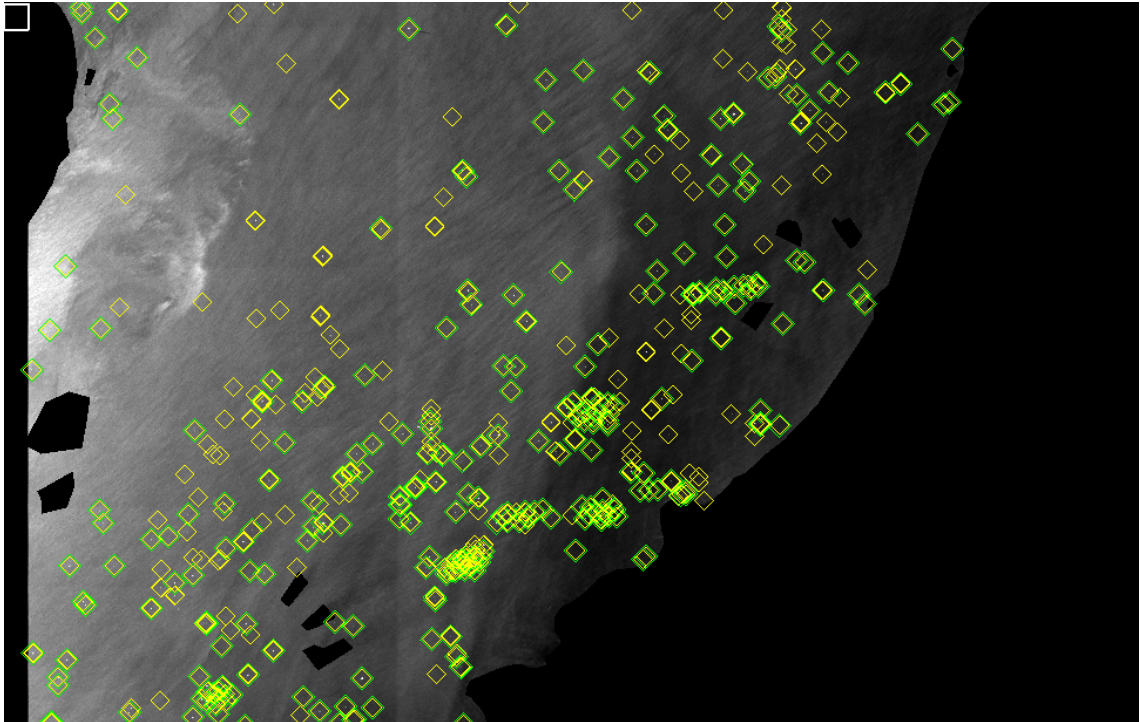


Figure 90 Sentinel-1A IW image on June 1<sup>st</sup> 2016 with land mask and ship detections done by Aegir in yellow. Green diamonds mean that the SAR ship detections are confirmed by AIS data.

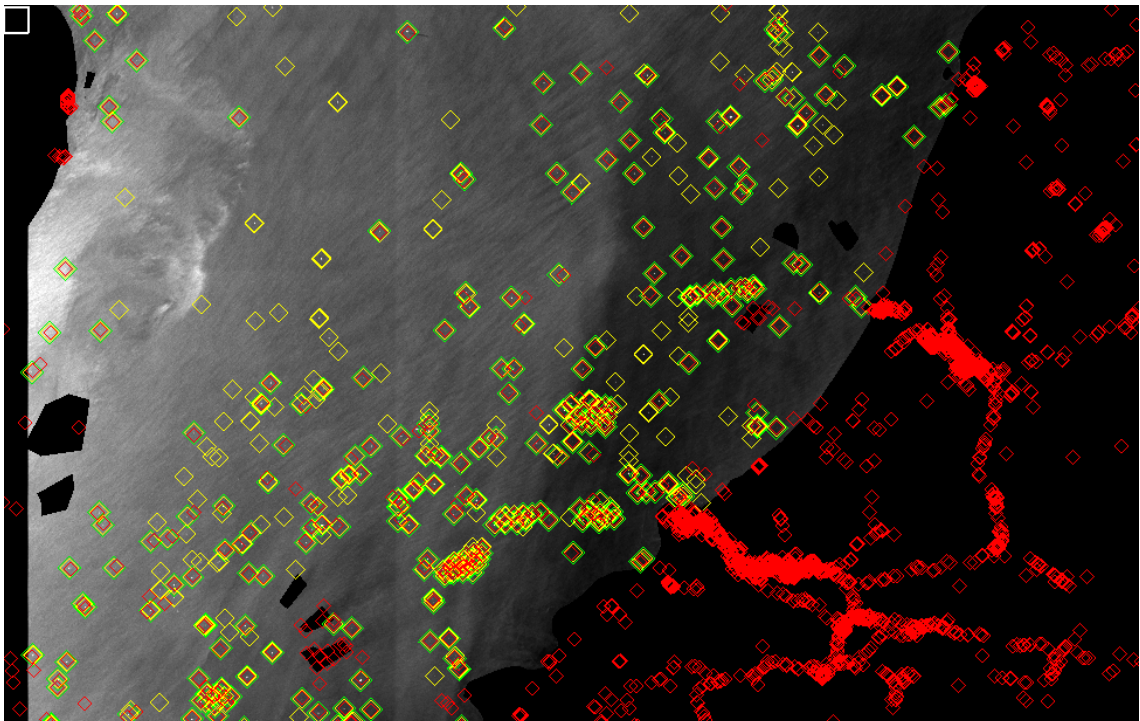


Figure 91 Sentinel-1A IW image on June 1<sup>st</sup> 2016 with ship detections done by Aegir (yellow) as well as AIS data (red). Green diamonds mean that the SAR ship detections are confirmed by AIS data.

### **CLASSIFICATION: UNCLASSIFIED**

All rights reserved. No part of this document may be reproduced or transmitted in any form or by any means, electronic, mechanical, photocopying, recording, or otherwise, without prior written permission of FFI, NLR or TNO.



### 5.3.1.5 Use case 5: UV2014

#### *High resolution radar data and replacements of airplanes and vehicles*

In this test case several spotlight images were collected with TerraSAR-X and COSMO-SkyMed (resolution in the order of 1 meter). Recordings were done 18 May 2014, 19 May 2014, 22 May 2014, 30 May 2014 (2x), and 10 June 2014 before, during and after the UV2014 trial. On and near the airfield, several displacements of aircrafts and vehicles are present, which can be detected using SAR change detection. Also camouflaged objects were deployed. Due to lack of ground truth information their possible detections are not further discussed here. Figure 92 shows Ørland airbase and the surroundings.



Figure 92 Overview of the radar data for the Ørland airbase.

## **CLASSIFICATION: UNCLASSIFIED**

All rights reserved. No part of this document may be reproduced or transmitted in any form or by any means, electronic, mechanical, photocopying, recording, or otherwise, without prior written permission of FFI, NLR or TNO.

### 5.3.1.6 Use case 6: Kaliningrad

#### *Sentinel data and harbour/airfield activities & activities near military complexes*

The Kaliningrad area is a Russian enclave in the EU close to Poland and Lithuania. Currently the interest in the enclave is increasing since Russia is moving modern missiles (S-400) to the enclave in response to the US protection shield to be deployed in Poland. The S-400 missiles cover a large range up to 500 km to create "Anti-access/area denial" (A2/AD) for NATO. See NATO Defence Collage document: <http://www.ndc.nato.int/news/news.php?icode=906>.

For the Kaliningrad area Sentinel data have been acquired for several dates in 2016. The area is covered using various orbits. To perform multi-temporal change detection, the same type of orbit has to be used in each image in order to avoid insignificant changes due to the radar illumination direction. An orbit can be identified using its relative orbit number (in this case 51). Below a Sentinel image is shown covering the complete Kaliningrad oblast. The main interest is to discover activities in the military harbour in Baltiejsk and the naval air base in Chkalovsk. Furthermore there are several military sites, also for missile-based air defence.

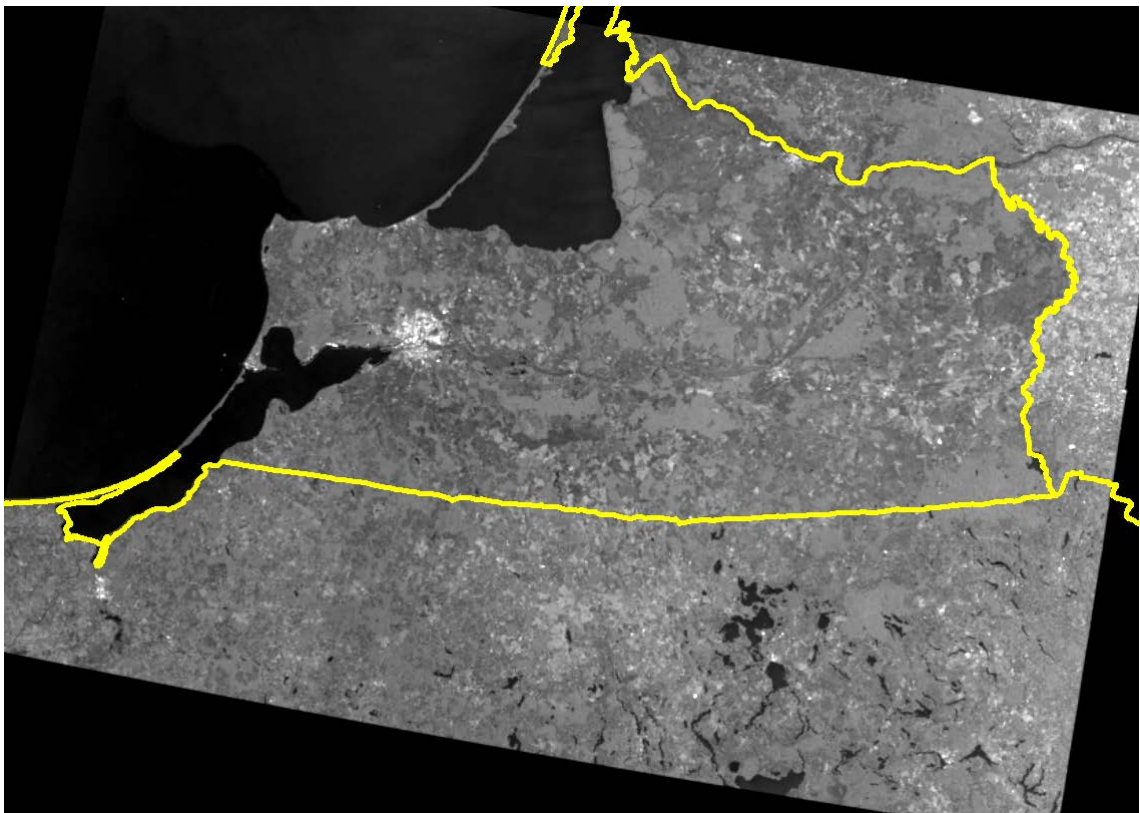


Figure 93 Sentinel image used for the Kaliningrad Oblast.

### **CLASSIFICATION: UNCLASSIFIED**

All rights reserved. No part of this document may be reproduced or transmitted in any form or by any means, electronic, mechanical, photocopying, recording, or otherwise, without prior written permission of FFI, NLR or TNO.

### *Ship monitoring (Aegir) and Sentinel data*

Figure 94 shows the coverage of the first Sentinel-1A image used in this use case. The image is IW GRDH dual-polarisation VV/VH from August 16<sup>th</sup> 2016 at 04:59. Figure 95 shows the SAR image with SAR detections done in Aegir in yellow, AIS detections in red and the green diamonds mean that the SAR ship detections are confirmed with AIS data.

Figure 96 shows the coverage of the second Sentinel-1A image used in this use case. The image is IW GRDH dual-polarisation VV/VH from September 9<sup>th</sup> 2016 at 04:59. Figure 97 shows the SAR image with a land mask and SAR detections done by Aegir in the VV-channel, while Figure 98 shows detections both in the VV- and the VH-channel. Figure 99 shows the SAR image with land mask and MMSI (Maritime Mobile Service Identity) numbers (from AIS data) on top of the image. Figure 100 shows the SAR image with SAR detections done in Aegir in yellow, AIS detections in red and the green diamonds mean that the SAR ship detections are confirmed with AIS data.

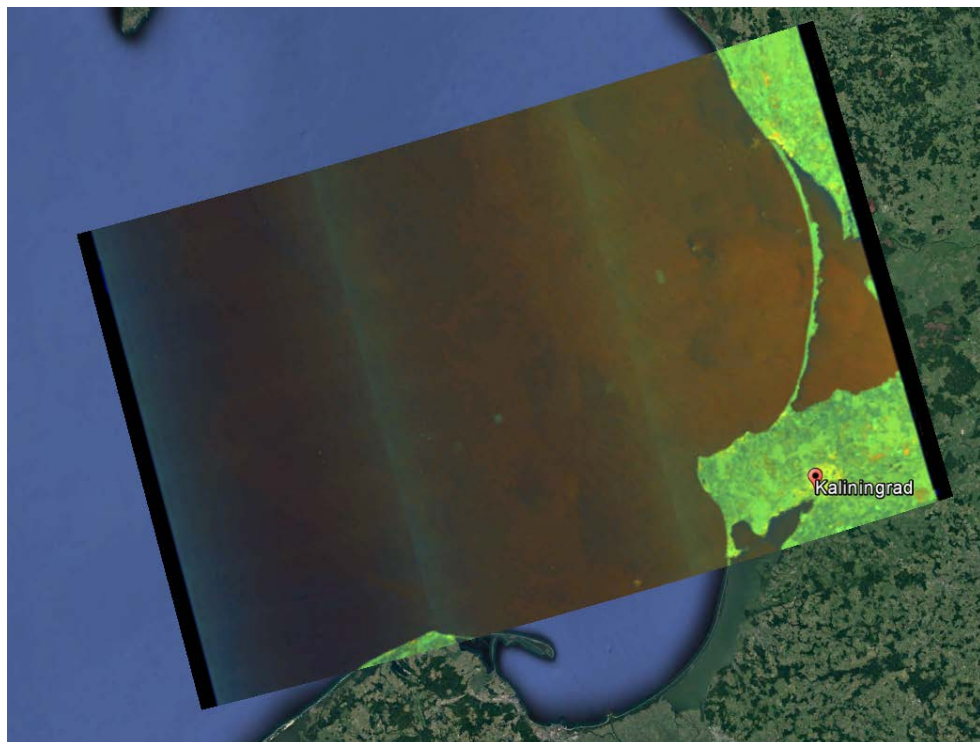


Figure 94 Coverage of Sentinel-1A image on August 16<sup>th</sup> 2016 covering Kaliningrad.  
© Google Earth

## **CLASSIFICATION: UNCLASSIFIED**

All rights reserved. No part of this document may be reproduced or transmitted in any form or by any means, electronic, mechanical, photocopying, recording, or otherwise, without prior written permission of FFI, NLR or TNO.



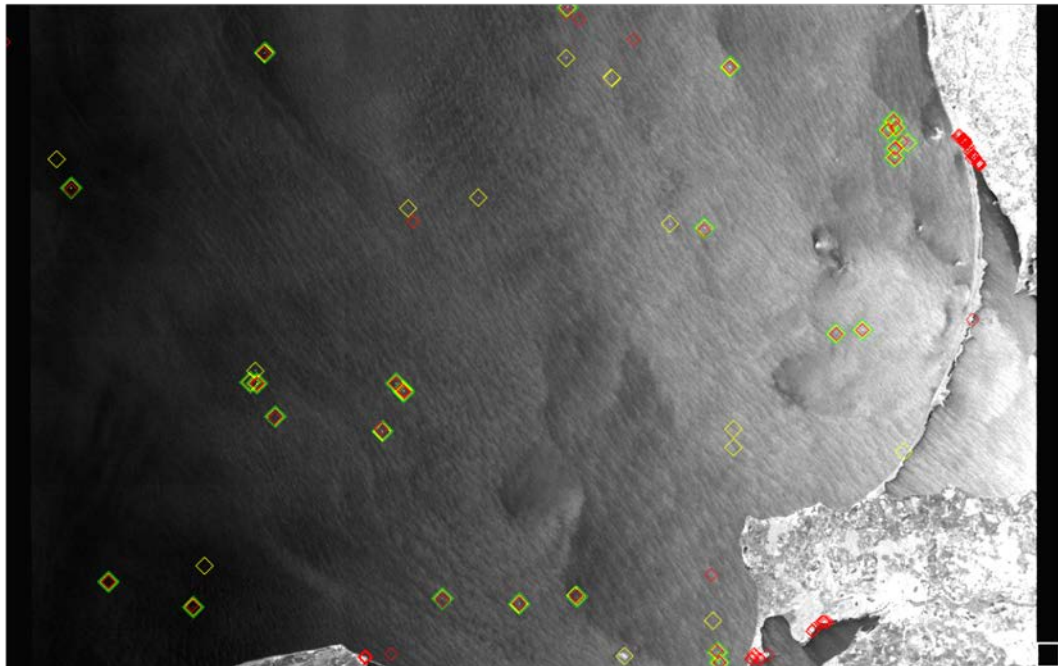


Figure 95 Sentinel-1A IW image on August 16<sup>th</sup> 2016 with ship detections done by Aegir (yellow) as well as AIS data (red) Green diamonds mean that the SAR ship detections are confirmed by AIS.



Figure 96 Coverage of Sentinel-1A image on September 9<sup>th</sup> 2016 covering Kaliningrad. ©  
Google Earth

**CLASSIFICATION: UNCLASSIFIED**

All rights reserved. No part of this document may be reproduced or transmitted in any form or by any means, electronic, mechanical, photocopying, recording, or otherwise, without prior written permission of FFI, NLR or TNO.



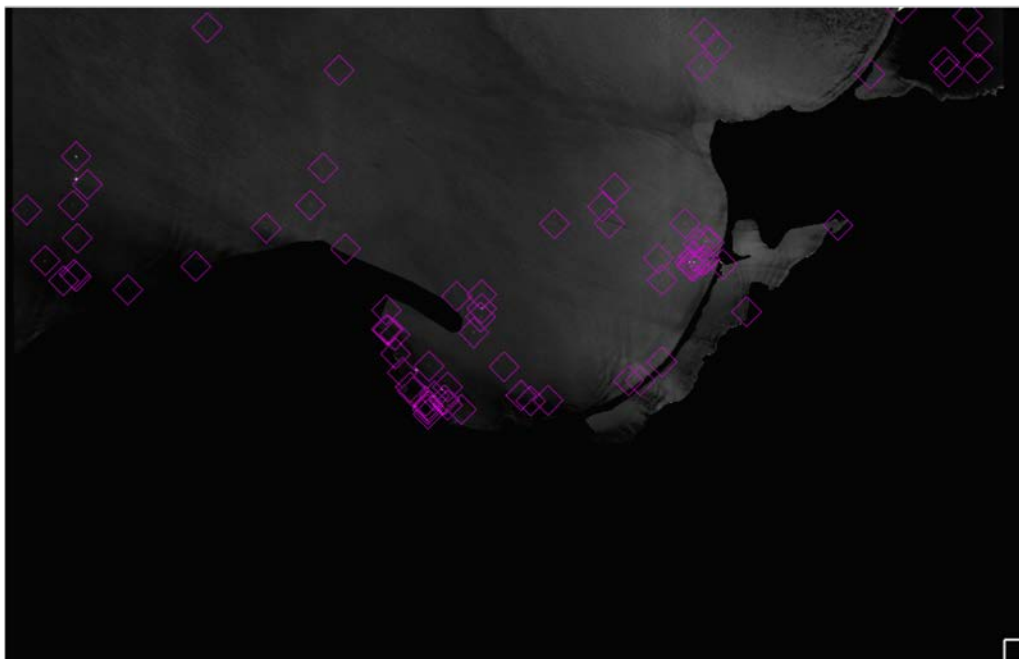


Figure 97 Sentinel-1A IW image on September 9<sup>th</sup> 2016 with land mask and ship detections in the VV-channel done by Aegir.

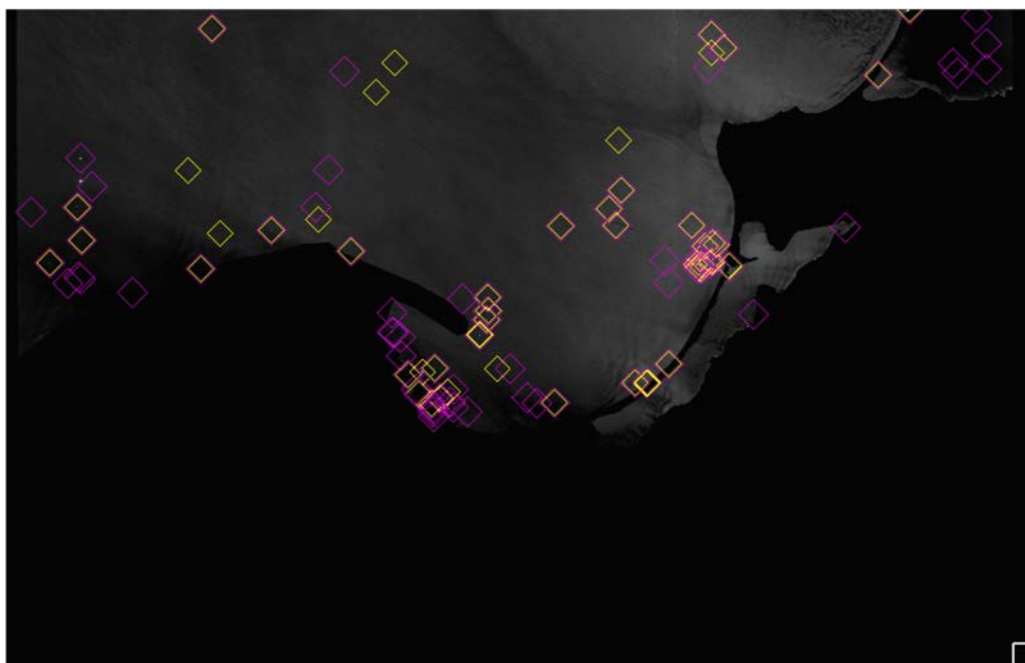


Figure 98 Sentinel-1A IW image on September 9<sup>th</sup> 2016 with land mask and ship detections in the VV- and VH-channel done by Aegir.

**CLASSIFICATION: UNCLASSIFIED**

All rights reserved. No part of this document may be reproduced or transmitted in any form or by any means, electronic, mechanical, photocopying, recording, or otherwise, without prior written permission of FFI, NLR or TNO.

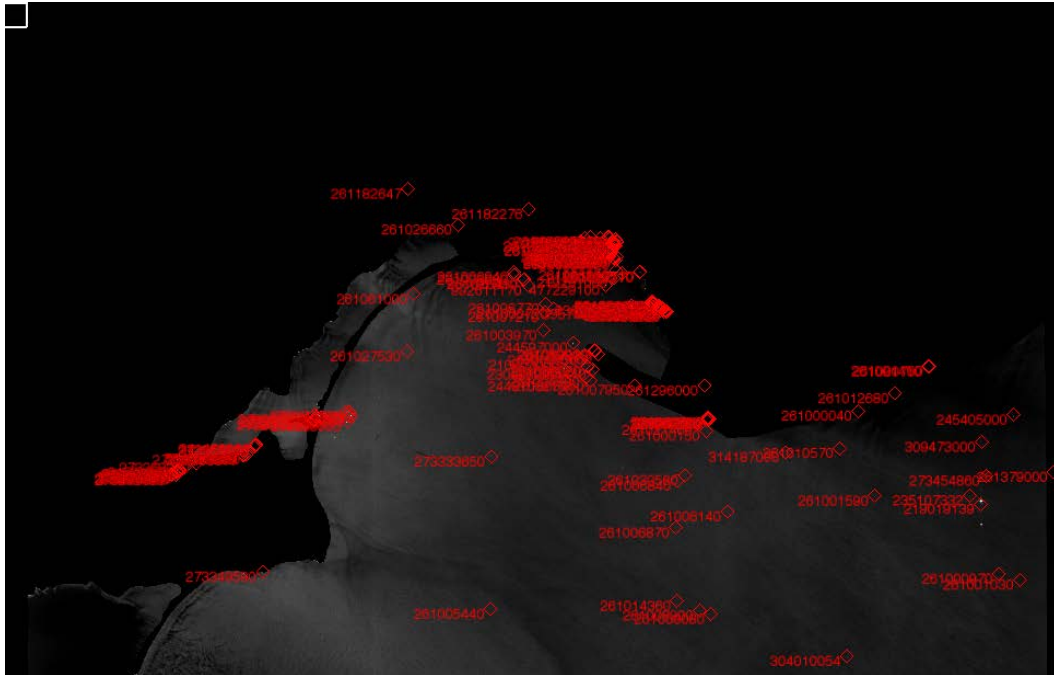


Figure 99 Sentinel-1A IW image on September 9<sup>th</sup> 2016 with land mask and AIS data.

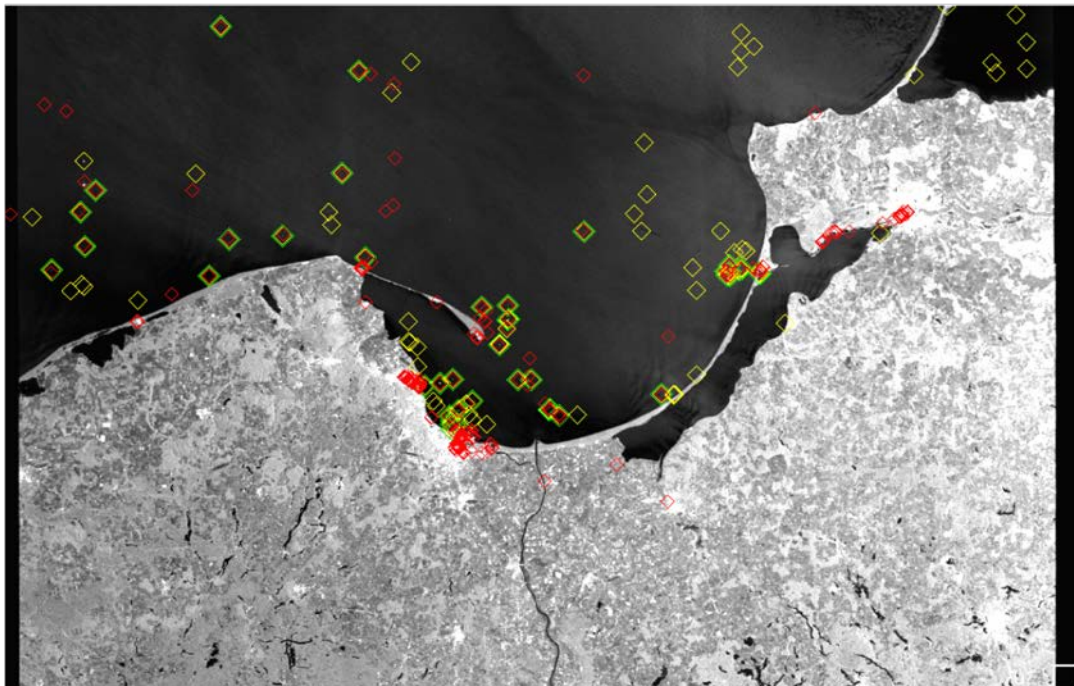


Figure 100 Sentinel-1A IW image on September 9<sup>th</sup> 2016 with ship detections done by Aegir (yellow) as well as AIS data (red) Green diamonds mean that the SAR ship detections are confirmed by AIS data.

**CLASSIFICATION: UNCLASSIFIED**

All rights reserved. No part of this document may be reproduced or transmitted in any form or by any means, electronic, mechanical, photocopying, recording, or otherwise, without prior written permission of FFI, NLR or TNO.

## 5.4 Description of optical test bed components

A demonstration system for the optical analysis has been developed in order to demonstrate the different optical analysis methods for a practical use case, to combine the processing steps in a workflow and to integrate the modules in a testbed system.

### 5.4.1 Technical setup

The NLR sub-demonstrations run within an Erdas Imagine environment. Erdas was chosen because Dutch IMINT analysts are familiar with this and the software provides possibilities to adapt the graphical user interface, define spatial processing models and integrate Python based processing components.

The two sub-demonstrations have an interactive Erdas Imagine GUI (Graphical User Interface) from where the workflow is executed, results are visualized and interactive editing of the automatically generated results can be done. With the main GUI, workflow buttons activate batch scripts with Erdas spatial models and Python programmes, which produce intermediate results and load data into the GUI. With the export command as last step in the chain, the sub demo end file products are created and made available to the integrated GeoInt demo.

Initially, the demonstrations are limited for the use of one specific dataset of 18 DMC or 19 Sentinel-2A images of the harbour of Rotterdam, where several routines and parameters are tuned for these data sets. In a later phase the demo can be made more generic for other DMC and Sentinel datasets (number of images, size of area), datasets from other type of sensors, and more generic detection functions (automated parameter settings).

### 5.4.2 Demonstration workflow

The workflows for the two sub-demonstrations Anomaly detection and Harbour ship intensity anomaly detection were worked out. It appeared that both workflows could be kept very similar.

The main steps involve:

- Data: load dataset.
- Detection: start automatic anomaly detection and load results.
- Evaluation: activate interactive editing and save results.
- Export: generate output files for GeoInt demo.

See also Figure 101 where the main workflow steps are visible in the button bar of the graphical user interface.

## **CLASSIFICATION: UNCLASSIFIED**

*All rights reserved. No part of this document may be reproduced or transmitted in any form or by any means, electronic, mechanical, photocopying, recording, or otherwise, without prior written permission of FFI, NLR or TNO.*

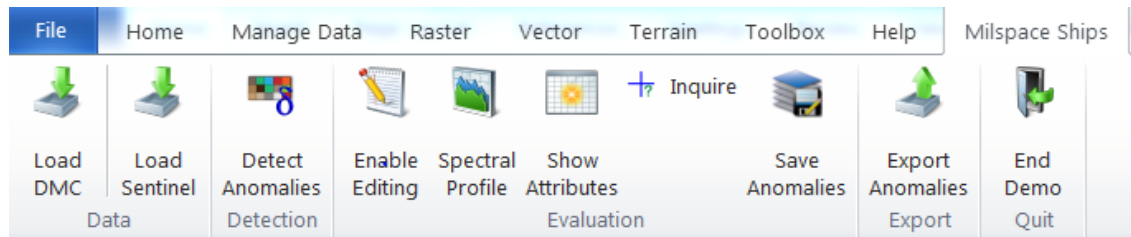


Figure 101 Milspace demonstration tab with user workflow (ships).

### 5.4.3 Graphical user interface

The graphical user interface (GUI) for the anomaly detection is based on the Erdas GUI. The GUI is based on a number of main components, see Figure 102.

- Demonstration Tab as part of the Erdas top button bar.  
 The buttons in this tab guide the user through the main steps of the demonstration workflow and activate the related processing, display and interactive functions.
- Overview window (Viewer-1).  
 This left image viewer shows the main results of each step (e.g. vector and raster based anomaly information) and reference information (e.g. maps, harbour sectors)
- Detail window (Viewer-2).  
 This right image viewer shows additional detail information to support the interpretation of the main results. Examples are the original satellite images, layer stacks of reflections, detected ships, heat maps of ship intensity.
- Table window.  
 This window at the bottom shows attribute information from anomaly vector files or thematic raster files. It is also used to display profiles of reflections or anomaly occurrences over time for a pointed pixel.

## CLASSIFICATION: UNCLASSIFIED

All rights reserved. No part of this document may be reproduced or transmitted in any form or by any means, electronic, mechanical, photocopying, recording, or otherwise, without prior written permission of FFI, NLR or TNO.



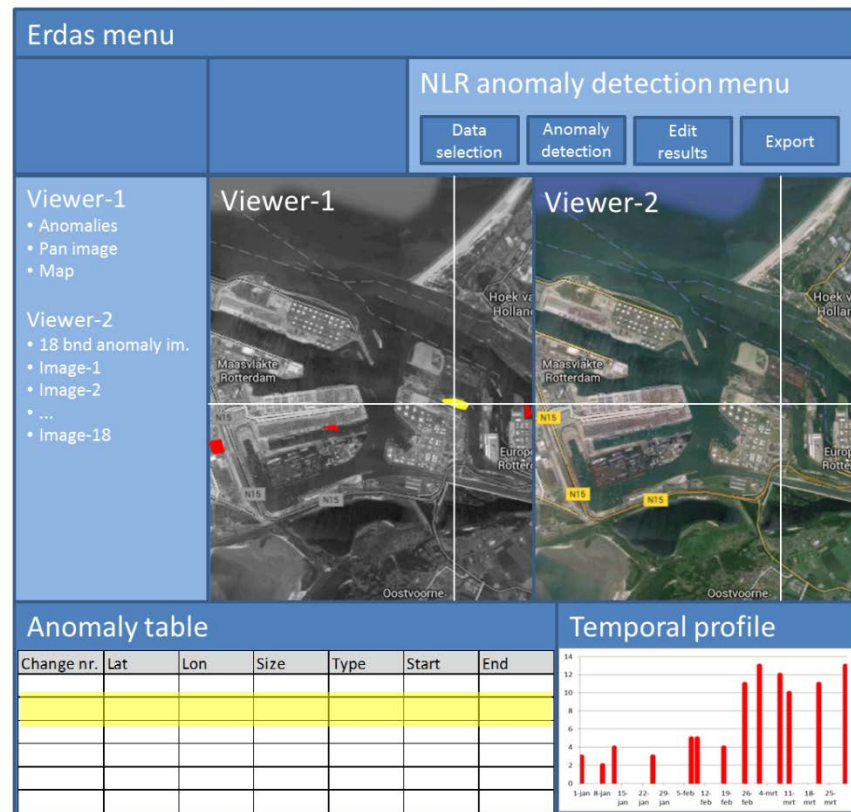


Figure 102. Main components of graphical user interface.

## 5.4.4 Technical implementation

### 5.4.4.1 Technical workflow

The main technical workflow contains the same four steps as the demonstration workflow. To initialize the demonstration two additional steps are required.

- Initialization steps
  - Start Milspace demo
  - Sub demonstration selection
- Main demonstration steps
  - Data Selection
  - Detection
  - Evaluation
  - Export

## CLASSIFICATION: UNCLASSIFIED

All rights reserved. No part of this document may be reproduced or transmitted in any form or by any means, electronic, mechanical, photocopying, recording, or otherwise, without prior written permission of FFI, NLR or TNO.

The different steps of the technical workflow will be described in more detail below for both sub demonstrations. First the initializing steps are discussed, followed with the Anomaly demonstration steps and Harbour ship anomaly steps.

### *Initialization*

- Start milspace demo.

The start of the workflow has to be done manually, by loading a session file (milspace\_demos.ixs). This session file loads the basic demo setup with two views and adds a milspace demo tab to the menu bar (see figure 102).

- Select demo.

In the milspace menu tab a selection can be made for the Anomaly demo or the Ships demo. Both selections load a session file with the basic setup for that specific demo and installs the appropriate menu in the menu bar (Milspace Anomalies or Milspace Ships), but with no data loaded yet.

### *Anomaly Detection*

- Select data.

A selection has to be made of which data is going to be used in the demo. In this case a dataset is available from DMC or Sentinel-2A. Both selections load a session file with the basic setup for that specific data set and install the appropriate menu in the menu bar. In Viewer-1 thematic harbour data is loaded and in Viewer-2 the used selected satellite images of DMC or Sentinel-2A are loaded.

- Detection.

Anomalies are detected and intermediate results are calculated. This is done by calling the script detect\_anomalies.bat. An Erdas spatial model determines for each pixel in an image if this has an anomalous reflection value in comparison to the other images of the time series and clusters neighbouring pixels to clumps. Next a python programme vectorises the clumps to a shape file. Finally the multi-band anomaly file and single-band clumped anomaly file are made available in the demo GUI by loading a new session file. See Figure 103 for an overview of the anomaly detection.

## **CLASSIFICATION: UNCLASSIFIED**

*All rights reserved. No part of this document may be reproduced or transmitted in any form or by any means, electronic, mechanical, photocopying, recording, or otherwise, without prior written permission of FFI, NLR or TNO.*

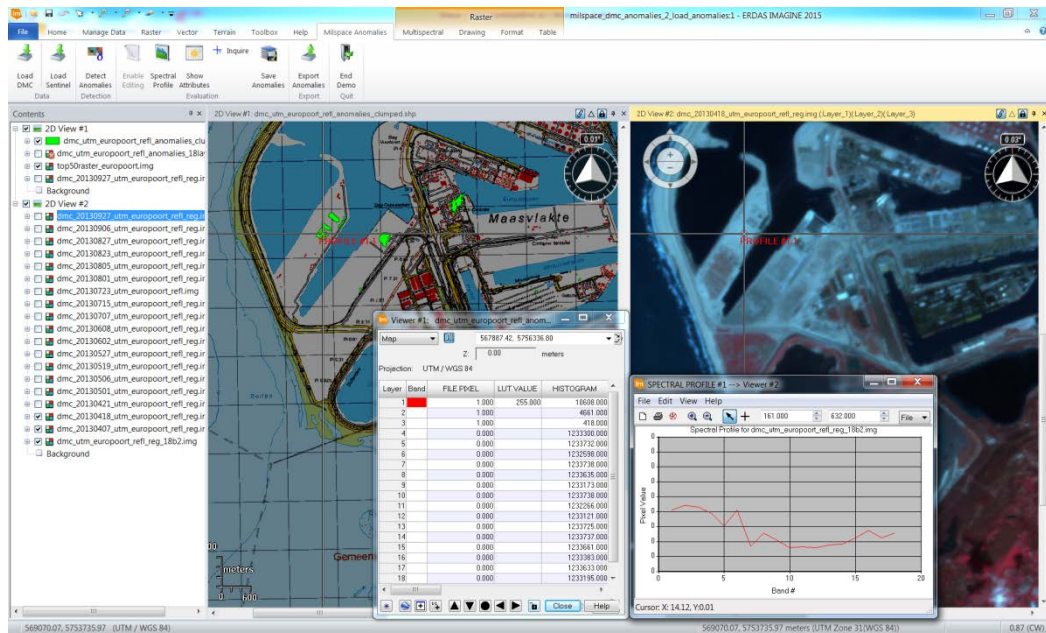


Figure 103. Overview of anomaly detection, with anomalies in green in left viewer, temporal profile of anomalies (0,1), and temporal profile of reflections (red curve) in separate windows.

- Evaluation.

The automatic derived anomalies can be interactively analysed and edited. To support this, a number of Erdas functions are made available in the ribbon. ‘Enable editing’ makes it possible to edit the anomaly shape file. ‘Show Attributes’ displays the attribute information from the anomalies and supports filtering, selection and deleting of anomalies. ‘Spectral Profile’ can be applied for the multi-band reflection file, so that for an anomalous pixel the temporal profile of the reflections can be evaluated. With ‘Inquire Cursor’ applied for the multi-band anomaly the temporal profile of anomaly moments can be evaluated. Further the different loaded reflection and anomaly images can be viewed. Finally with ‘Save Anomalies’ the edited anomaly shape file can be saved with ‘\_edit’ added to the filename.

- Export.

Final results as required by the GeoInt Integrated Demo are calculated using the edited intermediate anomaly results and then exported. This is done by calling the script export\_anomalies.bat. The anomaly shape file is converted to raster with a python programme. An anomaly overview raster file is generated with anomaly areas in red and a grey image background, using a spatial model. An output text file is created by a Python programme with information of the input images, area, and anomalies with details. And this same programme also creates image chips around the centre of the

**CLASSIFICATION: UNCLASSIFIED**

All rights reserved. No part of this document may be reproduced or transmitted in any form or by any means, electronic, mechanical, photocopying, recording, or otherwise, without prior written permission of FFI, NLR or TNO.





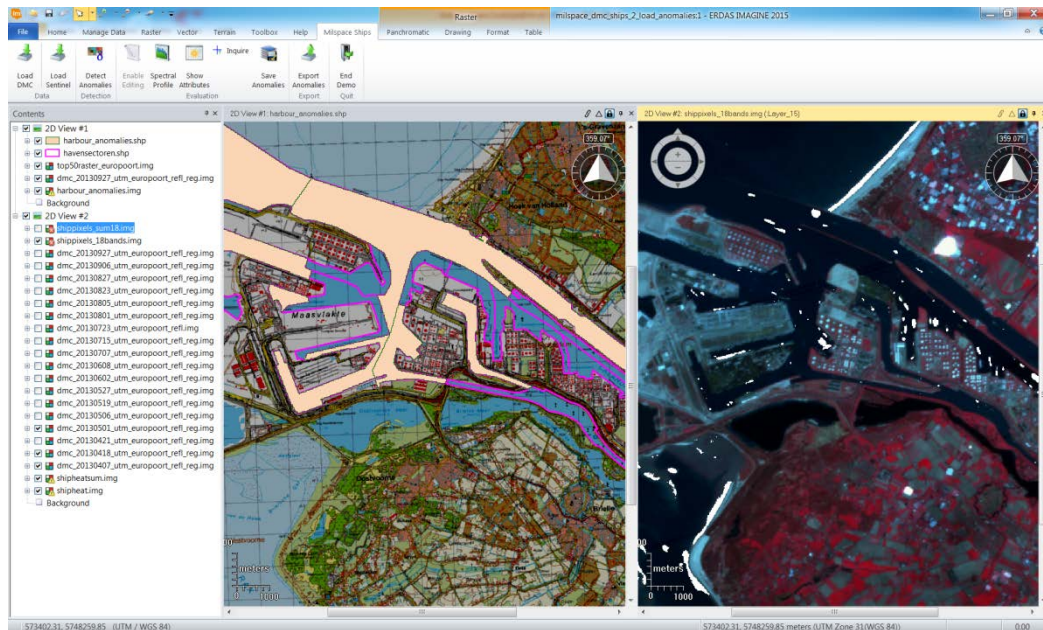


Figure 105 Results of ship intensity detection activities: anomalous harbour sections (left, yellow) and detected ships at a selected data (right).

- Detection.

Anomalies are detected and intermediate results are calculated. This is done by calling the script `ship_detect_anomalies.bat`, which calls in turn 3 sub batch scripts, and loads the results in the demo GUI. Three processing steps are carried out (see also section 3.2):

- Ship detection. For each input image a file with clumps of ship pixels is computed with a spatial model.
- Ship statistics computation. With a Python programme for each ship detection results the detected ships are filtered for too small (noise) and too large (mostly clouds) clumps, classified in small or large ships and summed per harbour sector.
- Harbour ship intensity anomaly detection. Per harbour sector is evaluated if anomalies occur in the ship intensity over time.

Intermediate products are created: a multi-band shippixels file, a summed shippixel heatmap file, a multi-band harbour sector intensity file, a summed harbour sector heatmap file, and a harbour sector anomaly shape file. Finally the intermediate results are made available in the demo GUI by loading a new session file. See Figure 105 for an example.

**CLASSIFICATION: UNCLASSIFIED**

All rights reserved. No part of this document may be reproduced or transmitted in any form or by any means, electronic, mechanical, photocopying, recording, or otherwise, without prior written permission of FFI, NLR or TNO.

- Evaluation.

Like in the Anomaly Detection case, the automatic derived harbour anomalies can be interactively analysed and edited, using the Erdas functions made available in the ribbon and viewing the different loaded intermediate products. After finishing with ‘Save Anomalies’ the edited anomaly shape file can be saved with ‘\_edit’ added to the filename. Figure 106 shows an overview of the ship anomaly evaluation.

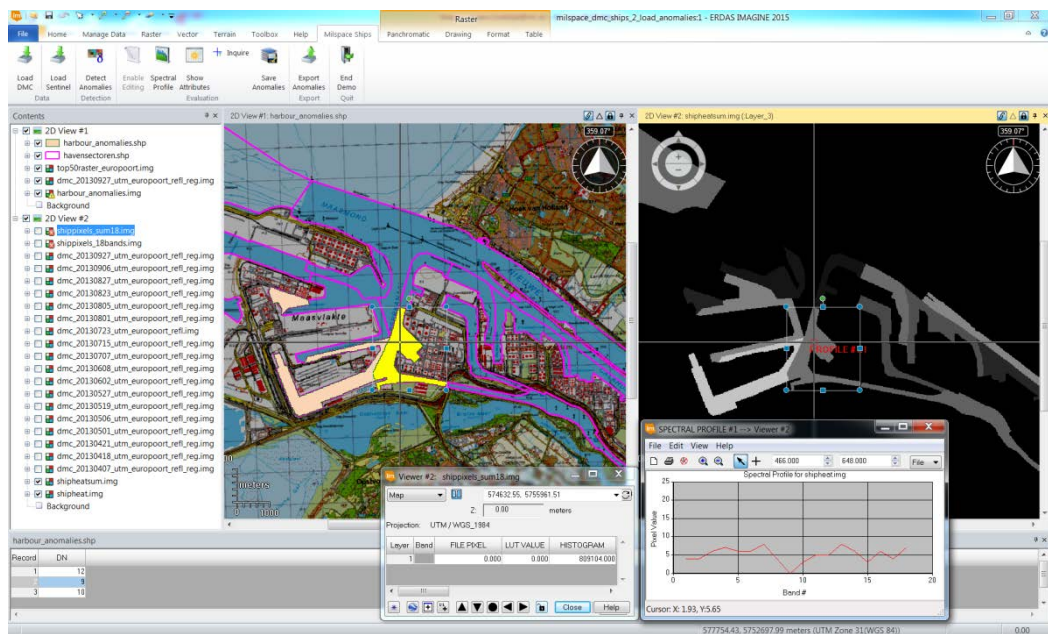


Figure 106 Overview of the ship anomaly evaluation: selected anomaly harbour sectors (left, yellow), and temporal profile of number of ships in the selected sector (red line in right window).

- Export.

Like in the Anomaly Detection case, final results as required by the GeoInt Integrated Demo are calculated using the edited intermediate anomaly results and exported. The products are similar. Finally the export results area displayed by loading a new session file.

#### 5.4.4.2 Erdas GUI customization

For customization of the Erdas Graphical user interface several principles can be applied.

- Additional buttons in the ribbon can be created by using ‘ribbon customization’ (starting from Erdas Imagine 2015 and later).
- The window layout can be manipulated manually and then saved
  - The settings and loaded files in a viewer can be saved as .vue

### CLASSIFICATION: UNCLASSIFIED

All rights reserved. No part of this document may be reproduced or transmitted in any form or by any means, electronic, mechanical, photocopying, recording, or otherwise, without prior written permission of FFI, NLR or TNO.

- The layout of all viewers can be saved as .ixw
- The complete window layout and loaded files can be saved as .ixs
- Functional macros. Sequences of actions can be built in macro's using the spatial modeller. The result is a .gmdx file that can be coupled to a button in the GUI.
- Specific button actions (like calling windows bat files) can be achieved by editing the ixw/ixs layout/session files by hand. Example: To call the batch file 'calculate.bat', the button type in the ixw/ixs file has to be changed from 'common' into the line:  
<type info="C:\batfiles\calculate.bat">Executable</type> . In the bat files, all kinds of actions can be started like:
  - Call Erdas Imagine spatial models. Use the Erdas executable: smprocess.exe in combination with a gmdx file.
  - Load Erdas session. Use the Erdas executable eWkspce.exe in combination with an ixS file. The session will replace the current session
  - Execute a python programme
  - Load a text file in notepad

#### 5.4.4.3 Python and Erdas

There are several options for the combined usage of Erdas and Python.

- Usage of Erdas within Python
  - Within a Python program a number of Erdas functions can be integrated, which all use the spatial modeller. To achieve this, an Erdas spatial modeller python module can be included within python.
  - A Python program can also be made that activates an Erdas model (.gmdx)
- Usage of Python within or in combination with Erdas
  - Within a spatial model python code can be integrated (with the limitation that Python can only generate one single output)
  - Python programs can be executed stand-alone without actually using the Erdas environment. Of course, they can also be coupled to an Erdas button.
  - To read and write (Erdas) image data in python, the GDAL(Geopsatial Data Abstraction Library) library can be used.

#### 5.4.5 Results

##### *Anomaly detection*

In the dataset of the Rotterdam area many anomalies occur when the complete images are evaluated. Most of them are not of interest for the operator however. Many anomalies are related to changes in vegetation, partly due to agricultural activities, but also as a consequence

### **CLASSIFICATION: UNCLASSIFIED**

*All rights reserved. No part of this document may be reproduced or transmitted in any form or by any means, electronic, mechanical, photocopying, recording, or otherwise, without prior written permission of FFI, NLR or TNO.*



of the seasons over the year. Therefore it was decided therefor for this case to filter out these anomalies, by evaluating the NDVI (Normalized Difference Vegetation Index) index. Secondly many anomalies were related to ship activities. These were of interest for the second demonstration case, but not for this one, and therefor filtered out based on the detection of water areas. The remaining anomalies were related to changes in built up urban or industrial areas. Some of the anomalies were found in the DMC images, but there were only a few, due to the coarse 22 meter spatial resolution of the data and the fact that apparently no significant infrastructural changes were present in the area of interest. Two interesting changes could be noticed, related to the realisation of two new buildings. One clear false alarm was generated by the smoke from a pipe at an industrial plant that was wiping in different directions due to the wind. Further multiple small false alarms were present. In Figure 107 part of the image is shown with a detected anomaly of a new building (left) and of the smoke (right). For the new building the temporal profile of the reflection values shows that the anomaly took place in the fourth observation, i.e. in the May 1 2013 data.

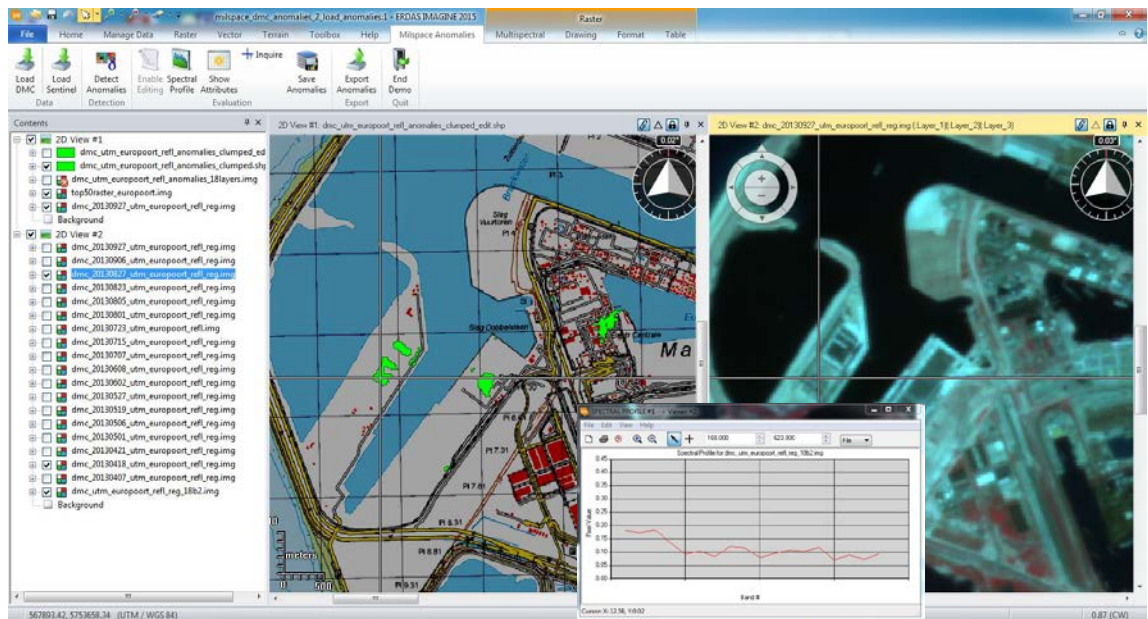


*Figure 107. Anomaly detection result (left), showing new buildings in green and the smoke plume of a power plant (right). The temporal reflection profile for the building anomaly shows that the anomaly occurs in the fourth observation (1 may 2013).*

At the end of the project the developed methodology was also applied on a series of 19 Sentinel-2A (S2A) images. The data was downloaded through the ESA Scientific Data Hub. Recently it is possible to download separate granules instead of a complete strip meaning data amounts of about 350 Mb (per granule) instead of 7 Gb (per strip). Level 1C products were used, which are

## **CLASSIFICATION: UNCLASSIFIED**

*All rights reserved. No part of this document may be reproduced or transmitted in any form or by any means, electronic, mechanical, photocopying, recording, or otherwise, without prior written permission of FFI, NLR or TNO.*



ortho rectified with a 12.5 meter absolute location accuracy and radiometric correction at Top Of Atmosphere reflectance.

Figure 108 shows the result of the anomaly detection. First a mask was generated to avoid water areas, vegetated areas, clouded areas and shadowed areas. In the areas left (industrial, built-up and infrastructure) the differences compared to the mean value were extracted by applying certain thresholds. The resulting product is a summation of anomalies detected over time for a specific pixel, displayed in a rainbow lookuptable. Clearly visible are the anomalies of the oil tanks where the shadow at the top changes with the oil level (1), the changes in storage of bulk goods (2) and the locations of the cranes for (un) loading the ships.

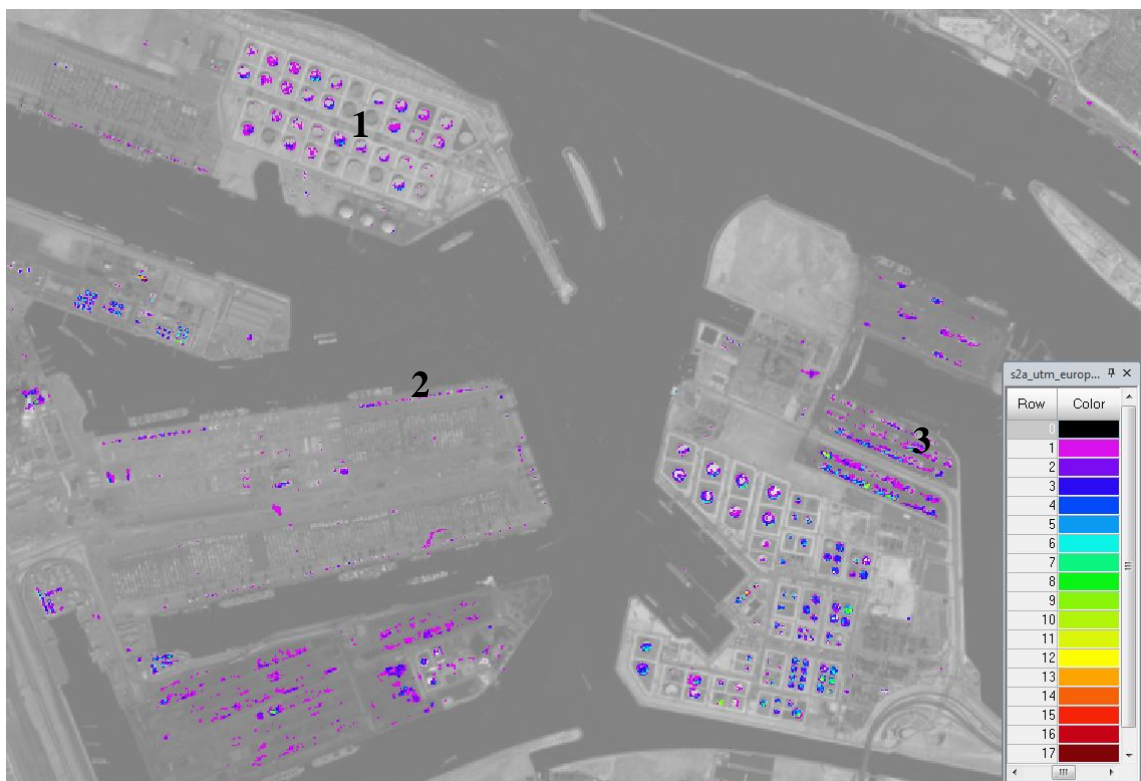


Figure 108 Anomalies detected in a series of 19 Sentinel-2A images. The colors show the number of detected anomalies over time.

### Ship detection

For the Rotterdam DMC dataset the ship detection and harbour intensity anomaly results have been evaluated. Conclusion is that the routines work quite well. Manual inspection gives an estimation that 80-90% of the ships are found and that not more than 10% of false alarms exist. Errors are made at places where the land-water mask is not detailed enough, e.g. when a pier is missing and two ships are located at both sides, these are connected to one area and thus

### **CLASSIFICATION: UNCLASSIFIED**

All rights reserved. No part of this document may be reproduced or transmitted in any form or by any means, electronic, mechanical, photocopying, recording, or otherwise, without prior written permission of FFI, NLR or TNO.

rejected to one ship or rejected as a too large ship. Also errors are made when the ship reflection is too close to the water reflection and when small scattered clouds in the size of a ship occur.

The temporal ship intensity of specific types of harbour sectors has been plotted in Figure 109. It is clear that there is good correlation between the ship intensity for harbour sectors with the same type of goods.

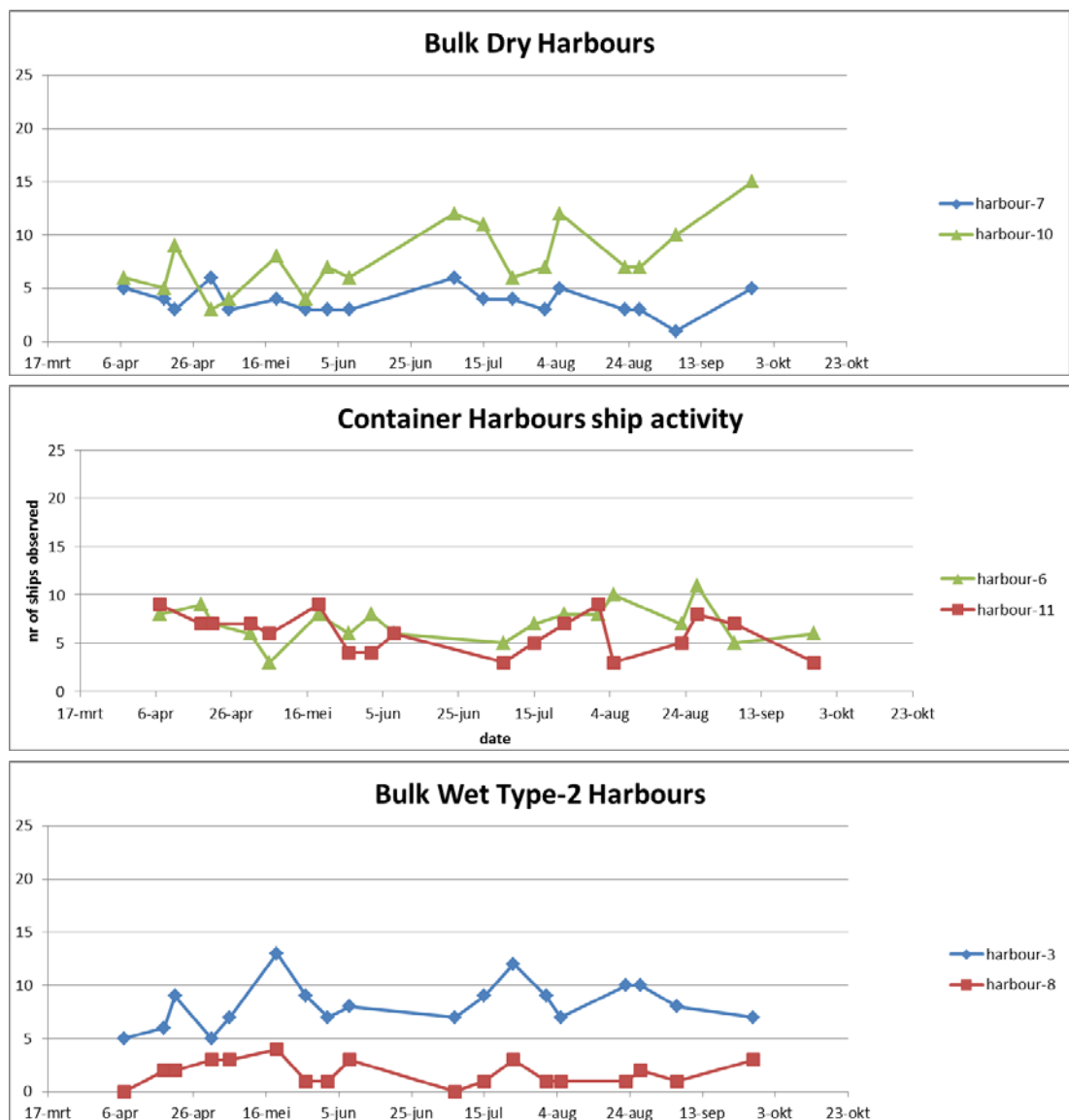


Figure 109. Temporal ship intensity plotted for different harbour types.

**CLASSIFICATION: UNCLASSIFIED**

All rights reserved. No part of this document may be reproduced or transmitted in any form or by any means, electronic, mechanical, photocopying, recording, or otherwise, without prior written permission of FFI, NLR or TNO.

At the end of the project also a test was done with the detection of ships in Sentinel-2A images. Due to the better spatial resolution the accuracy of the detection is better, as can be seen in Figure 110. Individual ships are detected more accurately, the size of the ships can be determined more accurately, the discrimination between ships close to each other is better and the influence of the land mask accuracy is less disturbing. At the other side ship wakes cause some more noise.

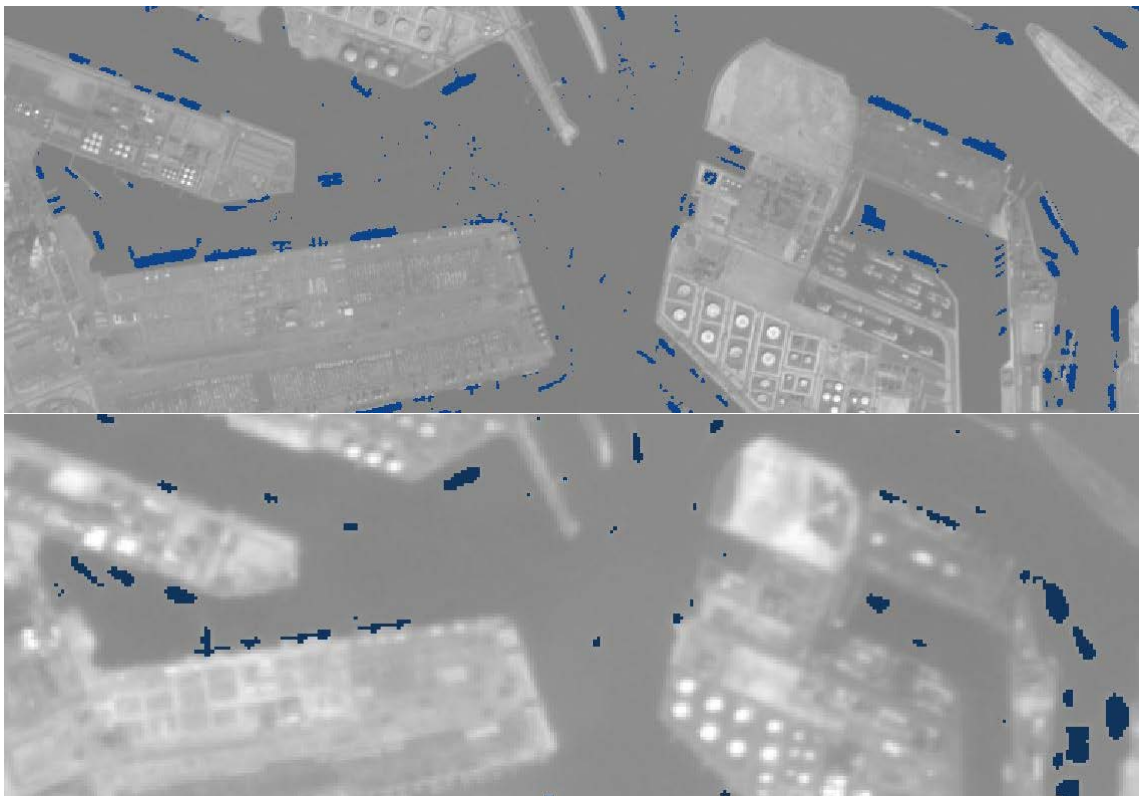


Figure 110 Results of ship detection in Sentinel-2A (top) compared to DMC (bottom).

#### 5.4.6 Evaluation.

A workflow has been realised for the analysis of anomalies in built up areas and in the harbour ship intensity. For the demonstration cases the workflow works quite well and guides the operator through the process.

The demonstration is not very generic yet in the sense that in the spatial models are specific for filenames of test dataset, number of images and the area of interest. Possibilities to further generalize the Erdas spatial models exist, but soon one encounters all kind of limitations of the spatial modeller environment. Programming in Python is much more flexible and the software mostly also runs faster. The Python routines easily can be integrated in the Erdas GUI. This

### **CLASSIFICATION: UNCLASSIFIED**

*All rights reserved. No part of this document may be reproduced or transmitted in any form or by any means, electronic, mechanical, photocopying, recording, or otherwise, without prior written permission of FFI, NLR or TNO.*

GUI has its limitations when fully automated workflows need to be generated. In case some expertise of the operator is assumed, and thus some more operator actions are allowed, the level of automation can be limited and the followed approach is sufficient.

The actual ship and anomaly detection routines are in fact relative simple routines, but can be built out to more complex ones that can operate in the same framework.

### 5.5 Description of SAR test bed components

The SAR component uses a co-registered data cube for a multi-temporal layered data-set. Original image data in amplitude format (16 bit) can be prepared with commercial image analysis software such as Erdas or Socket GXP. The data of the various layers should be co-registered and be projected into UTM ground range. Next the various dates are combined into a layer stack to produce the data cube. In general a subset of the total area is taken for the data cube in order to restrict the total data volume. The output is a multi-layer file (16 bit) in tiff format and a world file in twf format containing the geographical information. The world file is used for adding information about the UTM zone and labels indicating the various dates in the multi-temporal data cube. To indicate this extended worldfile the extension twfz is used. Figure 111 shows the workflow for the multi-temporal change detection tool.

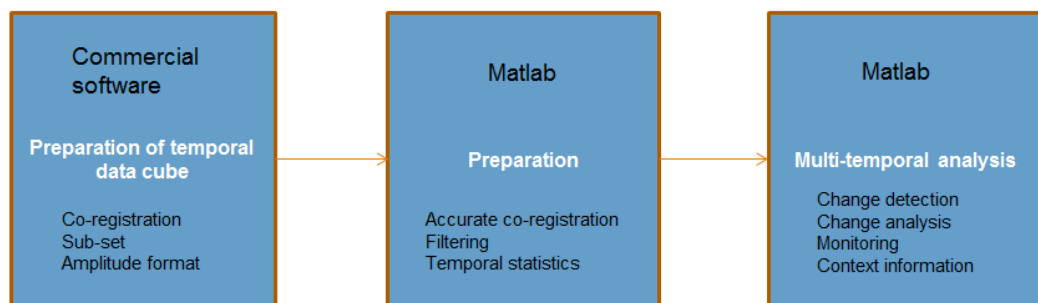


Figure 111 Workflow for the multi-temporal change detection tool.

The tiff and twfz files are input for the Matlab modules: a preparation module and an analysis module. In the preparation module a fine tuning of the co-registration is done by selecting an area with sufficient texture. Next a spatial Gaussian filter is applied to reduce speckle and to prevent false alarms. This is at the cost of some spatial resolution (spatial resolution reduction by a factor of 2). Finally for each location temporal statistics are calculated (median, mean, maximum, minimum values etc.). All relevant information is stored in an output file in an internal Matlab format. In this way several data-cubes can be prepared.

In the analysis module a prepared data-cube can be selected. In the first steps after reading the data the detection level should be set. Then zooming and panning are possible and a target

### **CLASSIFICATION: UNCLASSIFIED**

All rights reserved. No part of this document may be reproduced or transmitted in any form or by any means, electronic, mechanical, photocopying, recording, or otherwise, without prior written permission of FFI, NLR or TNO.



should be selected. This is done by two mouse clicks in the image to create a box around the target. Figure 112 shows multi-temporal change analysis with multi-temporal information (top-right panel) and a Google Earth (GE) image when internet connection exists (bottom-right panel). The GE image can be adjusted by selecting another zoom factor and by changing the centre of the GE image (mouse click on the location for the centre). In this way inaccurate registration of the radar imagery with respect to the map can be corrected.

Figure 112 and figure 113 below show the analysis GUI for two use cases: Nikel and Rotterdam with RADARSAT data (2 and 5 meter resolution). The Nikel use case is focussed on the activities near the Nikel melt plant which causes extensive environmental pollution. The RADARSAT imagery was collected every month for 2 years. Below the temporal development is shown for a change target selected over a parking and storage area. The temporal trend shows that especially in the summer of the second year goods were stored there. The GE image shows the area without storage.

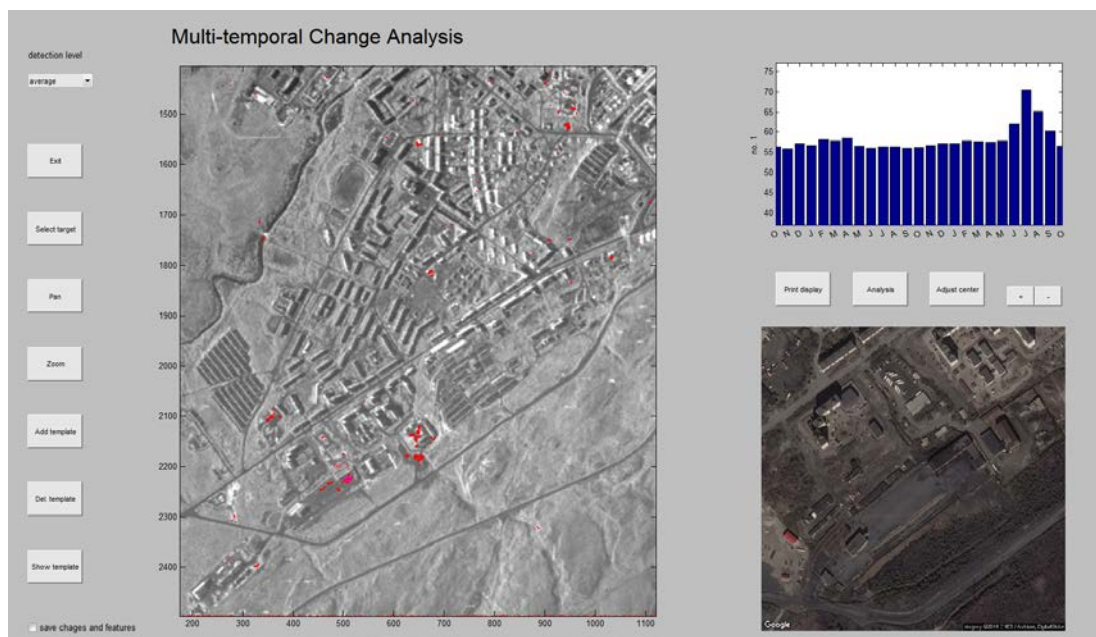


Figure 112 Interface of the multi-temporal change detection tool showing use case Nikel

The figure below shows the GUI for Rotterdam harbour for 7 dates in the second half of 2015. Changes are visible due to replacement of ships, goods and oil-terminals. A ship replacement is selected and the temporal development is shown in the right upper corner indicating the presence of ships during the first, third and last date. The fourth date is more uncertain, due the lower backscatter level. This can be verified by further analysis.

### **CLASSIFICATION: UNCLASSIFIED**

All rights reserved. No part of this document may be reproduced or transmitted in any form or by any means, electronic, mechanical, photocopying, recording, or otherwise, without prior written permission of FFI, NLR or TNO.

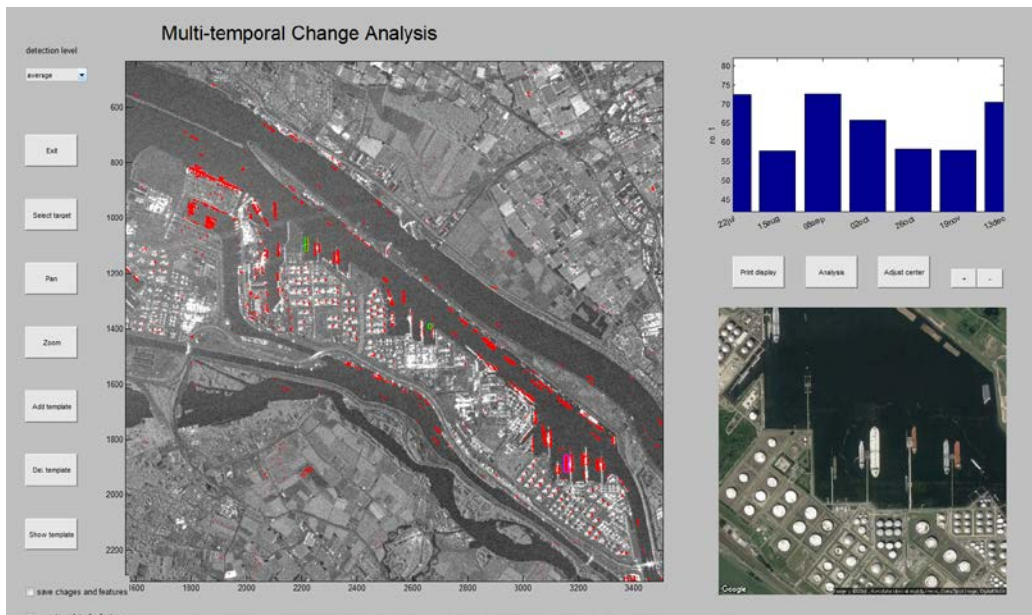


Figure 113 Interface of the multi-temporal change detection tool showing use case Rotterdam.

To allow further inspection of a change target the analysis button should be use. In the follow-on the GUI indicates a radar imagery extract focused on the target. It is possible to select three dates to create an RGB image, showing colours where changes are present. It is also possible to play a sequence of images (animation), so that changes become apparent. The results can also be stored in GIF (Graphics Interchange Format) format (see figure 114).

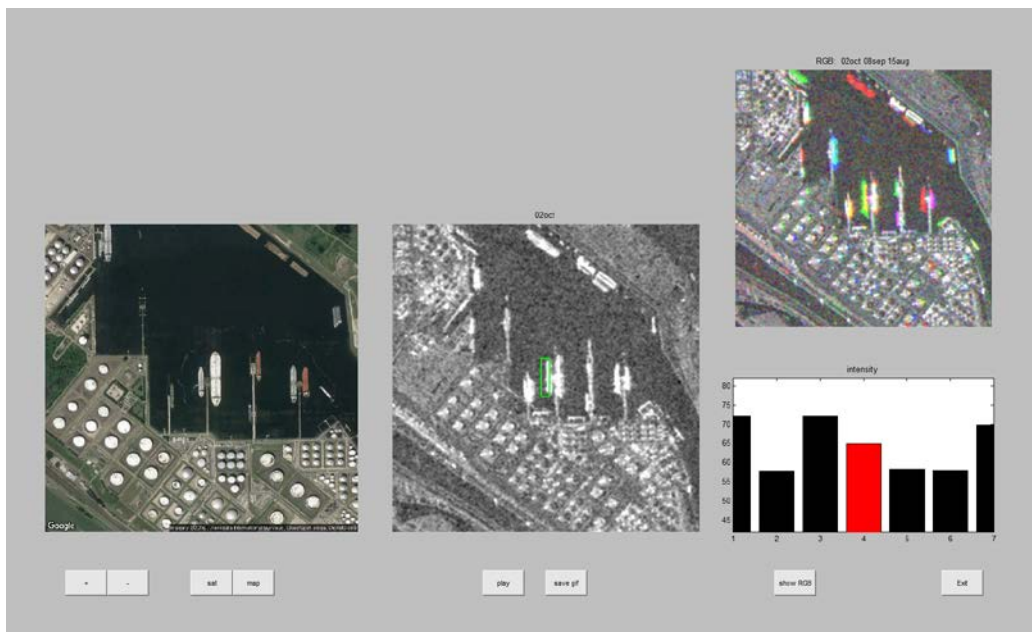


Figure 114 Interface of the multi-temporal change detection tool showing analysis results for use case Rotterdam.

**CLASSIFICATION: UNCLASSIFIED**

All rights reserved. No part of this document may be reproduced or transmitted in any form or by any means, electronic, mechanical, photocopying, recording, or otherwise, without prior written permission of FFI, NLR or TNO.

It is also possible to define a template over a location in the image which stores the changes and which might be applied to a new data cube, for example when the number of dates increases. The results can be shown in a separate GUI and is also written to a text file. In this way changes can be monitored over time, for example showing the presence/absence of ships. If the resolution is sufficient also changes in the roof level of oil terminals can be monitored in this way. Figure 115 shows these changes for a set of oil terminals in Rotterdam. To the right the temporal development level is accompanied with an indication whether the terminal is full or not.



Figure 115 Interface of the multi-temporal change detection tool showing temporal behaviour of oil terminal content.

During the UV2014 trial COSMO-SkyMed and TerraSAR-X spotlight data with corresponding imaging geometries have been co-registered. Here we present multi-temporal change detection results showing changes due to displacements of aircrafts on a platform (Figure 116 top). Due to the higher resolution not only the presence and absence of aircrafts are detected but also replacement of aircrafts which can be inferred when the animation and RGB image is inspected (Figure 116 bottom)

**CLASSIFICATION: UNCLASSIFIED**

All rights reserved. No part of this document may be reproduced or transmitted in any form or by any means, electronic, mechanical, photocopying, recording, or otherwise, without prior written permission of FFI, NLR or TNO.



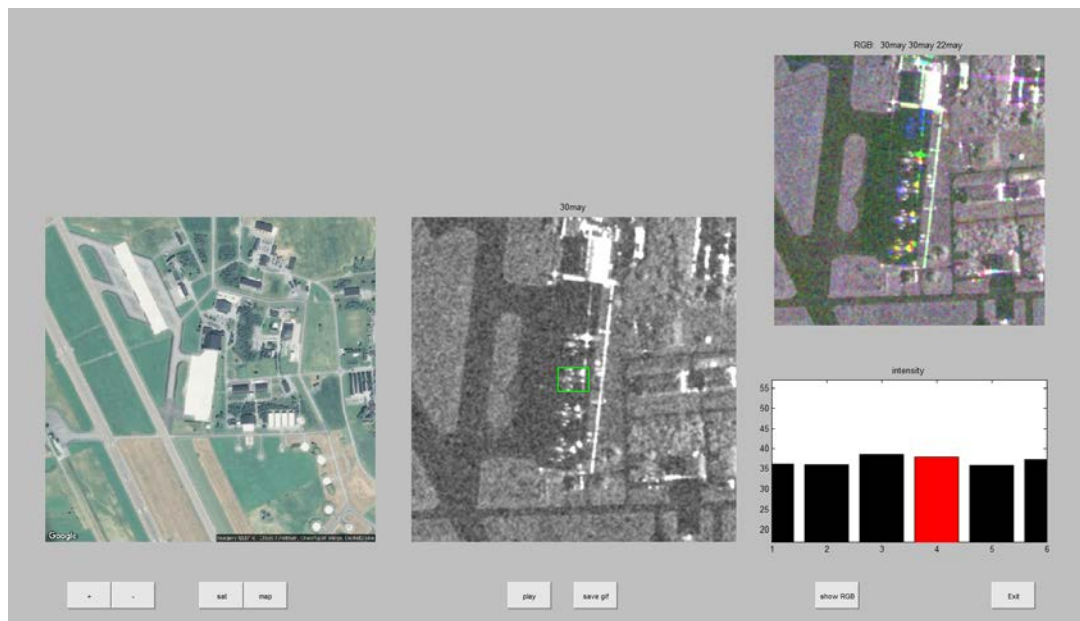
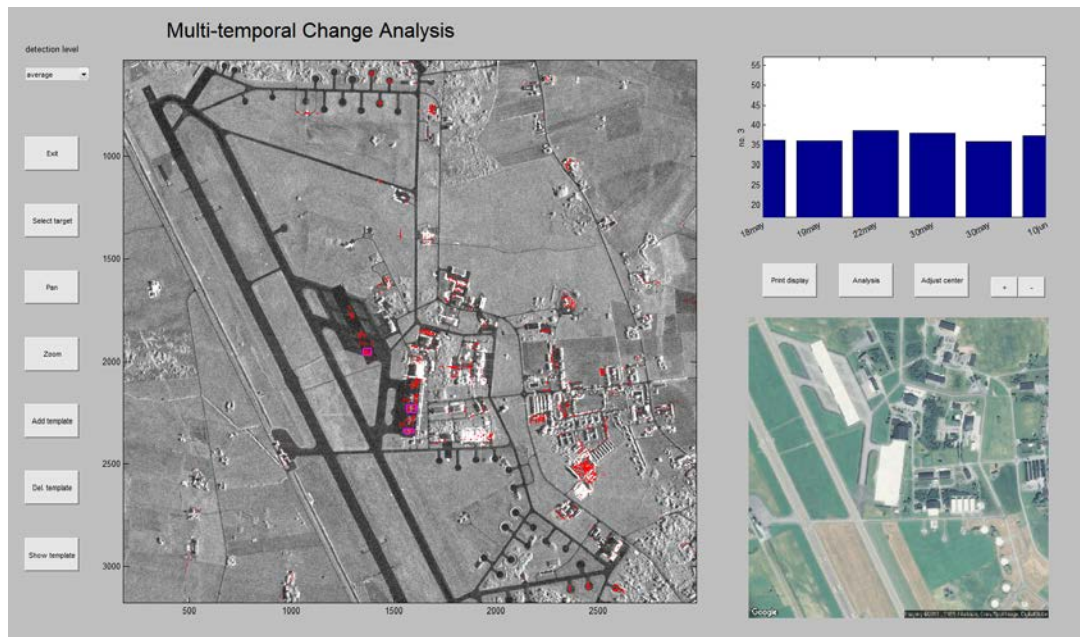


Figure 116 Interface of the multi-temporal change detection tool showing use case UV2014 (top) and the analysis for displacement of aircraft (bottom).

## 5.6 Description ship detection test bed component

SAR satellites have the unique capability to monitor large and difficult accessible ocean areas for shipping and fishing activity that are difficult to monitor using more traditional methods, such as Coast Guard vessels. Ships have many corner reflectors and scatter efficiently back towards the radar when illuminated by radar waves. They appear as bright targets against a

### **CLASSIFICATION: UNCLASSIFIED**

All rights reserved. No part of this document may be reproduced or transmitted in any form or by any means, electronic, mechanical, photocopying, recording, or otherwise, without prior written permission of FFI, NLR or TNO.



darker sea background in SAR satellites images. How dark the sea background appears in a SAR image depends on the incidence angle, the polarisation of the radar, the wind strength, wave height, direction of the waves compared to the radar etc. Today's commercial available SAR satellites are well suited to do ship detection, compared with optical satellites, due to the all-weather and day-night capability. ScanSAR images from RADARSAT-2 and TOPSAR images from the Sentinel-1 satellites give good ship detection results in the open ocean for vessels of Norwegian interest. Higher resolution data can be used in harbour areas or if smaller vessels are of interest.

Norwegian interest areas are for example Norwegian coastal areas, the Barents Sea between Spitsbergen and the Norwegian mainland where ship traffic, illegal fisheries and smuggling need to be monitored by the Norwegian Coastguard and the Norwegian intelligence services. To ease the task of monitoring these large ocean areas, it is helpful to have an automatic ship detector. FFI has developed an automatic ship detector, Aegir. The algorithm used in Aegir is based on the K-distribution algorithm. The image is divided in overlapping frames of 100 pixels x 100 pixels. A PDF (Probability Density Function) is adapted to the data and a threshold value is estimated based on the PDF. Model parameters are estimated for each frame.

There is one fully automatic version of Aegir and one version which offer the possibility for the user to actively manage how the program shall run. Aegir ingests and loads the satellite data on screen, and applies a land mask on the image if necessary. If ice or anything else that the user does not want to be analysed is in the image, it is possible to make a manual mask to mask out these areas. The ship detection algorithm is run, confidence estimates are calculated and alarms on detections are presented on screen and in ship detection reports. Figure 117 shows the workflow for Aegir.

## **CLASSIFICATION: UNCLASSIFIED**

*All rights reserved. No part of this document may be reproduced or transmitted in any form or by any means, electronic, mechanical, photocopying, recording, or otherwise, without prior written permission of FFI, NLR or TNO.*

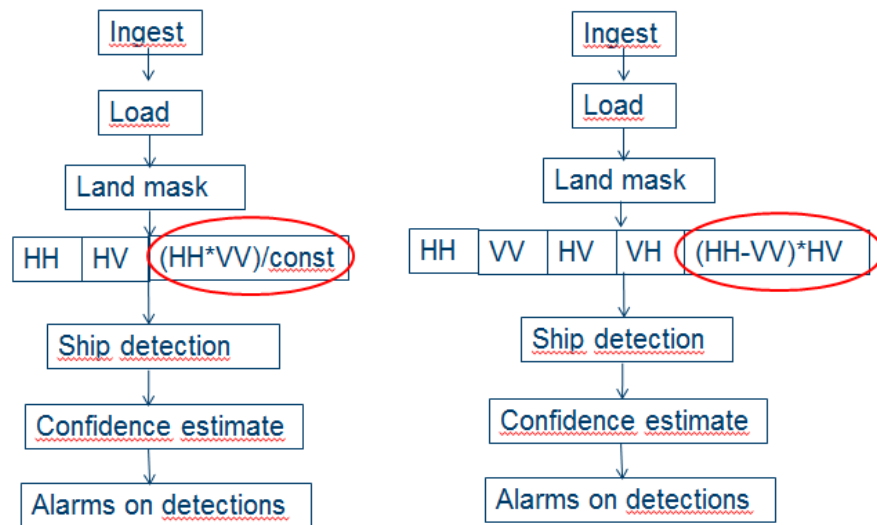


Figure 117. Workflow for the automatic ship detector Aegir for dual-polarisation or quad-polarisation data.

Figure 118 shows Aegir’s main image display GUI and what it looks like when Aegir is running. The largest window shows an overview of the image being analysed. In the semi-automatic version, the square cursor in white shown in the big image can be moved around to see more details in the zoomed image to the right. The upper left part is where you can choose what action to take in the semi-automatic ship detector, while the upper right panel shows a status window where the user can follow the ship detection process. Figure 119 shows how the land and ice is masked out in an image which includes ice and Jan Mayen.

**CLASSIFICATION: UNCLASSIFIED**

All rights reserved. No part of this document may be reproduced or transmitted in any form or by any means, electronic, mechanical, photocopying, recording, or otherwise, without prior written permission of FFI, NLR or TNO.

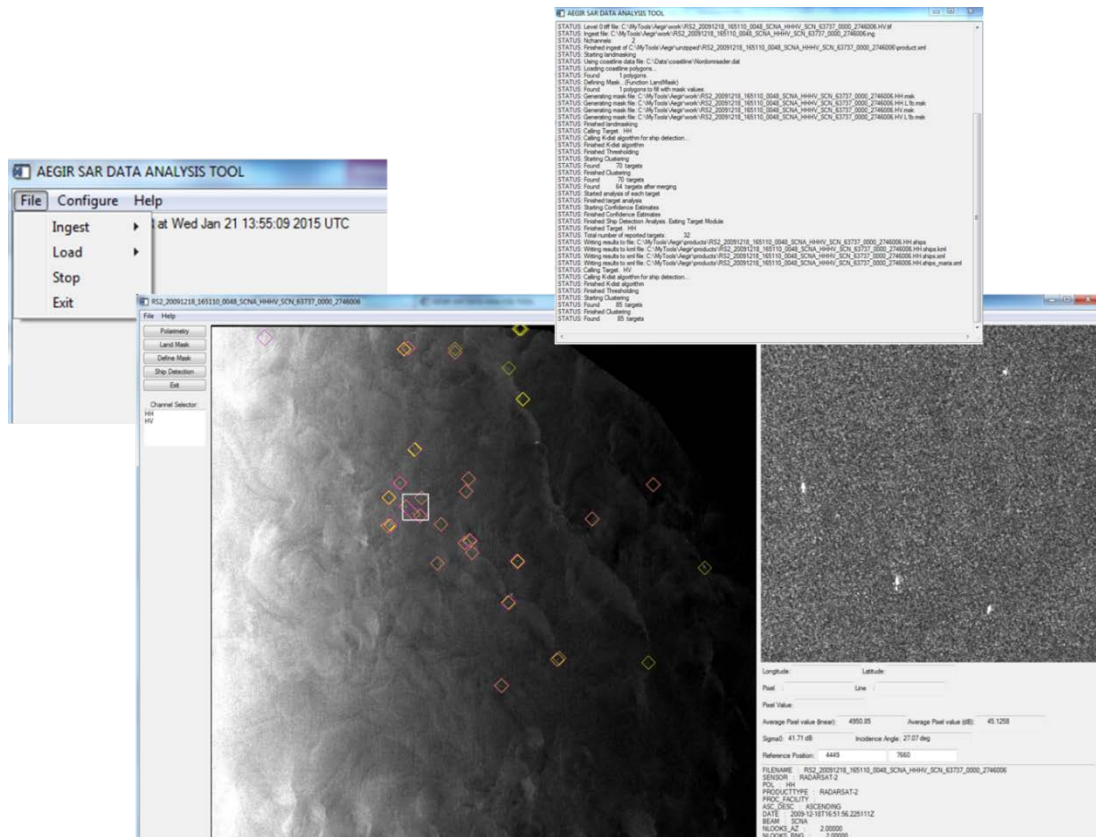


Figure 118 Aegir's main image display and GUI when Aegir is running.

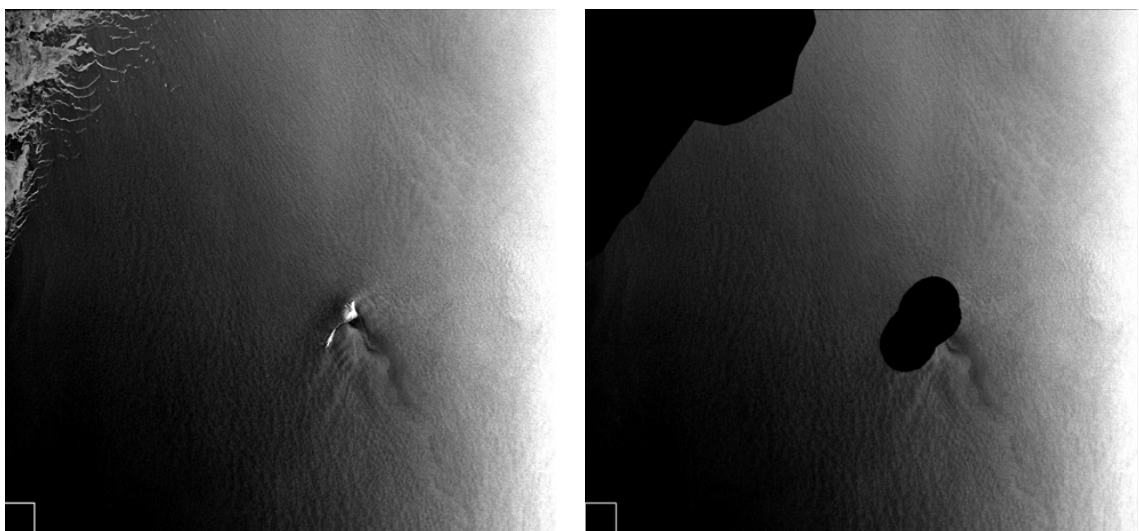


Figure 119 When ice is present in the image, a manual mask can be created over the ice in addition to the automatic land mask over Jan Mayen in this RADARSAT-2 image.

**CLASSIFICATION: UNCLASSIFIED**

All rights reserved. No part of this document may be reproduced or transmitted in any form or by any means, electronic, mechanical, photocopying, recording, or otherwise, without prior written permission of FFI, NLR or TNO.

As shown in Figure 119, Aegir analyses all available polarisation channels separately. In addition, it has the possibility to combine the available polarisation channels to enhance the ship to sea contrast. The ship detector can be run on the fused polarisation channel, giving the opportunity to detect more vessels. Two different ways of fusing the polarimetric channels have been implemented in Aegir, one for dual-polarisation data and one for quad-polarisation data. Aegir multiplies the amplitude of the two polarisation channels when dual-polarised data is available. For quad-polarised data, double bounce is multiplied with cross-polarisation. Figure 120 shows where it is possible to choose to fuse the polarisation channels. It is also possible to fuse the channels automatically in the fully automatic version of Aegir.

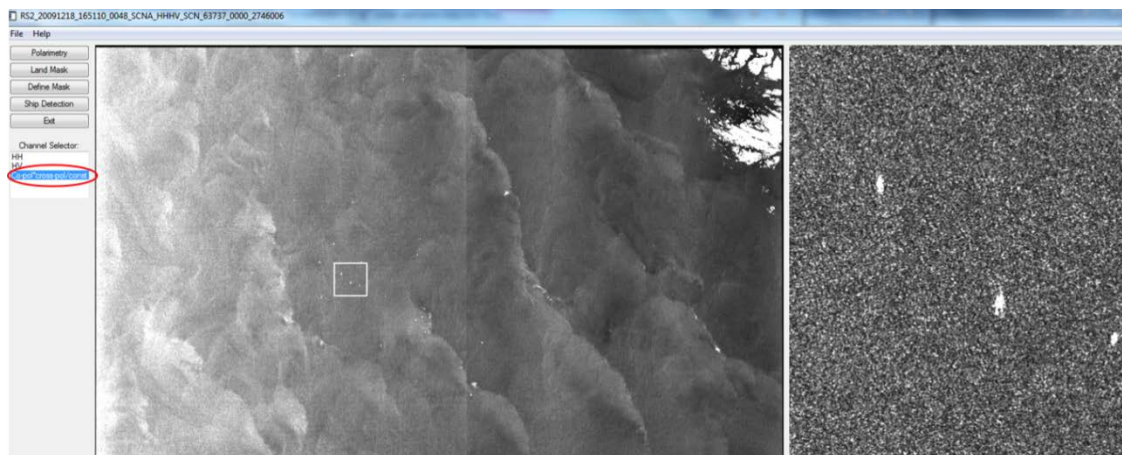


Figure 120. Location where it is possible to choose the fused polarimetric “channel” (see red circle to the left).

The ship detection results can be compared with AIS data for verification. Reports from the ship detector are for example report files in different formats with ship positions including attributes with more information about the vessels (see Table 12). The kml file can be opened in Google Earth. This functionality can be used to compare targets detected in SAR images with AIS (Automatic Identification System) messages from vessels in the same area, since these also can be viewed in Google Earth (see Figure 121). Now FFI has developed an MHT (Multi Hypothesis Tracker) which can combine SAR detections with AIS, VMS (Vessel Monitoring System), LRIT (Long Range Identification and Tracking), and other data sources [11]. All this information can be used for picture building and to determine the normal pattern. Operationally the results from all the different data sources can be used to catch indications of abnormal presence of vessels as well as finding vessels not reporting through AIS or vessels reporting wrong AIS position on purpose. It is also useful for the Coast Guard to get an overview of where the fishing fleets are.

**CLASSIFICATION: UNCLASSIFIED**

All rights reserved. No part of this document may be reproduced or transmitted in any form or by any means, electronic, mechanical, photocopying, recording, or otherwise, without prior written permission of FFI, NLR or TNO.



Table 12 Reports produced after ship detection is done.

File name	File purpose
.ships	Common ship detection report where the results from all detections in all polarisation channels available are combined into one report
Ships.gml	Common gml report produced that can be read by the MHT (Multi Hypothesis Tracker) at FFI.
XX.ships	One text report for each polarisation, where 'XX' can be 'HH', 'VV', 'VH', or 'HV' according to transmitted and received polarisation.
XX.ships.kml	One report for each polarisation that can be opened in Google Earth.
XX.ships_maria.xml	One xml report for each polarisation that can be opened in Maria.
XX_IncConf.ships	One text report for each polarisation with increased confidence estimates after using the incidence angle and detection information from all polarisation channels.

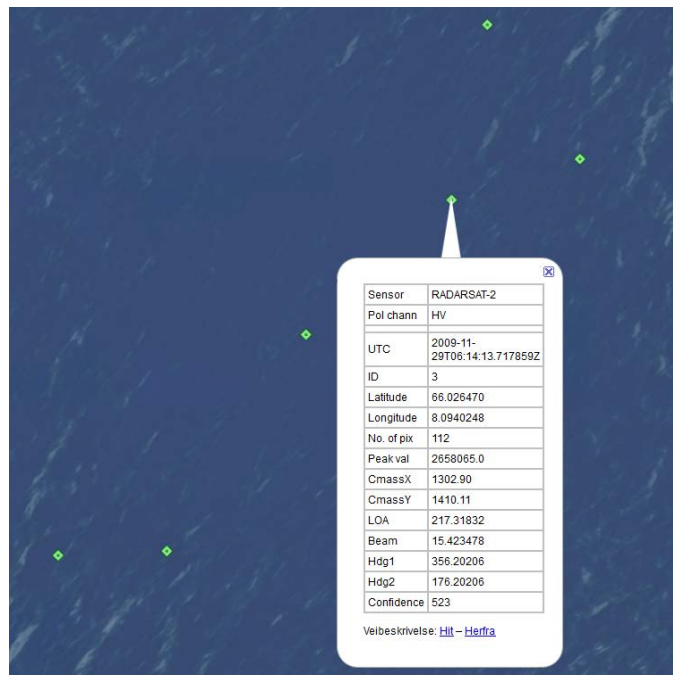


Figure 121 SAR detections can be shown in Google Earth. © Google Earth.

For application of Aegir to the use cases Rotterdam and Kaliningrad we refer to section 5.3.1.4 and 5.3.1.6 respectively.

### CLASSIFICATION: UNCLASSIFIED

All rights reserved. No part of this document may be reproduced or transmitted in any form or by any means, electronic, mechanical, photocopying, recording, or otherwise, without prior written permission of FFI, NLR or TNO.

### 5.7 Description of fusion test bed component

In the section we describe the fusion component of the test bed. The fusion component is a viewer which allows to combine the output of the various modules described in the previous sections and to present these outputs in the context of other geographic oriented information. Figure 120 shows the test bed implementation highlighting the fusion viewer component and the various components described in the previous sections. The ELINT satellite is not implemented as it is studied as a future capability in Milspace II. In the fusion viewer simulated data can be used.

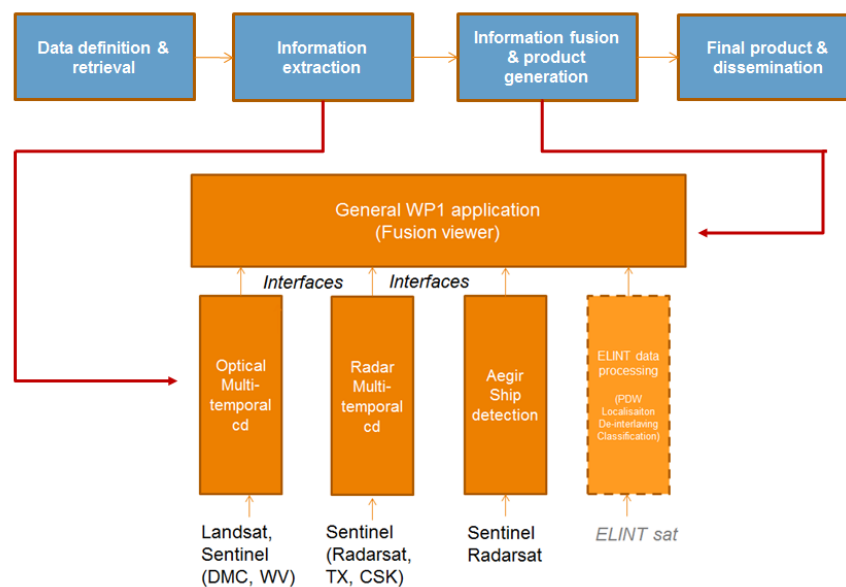


Figure 122 Overview of test bed components and workflow

The input for the fusion component is an area of interest for which several data sets should be available. Basis data are a map, an optical image, a radar image, as well an optional emitter density picture.

The various components produce optical and radar multi-temporal change products, as well as a ship detection list and an emitter list. Detailed information contained in these products can be inspected (info button) in the fusion viewer so that correlations between the various features (ship, changes, emitter) can be made.

### CLASSIFICATION: UNCLASSIFIED

All rights reserved. No part of this document may be reproduced or transmitted in any form or by any means, electronic, mechanical, photocopying, recording, or otherwise, without prior written permission of FFI, NLR or TNO.

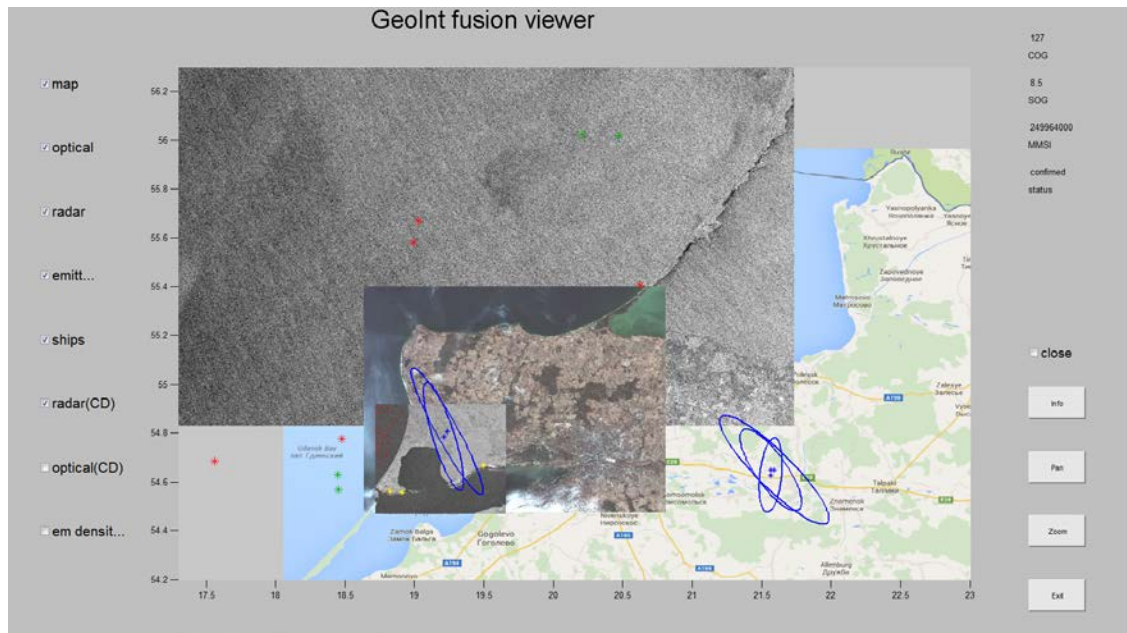


Figure 123 Interface of the fusion component showing use case Kaliningrad.

Two use cases in combination with the integrated demonstrations A & B (see 5.3.1) are elaborated: the Rotterdam case and the Kaliningrad case. Figure 123 shows the Kaliningrad area. In the background an optical Sentinel-2A image is presented along with (simulated) emitter detections. Information is presented from ships detected in a Sentinel1A image (Aegir) and which are cross-checked with AIS data of the time of satellite overpass. Information about the ships can be made visible. Also a multi-temporal change image from a radar data cube is presented and the monitored changes (yellow dots) which can be inspected (see figure 124 and 125) for the detailed information produced in the radar component.

**CLASSIFICATION: UNCLASSIFIED**

All rights reserved. No part of this document may be reproduced or transmitted in any form or by any means, electronic, mechanical, photocopying, recording, or otherwise, without prior written permission of FFI, NLR or TNO.

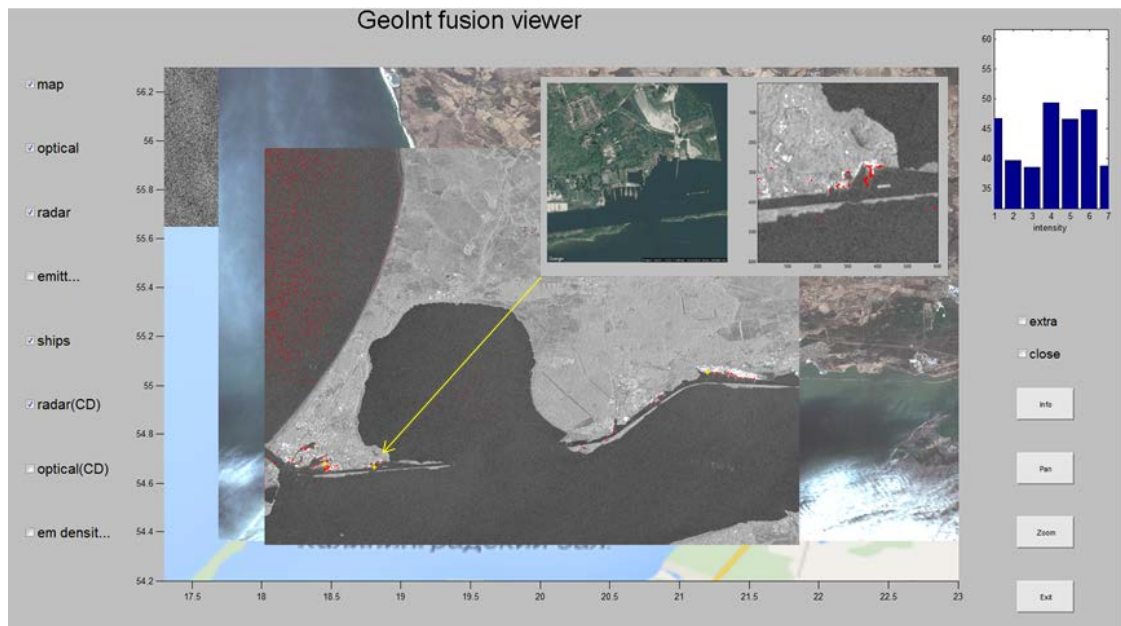


Figure 124 Interface of the fusion component showing use case Kaliningrad and retrieval of radar change detection results.

The Rotterdam use case (Figure 125) shows an area of interest of the Southern North Sea and the west coast of Holland. Both an optical image (Landsat) and a Sentinel-1A radar image are shown, as well as ships detected in a Sentinel-1A image using Aegir (partly shown). Green dots are confirmed by AIS data collected during the overpass, while red dots are not confirmed by AIS. This might be due to the fact that the AIS coverage was not complete. Also three simulated emitters are shown where one is inspected.

**CLASSIFICATION: UNCLASSIFIED**

All rights reserved. No part of this document may be reproduced or transmitted in any form or by any means, electronic, mechanical, photocopying, recording, or otherwise, without prior written permission of FFI, NLR or TNO.



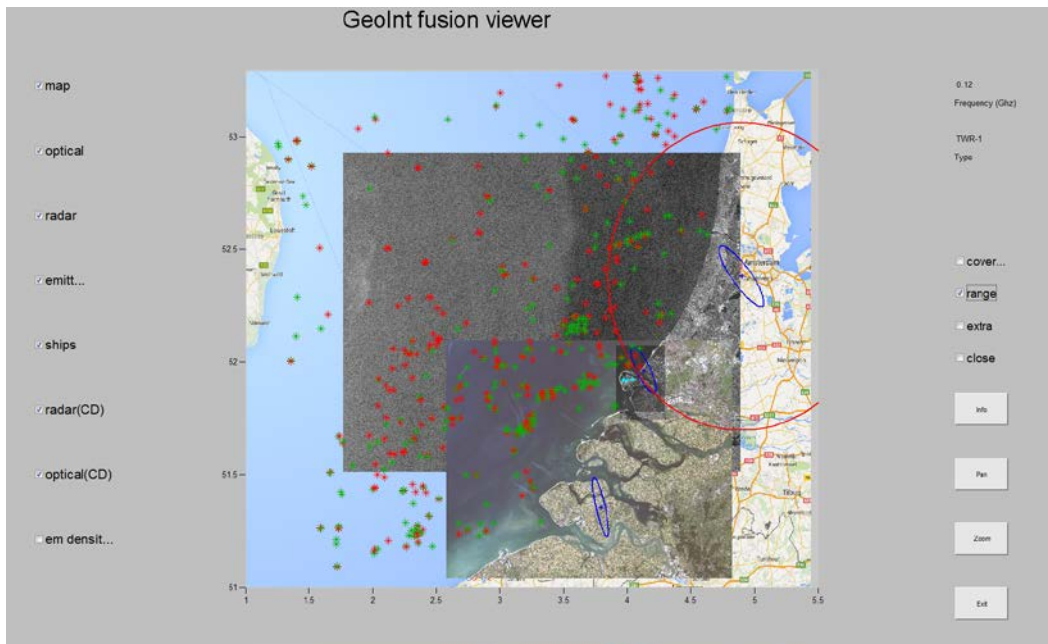


Figure 125 Interface of the fusion component showing use case Rotterdam.

Near Rotterdam the optical change image is present indicating changes (cyan crosses) which can be inspected in more detail (see Figure 126). The fusion viewer can be considered as a GIS viewer which has been dedicated to the test bed components studied in Milspace. It is implemented in Matlab, which allows easy and fast manipulation of changes to be made in the test bed. In operational condition the functionality should be incorporated in commercial software (such as ArcMap) used by the MOD.

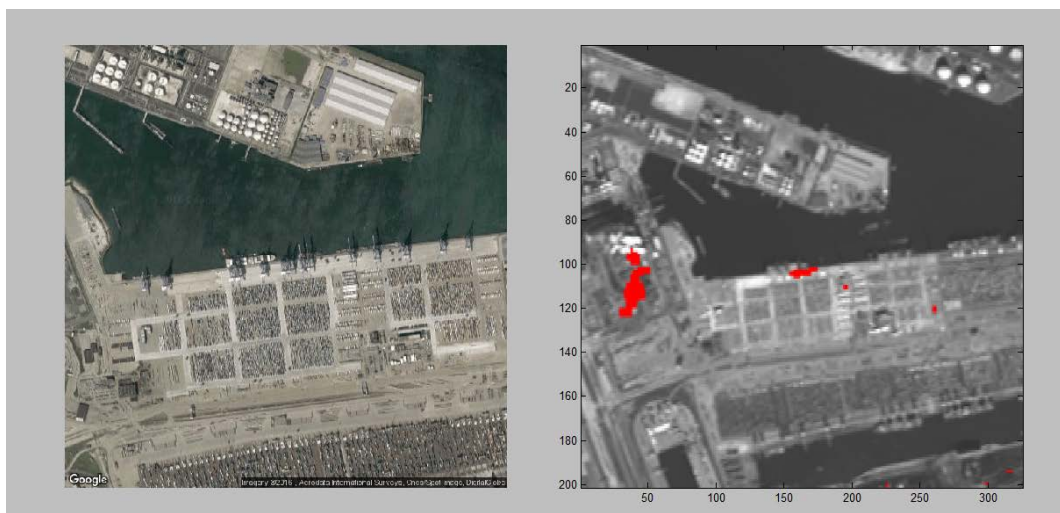


Figure 126 Interface of the fusion component showing use case Rotterdam and retrieval of optical change detection results.

**CLASSIFICATION: UNCLASSIFIED**

All rights reserved. No part of this document may be reproduced or transmitted in any form or by any means, electronic, mechanical, photocopying, recording, or otherwise, without prior written permission of FFI, NLR or TNO.

## 6 Conclusions

### 6.1 Summary

#### *Requirements*

- Enhanced insight has been gained on the usability of open source satellite observation data for obtaining geospatial intelligence. Because of the frequent and easy availability of medium resolution imagery analysis can be made of time sequences of observations, based on which patterns of environmental or human activities can be recognized and anomalies with respect to normal behaviour can be detected. Typical applications for which this can be used is information on the terrain in the framework of Intelligence Preparation of the Battlefield, such as monitoring of ship activities at sea or in the harbour area, monitoring of aircraft, cars, goods activities at airports, industrial areas or barracks, monitoring of changes in infrastructure or around strategic positions. Due to the medium resolution the details of the changes are limited, but the detections can be used as triggers that can initiate further analysis with more detailed observations. Advantage of the open source data is that large areas can be monitored relatively easy in an automated way.
- An indication has been given of potential products that can be produced by the analysis of series of open data, based on which further discussion on the requirements and applicability could take place.

#### *Acquisition*

- Military access to satellite observations is organized differently in Norway and The Netherlands. In The Netherlands the MOD has no direct contact with satellite operators and data are bought from local resellers. Main clients are the military intelligence service (MIVD) and the Military Geographic Service. Main type of data currently used is high resolution optical imagery. In Norway a central military entity FSGI is formed that collects all information requests and orders satellite data or observations directly from KSAT, where also satellite tasking can be supported. SAR imagery is delivered operationally to monitor ship activities, and geographic or intelligence information products can be generated based on SAR or optical data.

### **CLASSIFICATION: UNCLASSIFIED**

*All rights reserved. No part of this document may be reproduced or transmitted in any form or by any means, electronic, mechanical, photocopying, recording, or otherwise, without prior written permission of FFI, NLR or TNO.*

- More and more actual and archived medium resolution open satellite data is coming available (Sentinel, Landsat , Aster).
- Constellations of large number of small medium resolution satellites are in development (TerraBella, Planet, Blacksky, Satellogic), providing daily or even more frequent observations of every place on earth. Pricing of the data is not clear yet.
- Access to satellite observation data is not easy yet. Several portals are available, but they work interactive and scene based. New service based concepts are in development, giving automated access to data stacks of pixels for a specified area of interest and period.

#### *Processing/analysis*

- An overview has been given of methods and related routines and tools for the processing and analysis of optical and SAR data.
- Proper pre-processing of the data is required to enable combined analysis. For the Landsat and Sentinel missions this is arranged better and better by the basic processing at ground station level. For other missions own routines are required to deal with this step.
- Several methods have been implemented and applied coupled with the demonstration datasets and scenarios. The maturity of the applied methodologies varies. The Aegir ship detection methodology is rather robust. The anomaly detection methodologies for SAR and optical data are more conceptual and require further testing and tuning for different situations (seasons, type of landscapes, type of targets).

#### *Fusion*

- For fused analysis supporting context information is required. One element of this is proper Digital Elevation Models. An analysis of available DEMs was made and concluded was that the SRTM based DTED2 is best usable. With the current TanDEM-X mission DTED3 level data are acquired that will come available in the next years.
- Different type of satellite half products can be delivered as input for the fusion process: land use classification products, change detection products, ship detection products, and detailed analysis products.
- Fusion methods for the combination of the satellite half products with context data have been defined and tested for the demonstration datasets and scenarios.

#### *Dissemination/architecture*

- An overview has been given of the architectures that are applied for the data management, processing, analysis and dissemination. In the military domain the NATO STANAG and the results on architectures, implementation and procedures as obtained in the MAJIIC project

### **CLASSIFICATION: UNCLASSIFIED**

*All rights reserved. No part of this document may be reproduced or transmitted in any form or by any means, electronic, mechanical, photocopying, recording, or otherwise, without prior written permission of FFI, NLR or TNO.*

are leading. In the civil world standards and architectures as defined in the framework of INSPIRE and the Open GIS Consortium are important. The standards in both worlds interact with each other.

- For the different levels of products (base, half, finished) military and civil formats have been defined.

#### *Demonstration workflows*

- Several demonstration datasets have been collected and related scenarios were defined (e.g. Rotterdam, Nickel, Carabean, North Sea, Kaliningrad). Based on these scenarios information products were defined. For these cases a demonstration environment was developed in which the data could be processed to products.
- A demonstration workflow has been realised where operators are guided in the process of extracting ships and anomalies in located aircraft, infrastructure or industrial activities, including the interactive combined analysis of the results obtained from different data sources and related processing tools.
- The demonstration illustrates that operator work environment can be based on different software components, either based on customized commercial tools or own developed tools, that can be integrated to a single environment.
- The current demonstration environment needs further operationalization for usage in practise. In many cases data input and processing routines are not generic and the operator interaction is not mature. Also the processing speed and related response times are not optimised, which means that for larger datasets practical working times will be too long.
- Processing optimization can be obtained by optimizing the software and software environment and also by applying big data technology so that the process is scalable when applying more processing nodes.

## **6.2 Recommendations**

It is recommended that a next step with the demonstration system can be made in which attention can be given to several aspects:

- Couple to data acquisition process (archive retrieval and possibly tasking) in an automated way.
- Further automation of the workflow, so that it can run as a background process.
- Increase robustness of the algorithms by testing them for different data sources, geographic environments and types of anomalies.

### **CLASSIFICATION: UNCLASSIFIED**

*All rights reserved. No part of this document may be reproduced or transmitted in any form or by any means, electronic, mechanical, photocopying, recording, or otherwise, without prior written permission of FFI, NLR or TNO.*



- Suitability of the processing chain for very large datasets. Big data processing technologies can be applied to make the processing scalable when applying large number of processing nodes.
- Possibility to test and apply the tools by military analysts in their own environment.
- Evaluation of the results for multiple cases and discuss with the military analysts on the relevance of the obtained information for different scenarios.

**CLASSIFICATION: UNCLASSIFIED**

*All rights reserved. No part of this document may be reproduced or transmitted in any form or by any means, electronic, mechanical, photocopying, recording, or otherwise, without prior written permission of FFI, NLR or TNO.*

## References

1. [Big Data, 2013] Anne-Claire Boury-Brisset, Defence Research and Development Canada, Managing Semantic Big Data for Intelligence, STIDS 2013 Proceedings, 2013.
2. [Del\_31b\_NLR, 2014] Infrastructure Technology Overview
3. [EC-INSPIRE, 2008] European Commission, INSPIRE, INSPIRE Network Services Drafting Team, Network Services Architecture (Version 3.0), 2008.
4. [NATO SG115, 2008] NATO NIAG Study SG115 Final Report, Infrastructures for Dissemination of Intelligence, Surveillance and Reconnaissance (ISR), Data to Field Commanders, 2008.
5. [OGC-WMS, 2006] OpenGIS® Web Map Server Implementation Specification, Version 1.3.0. Open Geospatial Consortium Inc., OGC 06-042, 2006.
6. [OGC-CSW, 2007] OpenGIS® Catalogue Services Specification, Version 2.0.2, Open Geospatial Consortium Inc., OGC 07-006r1, 2007-02-23.
7. [OGC-WCS, 2008] OpenGIS® Web Coverage Service (WCS) Implementation Standard, Version 1.1.2. Open Geospatial Consortium Inc., OGC 07-067r5, 2008.
8. [STANAG 4559, 2007] STANAG 4559 AIR (EDITION 2) - NATO Standard ISR Interface, NSA/336(2007)-AIR14559, 2007.
9. Bert van den Broek, Eric den Breejen, Rob Dekker, Arthur Smith, Change detection and maritime situation awareness in the channel area - Feasibility of space borne SAR for maritime situation awareness, *IGARSS 2012*, 7436-7439
10. E. J. M. Rignot and J.J. Van Zyl, 1993, Change detection techniques for ERS-1 SAR data. *IEEE Transactions on Geoscience and Remote Sensing*, Vol. 31, No. 4, p. 896-906.
11. Gade, B.H.H. LAMU Tracker, a Tracker for Sensors with large Angular Measurement Uncertainty. FFI-rapport 2006/03576.
12. Hannevik, T.N.A., K. Eldhuset and R.B. Olsen. Improving Ship Detection by using Polarimetric Decompositions. FFI-rapport 2015/01554.
13. Nord, M.E., T.L. Ainsworth, J.-S. Lee and N.J.S. Stacy. Comparison of Compact Polarimetric Synthetic Aperture Radar Modes. *IEEE Trans. Geosc. Rem. Sens.*, Vol. 47, No. 1, January 2009.
14. R. Dekker, C. Kuenzer, M. Lehner, P. Reinartz, I. Niemeyer, S. Nussbaum, V. Lacroix, V. Sequeira, E. Stringa, and E. Schöpfer, 2009, Change Detection Tools. In: *B. Jasani, M. Pesaresi, S. Schneiderbauer, and G. Zeug (editors), Remote Sensing from Space: Supporting International Peace and Security, Springer Science and Business Media, Germany*

**CLASSIFICATION: UNCLASSIFIED**

All rights reserved. No part of this document may be reproduced or transmitted in any form or by any means, electronic, mechanical, photocopying, recording, or otherwise, without prior written permission of FFI, NLR or TNO.

15. Weydahl, D.J. Personal Communication 2010.
16. Weydahl, D.J., 2011. The Potential of Commercial Satellite SAR Images for IED Prediction. NATO MP-SET-175-12. Presentation done under SET-175 meeting in Copenhagen, June 6-7 2011.
17. Yamaguchi, Y., A. Sato, W.-M. Boerner, R. Sato, H. Yamada. Four-Component Scattering Model for Polarimetric SAR Image Decomposition. *IEEE Transactions on Geoscience and Remote Sensing*, Vol. 39, No. 8, pp. 1699-1706, 2005.
18. Zebker, H.A., and Villasenor, J., 1992. Decorrelation in Interferometric Radar Echoes. *IEEE Transactions on Geoscience and Remote Sensing*, Vol. 30, No. 5, pp. 950-959.
19. Xu, H. 2007. Extraction of Urban Built-Up Land Features from Landsat Imagery Using a Thematic-oriented Index Combination Technique. From: *Photogrammetric Engineering and Remote Sensing*. Vol. 73, No. 12.

**CLASSIFICATION: UNCLASSIFIED**

*All rights reserved. No part of this document may be reproduced or transmitted in any form or by any means, electronic, mechanical, photocopying, recording, or otherwise, without prior written permission of FFI, NLR or TNO.*

## **Appendix A Geospatial analysis workshop, DIVI, 't Harde, 18-20 November 2014**

A geospatial analysis workshop was held at the Dutch school of intelligence (DIVI), and addressed the use of satellite data by geospatial analysts for the intelligence preparation of the environment. For this workshop the Nickel test site from the NL/NO Milspace research programme work package 1 on GeoInt was chosen. Experiences collected during the workshop are used as input to the project on military requirement for the use of satellite data.

The goal was to practice the first steps for IPE for an unfamiliar area (terrain analysis and activity mapping). As preparation articles from the Barents Observer, YouTube movies and scientific papers on change detection were distributed. Examples of data collected were time series of Landsat data and RADARSAT spotlight data, as well as open street map data were collected.

Participants were from the Dutch school of intelligence, geospatial analysts (DIVI, JSTARC), TNO, NLR, ESRI and Imagemn. The following agenda was used:

### **Day 1 Terrain Analysis (DIVI)**

- Introduction to the workshop and Milspace project
- Hydrology with ArcGIS and with Erdas
- Vegetation mapping with Erdas
- Infrastructure mapping with ArcGIS

### **Day 2 Activity and change monitoring with Landsat imagery (NLR)**

- Time series analysis – calibration of Landsat data
- Time series analysis – use of Landsat data
- Time series analysis – use of Erdas

### **Day 3 Activity monitoring with radar imagery (TNO)**

- Introduction to radar imagery
- Radar change detection with Erdas
- 3D mapping with Erdas

## **CLASSIFICATION: UNCLASSIFIED**

*All rights reserved. No part of this document may be reproduced or transmitted in any form or by any means, electronic, mechanical, photocopying, recording, or otherwise, without prior written permission of FFI, NLR or TNO.*



- Time series analysis with RADARSAT data
- Discussion and evaluation



Figure A.1 Participants working on Landsat data of test case Nickel during the workshop.

**CLASSIFICATION: UNCLASSIFIED**

*All rights reserved. No part of this document may be reproduced or transmitted in any form or by any means, electronic, mechanical, photocopying, recording, or otherwise, without prior written permission of FFI, NLR or TNO.*

## Day 1 Terrain analysis (DIVI)

Day 1 started with the necessary welcoming presentations as well as an introductory presentation by TNO on the Milspace project. The project goal is to facilitate the military use of open source satellite data for producing GeInt products. This is done by developing tools and algorithms for automating workflows. The workflow components are demonstrated in a test bed. This was followed by a few hands-on sessions on the subject of terrain analysis. The objective was to show methods what data is needed for the IPE (Intelligence Preparation of the Environment) that can be generated from open source geodata (DTED2, Landsat8 and Open Street Map). In this workshop we focused specifically on hydrology (open water, streams), vegetation and infrastructure mapping using the available tools in ArcGIS and Erdas.

### 1. Hydrology - open water

If no information on open water bodies is available, Landsat8 data is a good source from which these data can be extracted (see figure A.2 to get an idea of the area, Landsat8 band combination RGB 564).

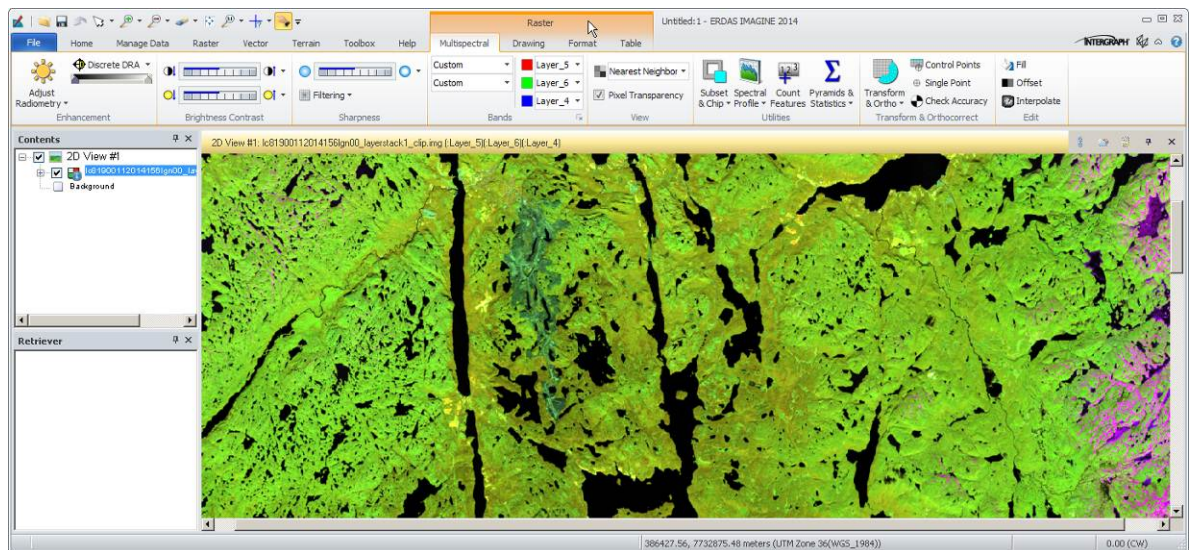


Figure A.2 A part of the study area, just north of Nikel.

The method to map open water bodies from Landsat8 discussed here, exploits the fact that clear water features absorbs nearly all infrared radiation. This is in contrast with other land cover features like vegetation or bare soil where infrared radiation is reflected back to the sensor. This spectral contrast enables the mapping of open water bodies. The first step is to calculate an NDVI (Normalised Difference Vegetation Index) of the area.

$$\text{NDVI} = \frac{\text{NIR} - \text{R}}{\text{NIR} + \text{R}}$$

## CLASSIFICATION: UNCLASSIFIED

All rights reserved. No part of this document may be reproduced or transmitted in any form or by any means, electronic, mechanical, photocopying, recording, or otherwise, without prior written permission of FFI, NLR or TNO.



Open water bodies usually have a very low NDVI index value – low reflectance in the red band (R) and no reflectance in the near infrared band (NIR (Near Infrared), figure A.3).

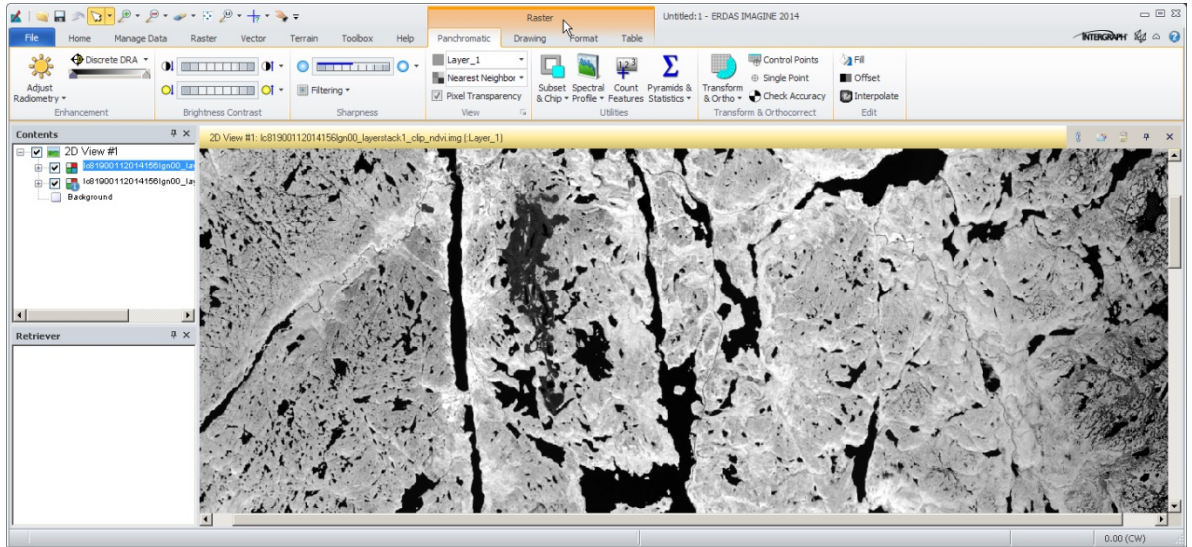


Figure A.3 NDVI of study area.

Another option is to calculate an NDWI (Normalised Difference Water Index).

$$NDWI: (G - NIR)/(G + NIR)$$

Open water bodies typically have a high index value in the NDWI – low reflectance in the green band (G) and no reflectance in the near infrared band (NIR, figure 1.3). In the study area the NDWI makes better distinction between mine dumps and water when compared to the NDVI.

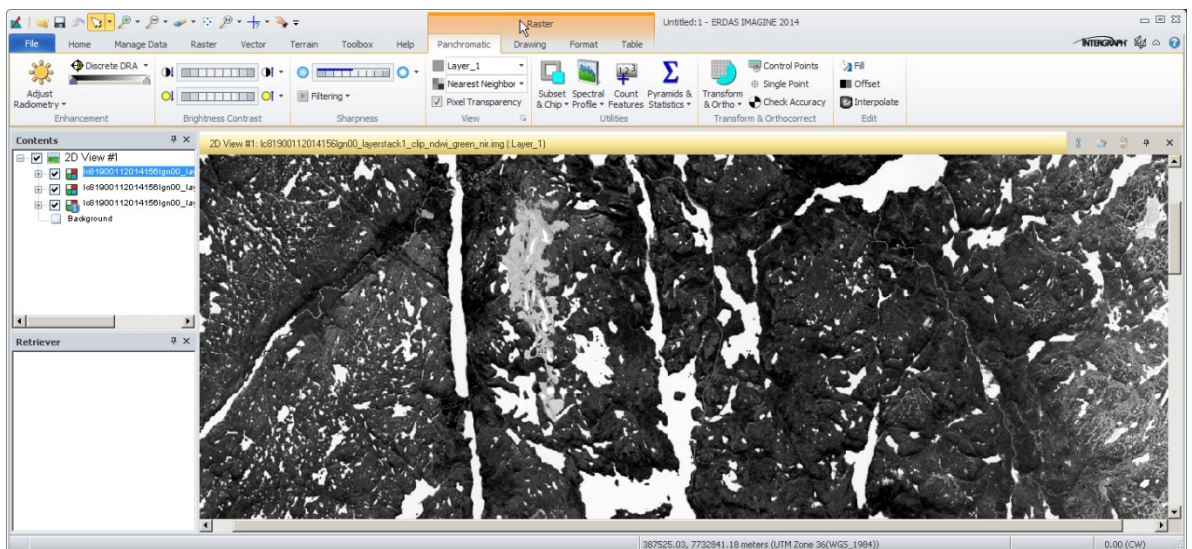


Figure A.4 NDWI of study area.

**CLASSIFICATION: UNCLASSIFIED**

All rights reserved. No part of this document may be reproduced or transmitted in any form or by any means, electronic, mechanical, photocopying, recording, or otherwise, without prior written permission of FFI, NLR or TNO.

The NDVI (and / or the NDWI) is then stacked together with the NIR and MIR (Middle Infrared band) bands of the original Landsat8 image into a new stack file. An unsupervised classification is then run on this stack file (parameters used in figure A.5).

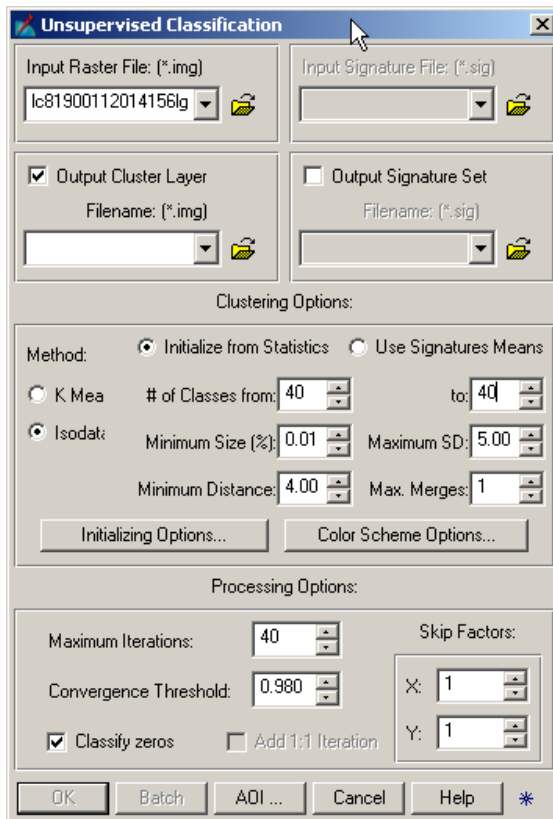


Figure A.5 Unsupervised classification parameters.

In the resulting classification one or two classes includes open water bodies (figure A.6). These classes can be extracted to a water mask. This mask contains the necessary information of the location of open water bodies for the IPE. It can subsequently be exported to a smoothed vector file in an IPE-related geodatabase, together with the raster mask file.

## CLASSIFICATION: UNCLASSIFIED

*All rights reserved. No part of this document may be reproduced or transmitted in any form or by any means, electronic, mechanical, photocopying, recording, or otherwise, without prior written permission of FFI, NLR or TNO.*



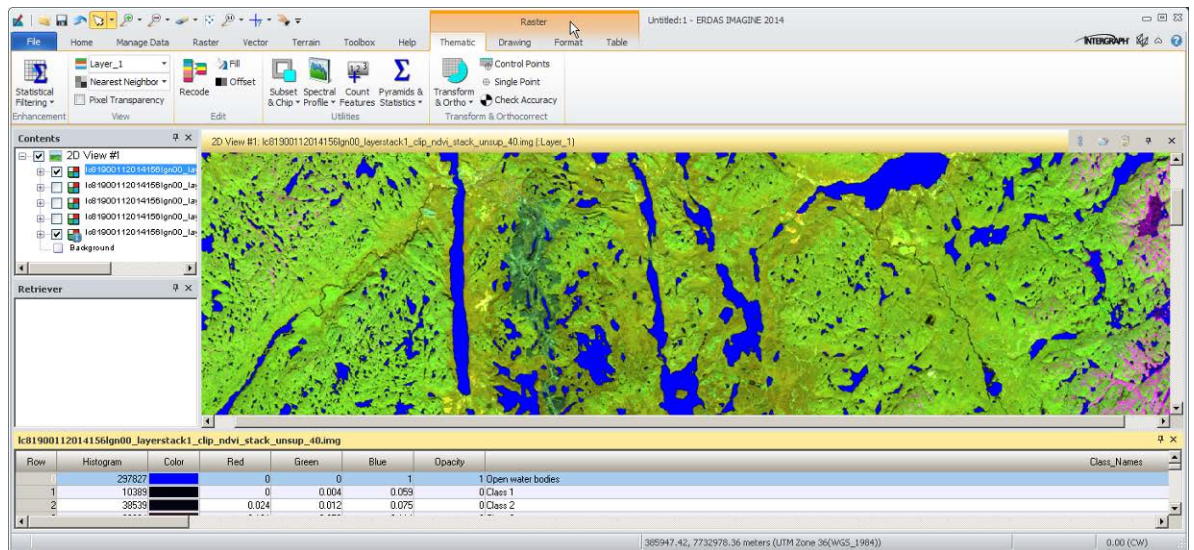


Figure A.6 Water mask of open water bodies.

## 2. Hydrology - streams

The Spatial Analyst extension toolbox in ArcGIS contains hydrology tools. These tools can be used to calculate streams, stream order and basins based on a DEM (Digital Elevation Model). These tools cannot be used to sketch a complete hydrologic picture of a specific area. Various elements of the hydrologic cycle are not taken into account (like evaporation and infiltration). For the purpose of mapping (perennial and non-perennial) streams only on a hard impermeable surface for IPE-purposes, the ArcGIS hydrology tools are sufficient.

An ArcGIS model, with the relevant hydrology tools, is used to calculate streams as well as other hydrological products (figure 1.6). The user interface of this model aids the user to specify input and output parameters and datasets (figure A.8).

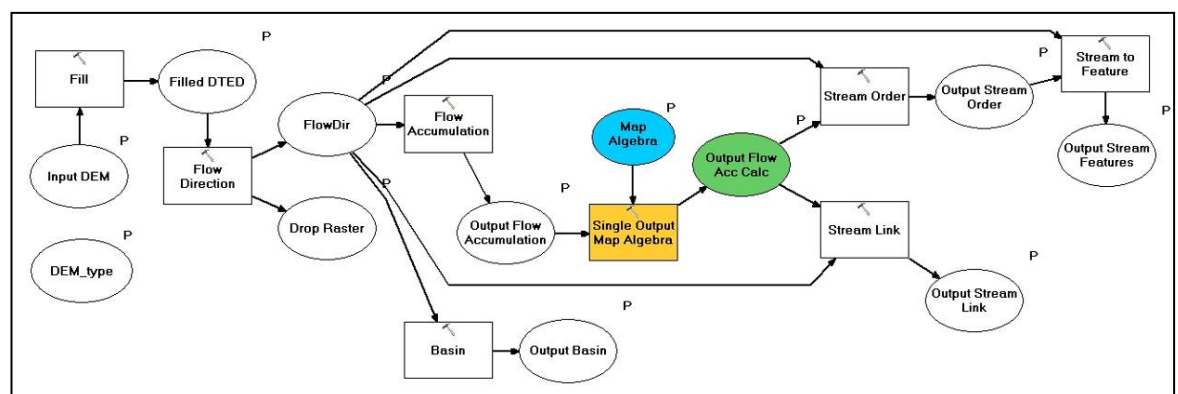


Figure A.7 Model with hydrology tools.

The resulting calculated streams can be draped over the 30 m DEM of the area used for the calculation, as well as over the Landsat8 image to verify the calculation. It is visible that

## CLASSIFICATION: UNCLASSIFIED

All rights reserved. No part of this document may be reproduced or transmitted in any form or by any means, electronic, mechanical, photocopying, recording, or otherwise, without prior written permission of FFI, NLR or TNO.

the streams follow the topography of the area. Over large lake surfaces, the model can however not resolve streams properly. This can be seen where many parallel streams are calculated (figure A.9). At some places the calculated stream does not follow the location of the stream on the satellite image. This is probably due to a time difference between the stream on the satellite image and the DEM, or due to the resolution of the DEM (figure A.10). When the open water bodies are draped over the streams, the streams and open water connect rather well (figure A.11). The basins product shows the areas that feed the rivers and open water bodies with water (figure A.12).

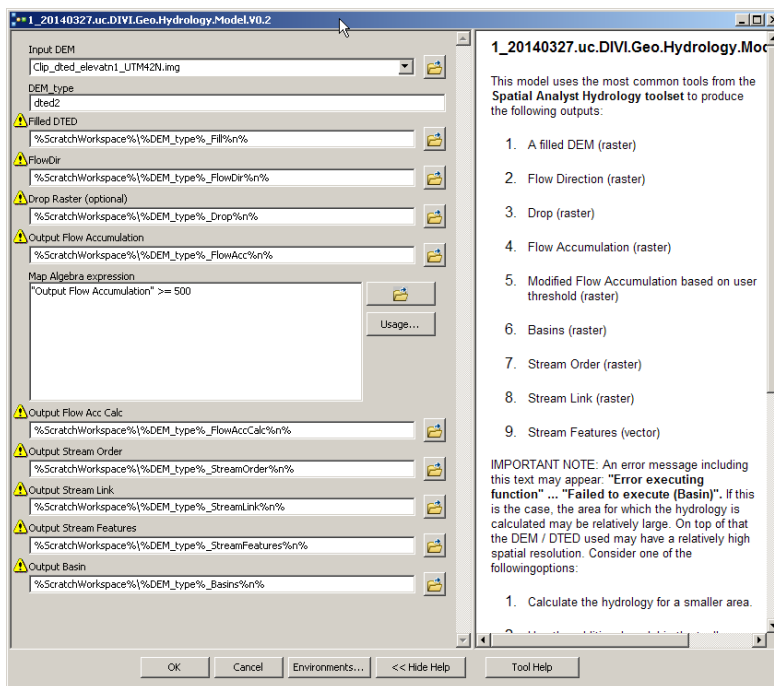


Figure A.8 User interface of hydrology model.

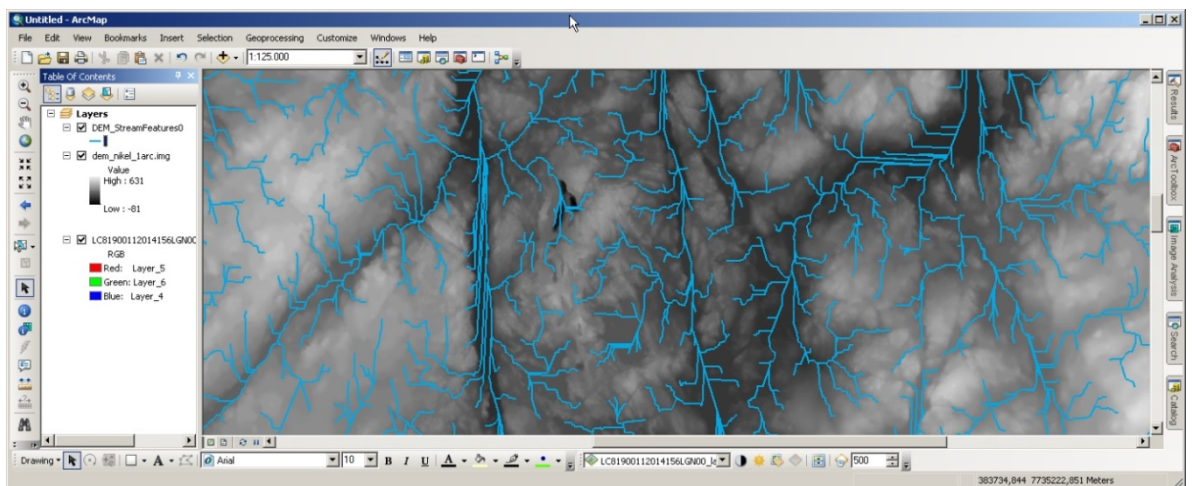


Figure A.9 Streams over the DEM.

**CLASSIFICATION: UNCLASSIFIED**

All rights reserved. No part of this document may be reproduced or transmitted in any form or by any means, electronic, mechanical, photocopying, recording, or otherwise, without prior written permission of FFI, NLR or TNO.



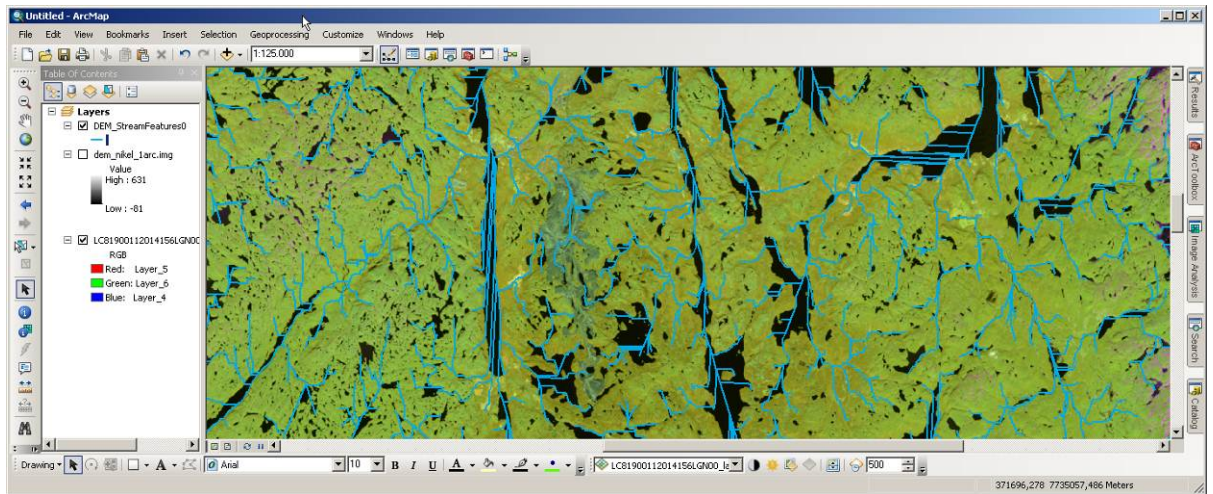


Figure A.10 Streams over the Landsat8 satellite image.

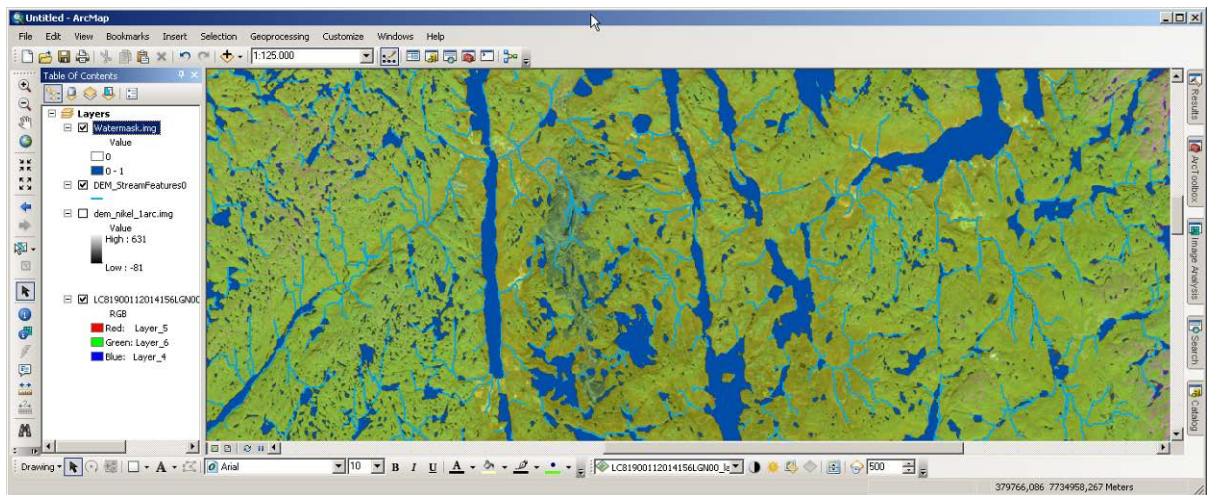


Figure A.11 Streams over the Landsat8 satellite image with open water bodies.

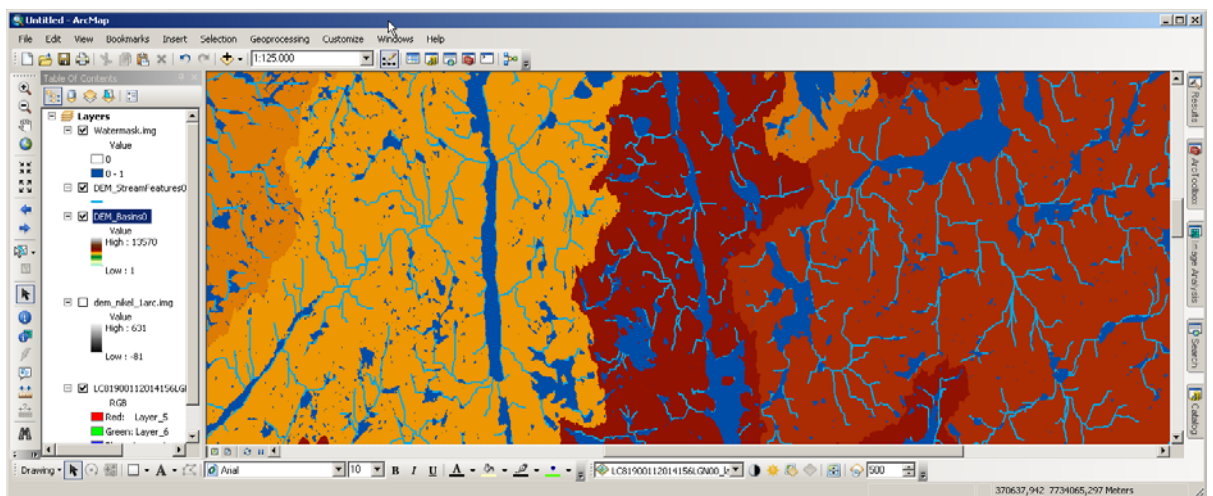


Figure A.12 Streams and open water bodies over the calculated basins.

**CLASSIFICATION: UNCLASSIFIED**

All rights reserved. No part of this document may be reproduced or transmitted in any form or by any means, electronic, mechanical, photocopying, recording, or otherwise, without prior written permission of FFI, NLR or TNO.

### 3. Vegetation

Landsat8 satellite imagery is an ideal source to map vegetation. Due to the differences between reflection of vegetation in the R and NIR bands of Landsat8 images, the location of vegetation can be mapped with an NDVI (formula described earlier).

The Spatial Modeler in Erdas is used to calculate the NDVI (up to 1, figure A.13-figure 1A.14). Next criteria is set based on an NDVI threshold value ( $< 0.2$ : not vegetation, figure A.15) to make a general division (a mask) between vegetated and non-vegetated areas (up to 2, figure A.13). These threshold values are not standard and should be set again for each new area. The threshold can be extracted visually from the histogram of the NDVI product (figure A.16). This mask is used to clip the input Landsat8 image to show only the vegetated areas (up to 3, figure A.13). The clipped Landsat8 image can be used to show with more contrast all different vegetated areas (figure A.17).

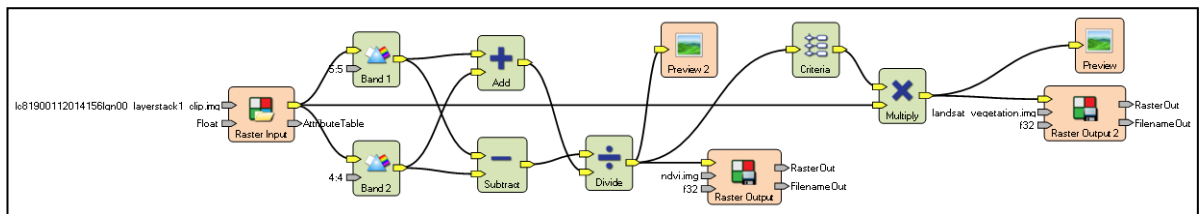


Figure A.13 Erdas model to calculate NDVI, NDVI-mask and output clipped satellite image.

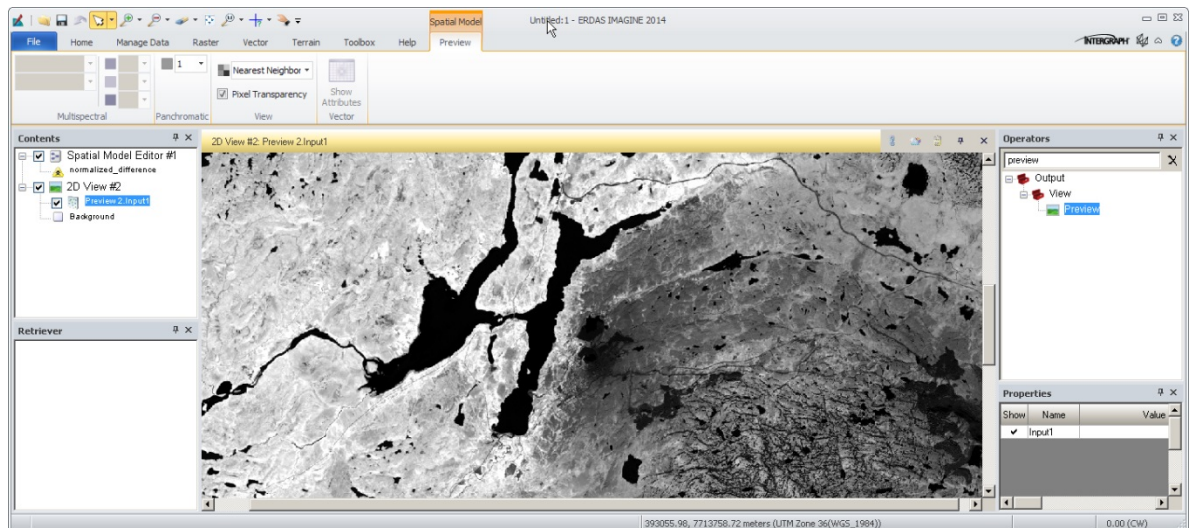


Figure A.14 Preview of the NDVI.

**CLASSIFICATION: UNCLASSIFIED**

All rights reserved. No part of this document may be reproduced or transmitted in any form or by any means, electronic, mechanical, photocopying, recording, or otherwise, without prior written permission of FFI, NLR or TNO.



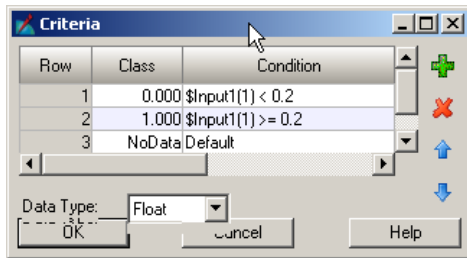


Figure A.15 Criteria set to separate vegetation from the rest.

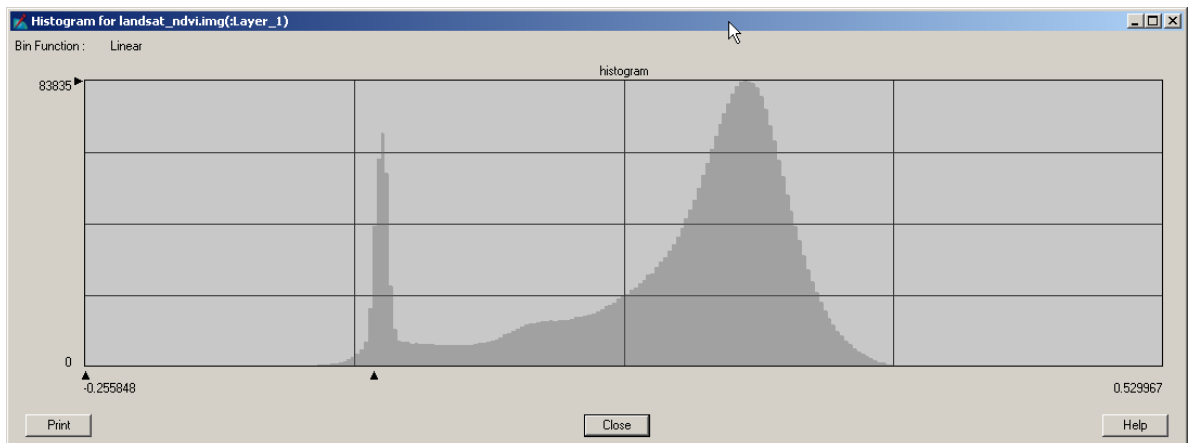


Figure A.16 Histogram of the NDVI product.

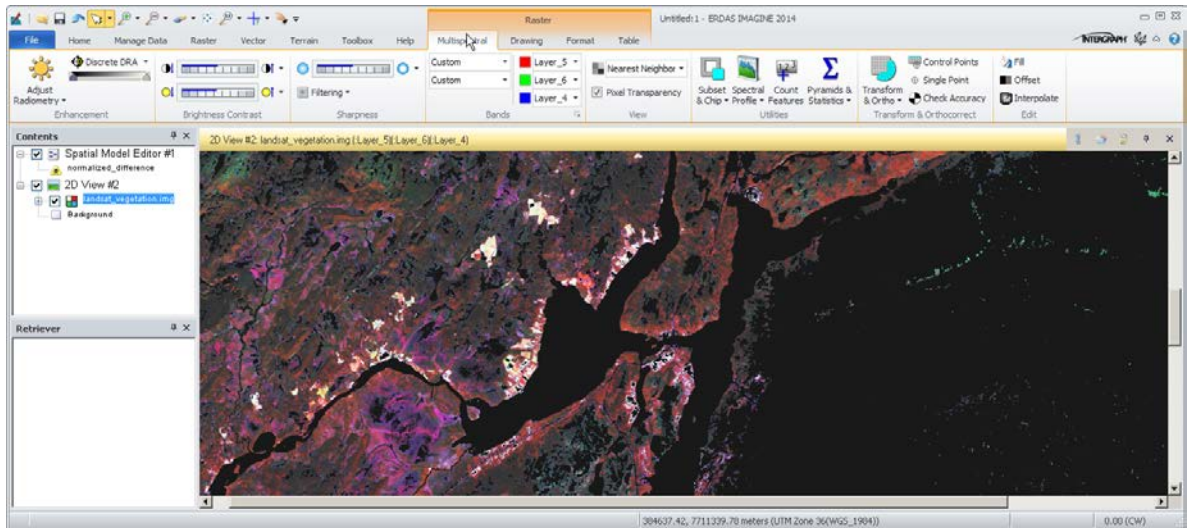


Figure A.17 Stretched vegetated areas only.

The clipped Landsat8 image (figure A.17) can subsequently be classified to make different thematic vegetation classes which can then be used as input data in the IPE. This step was not performed during the workshop.

## CLASSIFICATION: UNCLASSIFIED

All rights reserved. No part of this document may be reproduced or transmitted in any form or by any means, electronic, mechanical, photocopying, recording, or otherwise, without prior written permission of FFI, NLR or TNO.

#### 4. Infrastructure - vector

Geodata on the infrastructure in a specific area is crucial for use in the IPE. One method to get geodata on infrastructure is to process OSM (Open Street Map) vector data with the ArcGIS toolbox specifically designed to work with OSM data. The ArcGIS Editor for Open Street Map can be downloaded from the internet and installed on a computer with ArcGIS.

In this toolbox (the Editor for Open Street Map) there is a tool (Download OSM Data) with which OSM data can be directly imported into ArcGIS. The limitation of this tool is that only up to (approximately) 16,000 nodes can be downloaded. Experience shows that this is not much data. Another option is to download the data from the Open Street Map website.

Open Street Map vector data can be downloaded from the internet in various forms from shape files to .osm files. In the case of the workshop, an .osm file of the Nikel area was downloaded from the Open Street Map website with the Export function (figure A.18). With the Load OSM File tool, the downloaded OSM vector data can be imported into an ArcGIS geodatabase feature dataset (figure A.19). The imported vector data merely consist of points, lines and polygons without any proper symbology added. Symbology can be added by using the Symbolise OSM Data tool (figures A.20-A.21). The vector data from OSM can subsequently be filtered as needed to extract the necessary geodata on infrastructure for the IPE.

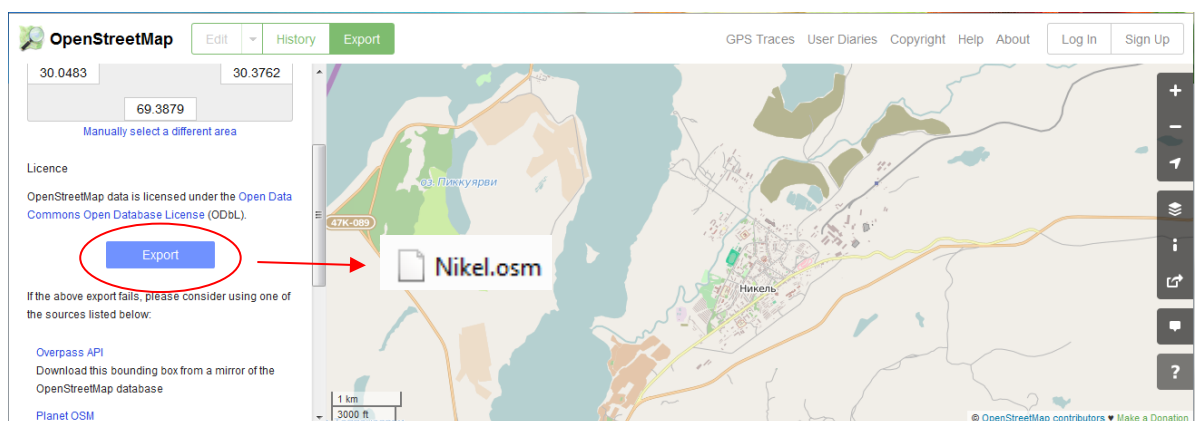


Figure A.18 Exporting vector data from the Open Street Map website.

### CLASSIFICATION: UNCLASSIFIED

All rights reserved. No part of this document may be reproduced or transmitted in any form or by any means, electronic, mechanical, photocopying, recording, or otherwise, without prior written permission of FFI, NLR or TNO.

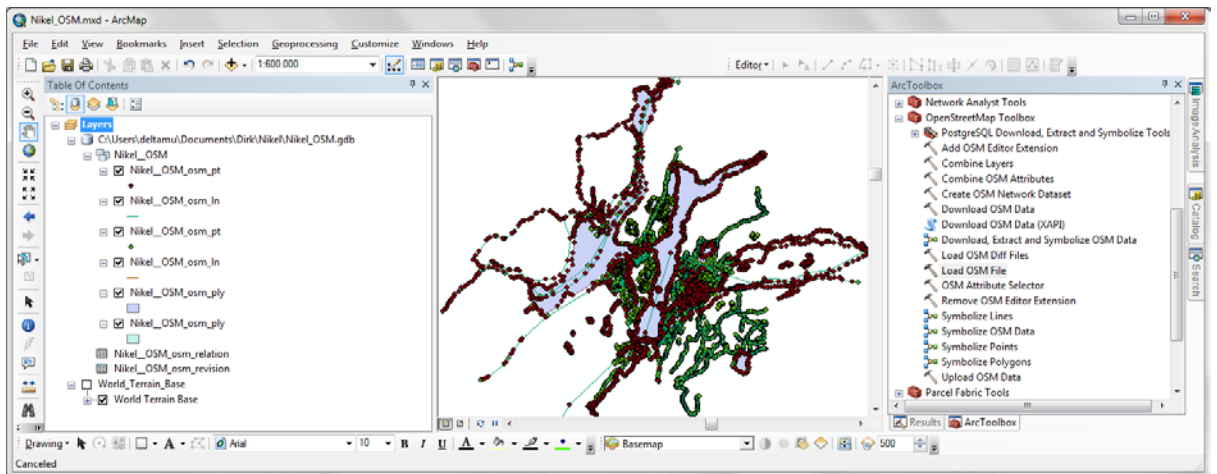


Figure A.19 Importing vector data from the Open Street Map website into a geodatabase.

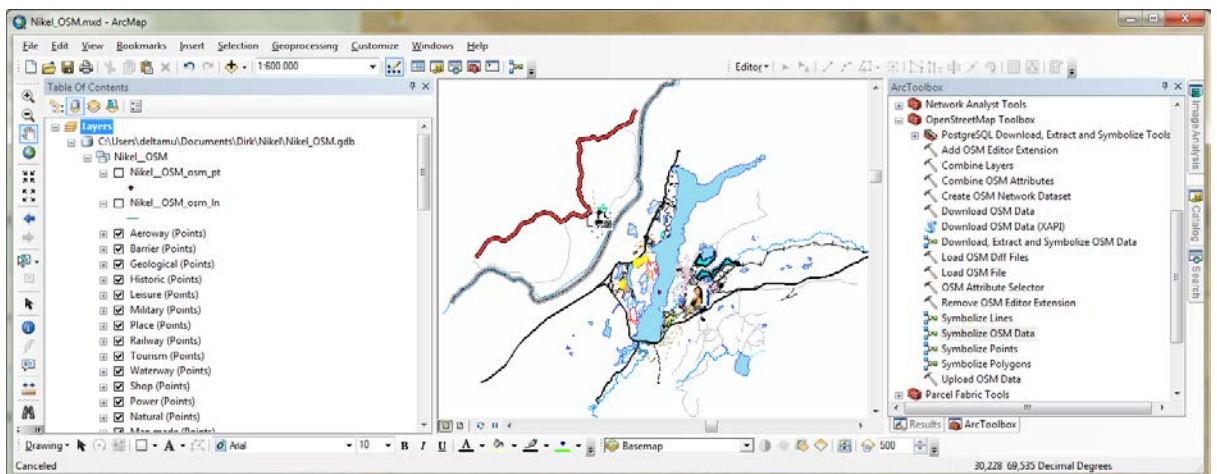


Figure A.20 Symbolising vector data from the Open Street Map website in ArcMap.

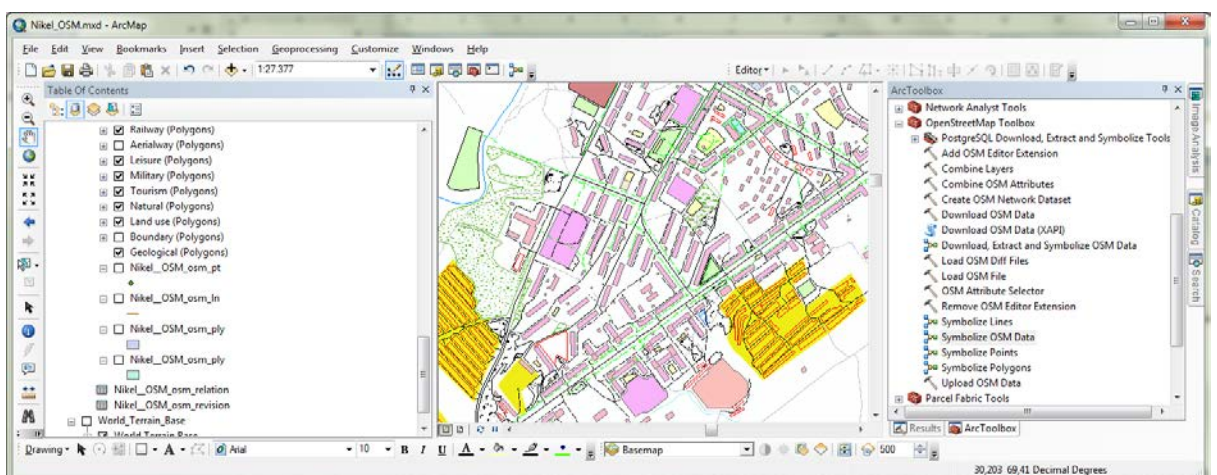


Figure A.21 Symbolising vector data from the Open Street Map website in ArcMap – zoomed in on Nikel.

**CLASSIFICATION: UNCLASSIFIED**

All rights reserved. No part of this document may be reproduced or transmitted in any form or by any means, electronic, mechanical, photocopying, recording, or otherwise, without prior written permission of FFI, NLR or TNO.



## 5. Infrastructure - raster

Depending on the type of raster data available it is possible to extract geodata on infrastructure. Landsat8 data can be used to a certain extent to produce geodata on infrastructure. Performing analysis on stacked indices based on the different multispectral bands is a method used in various studies.

The following example was used in the workshop from a study by Xu [19], H. 2007, *Extraction of Urban Built-Up Land Features from Landsat Imagery Using a Thematic-oriented Index Combination Technique*. From: Photogrammetric Engineering and Remote Sensing. Vol. 73, No. 12. In this study three indices are stacked together and analysed with 1.a Supervised Classification, 2.a Principle Components Analysis and 3.a Logical Calculation.

The first index used is the SAVI (Soil Adjusted Vegetation Index).

SAVI:  $(NIR - R)(1 + I)/(NIR + R + I)$  where  $I$  is a correlation factor related to vegetation density.

Visually the SAVI (figure A.22) is not much different when compared to the NDVI. It is however more capable to detect vegetation in low plant-covered areas.

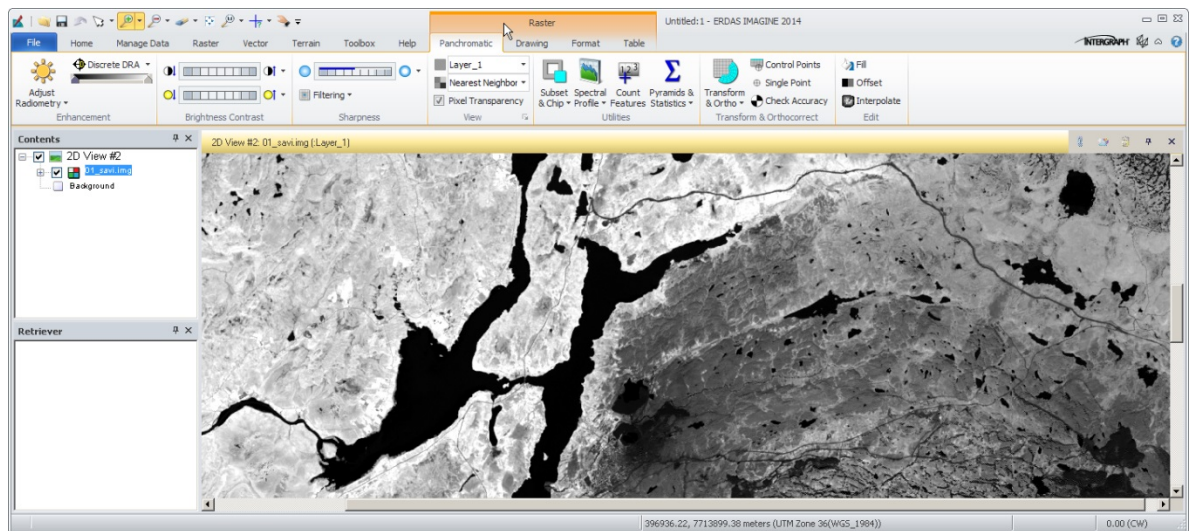


Figure A.22 Soil Adjusted Vegetation Index.

The second index used is the MNDWI (Modified Normalised Difference Water Index).

$$MNDWI: (G - MIR)/(G + MIR)$$

The MNDWI (figure A.23) uses the MIR band instead of the NIR band as used in the NDWI (figure A.4). This results in more distinction between reflectance of built-up areas and water in the green and MIR bands.

## CLASSIFICATION: UNCLASSIFIED

All rights reserved. No part of this document may be reproduced or transmitted in any form or by any means, electronic, mechanical, photocopying, recording, or otherwise, without prior written permission of FFI, NLR or TNO.



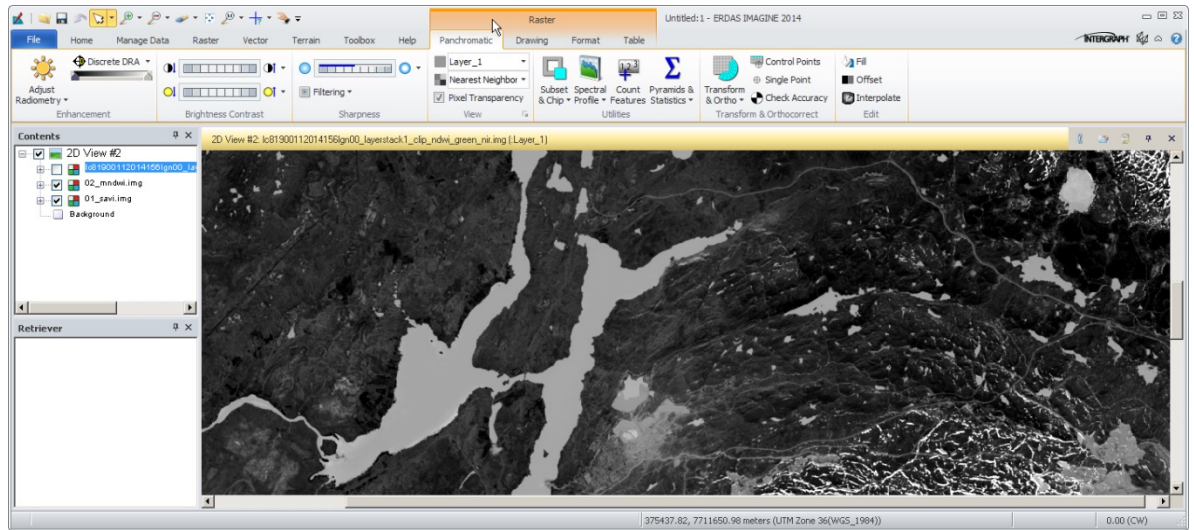


Figure A.23 Modified Normalised Difference Water Index.

The third index used is the NDBI (Normalised Difference Built-up Index).

$$\text{NDBI} = (\text{MIR} - \text{NIR}) / (\text{MIR} + \text{NIR})$$

The NDBI is based on the unique spectral response of built-up areas that reflect more in MIR than in NIR (figure A.24).

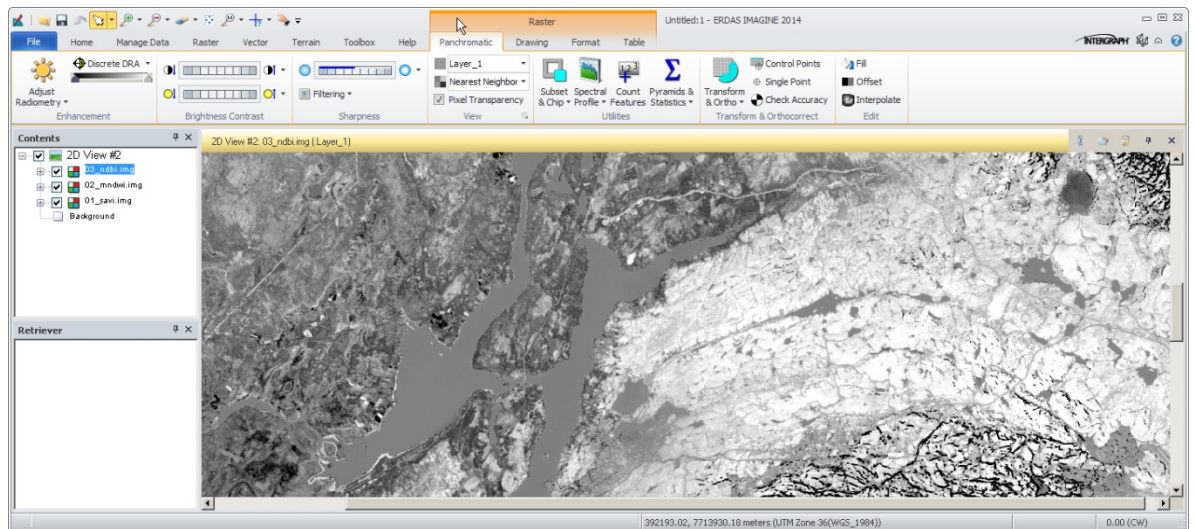


Figure A.24 Normalised Difference Built-up Index.

The three indices mentioned above are subsequently stacked together in a 3-band raster layer (figure A.25). An RGB composite of this layer shows good contrast between different land cover classes. Vegetated areas are clearly depicted in reddish, orange colours; water in dark cyan; snow in dark blue and bare soil/rock areas in light green.

### **CLASSIFICATION: UNCLASSIFIED**

*All rights reserved. No part of this document may be reproduced or transmitted in any form or by any means, electronic, mechanical, photocopying, recording, or otherwise, without prior written permission of FFI, NLR or TNO.*

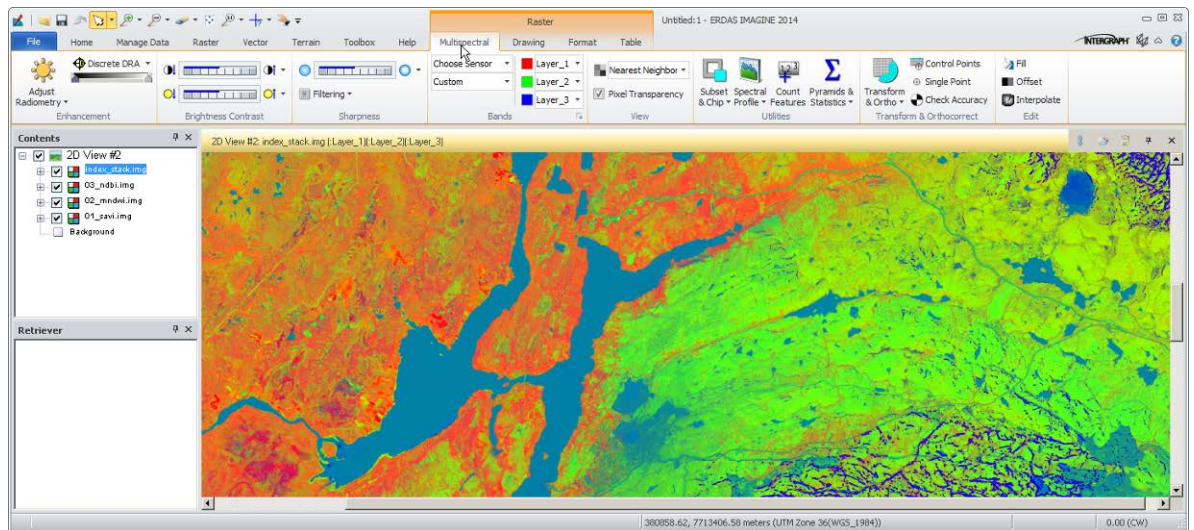


Figure A.25 Index stack, RGB: SAVI, MNDWI, NDBI.

In the workshop not all classification methods applied to this 3-band raster layer were used. A Principle Components Analysis is performed on the three input bands. Three principle components are set to be the output of which an RGB colour composite is shown in figure A.26. In this colour composite even more contrast can be seen between the different land cover classes as discussed in the paragraph above.

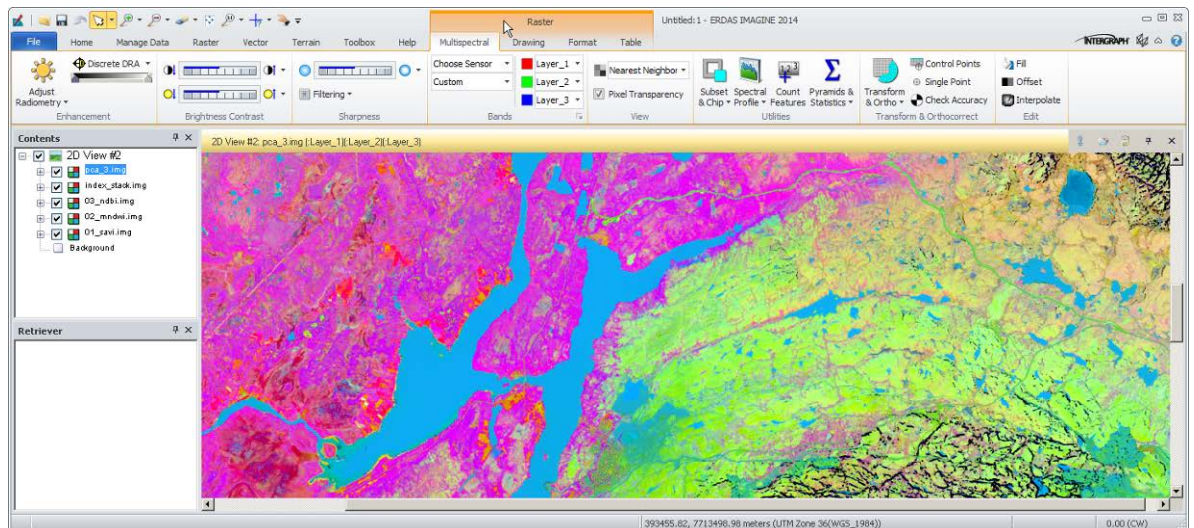


Figure A.26 PCA-3, RGB: PC-1, PC-2, PC-3.

According to Xu (2007, [19]), the second principle component contains the most information relevant to built-up areas (figure A.27). In this raster layer it is clear that bare soil/rock areas have a high value (bright) while snow vegetation and water areas have low values (dark).

## CLASSIFICATION: UNCLASSIFIED

All rights reserved. No part of this document may be reproduced or transmitted in any form or by any means, electronic, mechanical, photocopying, recording, or otherwise, without prior written permission of FFI, NLR or TNO.



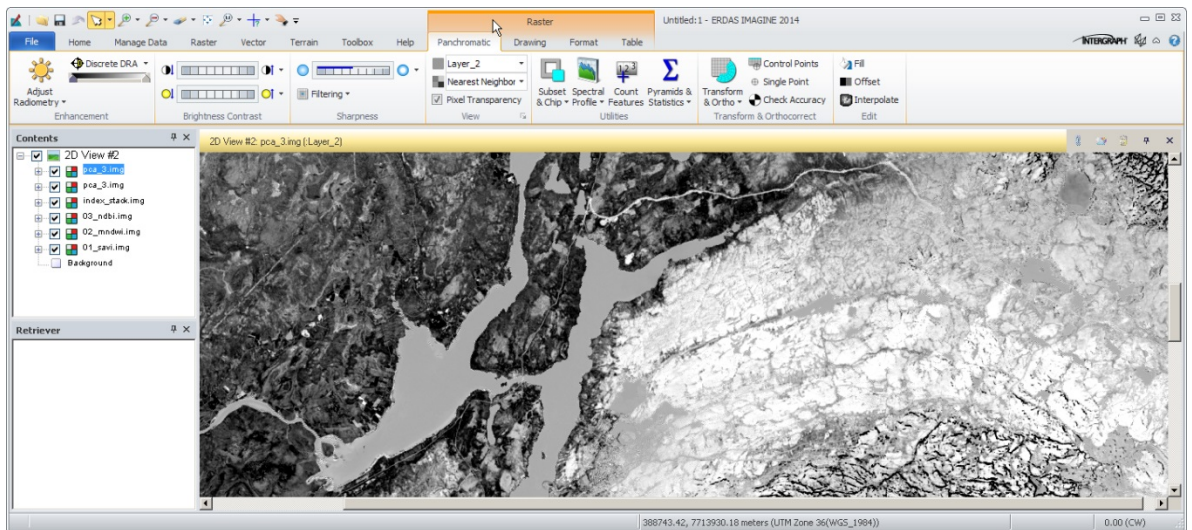


Figure A.27 Principle Component 2.

When comparing the second principle component to the original Landsat8 image (figures A.28-A.29), it is clear that built-up areas do not have the same bright values when compared to bare soil/rock. This is inherent to the multispectral characteristics of built-up areas. They contain a mix of many different reflections: plants, bare soil, water etc. It may be that the cities in China (as mapped by Xu, 2007, [19]) are more homogenous in reflectance compared to Nikel in Russia.

Unfortunately there was not enough time to delve deeper into this during the workshop. What can be taken from this however is that in order to map various land cover classes from a Landsat8 image, one index is not always enough. A combination of indices with further processing on them may lead to more accurate results.

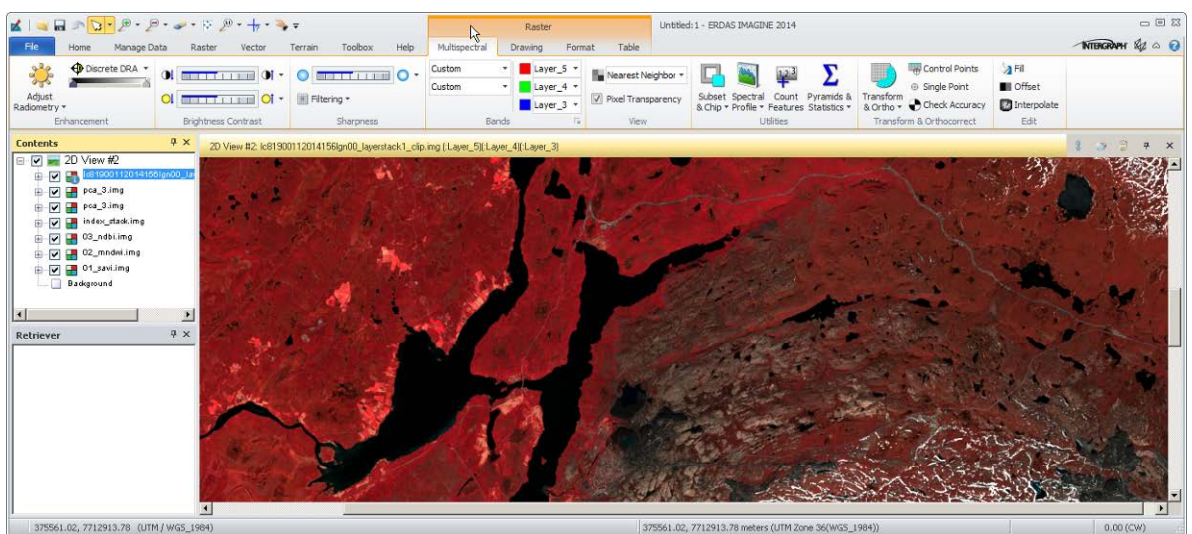


Figure A.28 Landsat8 RGB 543.

## CLASSIFICATION: UNCLASSIFIED

All rights reserved. No part of this document may be reproduced or transmitted in any form or by any means, electronic, mechanical, photocopying, recording, or otherwise, without prior written permission of FFI, NLR or TNO.

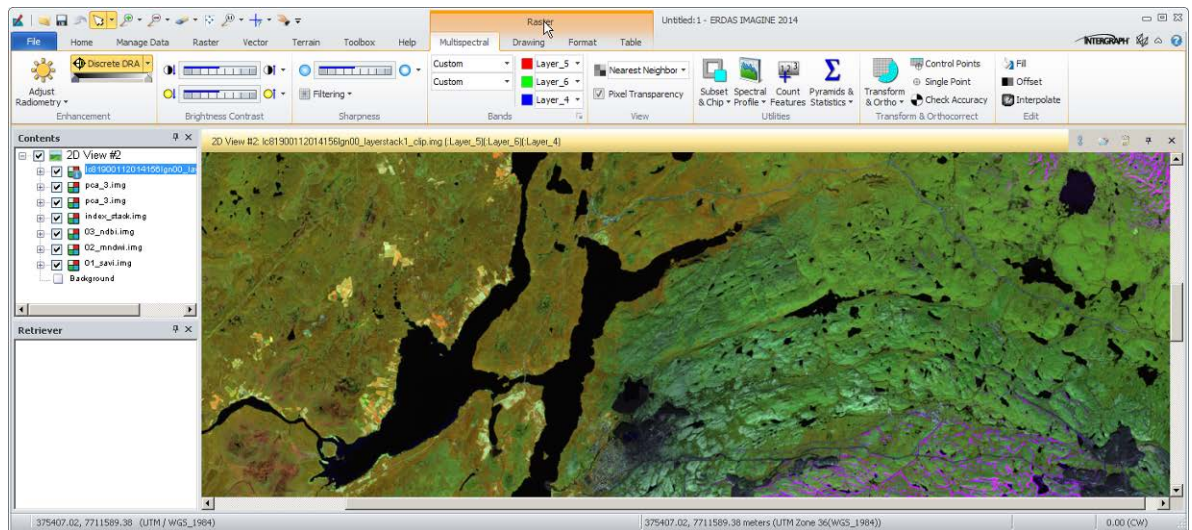


Figure A.29 Landsat8 RGB 564.

## ***Day 2 Activity and change monitoring with Landsat imagery (NLR)***

### Presentation on time series analysis of optical satellite data

A presentation was given by NLR on Time series analysis with Landsat data. Attention is paid to the spatial, spectral and temporal characteristics of the Landsat imagery and the developments in the Landsat program. It is important that Landsat images have relatively low spatial resolution (30 m, latest Landsat-8 with a 15 m pan band added), but spectral channels over the full optical spectral region, and a continuous observation of the complete Earth during 40 years, with a repetition frequency of about 15 days. Currently all data is made available in a single online database, and older data is reprocessed with the latest algorithms (see <http://landsat.gsfc.nasa.gov/>).

Attention is paid to the good geometry of the imagery (no additional correction is required) and the radiometry. The procedure for applying a radiometric and atmospheric correction in order to obtain ground reflection values is explained. NLR implemented the Landsat correction in an Erdas Imagine routine. A selection of Landsat images of Nikel was downloaded as a test dataset and the images were calibrated using the model (see figure A.30) A multi-year dataset of summer images over 10 years and a multi-month dataset from May to September in 2013 were composed.

### **CLASSIFICATION: UNCLASSIFIED**

*All rights reserved. No part of this document may be reproduced or transmitted in any form or by any means, electronic, mechanical, photocopying, recording, or otherwise, without prior written permission of FFI, NLR or TNO.*



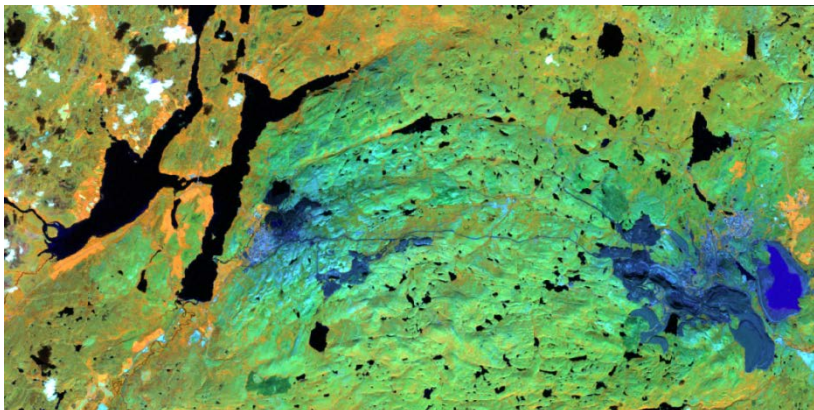


Figure A.30 Nickel Landsat8 image of 13 September 2013 (bands 4,5,3).

Next the analysis of these datasets was discussed. An analysis of the spectral characteristics of the Landsat images for the typical land classes in the Nickel area was presented, as well as the relevance of some vegetation and mineral indexes for the classification (see figure A.31). Based on this classification rules were defined and applied, using the Erdas Imagine Knowledge Engineer.

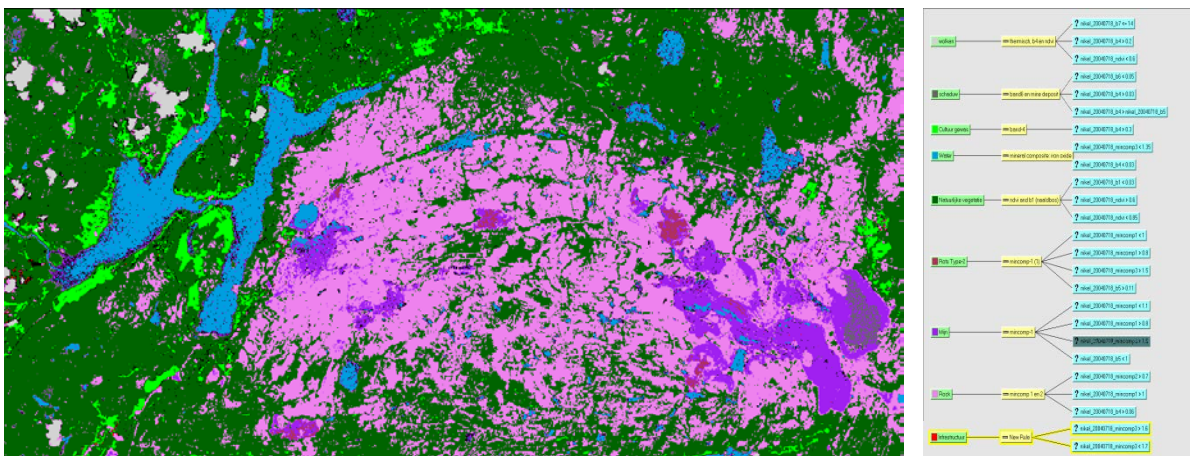


Figure A.31 Classified Landsat image and the set of rules used for this.

Finally, attention was paid to the temporal analysis. First, additional temporal parameters can be extracted (like variation of the reflectance over time (min,max,average), start and end moment of vegetation activity), and based on this additional classification rules can be formulated to obtain a better single classification result. Secondly, the temporal trend of a pixel can be determined, and for new images deviations from the expected trend (changes) can be detected. Thirdly, specific objects can be detected in the images, like ships, for which the statistical behaviour in time can be analysed. Examples are given based on a dataset of Rotterdam and environment. Finally, video-clips of multi-temporal image series were shown,

### **CLASSIFICATION: UNCLASSIFIED**

*All rights reserved. No part of this document may be reproduced or transmitted in any form or by any means, electronic, mechanical, photocopying, recording, or otherwise, without prior written permission of FFI, NLR or TNO.*

in which relatively easy detection of specific changes could be done (new roads, deposits, agricultural activities).

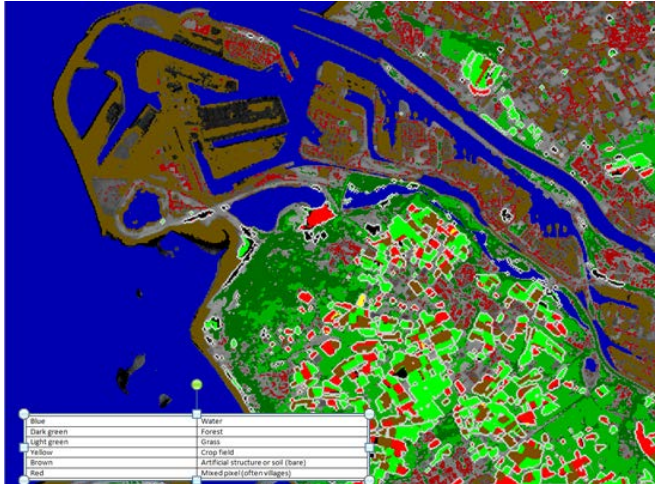


**Figure A.32** Classification of agricultural fields using multi-temporal information.

Next three exercises were done by the participants:

#### Exercise 1: Calibration of Landsat image

A downloaded recent Landsat scene of Nikel was made available. Calibration of this image was done by all participants using the Erdas calibration model as provided by NLR. Values for the gain/offset and darkest pixels in the bands had to be filled in by the participants. Application of the model gave a reflectance image that was radiometrically and atmospherically corrected. With Imagem it was discussed that the model can be farther automated by reading the calibration parameters directly from the metadata file.

#### Exercise 2: Rule based classification of Landsat image

The formulated rules in the Expert Classifier model were made available to the participants together with a Landsat scene. Some changes were made to the model by adding additional rules and constraints and evaluating the results. In this way everyone could get more idea on the working of the Expert Classifier and the sensitivity of the rule set to variations in the parameter levels. The model is made available to the participants.

#### Exercise 3: Visual inspection of multi-year and multi-month video of Landsat imagery

Videos with a 10 year sequence and one season sequence of the Landsat images were played, and were provided to the participants. The participants were asked to look for a longer time to this videos, discover changes over time in the image sequences, and determine how far the observed changes might be relevant for military practice.

### **CLASSIFICATION: UNCLASSIFIED**

*All rights reserved. No part of this document may be reproduced or transmitted in any form or by any means, electronic, mechanical, photocopying, recording, or otherwise, without prior written permission of FFI, NLR or TNO.*

It was concluded that such a relatively simple video could be a very strong means to provide insight in the characteristics of an area, both for the analyst and the commander. Relevant changes that could be observed were:

- Period and extend of snow cover, leaves on trees
- Location and type of agricultural fields, time of harvesting
- Infrastructural activities: renewal of existing road, construction of new pipe- or powerline
- Detection of secondary routes in landscape as indication of activity or smuggling
- Activity/extension of open mine areas
- Dumping of waste at specific sites
- Variation of water level in (reservoir) lakes and rivers
- Landscape changes due to nuclear power plant or industrial activities

It was remarked that in many cases first an information requirement is given, based on which an image analyst starts analysis activities on imagery. The imagery is analysed to see if any interesting information is found. In a more strategic monitoring case an area can be kept under observation in order to detect deviating or abnormal things that can be triggers for relevant activities or developments in that area.

#### Presentation on Leica Erdas Imagine functionality

During the second part of the afternoon a presentation/demonstration on the of Erdas Imagine data analysis functions was given by Dirk Voets from Imagem. Attention was paid to many functions and features of the software:

- Automatic reading of downloaded Landsat imagery
- Atmospheric correction functions
- Automatic geometric correction functions and DEM generation
- Classification functions, including object based classification
- Functions for computation of several indices (mineral, vegetation, water etc)
- Change detection
- Automation of sequences of functions, using the modeller and python

### **CLASSIFICATION: UNCLASSIFIED**

*All rights reserved. No part of this document may be reproduced or transmitted in any form or by any means, electronic, mechanical, photocopying, recording, or otherwise, without prior written permission of FFI, NLR or TNO.*



### ***Day 3 Activity monitoring with radar imagery (TNO)***

The day started with a TNO presentation about Radar basics:

- 1) Geometrical properties, slant/ground range, relief distortion etc.
- 2) Radiometric properties: dielectric properties, geometrical properties, local incidence.
- 3) Interpretation of terrain and manmade objects
- 4) Change detection with radar

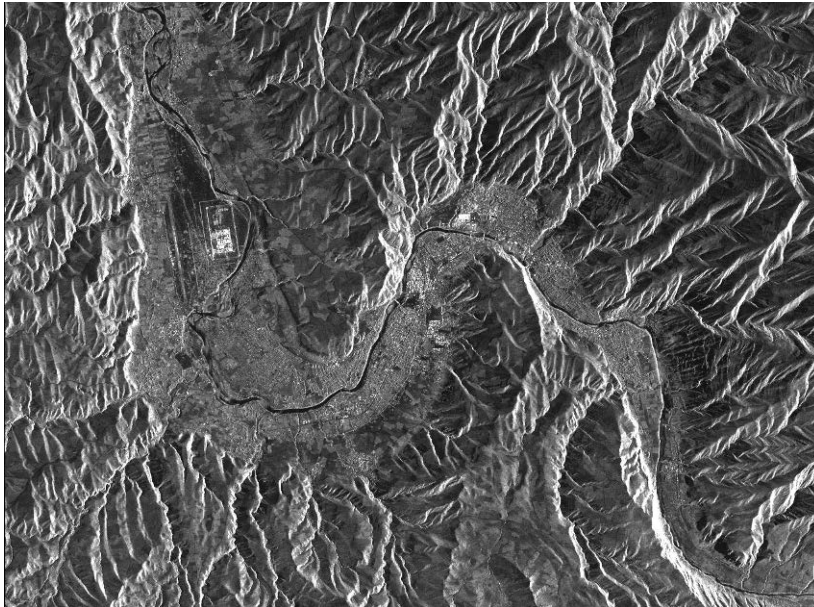


Figure A.33 TerraSAR-X image of Feyzabad showing relief distortion.

A second presentation was given by Imagem of the Erdas Imagine radar processing module (Radar Analyst), followed by a change detection exercise over the Rotterdam test site with a TerraSAR-X HS (High resolution Spotlight) image and TerraSAR-X ST (Staring Spotlight) image. Changes can be made visible in blue or red in overlay. A swipe function can be used to inspect the underlying images. The ST clearly showed better resolution and less noise.

### **CLASSIFICATION: UNCLASSIFIED**

*All rights reserved. No part of this document may be reproduced or transmitted in any form or by any means, electronic, mechanical, photocopying, recording, or otherwise, without prior written permission of FFI, NLR or TNO.*



**HS sliding**



**ST Staring**



Figure A.44 TerraSAR-X images of Rotterdam harbour showing oil drums. A comparison between HS and ST modes is shown.

Erdas Imagine interferometric processing: a demonstration was given of a pair of TerraSAR-X images with one week interval of a desert area in Australia. Because of the rocky and dry conditions coherence between the single look complex (SSC) images was kept and a DEM more accurate than the SRTM DEM could be produced during the demonstration.

As side step to height retrieval using radar, an Erdas module was shown to derive height information from a high resolution optical stereo pair. The  $x,y,z$  information is stored in a point cloud. This point cloud can be visualized as a 3-dimensional model with the original colour image in overlay. In this way a quick and good impression of the environment can be obtained. The point-cloud should be dense so that high resolution is required and enough texture should be available in the image to avoid holes in the height model.

For the Nickel test case a multi-temporal radar change detection module developed at TNO was available. A set of 25 spotlight images from RADARSAT provided by FFI was analysed using an interactive tool (see Figure A.45). Various changes could be seen such as changes near the nickel melting plant, displaced trains, and changes at parking lots and at assembly places.

The tool uses a data cube of co-registered and calibrated images. Such a data cube can be prepared using Erdas image, using optional standard preprocessing steps for co-registration and calibration. The cube can then be produced using layer stacking and an optional subset operation to reduce the data volume.

A first step is a change detection step where locally outliers are detected using a median filter. In a following step these detections can be inspected, and in an additional window the temporal behaviour is shown. Also shown in a separate window is a Google map image focused on the inspected detection to facilitate the interpretation.

### **CLASSIFICATION: UNCLASSIFIED**

*All rights reserved. No part of this document may be reproduced or transmitted in any form or by any means, electronic, mechanical, photocopying, recording, or otherwise, without prior written permission of FFI, NLR or TNO.*

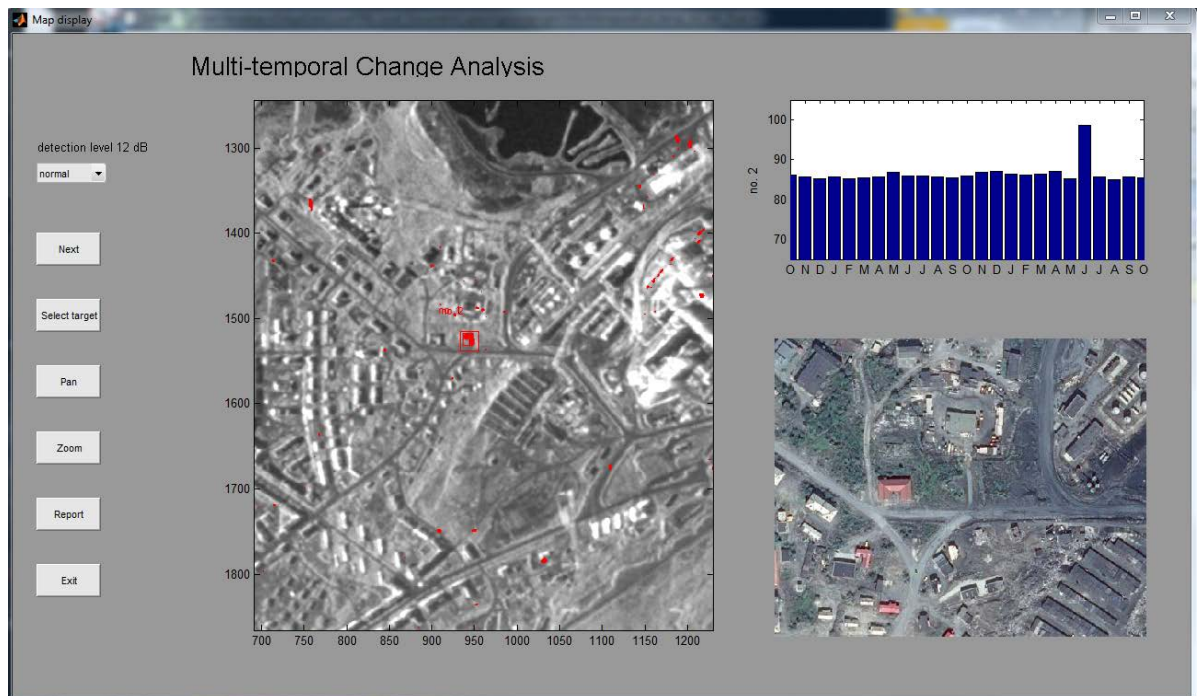


Figure A.45 Multi-temporal analysis showing a significant change in June.

Discussion about the usefulness:

- 1) The interval between the images should match the dynamics of the process to be studied. For example with the monthly interval the seasonal vegetation growth could be seen and the gradual change of the increasing deposits.
- 2) In the multi-temporal change detection tool also a RGB image containing the image with the detection, the previous, and the next should be shown.
- 3) Sentinel images are interesting since these are freely accessible. Procedure how to access and how to handle these images should be studied.
- 4) The role of radar imagery in desert areas is interesting due to the possibility of detecting vehicles.
- 5) Preparation of imagery could be done by the Dienst Geografie (DG). Analysis should be done by the GSAs (Geospatial Analysts).

### **CLASSIFICATION: UNCLASSIFIED**

*All rights reserved. No part of this document may be reproduced or transmitted in any form or by any means, electronic, mechanical, photocopying, recording, or otherwise, without prior written permission of FFI, NLR or TNO.*

## About FFI

The Norwegian Defence Research Establishment (FFI) was founded 11th of April 1946. It is organised as an administrative agency subordinate to the Ministry of Defence.

### FFI's MISSION

FFI is the prime institution responsible for defence related research in Norway. Its principal mission is to carry out research and development to meet the requirements of the Armed Forces. FFI has the role of chief adviser to the political and military leadership. In particular, the institute shall focus on aspects of the development in science and technology that can influence our security policy or defence planning.

### FFI's VISION

FFI turns knowledge and ideas into an efficient defence.

### FFI's CHARACTERISTICS

Creative, daring, broad-minded and responsible.

## Om FFI

Forsvarets forskningsinstitutt ble etablert 11. april 1946. Instituttet er organisert som et forvaltningsorgan med særskilte fullmakter underlagt Forsvarsdepartementet.

### FFI's FORMÅL

Forsvarets forskningsinstitutt er Forsvarets sentrale forskningsinstitusjon og har som formål å drive forskning og utvikling for Forsvarets behov. Videre er FFI rådgiver overfor Forsvarets strategiske ledelse. Spesielt skal instituttet følge opp trekk ved vitenskapelig og militærteknisk utvikling som kan påvirke forutsetningene for sikkerhetspolitikken eller forsvarsplanleggingen.

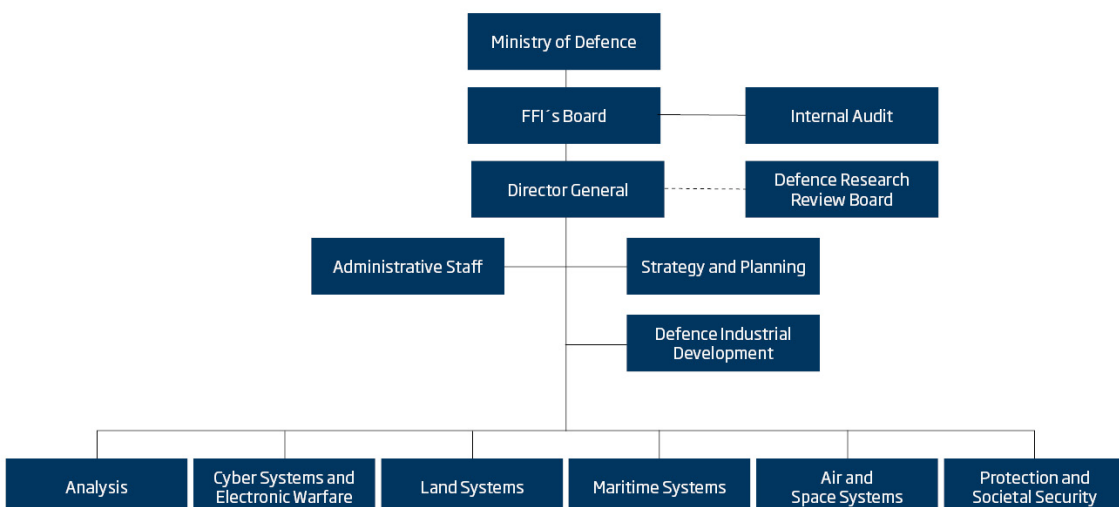
### FFI's VISJON

FFI gjør kunnskap og ideer til et effektivt forsvar.

### FFI's VERDIER

Skapende, drivende, vidsynt og ansvarlig.

## FFI's organisation



**Forsvarets forskningsinstitutt**  
Postboks 25  
2027 Kjeller

Besøksadresse:  
Instituttveien 20  
2007 Kjeller

Telefon: 63 80 70 00  
Telefaks: 63 80 71 15  
Epost: [ffi@ffi.no](mailto:ffi@ffi.no)

**Norwegian Defence Research Establishment (FFI)**  
P.O. Box 25  
NO-2027 Kjeller

Office address:  
Instituttveien 20  
N-2007 Kjeller

Telephone: +47 63 80 70 00  
Telefax: +47 63 80 71 15  
Email: [ffi@ffi.no](mailto:ffi@ffi.no)